REPORT DOCUMENTATION PAGE

Form Approved
OMB No. 0704-0188

1. AGENCY USE ONLY (Leave blank)	2. REPORT DATE	3. REPORT TYPE AND DATES COVERED
	March 15, 1996	Final Technical Report

4. TITLE AND SUBTITLE

Chemical Mechanisms at the Burning Surface

5. FUNDING NUMBERS

PE-61102F
PR-2308
SA-AS
G-F49620-94-1-0053

6. AUTHOR(S)

Thomas B. Brill

7. PERFORMING ORGANIZATION NAME(S) AND ADDRESS(ES)

Department of Chemistry
University of Delaware
Newark, DE 19716

8. PERFORMING ORGANIZATION REPORT NUMBER

9. SPONSORING / MONITORING AGENCY NAME(S) AND ADDRESS(ES)

AFOSR/NA
110 Duncan Avenue, Suite B115
Bolling AFB, DC 20332-0001

NA

10. SPONSORING / MONITORING AGENCY REPORT NUMBER

94-1-0053

11. SUPPLEMENTARY NOTES

12a. DISTRIBUTION / AVAILABILITY STATEMENT

Approved for public release; distribution is unlimited

12b. DISTRIBUTION CODE

13. ABSTRACT *(Maximum 200 words)*

Chemical mechanisms and kinetics are described for the surface reaction zone of materials of interest in solid rocket propellants. The technique used is flash thermolysis of films by T-jump-Fourier transform infrared spectroscopy. The potential for burn rate modification by a wide variety of related nitrogen heterocyclics was uncovered. The kinetics of decomposition of HMX, RDX and NTO were evaluated and critically analyzed. It was found that a kinetic compensation effect exists. Lower values of the activation energy for NTO were all shown to result from sublimation kinetics rather than decomposition kinetics. A three-stage reaction mechanism for HMX and RDX in the condensed phase was proposed which involves two competitive decomposition reactions and one strongly exothermic reaction. This model is now being adopted in most combustion models of nitramines. The decomposition kinetics and mechanism of HNF were determined for the first time at flash heating conditions. The kinetics of product evolution was determined for HTPB at combustion temperatures. It was found that desorption kinetics rather than bulk-phase decomposition kinetics control the rate of volatilization at temperatures above about 500°C.

14. SUBJECT TERMS		15. NUMBER OF PAGES
-RDX	-HMX	126
-Thermal decomposition	-NTO	16. PRICE CODE
-Kinetics	-HTPB	
-IR spectroscopy	-HNF	

17. SECURITY CLASSIFICATION OF REPORT	18. SECURITY CLASSIFICATION OF THIS PAGE	19. SECURITY CLASSIFICATION OF ABSTRACT	20. LIMITATION OF ABSTRACT
unclassified	unclassified	unclassified	UL

DISCLAIMER NOTICE

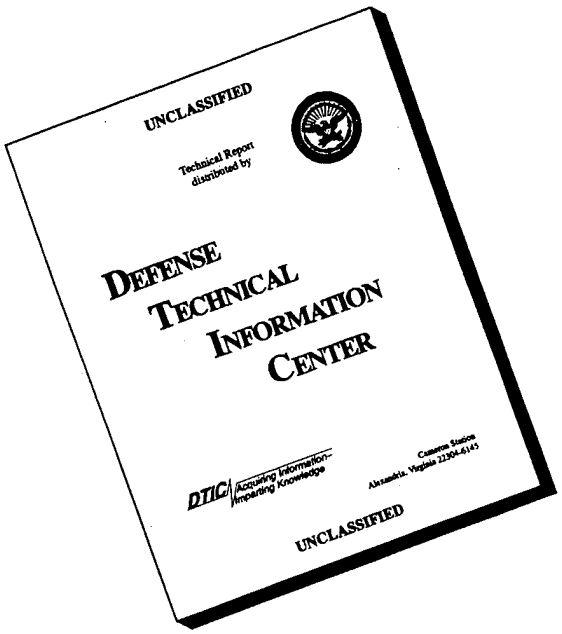

THIS DOCUMENT IS BEST QUALITY AVAILABLE. THE COPY FURNISHED TO DTIC CONTAINED A SIGNIFICANT NUMBER OF PAGES WHICH DO NOT REPRODUCE LEGIBLY.

I. Background and Objectives

The research summarized in this Final Report on F49620-94-1-0053 covers the period of November 5, 1993 to March 4, 1996. The objective was to determine the kinetics and mechanisms of chemical processes which occur in the surface reaction zone of burning energetic materials and fuel/binders. The main application of this work is in development of large scale combustion models of solid rocket propellants in which reduced chemistry at the surface replaces global Arrhenius chemistry. However, there is fundamental scientific interest in this work as evidenced in various invitations to speak in pure science forums.

The problems faced in defining the heterogenous pyrolysis chemistry in the surface reaction zone of burning materials are both experimentally and conceptually challenging. The reactions occur over a short linear dimensions, in multiple phases, at high temperatures, and with a steep temperature gradient. The experiments are mostly being performed by using T-jump/FTIR spectroscopy by which a film of material is flash-heated to temperatures that are believed to be representative of the burning surface. This experiment is a "snapshot" simulation of a layer element of the burning surface during steady combustion. The experiment is the first of its type designed both to create combustion-like conditions and to capture chemical details at the same time.

The compounds selected for study are among those of interest to the Air Force in propulsion and explosion applications. They

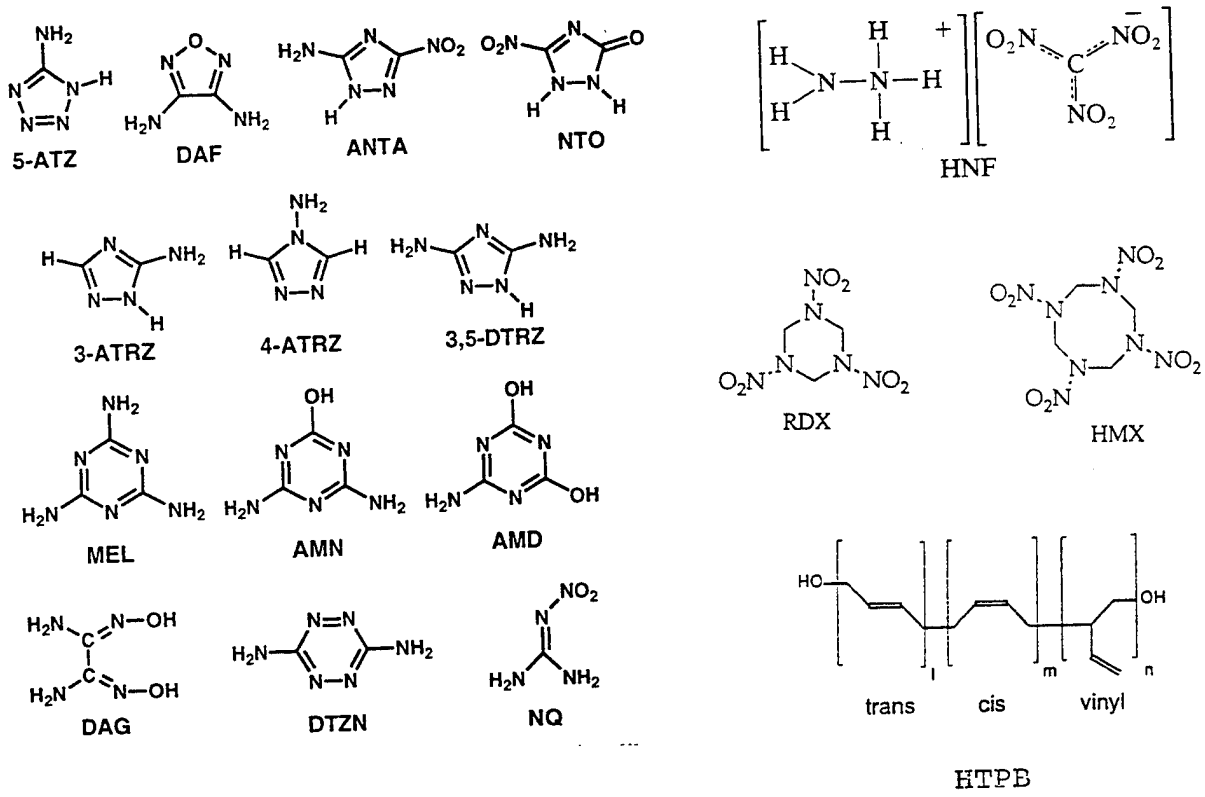

Figure 1. Compounds studied

are shown in Figure 1. In addition, considerable effort has been made in this program to support the AFOSR-URI on Combustion Instability. A major effort has also been made to evaluate the chemical kinetics which have been reported for important energetic materials. The publications appended to this report detail of these efforts.

II. Major Accomplishments

A. Burn-rate Modification

Selected triazole, tetrazole, triazine, furazan, and acyclic backbone compounds were shown by IR spectroscopy to convert to polymeric, melon-like, cyclic azine residues upon

heating to T≥ 500°C. These compounds include the insensitive explosives 3-nitro-1,2,4-triazol-5-one (NTO), 3-amino-5-nitro-1,2,4-triazole (ANTA), and nitroguanidine. The melon-like residue could suppress the burn rate if these compounds are formulated into solid rocket propellants. The IR-active gaseous products from thermolysis were determined as a function of pressure and are related to the atom connectivity in the parent molecules.

B. Analysis and Critical Evaluation of HMX, RDX and NTO Kinetics.

Widely different Arrhenius parameters have been published for thermal decomposition of HMX (octahydro-1,3,5,7-tetranitro-1,3,5,7-tetrazocine) and RDX (1,3,5-trinitrohexahydro-s-triazine). Evaluation of these data reveals that an approximately linear relationship exists between ln A and E_a for each compound irrespective of the phase. This kinetic compensation effect accounts for and unifies most of the differences in the reported rates. The range of data is qualitatively attributable to differences in the sample characteristics and experimental conditions. All E_a-ln A sets lying on or close to the compensation regression line consistently account for the rate of thermal decomposition under the conditions reported. E_a-ln A sets not lying on or near the compensation regression line represent a different process or are incorrect. The kinetic compensation effect provides a rational

method to select Arrhenius parameters to describe the global thermal decomposition rate of an explosive.

Seven previously published global kinetic measurements for thermal decomposition of the energetic compound 5-nitro-2,4-dihydro-3H-1,2,4-triazol-3-one (NTO) report Arrhenius activation energies ranging from 40.7 to 120.4 kcal/mol. To resolve this large discrepancy, two potentially dominating processes (sublimation and thermal decomposition) were isolated and their kinetics determined. For sublimation E_a = 25.8 kcal/mol, ln A (s^{-1}) = 29.2 (isothermal at 0.002 atm); E_a = 28.6 kcal/mol, ln A(s^{-1}) = 31.3 (non-isothermal at 0.002 atm). Decomposition kinetics on semi-confined NTO (20 atm pressure) by flash-heating with T-jump/FTIR spectroscopy yield E_a = 87.1 kcal/mol and ln A(s^{-1}) = 74.8. From these data and selected, evaluated, previous measurements, the kinetic constants for decomposition alone were E_a = 78 - 87 kcal/mol and ln A(s^{-1}) = 67-78. Smaller values of the Arrhenius parameters reported previously were shown to result predominantly or partly from sublimation.

C. Analysis and Critical Evaluation of the Surface Chemistry of Burning Nitramine Propellants.

The surface reaction zone of a solid propellant is increasingly acknowledged as imparting major, if not dominant, characteristics to combustion. An overview of this evolving issue is given. Chemistry considerations associated with the multiphase surface layer of the nitramine monopropellants HMX and RDX were evaluated critically. These include global rates,

specific decomposition and exothermic reactions, evaporation, and surface temperatures. A chemistry description was offered which involves the competition of two decomposition branches and one strongly exothermic reaction. Based simply on rationally derived reaction rates, reasonable deductions may be made about the surface temperature and reaction-zone thickness during combustion of HMX and RDX.

D. Determination of Rates and Pathways of Hydrazinium Nitroformate under Combustion-like Conditions.

Hydrazinium nitroformate (HNF), $N_2H_5[C(NO_2)_3]$, holds promise as a clean-burning, high-energy oxidizer for solid rocket propellants. By using T-jump/FTIR spectroscopy, the thermal decomposition process was outlined in the 130-400°C range, which includes surface melt/foam formation and self-ignition events. Reaction regimes containing evaporation, conversion to $NH_4[C(NO_2)_3]$, and progressive decomposition into CO_2, CO, N_2O, NO, and H_2O were observed. Based on the products these reaction regimes become increasingly exothermic at higher temperature. Decomposition induction-time kinetics (E_a = 25 kcal/mol, ln B(s) = 25.3) of the melt/foam layer were determined from time-to-exotherm data and give reasonable agreement with the combustion characteristics of HNF measured by others.

E. Kinetics and Species Analysis of Hydroxyl-terminated Polybutadiene (HTPB) under Combustion-like Conditions.

Flash pyrolysis of structurally different hydroxyl-terminated polybutadiene polymers (HTPB) was conducted at 600°C/s

to constant temperatures in the 450-609°C range under 2 and 11 atm of applied pressure. With chemometric procedures based on the entire mid-IR spectrum, thirteen gaseous products representing at least 70 percent of the polymer were identified and quantified. Contrary to previous indications that butadiene and 4-vinyl-1-cyclohexene dominate, the *trans*-butadiene oligomers are major products. These oligomers are probably responsible for smoke formation. The product concentrations are sensitive to the temperature below 500-530°C and 2 atm Ar, but are relatively insensitive to the temperature above 500-530°C.

The rates of formation were determined for the six most prevalent volatile products from HTPB heated at 600°C/s to constant temperatures in the 450-609°C range under 2 and 11 atm of applied pressure. The resulting Arrhenius parameters reveal that mildly exothermic, bulk-phase, heterogeneous decomposition reactions control the rate of gaseous product evolution at T<500-530°C under 2 atm Ar. The exact temperature depends on the product and the polymer microstructure. The rate evolution of most of the gaseous products at T>500-530°C is controlled by desorption of fragments of the polymer rather than by bulk-phase decomposition. When P = 11 atm Ar, the formation and desorption of these fragments controls the rate of product of evolution over the entire 460-600°C range. These individual rate constants combined into a single rate yield macro kinetics of gas evolution from R45M as follows: E_a = 51 kcal/mol, ln A (s^{-1}) = 31 for 2 atm and 450-530°C; E_a = 18 kcal/mol, ln A (s^{-1}) = 11 for 2 atm and

530-609°C; E_a = 12 kcal/mol, ln A (s^{-1}) = 6.6 for 11 atm and 460-600°C. A generalized equation that qualitatively matches the kinetics of gaseous product evolution as a function of pressure is given.

III. Publications (attached as appendices)

195. T. B. Brill "FTIR Spectroscopy for Surface Pyrolysis and Flame Diagnostics," in Non-Instrusive Combustion Diagnostics, K. K. Kuo and T. P. Parr, Eds. Begell House, Inc. New York, 1994, p. 191 (Invited).

196. D. G. Patil and T. B. Brill, "Thermal Decomposition of Energetic Materials 64. Kinetics of Decomposition of Furazano[3,4,b]piperazine and its 1,4-Dinitro Nitramine Derivative," Thermochim. Acta, **235**, 225 (1994).

197. G. K. Williams, S. F. Palopoli and T. B. Brill, "Thermal Decomposition of Energetic Materials 65. Conversion of Insensitive Explosives (NTO, ANTA) and Related Compounds to Polymeric Melon-like Cyclic Azine Burn-Rate Suppressants," Combust. Flame, **98**, 197 (1994).

199. T. B. Brill, P. E. Gongwer and G. K. Williams, "Thermal Decomposition of Energetic Materials 66. Kinetic Compensation Effects in HMX, RDX, and NTO," J. Phys. Chem., **98**, 12242 (1994).

200. T. B. Brill, H. Arisawa, P. J. Brush, P. E. Gongwer and G. K. Williams, "Surface Chemistry of Burning Explosives and Propellants," J. Phys. Chem., **99**, 1384 (1995) (Invited Feature Article).

201. T. B. Brill, "Chemistry of a Burning Surface," in Combustion Efficiency and Air Quality, Chapter 3, Plenum Press, New York, 1995, p. 63 (Invited).

202. G. K. Williams and T. B. Brill, "Thermal Decomposition of Energetic Materials 67. Hydrazinium Nitroformate (HNF) Rates and Pathways under Combustion-like Conditions," Combust. Flame, **102**, 418 (1995).

203. T. B. Brill, "Multiphase Chemistry Considerations at the Surface of Burning Nitramine Propellants," J. Propuls. Power, **11**, 740 (1995) (Invited).

204. G. K. Williams and T. B. Brill "Thermal Decomposition of Energetic Materials 68. Decomposition and Sublimation Kinetics of NTO and Evaluation of Prior Kinetic Data," J. Phys. Chem., **99**, 12536 (1995).

207. H. Arisawa and T. B. Brill "Flash Pyrolysis of Hydroxyl-terminated Polybutadiene (HTPB) I. Analysis and Implications of the Gaseous Products," Combust. Flame, in press.

208. H. Arisawa and T. B. Brill, "Flash Pyrolysis of Hydroxyl-terminated Polybutadiene (HTPB) II: Implications of the Kinetics to Combustion of Organic Polymers," Combust. Flame, in press.

213. G. K. Williams and T. B. Brill, "Toward Quantitative Thermodynamics and Kinetics of Pyrolysis of Bulk Energetic Materials at High Temperature and Pressure," in Decomposition, Combustion and Detonation Chemistry of

Energetic Materials, T. B. Brill, T. P. Russell, W. C. Tao, and R. B. Wardle, Eds., Materials Research Society, Pittsburgh, PA, Vol. 418, 1996, in press.

IV. Persons Supported

1. Thomas B. Brill, Principal Investigator.
2. Graylon K. Williams is a Ph.D. student who is near completion of his studies.
3. Haruyuki Arisawa is a Ph.D. student who is supported by this Japan Defense Agency (Third Research Center). He is working on this project.

Non-Intrusive Combustion Diagnostivs, K. K. Kuo and T. P. Parr, Eds. Begell House, New York, 1994.

SURFACE PYROLYSIS PHENOMENA AND FLAME DIAGNOSTICS BY FTIR SPECTROSCOPY

Thomas B. Brill

Department of Chemistry, University of Delaware, Newark, DE 19716

INTRODUCTION

Chemical description of the combustion and explosion of bulk energetic materials continues to be one of the greatest challenges to the energetics community. Laser diagnostic and microprobe mass spectrometry are established techniques for characterizing the homogeneous flame zone in terms of species, concentrations and temperature profile.[1] A particularly daunting problem has been the chemical description of the heterophase reaction zone at the surface of a burning propellant. The chemistry of this region is important because it connects the flame characteristics to the formulation of the propellant. During combustion, this condensed phase-to-gas phase transition zone is spacially thin, has a steep temperature gradient and a microstructure of mixed phases that are shown in Figure 1. No experimentally based description of the chemical details of this reaction zone has been possible while the flame is present. An alternate approach to gain the required information is to simulate the conditions of the surface zone in a manner that enables spectroscopic diagnostics to be conducted. Hence, the larger part of this article is devoted to the use of FTIR spectroscopy to characterize dynamically the simulated surface reaction zone of a burning propellant. The applications of FTIR spectroscopy to characterize the flame zone conclude the article. The use of FTIR spectroscopy to characterize recovered samples or with time-delayed analysis is not covered because of space limitations.

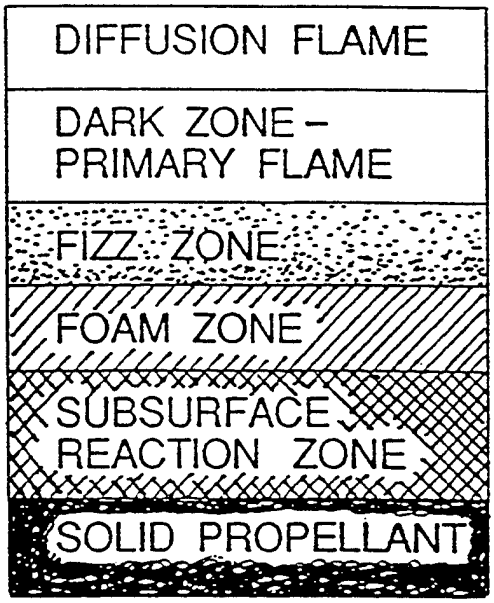

Figure 1. The generalized 1-D surface reaction zone of a burning propellant

FTIR SPECTROSCOPY

FTIR spectroscopy has the advantage over dispersive IR methods when high energy throughput, rapid data acquisition and broad band IR spectra are required. For real or near real-time data acquisition, a research grade rapid-scanning FTIR spectrometer (RSFTIR) is invaluable. Fortunately, commercial instrumentation is available so that little space needs to be devoted to the theory and practice of FTIR spectrometry.[2]

The RSFTIR spectrometer takes advantage of the fact that both the forward and reverse motions of the moving mirror of a Michelson interferometer can generate all of the spectral information. This fact, coupled with a high mirror velocity and a very stable interferometer, allows mid-IR spectra to be collected at 60-80 scans per second with 16-32 cm^{-1} resolution. A mercury-cadmium-telluride (MCT) detector and digital signal processing provide a low-noise signal in which absorbances from all IR active species are clearly evident in a single-scan spectrum. The interferograms acquired in this way are stored independently by fast analog-digital transfer with the time attached to each interferogram. At a later time, the interferograms are transformed to spectra. The operator can manipulate many of the parameters of the data collection and Fourier transformation to optimize the scan speed, resolution and spectra details. We settled on a scan speed of ten scans/sec at 4 cm^{-1} resolution as optimal for our research. However, a faster scan speed could have been chosen while sacrificing resolution. Modifications of the sample compartment may also be required to be compatible with the conditions of the experiment. For example, a high temperature flame can heat the optics and create interference patterns. This can be eliminated by the use of wedged windows.

Perhaps the most important consideration in the solution of combustion and explosion problems by FTIR spectroscopy is the design of sample cells that simulate the conditions appropriate for the event being sought. Most of our effort has gone into this area and is described next.

ANALYSIS OF SURFACE PYROLYSIS PROCESSES BY FTIR SPECTROSCOPY

FTIR spectroscopy is an effective method to identify and quantify gases produced by fast reactions of solids and liquids, such as burning energetic materials.[3] When studying ignition, combustion and explosion phenomena, the sample must be heated rapidly. To capture the important events, the FTIR analysis must be performed with minimal time delay between the event and analysis. Hence, the IR beam should be focused as close to the reacting surface as possible and the data collected by RSFTIR. If the gases evolve into a cool non-reactive atmosphere, they will quench and be detected. Since the time delay between the reaction and the detection is minimal, many relatively reactive species are observed with concentrations more close to the original than when longer time delays exist. Of course, the time delay is still large relative to the rates of the elementary reactions. Nevertheless, the instantaneous relative concentrations of the gases that feed the flame zone are observed if a flame were present. Analysis of the gas products can be made if the flame is present, but the flame zone products tend to dominate the reactive, near-surface products in this case.

The most powerful FTIR-based technique for determining the chemical processes in the burning surface reaction zone is T-jump/FTIR spectroscopy.[4] The technique is based on recreating a "snap-shot" view of the reaction zone of a burning surface (Figure 1), which is a thin layer of rapidly heated material. This scenario is produced by T-jump/FTIR spectroscopy in which a thin film of material is heated at 2000°C/sec to a constant chosen temperature while simultaneously monitoring the heat flow to the film and determining the gaseous products released in near real time. Figure 2 shows the essential details of this experiment.

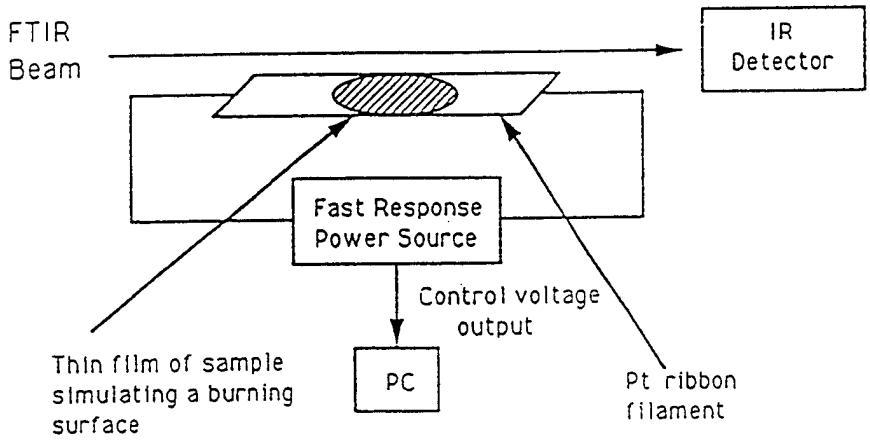

Figure 2. The T-jump/FTIR experiment

Typically, approximately 200 μg of polycrystalline sample is spread on a Pt ribbon filament that is housed in a gas-tight IR cell having about 25 cm^3 internal volume. The cell is flushed with Ar and pressurized as desired. The filament is heated by a power control unit at about 2000°C/sec to a constant temperature in the 240-500°C range depending on the sample. Control is achieved by rapidly sensing the Pt resistance. Endothermicity and exothermicity of the sample are detected by monitoring the control voltage required to maintain constant resistance. The difference control voltage is obtained by subtracting the voltage of the filament without sample from the voltage when the sample is present. A negative excursion represents an exotherm of the sample.

Because of the small mass, the sample temperature is relatively uniform. However, the interfacial heat transfer is complex. The sample and the filament form a reaction zone that contains the gas and condensed phase in close contact with the heat source. From the point of view of the chemistry of the heterophase surface, this condition qualitatively resembles a surface during combustion. Instead of forming a flame, the decomposition products rise into and are quenched by the cool Ar atmosphere. The beam of the RSFTIR spectrometer is positioned about 3 mm above the sample surface. Collection of complete IR spectra every 100 msec gives the identity, sequence of formation, and relative concentrations of the products.

The IR absorbances of each product are converted to concentrations by multiplying the absorbance of a characteristic vibrational mode

Table 1 The Multiplicative Factor F used in Relative Percent Concentration Calculations		
Gas	Absorbance, cm^{-1}	F
CO_2	2349 (R)	1[a]
HNCO	2274 (R)	1.5[b]
N_2O	2224 (R)	2
CO	2143 (P)	25
NO	1876 (R)	32
CH_2O	1744 (R)	15
HNO_3	1709	8
NO_2	1621	2
HCOOH	1103	3.7
NH_3	968 (Q)	5
HONO (cis)	856 (Q)	3.2[c]
HONO (trans)	794 (Q)	
HCN	713 (Q)	3
CH_4	3020 (Q)	11
C_2H_4	949	7.5
C_2H_2	729	3.4
HCl	2974 (R)	10.3
[a]reference compound [b]estimated [c]sum of cis and trans intensity		

by a factor F derived from the absolute absorbance.[5] Table 1 gives the values of F used. In this way the rate of evolution of the product is ascertained. IR inactive products are not detected. H_2O is frequently detected but was not quantified.

Surface Chemistry of Nitramines

Nitramines, such as HMX and RDX, are especially important as minimum smoke, high energy explosive and propellant ingredients. The decomposition of HMX [6] and RDX [7] is similar, so only RDX will be described.

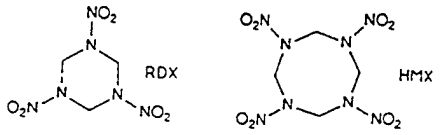

Figure 3 shows T-jump/FTIR data for a thin film of RDX heated at 2000°C/sec to 263°C and then held isothermally while IR spectra of the near-surface gas products are recorded. The global decomposition branches, R1 and R2, occur for bulk RDX and HMX. R1 and R2 imply that N_2O and NO_2 should form simultaneously with CH_2O and HCN. This is not found at any temperature studied. Rather, N_2O and NO_2 appear before

$$RDX \longrightarrow 3\ (N_2O + CH_2O) \qquad \textbf{(R1)}$$

$$RDX \longrightarrow 3\ (NO_2 + HCN + H) \qquad \textbf{(R2)}$$

CH_2O and HCN, which form from the residue left by elimination of N_2O and NO_2. This residue is a mixture of products like hydroxymethylformamide and acetamide [8-11] which decompose and delay the release of CH_2O, HCN and HNCO.[11,12]

The total IR absorbance of the products accelerates between 3.5 and 5.0 sec despite the constant heat flow from the filament, which implies that autocatalysis occurs in this stage of decomposition of HMX and RDX. Moreover, the control voltage trace in Figure 3 reveals only mild exothermicity between 3.5 and 4.5 sec when R1 and R2 dominate. Thus, these reactions release little energy in the condensed phase.

A runaway exotherm develops at 4.5 sec. The secondary reaction R3 appears to be responsible because CH_2O and NO_2 are consumed as NO,

CO, and H_2O appear. Figure 3 shows that more NO than CO forms in

$$5CH_2O + 7NO_2 \longrightarrow 7NO + 3CO + 2CO_2 + 5H_2O \qquad \textbf{(R3)}$$

accordance with R3. R3 is highly exothermic as written (ΔH = -320 kcal) and, by the large exotherm in Figure 3, it is the main source of heat in the heterogeneous condensed phase. These conclusions also apply at 360°C (Figure 3) except that the time scale is compressed. Hence, this description of the decomposition of RDX at 263°C applies as well at the surface reaction zone temperature (350 - 400°C) during combustion. However, the branching ratio of R1 and R2 depends on temperature and favors R2 at higher temperature. [6] This finding is illustrated by Figure 4, where the final

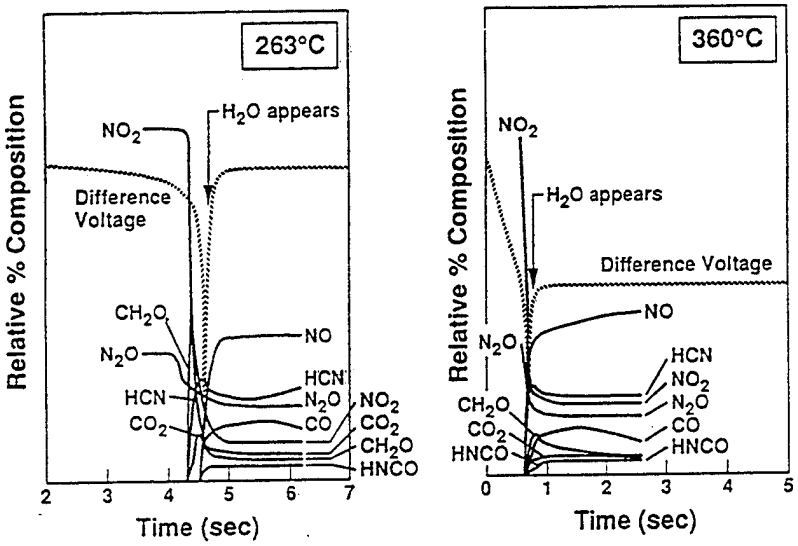

Figure 3. The gas products and heat change of RDX at 263°C and 360°C under 4 atm Ar

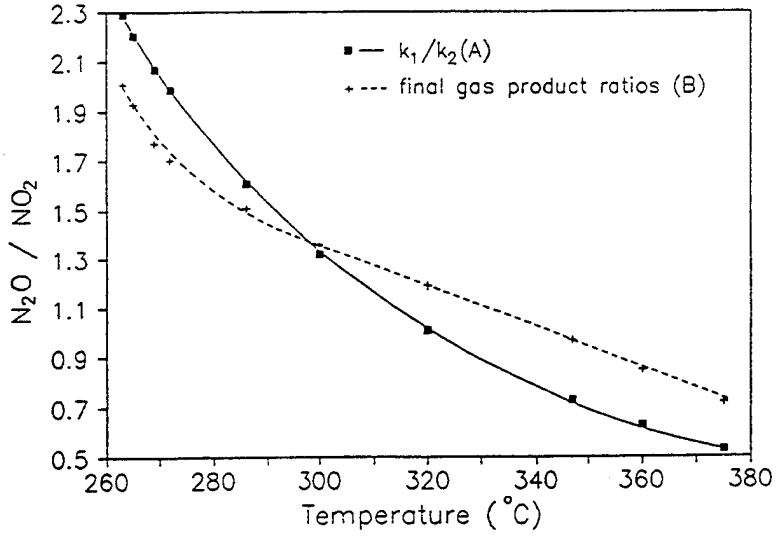

Figure 4. The calculated and experimental temperature dependence of the R1/R2

N_2O/NO_2 product concentration ratio is plotted vs. the temperature to which the sample was T-jumped. Also shown is the ratio of the rate constants k_1 and k_2 representative of R1 and R2, respectively, given by Melius.[13] The agreement in the trends is reasonably good, indicating that the rates of the semi-global decomposition branches R1 and R2 can be experimentally verified.

$$k_1 = 10^{13} \exp(-36000/RT) \text{ sec}$$

$$k_2 = 2 \times 10^{16} \exp(-45000/RT) \text{ sec}$$

Surface Chemistry of NH_4ClO_4

In excess of 1000 reactions may be involved in the decomposition and combustion of ammonium perchlorate (AP), NH_4ClO_4 [14] because of the presence of four elements and the full range of oxidation states utilized by nitrogen and chlorine. A limited chain reaction scheme of 10 reactions employed by Guirao and Williams [15] to model AP combustion was expanded to 80 reactions by Ermolin et al. [14] to simulate the gas products in the flame zone measured by microprobe-mass spectrometry.[16] Of the many reactions, Guirao and Williams and Ermolin et al. emphasize the important role that R4 plays in controlling the rate of the gas phase scheme.

$$HClO_4 + HNO \longrightarrow NO + ClO_3 + H_2O \qquad \textbf{(R4)}$$

T-Jump/FTIR spectroscopy [4] has the potential to provide evidence of R4 as well as other aspects of the rapid decomposition mechanism of AP. For example, during the rapid decomposition of bulk AP, a drop in the $HClO_4$(g) production accompanied by a sharp rise in the NO and H_2O concentrations during the stage of rapid heat release would be good evidence for R4 in the heterogeneous gas-condensed phase. Figure 5 shows the change of concentration of the gas products from AP measured from the absorbances by RSFTIR, along

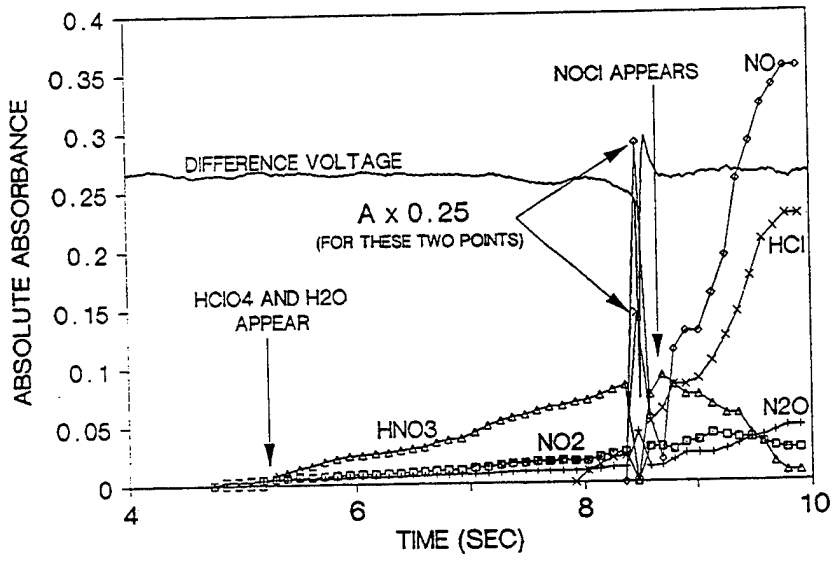

Figure 5. Gas products and the heat change of NH_4ClO_4 at 440°C under 13 atm Ar

with the heat balance sensed by the Pt control voltage.[17] Before the exotherm, IR active gas products are first detected at about 5 sec and consist of HNO_3, NO_2, N_2O, H_2O, $HClO_4$, and $HClO_4$(aq). The rise in gas product concentrations over the next few seconds indicates that the amount of sample decomposing gradually increases. The overall process is exothermic because the control voltage acquires a slight negative slope during this time.

The initial decomposition reaction of AP is widely regarded to be dissociative evaporation R5. Evidence of this reaction exists

$$NH_4ClO_4(s) \longrightarrow NH_3(absd) + HClO_4(absd) \longrightarrow NH_3(g) + HClO_4(g) \quad \textbf{(R5)}$$

below 3 atm where recombination of NH_3(g) and $HClO_4$(g) to form NH_4ClO_4(aerosol) is observed in the IR spectrum. Below 13 atm Ar, no NH_4ClO_4(aerosol) and NH_3 are detected, but $HClO_4$ is present, mostly in the hydrated form. The fact that some $HClO_4$ survives to reach the cool atmosphere, whereas NH_3 does not, may simply result from the fact that AP is over-oxidized. Not all of the $HClO_4$ is needed to oxidize NH_3. Hydrated $HClO_4$ from AP was confirmed by the match of the ClO_4^- asymmetric stretching mode with that of the gas phase above a rapidly heated 70% $HClO_4$ solution.[17]

The NH_3 from R5 is oxidized very rapidly in the heterogeneous gas-condensed phase zone by $HClO_4$. No NH_3 survives to reach the IR beam because the inversion doublet at 968 and 932 cm^{-1} is absent. The reduction product of $HClO_4$ is Cl_2 because no HCl(g), hydrated HCl, or NH_4Cl(aerosol) is observed in this stage of decomposition. NO_2, N_2O, HNO_3 and H_2O are products of ammonia oxidation. HNO_3 may simply result from hydrolysis of NO_2 and, as such, would not be an important product were a flame present. N_2O can form by R6. Preventing the buildup of HNO (*vide infra*) by R6 would be one of the chemical ways that AP is able to decompose slowly at lower temperature without developing a runaway release of heat.

$$2HNO \longrightarrow N_2O + H_2O \quad \textbf{(R6)}$$

The development and growth of the exotherm of AP in Figure 5 is a rapid event. The gas product concentrations during the exotherm are unusual in the occurrence of the large pulse of NO, HCl and H_2O. The $HClO_4$ concentration remains at or below the pre-exotherm level. The behavior of $HClO_4$, NO and H_2O is fully consistent with a major role of R4 in the acceleratory exothermic phase of AP decomposition. R4 increases in importance and ultimately controls the overall rate because HNO accumulates with time.[14] At the time when R4 dominates the rate, R6 is largely bypassed, as evidenced by the fact that the final concentration of N_2O is only approximately double the pre-exotherm value. Because of their reactivity and short life time at the temperature of the experiment, HNO and ClO_3 are not detected. In fact, for the same reason, no chlorine oxides or HClO are observed, but they are by mass spectrometry.[14,16] HNO has also been detected by mass spectrometry in the decomposition of AP in other work.[18]

The importance of Cl-O homolysis of $HClO_4$ in initiating and perhaps controlling rapid decomposition of AP has been repeatedly emphasized in many studies. It is highly likely that a fundamental role exists for HNO in the sense that products of both the early stage and exothermic stage are consistent with reactions involving HNO. R4 plays a major role in the regression rate of AP.

Surface Chemistry of Ammonium Nitrate and Ammonium Dinitramide

Interest is growing in oxidizers that might replace AP in solid propellants. Upon combustion, AP liberates HCl and H_2O that form an environmentally undesirable plume of HCl(aq). Nucleation of H_2O into droplets by HCl contributes to a prominently visible signature. These detracting features have rekindled interest in ammonium nitrate (AN). Unfortunately, AN has a low surface temperature and a low burn rate. The decomposition chemistry of AN is largely responsible for the low energy release. For example, two major decomposition reactions of AN, R7 and R8, are endothermic and mildly exothermic, respectively.

$$NH_4NO_3 \longrightarrow NH_3(g) + HNO_3(g) \qquad \textbf{(R7)}$$

$$NH_4NO_3 \longrightarrow N_2O + 2H_2O \qquad \textbf{(R8)}$$

The decomposition of AN is compared to that of ammonium dinitramide (ADN), $NH_4[N(NO_2)_2]$.[19] Unlike AN, ADN decomposes very rapidly. Part of the additional energy release is attributable to the higher heat of formation of ADN (-35 kcal/mol [20]) compared to AN(-78 kcal/mol). Beyond this difference, the chemical reactions that cause ADN to decompose very exothermically are not obvious because the gas products from rapid thermolysis of ADN are similar to those of AN. Both compounds liberate HNO_3, NH_3, N_2O, NO_2, NO, H_2O and N_2, although the mole fractions differ somewhat. By T-jump/FTIR spectroscopy it seems likely that the reaction of NH_3 and NO_2 near the surface plays a major role in driving the regression of the surface.[19]

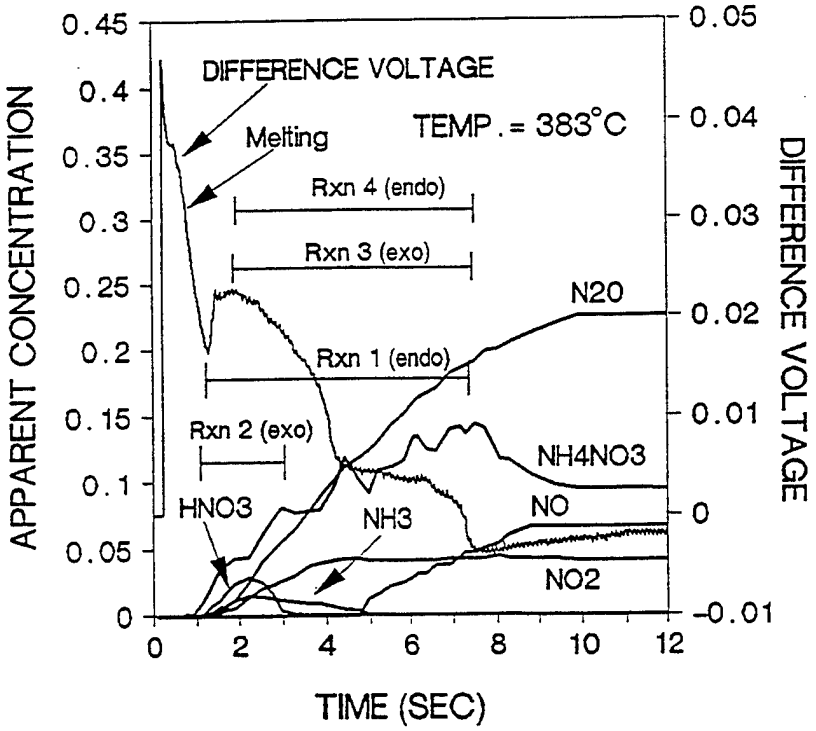

Figure 6. Gas products and the heat changes of NH_4NO_3 at 383°C under 1 atm Ar. The reactions are shown in Scheme I.

Although pure AN will not burn at 1 atm, a sample can be driven by the T-jump method to a temperature that is at or above the measured surface temperature of AN burning at 25 atm or above (300-350°C). [21] Figure 6 shows the gas products and thermal response of a 200μg film of AN heated at 2000°C/sec to 383°C and held at 383°C. The concentration data in this plot are based on the scaled growth of the IR absorbance values for each product. The superposition of several stoichiometric reactions is indicated. Of course, many elementary steps are imbedded in each of these stoichiometric reactions, but they are not determinable by T-jump/FTIR spectroscopy.

The first event is rapid endothermic melting of AN as indicated by the upward deflection in the difference control voltage trace. The control voltage decreases upon completion of melting from 0.5 - 1 sec. The process turns markedly endothermic again at about 1 sec. This second endothermic event corresponds to the appearance and growth of AN aerosol. AN aerosol forms from the endothermic dissociation of AN and desorption to $HNO_3(g) + NH_3(g)$, followed by recombination of NH_3 and HNO_3 in the gas phase (Scheme I, reaction

SCHEME I. PROPOSED REACTIONS THAT ACCOUNT FOR THE PRODUCTS OF HIGH TEMPERATURE DECOMPOSITION OF AN (see Figure 6).

	Approx ΔH, kcal
A. $4[NH_4NO_3(l) \longrightarrow HNO_3(g) + NH_3(g) \longrightarrow NH_4NO_3(\text{solid aerosol})]4$	$(44)^1$
B. $3[5NH_4NO_3(l) \longrightarrow 2HNO_3 + 4N_2 + 9H_2O]$	3(-35)
C. $5[NH_4NO_3(l) \longrightarrow N_2O + 2H_2O]$	5(-13)
D. $4NH_4NO_3(l) \longrightarrow 2NH_3 + 3NO_2 + NO + N_2 + 5H_2O$	81
A-D[2]. $28NH_4NO_3(l) \longrightarrow 6HNO_3 + 3NO_2 + NO + 2NH_3 + 5N_2O + 13N_2 + 42H_2O + 4NH_4NO_3(\text{aerosol})$	87

[1] ΔH for the desorption step only (see text).
[2] Gives the approximate IR active gas product ratios at 2 sec at 383°C (Figure 6).

A). Only the endothermic first step of reaction A is included in ΔH given for reaction A, because the second step occurs in the cooler region of the cell away from the filament. Hence, the exothermic second step is not sensed by the filament. However, a white smoke of AN aerosol is visually observed.

Despite the continuation of reaction A throughout the decomposition process, as evidenced by the growth of the AN (aerosol) concentration, the decomposition process becomes less endothermic again at about 2 sec. H_2O (not quantified) and excess HNO_3 form at this time which is consistent with the occurrence reaction B. This reaction is known, and its enthalpy has been deduced.[22] It is exothermic and would reduce the overall endothermicity of the decomposition process.

The process becomes still less endothermic from 2-4 sec as the amount of HNO_3 diminishes. However, N_2O grows rapidly in concentration through this time, suggesting that the exothermic reaction C plays an increasingly important role. However, there is evidence of yet another reaction that occurs in parallel, as indicated by the appearance of NO_2 and the eventual decrease in exothermicity again between 4-6 sec. Also, NO, whose IR absorbance

is very small, probably forms earlier than is indicated in Figure 6. Reaction D [23] accounts for these observations. Its endothermicity is superimposed on the exothermicity of reaction C and results in a leveling of the control voltage trace (heat flow is balanced) at 4-7 sec. Reaction D is also a source of NH_3, which appears as a product for a much longer time than HNO_3.

The multiplicative factors of the reactions in Scheme I were determined by the need to match the approximate relative concentrations of the gas products at a time when all of the reactions contribute. Concentrations at 2 sec were chosen. The stoichiometry of the net reaction in Scheme I approximates that found at 2 sec in Figure 6. Although the enthalpy of the net reaction is slightly exothermic as written, the relative contribution of reaction A needs only be increased somewhat to produce a net endothermic process.

The formation of NH_3 and NO_2 by reaction D raises the possibility that the process could become exothermic when confined by pressure. The reaction of NH_3 and NO_2 becomes rapid and exothermic in the 330-530°C range.[24,25] However, significant generation of heat requires confinement to enhance the concentration of NH_3 and NO_2 in the hot zone around the condensed phase.

Figure 7 shows the decomposition process of a 200μg film of AN heated at 2000°C/sec to 415°C under 33 atm of Ar. The concentrations are shown as relative percents throughout so that the behavior early in the decomposition process can be clearly seen. The melting endotherm initially dominates. The heat of reactions A-D leading to the formation of AN aerosol, N_2O, HNO_3, NH_3, and NO_2 are overall endothermic until 1.5 sec. At this time the concentrations of NH_3 and NO_2 formed by reaction D drop markedly and are accompanied by an exotherm which suggests that R9 occurs. ΔH is about -148 kcal for this reaction as written. Under pressure, this nominally gas-phase reaction could occur in the heterogeneous

$$2NH_3 + 2NO_2 \longrightarrow N_2O + N_2 + 3H_2O \qquad \textbf{(R9)}$$

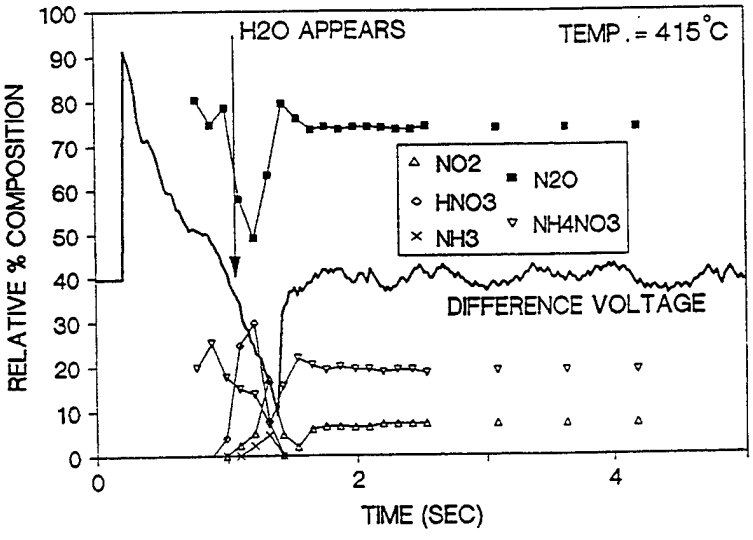

Figure 7. Gas products and the heat changes of NH_4NO_3 at 415°C under 33 atm of Ar

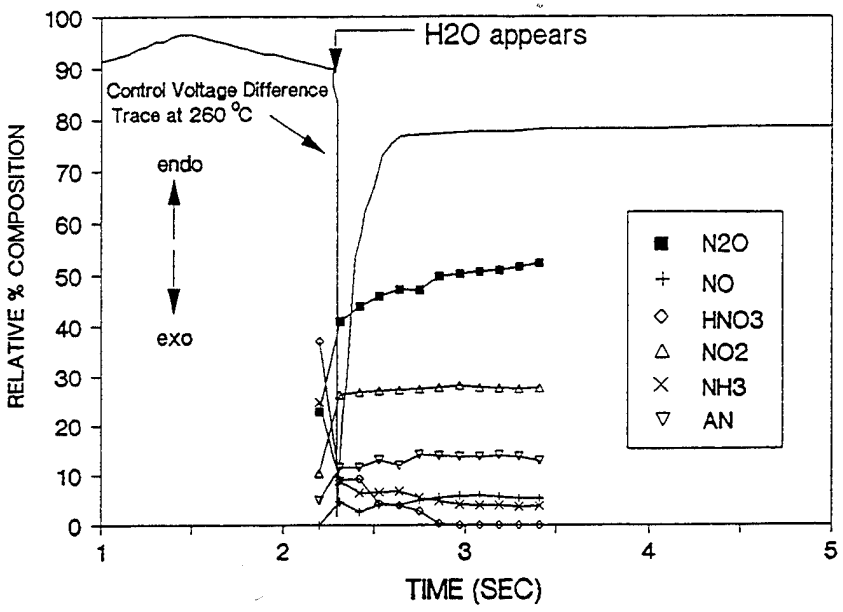

Figure 8. Gas products and the heat change of $NH_4N(NO_2)_2$ (ADN) at 260°C under 1 atm Ar

SCHEME II: PROPOSED REACTIONS RESPONSIBLE FOR THE GASES RELEASED BY ADN DURING HIGH RATE PYROLYSIS

		Approx. ΔH, kcal
	Branch A[1]	
	$3[ADN \longrightarrow NH_3 + HNO_3 + N_2O]$	3(+11.5)
	Branch B	
a	$9[ADN \longrightarrow NH_3 + HN(NO_2)_2]$	
b	$9[HN(NO_2)_2 \longrightarrow NO_2 + HNNO_2]$	
c	$6[HNNO_2 \longrightarrow N_2O + OH]$	
d	$2[HNNO_2 + OH \longrightarrow 2NO + H_2O]$	
e	$HNNO_2 + NO \longrightarrow NO_2 + HNNO$	
f	$HNNO + OH \longrightarrow N_2O + H_2O$	
g	$3[NH_3 + OH \longrightarrow H_2O + NH_2]$	
h	$3[NH_2 + NO \longrightarrow N_2 + H_2O]$	
i[2]	$9ADN \longrightarrow 6NH_3 + 7N_2O + 10NO_2 + 9H_2O + 3N_2$	-49
j[3]	$12ADN \longrightarrow 9NH_3 + 10N_2O + 10NO_2 + 9H_2O + 3N_2 + 3HNO_3$	-14
k	$4NH_3 + 4NO_2 \longrightarrow 3N_2 + 2NO + 6H_2O$	-309
l[4]	$12ADN \longrightarrow 5NH_3 + 10N_2O + 6NO_2 + 15H_2O + 2NO + 6N_2 + 3HNO_3$	-323
m[5]	$2NH_3 + 2HNO_3 \longrightarrow 2NH_4NO_3$ (aerosol)	
n[6]	$12ADN \longrightarrow 3NH_3 + 10N_2O + 6NO_2 + 15H_2O + 2NO + 6N_2 + HNO_3 + 2NH_4NO_3$	-323

[1] Assumes ΔH_f (ADN) = -35 kcal/mol, and ΔH [HNO_3(g)] is -33 kcal/mol.
[2] Sum of a-h.
[3] Sum of Branches A & B.
[4] Sum of reactions i+k.
[5] Occurs in gas phase away from surface so reaction m is not included in ΔH.
[6] Sum of l and m gives the approximate gas-phase stoichiometry at the end of the exotherm (Figure 8).

gas-condensed phase (e.g., bubbles and voids) and contribute to the condensed phase heat balance under combustion conditions. The thermal decomposition behavior of bulk ADN is very different from that of AN despite the fact that similar gas products are formed upon rapid decomposition. Figure 8 shows T-jump/FTIR data for a 200μg film of ADN heated at 2000°C/sec to 260°C. This temperature compares with a preliminary surface temperature measurement of burning ADN of about 300°C, [26] which is surprisingly similar to that of AN. At the onset of decomposition, gas products and, in contrast to AN, sharp exothermicity occur instantly. The first detected products are mostly HNO_3, NH_3 and N_2O in roughly similar amounts. Minor quantities of NO_2, AN and H_2O are also present in the initial spectrum.

The formation of HNO_3, NH_3 and N_2O in comparable amounts at the beginning suggests the presence of Branch A in Scheme II. This mildly endothermic reaction may have a role during slow decomposition at lower temperatures. It appears to be a minor branch during rapid heating, especially because it does not account for the major heat release that is experimentally observed.

Branch B of Scheme II is proposed to dominate under rapid thermolysis conditions.[19] Reaction a of Branch B is dissociation of ADN to produce NH_3 and $HN(NO_2)_2$. $HN(NO_2)_2$ is not detected, and probably homolyses in the condensed phase at high temperature by reaction b to NO_2 and $HNNO_2$. Reactions a and b are endothermic. Because relatively large quantities of NH_3 and NO_2 occur early in Branch B, much heat can be generated by reaction k in the gas phase near the surface or even as part of the heterogeneous gas-liquid zone at the surface. The high exothermicity is evident in the large control voltage deflection at 2.3 sec, and provides the energy to complete the decomposition process very rapidly. Some of the NH_3 and NO_2 remains unreacted because it escapes to the cooler region of the atmosphere. Reactions c-h are plausible subsequent steps for decomposition of $HNNO_2$, but are not determined by T-jump/FTIR spectroscopy. They are simply proposed as reasonable sources of stable products in the quantities detected. The net reaction i of Branch B is mildly exothermic. Combining Branches A and B yields the exothermic reaction j. Adding some gas-phase recombination of NH_3 and HNO_3 (reaction m) to account for the observed AN solid aerosol yields reaction n, whose stoichiometry approximates the experimentally observed gas product ratios observed at 2.5 sec in Figure 8. Reaction n is strongly exothermic largely because of reaction k, which is the reaction of NH_3 with NO_2.

For both AN and ADN, the exothermic NH_3 + NO_2 reaction appears to dominate the heat release stage. In the case of AN, the exotherm occurs only under a large applied pressure accompanied by a drop in the amount of NH_3 and NO_2 that appear in the gas phase. Although the reaction of NH_3 and NO_2 appears to be responsible for this exotherm, the amount of NH_3 and NO_2 is smaller for AN than for ADN, and therefore much less heat is generated.

The rapid decomposition process of ADN is strongly exothermic early in the reaction scheme. This behavior is consistent with the ease of formation of a large amount of NH_3 and NO_2 in the early decomposition steps. Because the reaction of NH_3 and NO_2 dominates early and produce a large amount of heat, the overall decomposition and gasification process is driven at a much higher rate for ADN than AN. Therefore, for both AN and ADN the reaction of NH_3 with

NO_2 is implicated as the main source of heat when the pure material is decomposed at high temperature. For AN this reaction only becomes important under confinement, e.g., by the application of pressure.

IS PYROLYSIS OF THIN FILMS RELATED TO THE BURNING SURFACE?

Good evidence that the rapidly heated thin film is a surface simulation comes from the SMATCH/FTIR method (SMATCH stands for simultaneous mass and temperature change) [27] in which a film of uniform, chosen thickness (20-60μm) is heated at $\geq$ 150°C/sec, while the dynamic mass change, temperature change, and gas products are all measured simultaneously. The burn rate $\dot{r}$ calculated from

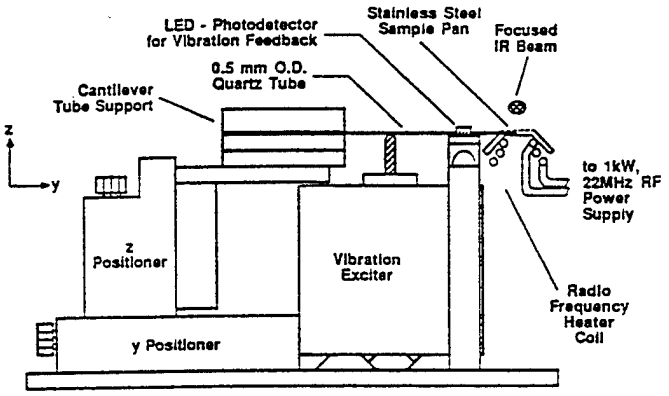

Figure 9. A side-view of the SMATCH/FTIR sampling device

SMATCH/FTIR kinetics matches $\dot{r}$ from bulk combustion measurements at the same pressure.[28-31] Hence, the heat flow conditions are similar to those of the surface reaction zone during bulk combustion. By inference, other techniques designed for fast, controlled heating of a thin film, such as T-jump/FTIR, [4] that are also specifically designed for chemical studies, give extensive details of the surface reaction zone.

Details of SMATCH/FTIR and spectroscopy are given elsewhere, [27-30] but are briefly summarized here. As shown in Figure 9, SMATCH/FTIR employs a cantilevered quartz tube whose vibrational frequency depends on the sample mass. Typically, 0.2 - 0.8 mg of sample was painted onto a metal tip attached to the tube, giving a uniform film of 16 - 64 μm thickness. If the film thickness is not uniform, then the experiment fails. The metal end-tip was heated by RF induction at a chosen rate in the 100 - 200°C/sec range. The sample atmosphere was 1 atm of Ar. The heating rate and film thickness are matched so that the heat transfer is fast enough to give a reasonably uniform temperature throughout the film.[28] The dynamic weight change of the sample was measured by the change in the vibrational frequency of the tube. Data were recorded at 160 Hz which provides enough points on the weight-loss curve to be confident of fitting the shape by E1. α is the degree of

$$1-\alpha = \sum_{i=0}^{3} a_i t^i \qquad \text{(E1)}$$

conversion and t is time. Typically, E1 was applied for the initial 50% of weight loss. The temperature was measured by a type E thermocouple spot-welded to the metal end-tip and in contact with the sample film. Infrared spectra of the decomposition gases were measured about 3 mm above the metal end-tip by using RSFTIR (10 scan/sec, 4 cm^{-1} resolution).

The reduction of SMATCH/FTIR temperature and weight change data from E1 and its derivative are related to Arrhenius parameters by E2.

$$\frac{d\alpha}{dt} = Ae^{-E/RT}(1-\alpha)^n \qquad \textbf{(E2)}$$

Rearrangement of E2 yields E3, which is a straight line by the appropriate choice of n. n=2 linearizes most SMATCH/FTIR data and has been rationalized elsewhere.[28] Modified versions of the pyrolysis law, E4 and E5, where h is the experimental film

$$\log\left[\frac{d\alpha}{dt}\left(\frac{1}{(1-\alpha)^n}\right)\right] = \log A - \frac{E}{2.3RT} \qquad \textbf{(E3)}$$

thickness, can be used to calculate the regression rate, $\dot{r}$, in mm/sec from the SMATCH/FTIR Arrhenius constants at the pressure and temperature of the experiment.[28-31] T is the average temperature during the initial 50% of the weight loss. E4 and E5 apply provided h approximates the surface reaction zone thickness at 1 atm. A value of h = 20 - 60 μm is reasonable at 1 atm [32].

Table 2
Burn Rate Comparisons

Compound	$\dot{r}$, mm/sec (1 atm)	
	SMATCH	Strand burner
AP	0.11	0.25
HMX	0.37	0.5
RDX	0.38	0.38
DNNC	0.27	0.27
13%N NC	0.3	0.4
GAP	1.35	1.7

$$\dot{r} = hAe^{-E/RT} \qquad \textbf{(E4)}$$

$$\dot{r} = hA^{1/2}e^{-E/2RT} \qquad \textbf{(E5)}$$

Table 2 compares the regression rates of various energetic materials computed by E4 and E5 at 1 atm from SMATCH/FTIR data and the values measured at 1 atm or extrapolated from higher pressure to 1 atm from combustion bomb data. The reasonably good match suggests that the rate and characteristics of heat transfer to the thin film are equal to or scale to those at the surface during combustion.

FTIR Measurements of Flames

Reactive two-phase flows, especially in flames, are usually produced when propellant formulations burn. This is because many solid rocket propellants contain fuels, such as Al or B, that burn to the solid oxide. Inert solids, such as ZrC, are sometimes added to help dampen combustion oscillations. The solid particles appear as smoke. A similar particle-laden flow can exist in hydrocarbon and coal combustion where the combustion gases might be mixed with soot, fly ash and char.

In recent years several techniques have been developed based on FTIR emission/transmission spectroscopy (FTIR E/T) that enable measurements to be made of particle and gas concentrations and temperatures in hot flows.[33-37] Specifically, 1) the temperature and concentration of the particle and soot phases have been measured separately in an ethylene-air diffusion flame, [34] 2) measurements have been made in densely loaded particle streams, [34] and 3) particle sizes have been measured.[35] Although most measurements have been line-of-sight, it has recently been shown that Fourier image reconstruction can be used to obtain absorbance and emittance spectra spacially resolved in about 1 x 1 x 4 mm volume.[37]

The FTIR E/T method offers promise for studying propellant flames in which the number of scattering particles is not unusually large. However, an additional experimental complication to propellant combustion studies is that the surface burns as a regressing front. Therefore, a moving stage is needed to maintain the position of the propellant flame relative to the IR beam. This requirement contrasts with the simpler flow reactor designs that can be used to study premixed gas flames and coal particle-gas flames. Recently, FTIR emission spectra have been recorded on flames of AP and HTPB binder.[38] A moving stage with servo feedback control was used to maintain the position of the propellant in the IR beam. Figure 10 shows the IR emission spectrum of the gas products. CO_2, CO, H_2O, HCl and fragments of HTPB were detected. In addition, NH_3 and $HClO_4$ were also detected, indicating that AP sublimes to some extent under combustion conditions. Recently considerable advancement has been made by Thynell, Kuo and coworkers [39] toward understanding IR spectral emission variables of propellant combustion in a manner that provides species concentration and temperature profiles. Further studies are described in a paper by Huang et al., in this Symposium.

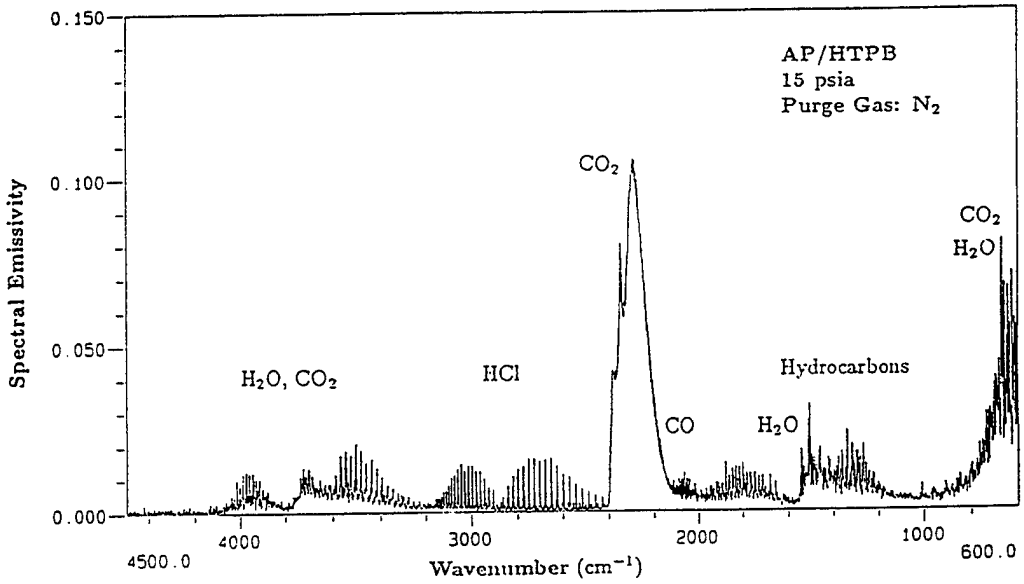

Figure 10. Sixteen coadded emission spectra of the AP-HTPB flame zone assuming T = 1500 K (ref. 38)

Computed tomographic reconstruction has recently been used by McNesby and Fifer [40] to obtain species profiles from FTIR spectra

as a function of height and lateral distribution above a CH_4/N_2O low pressure, premixed, flat-flame burner. Discrimination of cold interferences from the hot gas distribution is made. FTIR spectroscopy has been used to obtain high resolution absorption spectra of the major steady-state species in premixed C_2N_2-NO_2 [41] and HCN-NO_2 [42] burner flames. Reactions involving these gases are believed to be among the more important ones in certain rocket and gun propellant flames produced by nitramines. The high temperature of these flames required modifications to be made to the IR spectrometer. For example, temperature gradients in various parts of the optical bench were caused by the flame and led to channel spectra. Plane windows were, therefore, replaced by wedge windows to reduce this problem. The high infrared emissivity of the flame required the use of a long-pass IR filter and a high intensity globar to obtain quality spectra. With these modifications, detailed studies have been made of the species concentration profiles and temperature as a function of distance above the burner surface. The temperature was extracted from the rotational band intensities of CO in various parts of the flame. When coupled with simulations of the kinetics, it could be concluded that the flame chemistry is dominated by oxygen atoms.[42] The production of oxygen atoms increases the burn rate, while their consumption decreases the burn rate.

ACKNOWLEDGMENTS

The support of the Air Force Office of Scientific Research, Aerospace Sciences, is gratefully acknowledged. Most of this overview is based on research of graduate and post-doctoral students Mark Timken, Peter Brush, Dilip Patil, and Janqkang Chen, whose work is referenced below.

REFERENCES

1. Alexander, M. H., Dagdigian, P. J., Jacox, M. E., Kolb, C. E., Melius, C. F., Rabitz, H., Smooke, M. D. and Tsang, W., 1991. Prog. Energy. Combust. Sci. **17**, 263.

2. Griffiths, P. R. and deHaseth, J. A., 1986. Fourier Transform Infrared Spectroscopy, Wiley-Interscience, New York.

3. Brill, T. B., 1990. In Chemistry and Physics of Energetic Materials. Bulusu, S., Ed. Kluwer Academic Press, Dordrecht, The Netherlands, p. 255.

4. Brill, T. B., Brush, P. J., James, K. J., Shepherd, J. E. and Pfeiffer, K. J., 1992. Appl. Spectrosc., **46**, 900.

5. Brill, T. B., 1992. Prog. Energy Combust. Sci., **18**, 91.

6. Brill, T. B. and Brush, P. J., 1992. Phil. Trans. Royal Soc. (Lond.) A, **339**, 377.

7. Brill, T. B., Brush, P. J., Patil, D. P. and Chen, J. K., July 1992. Proc. 28th Symp. (Int.) Combustion, Sydney, Australia, p. 1907.

8. Cosgrove, J. D. and Owen, A. J., 1974. Combust. Flame, **22**, 13.

9. Kimura, J. and Kubota, N., 1980. Prop. Explos., **5**, 1.

10. Karpowicz, R. J. and Brill, T. B., 1984. Combust. Flame, **56**, 317.

11. Behrens, R., 1990. J. Phys. Chem., **94**, 6706.

12. Palopoli, S. F. and Brill, T. B., 1991. Combust. Flame, **87**, 45.

13. Melius, C. F., 1990. In Chemistry and Physics of Energetic Materials, S. Bulusu, Ed. Kluwer Academic Publ., Dordrecht, The Netherlands, p. 51.

14. Ermolin, N. E., Korobeinichev, O. P., Tereshenko, A. G. and Fomin, V. M., 1992. Comb. Explos. Shock Waves, **18**, 180.

15. Guirao, C. and Williams, F. A., 1971. AIAA J., **9**, 1345.

16. Korobeinichev, O. P. and Tereshenko, A. G., 1978. In Tenth Mat. Res. Symp. Charact. High Temp. Vapors and Gases, NBS publ. 561, Gaithersburg, MD, p. 479.

17. Brill, T. B., Brush, P. J. and Patil, D. G., 1993. Combust. Flame, **94**, 70.

18. Hackman, E. E., Hesser, H. J. and Beachell, H. C., 1972, J. Phys. Chem., **76**, 3545.

19. Brill, T. B., Brush, P. J. and Patil, D. G., 1993. Combustion Flame, **92**, 178.

20. Swett, M., 1992. NWC, personal communication.

21. Whittaker, A. G. and Barham, D. C., 1964. J. Phys. Chem., **68**, 196.

22. Federoff, B. T., 1960, Encyclopedia of Explosives and Related Items, Vol. I, Picatinny Arsenal, Dover, NJ, A3111.

23. Kaiser, R., 1935. Angew. Chem., **48**, 149.

24. Rosser, W. A. and Wise, H., 1956. J. Chem. Phys., **25**, 1078.

25. Bedford, G. and Thomas, J. H., 1972. J. Chem. Soc. Farad. Trans. **I**, 2163.

26. Fetherolf, B. L. and Litzinger, T. A., 1992. Penn State Univ., personal communication.

27. Timken, M. D., Chen, J. K. and Brill, T. B., 1990. Appl. Spectrosc., **44**, 701.

28. Chen, J. K. and Brill, T. B., 1991. Combust. Flame, **85**, 479.

29. Chen, J. K. and Brill, T. B., 1991. Combust. Flame, **87**, 157.

30. Chen, J. K. and Brill, T. B., 1991. Combust. Flame, **87**, 217.

31. Brill, T. B., Patil, D. P., Duterque, J. and Lengelle, G., 1993. Combust. Flame, **95**, 183.

32. Kubota, N. and Sakamoto, S., 1989. Prop. Explos. Pyrotech., **14**, 6.

33. Best, P. E., Carangelo, R. M., Markham, J. R. and Solomon, P. R., 1986. Combust. Flame, **66**, 47.

34. Soloman, P. R., Best, P. E., Carangelo, R. M., Markham, J. R., Chien, P-L., Santoro, R.J. and Semerjian, H.G., 1986. Proc. 21st Symp. (Int.) Combustion, 1763.

35. Solomon, P. R., Carangelo, R. M., Hamblen, D. G. and Best, P. E., 1986. Appl. Spectrosc., **40**, 746.

36. Solomon, P. R., Chien, P-L., Carangelo, R. M., Best, P. E., and Markham, J. R., 1988. Proc. 22st Symp. (Int.) Combustion, 211.

37. Markham, J. R., Zhang, Y. P., Carangelo, R. M. and Solomon, P. R., 1990. Proc. 23rd Symp. (Int.) Combustion, 1869.

38. Klotz, S., Thynell, S. T., Huang, I. T., Kuo, K. K., 1992. J. Propuls. Power, **8**, 537.

39. Huang, I. T., Thynell, S. T. and Kuo, K. K., 1992. Appl. Spectrosc., **46**, 1182.

40. McNesby, K. L. and Fifer, R. A., April 1992. BRL-TR-3333, Ballistic Research Laboratory, Aberdeen Proving Ground, MD.

41. Thorne, L. R. and Smith, O. I., 1988. CPIA Publ. 481, Vol II, 143.

42. Thorne, L. R. and Melius, C. F., 1990. Proc. 23rd Symp. (Int.) Combustion, 397.

COMMENTS

G. Vaghjiani, University of Dayton Research Institute, USA. The ratio of k_1/k_2 for the two decomposition channels in RDX shows that the difference in activation energies is changing with temperature for the T range used. Is this an experimental artifact? If not, what explanation do you have for this observation?

Author's Reply. The fact that the experimental k_1/k_2 decreases at a lower rate at higher temperatures compared to lower temperatures most likely results from the difficulty of achieving rapid heat transfer between the filament and sample at higher temperatures. The highest temperatures shown in Fig. 4, therefore, are probably somewhat higher than actually exist at the sample. If this effect could be confidently accounted for, then the flattening of k_1/k_2 would be less pronounced.

A. Gany, TECHNION - Israel Institute of Technology. (1) Have you tested pure binders or polymers? What decomposition products have you found? (2) Have you tested composite propellants or combinations of binders with the same amount of oxidizer? I wonder what kind of ingredients emerge from the surface?

Author's Reply. (1) Yes. Reference 30 of this article describes our most thorough study to date. In the forthcoming several years, we will report many more binder studies. (2) We have done very little work with oxidizer-binder mixtures, but we may also work more on these in the future.

Thermochimica Acta, 235 (1994) 225–230
Elsevier Science B.V., Amsterdam
SSDI 0040-6031(93)01551-D

The thermal decomposition of energetic materials. Part 64. Kinetics of decomposition of furazano[3,4,*b*]piperazine and its 1,4-dinitro nitramine derivative

D.G. Patil and T.B. Brill *

Department of Chemistry, University of Delaware, Newark, DE 19716 (USA)

(Received 3 May 1993; accepted 28 July 1993)

Abstract

The Arrhenius kinetics of decomposition of the nitramine explosive 1,4-dinitrofurazano[3,4,*b*]piperazine (DNFP) and the less energetic parent amine furazano[3,4,*b*]piperazine (FP) were determined by isothermal TGA and from the rate of change of selected vibrational modes in the IR spectra. For DNFP, $E_a = 136$ kJ and $\log A = 15.5\ \text{min}^{-1}$. The IR spectra show that $N-NO_2$ homoloysis is the dominant initial reaction. For FP, $E_a = 202$ kJ and $\log A = 22.1\ \text{min}^{-1}$. The value of E_a is the same as the N–O bond strength of the furazan ring.

INTRODUCTION

Compounds containing the furazan ring decompose exothermically and have, therefore, potential interest in the explosives and solid rocket-propellant fields. The relatively high density and stored energy of 1,4-dinitrofurazano[3,4,*b*]piperazine (DNFP) make it an attractive energetic molecule [1–4]. A detailed study has been made of the crystal structure, solid–solid

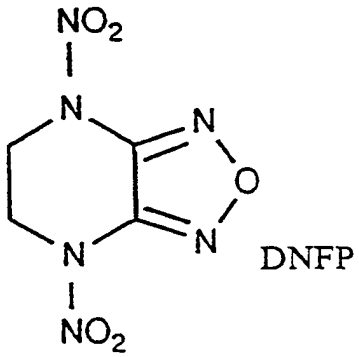

DNFP

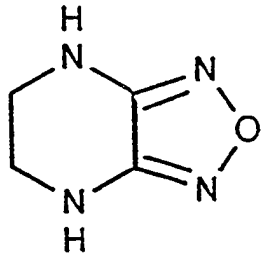

FP

*Corresponding author.

phase transitions and rapid thermal decomposition of DNFP [5]. However, the kinetics of its decomposition are unknown. The gas products suggest that $N-NO_2$ homoloysis dominates in the early decomposition process. However, furazano[3,4,*b*]piperazine (FP) decomposes in a more complicated fashion as evidenced by the gas products [5, 6].

Some researchers believe that the rate of slow, lower temperature thermal decomposition of energetic molecules correlates with the explosive [7–10] and combustion characteristics [11]. However, care must be taken because this connection frequently does not exist [12]. In this paper, we wish to show that the thermal decomposition kinetics of DNFP and FP are different and relate to the structure and composition of the molecules.

EXPERIMENTAL

Samples of DNFP and FP were supplied by Dr. R.L. Willer of the Thiokol Corporation, Elkton, MD. Isothermal thermogravimetric analysis (TGA) was conducted in air on a DuPont Instruments 951 analyzer in the temperature range 388–403 K for DNFP and 428–443 K for FP. The sample size was 2–3 mg and the temperature control was ± 1°C.

The kinetics of decomposition of DNFP from the solid phase was studied in air in the 379–395 K range by transmission IR spectroscopy. DNFP was dissolved in acetonitrile and spread onto an NaCl plate. The solvent was then evaporated to leave the DNFP residue as a thin film. This plate was then placed uncovered in the solid-phase IR cell, described previously [13, 14], so that gases could escape. The temperature was then maintained isothermally by a time-proportioning controller. Thirty-two spectra were summed per file using a Nicolet 60SX FTIR spectrometer operating at 2 cm^{-1} resolution. The rate of decrease in intensity with time of the $-NO_2$ asymmetric and symmetric stretching modes of the nitramine, and the CH_2 asymmetric stretch and bending modes, afforded the rate data.

KINETICS OF DECOMPOSITION

The decompositions of DNFP and FP were determined isothermally by TGA over a range of temperatures where the reaction is relatively slow. The rate of the initial 20–50% weight loss by gas evolution was calculated at each temperature from Figs. 1 and 2, and was fitted by eqn. (1)

$$\log(1-\alpha) = kt + c \tag{1}$$

where $\alpha = (W_0 - W_t)/W_0$, t is time and k is the rate constant at a given temperature. W_0 is the initial sample weight and W_t is the weight at time t. Values of k are tabulated in Table 1. Plots of $\log(1-\alpha)$ versus t (Figs. 3 and 4) are linear, indicating that a global first-order process is representative. The global activation energy E_a and pre-exponential factor A from an

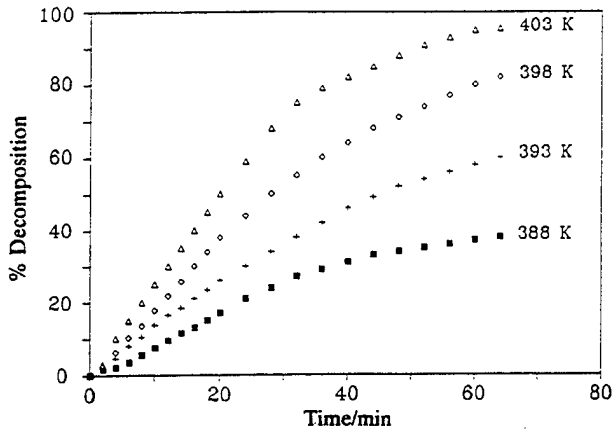

Fig. 1. The time dependence of the weight loss from DNFP determined by TGA.

Arrhenius plot of the rate constant at each temperature are given in Table 1. The accuracy of E_a is estimated to be ± 2 kJ mol^{-1}.

While the activation energy of a condensed-phase thermal decomposition process of a complex molecule is rarely the result of simple bond rupture, further insight into the molecular processes contained in the initial decomposition steps is obtained from transmission IR spectroscopy during the reaction. Because the spectral changes involve a decrease in intensity of modes due to gas-producing reactions, the solid phase IR transmission cell [13, 14] was designed to allow the gases to escape. Detailed IR spectra of DNFP have been analyzed before [5]. The modes assigned to the $-NO_2$ functional groups of DNFP are not pure because of coupling with the N–N bond [15]. The rate of decrease of the area B of these modes, however, qualitatively reflects cleavage of the N–N bond and liberation of NO_2(g). The rate constant k was calculated for the initial 50% of decomposition

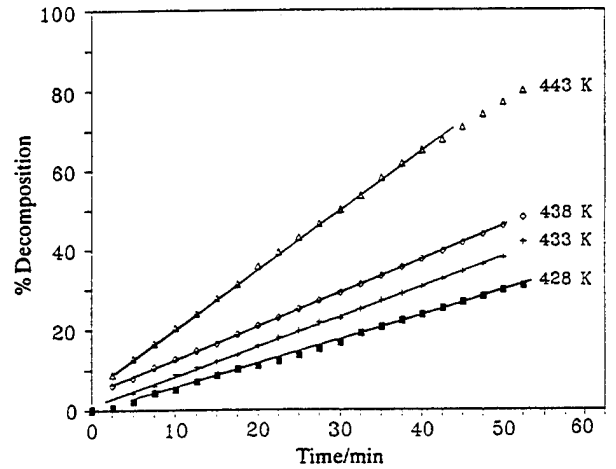

Fig. 2. The time dependence of the weight loss from FP determined by TGA.

TABLE 1

Rate constants and Arrhenius parameters for DNFP and FP

T/K	$k \times 10^3$/min	E_a/(kJ mol^{-1})	log(A/min^{-1})
DNFP			
388	4.0		
393	6.6	136	15.5
398	11.0		
403	18.0		
FP			
428	2.0		
433	3.8	202	22.1
438	4.7		
443	10.5		

from eqn. (1), where $\alpha = (B_0 - B_t)/B_0$. As with the TGA data, a first-order rate expression fits the change of absorbance. Table 2 gives the resulting Arrhenius constants. The kinetics of change of both the symmetric and asymmetric stretching modes of $-NO_2$ are the same within experimental error and closely resemble the Arrhenius values determined from the weight loss. This is good evidence that the rate of N–NO_2 homolysis dominates the rate of thermal decomposition of DNFP in this temperature range. Conversely, the kinetic constants for the decrease in the area of the CH_2 asymmetric stretch are very different from the kinetics of overall weight loss, indicating that C–H homolysis does not dominate the rate of decomposition in this temperature range. The decomposition of the C–H bond is not likely to involve simple homolysis in these compounds, but might rather be a bimolecular, concerted process in the condensed phase.

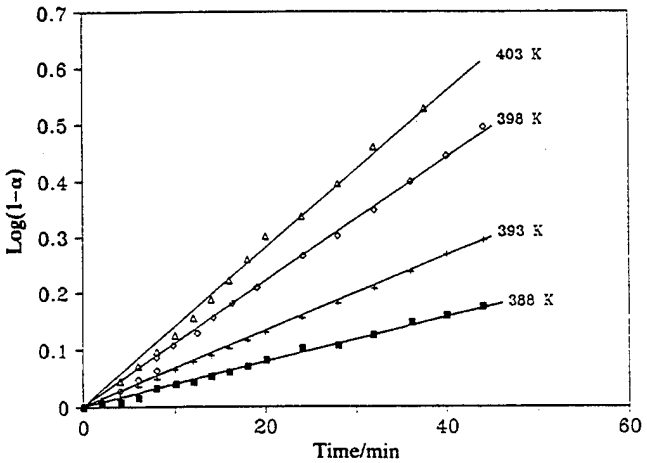

Fig. 3. Rate constant plots for the initial 50% of decomposition of DNFP.

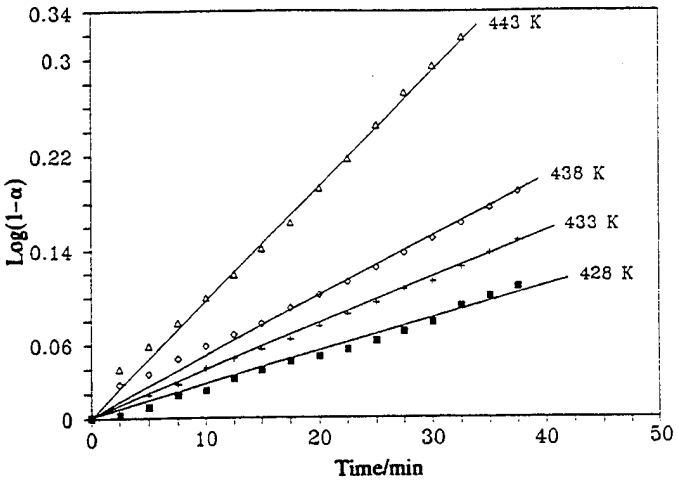

Fig. 4. Rate constant plots for the initial 50% of decomposition of FP.

The global activation energy for decomposition of DNFP is somewhat lower than the N–NO_2 bond dissociation energy of a secondary nitramine (190–210 kJ) [16]. However, the molecular structure of DNFP reveals that the C_2NNO_2 linkage is not a typical secondary nitramine [5]. The C–N bond distance to the carbon atom of the furazan ring is rather short, indicating multiple bond character, while the C–N bond distance to the ethylene carbon atom is typical of a C–N single bond. Hence, there is *nitrimine* character in the nitramine unit. Nitrimines have a bond dissociation energy of approximately 155 kJ mol^{-1} [16]. This ground-state distribution of electron density in DNFP is also reflected in an anomalously long N–N bond and a tendency to release a large amount of NO_2 upon fast thermolysis [5, 17, 18].

Furazanopiperazine is the parent amine of DNFP and lacks the $-NO_2$ groups. The kinetic constants for the initial 50% of decomposition of FP are given in Table 1. While the activation energy resembles the values obtained for the CH_2 unit of DNFP, we regard this similarity as coincidental. A more probable reason for the activation energy value of FP is the decomposition

TABLE 2

Arrhenius parameters for decrease in absorbance of characteristic vibrational modes as determined isothermally by IR spectroscopy

Wavenumber	Mode	E_a/kJ mol^{-1}	$\log(A/min^{-1})$
1597	$\nu_{as}(NO_2)$	140	15.5
1315	$\nu_s(NO_2)$	136	15.7
1267	$\nu_s(NO_2)$	138	15.6
3028	$\nu_{as}(CH_2)$	200	22.5
867	$\delta(CH_2)$	199	22.5

of the furazan ring at the weakest bonds. In particular, the N–O single-bond energy is 200 kJ [19]. This value closely resembles the activation energy of thermal decomposition of FP. Vibrational spectroscopy is not especially helpful in substantiating the dominance of cleavage of an N–O bond in the initial decomposition stage of FP because no pure vibrational motion dominates the furazan ring [20]. Extensive coupling exists, so that almost all of the modes will change simultaneously and in a complex manner upon thermal decomposition.

REFERENCES

1 D.A. Cichra, J.R. Holden and C. Dickenson, NSWC Report TR79-273, Naval Surface Weapons Center, Silver Spring, MD, 1980.
2 L.R. Rothstein and R. Peterson, Propellants and Explos., 4 (1979) 56.
3 L.R. Rothstein, Propellants and Explos., 6 (1981) 91.
4 R.L. Willer and D.W. Moore, J. Org. Chem., 50 (1985) 5123.
5 Y. Oyumi, A.L. Rheingold and T.B. Brill, J. Phys. Chem., 90 (1986) 4686.
6 C.E. Stoner, Jr., A.L. Rheingold and T.B. Brill, Inorg. Chem., 30 (1991) 360.
7 S. Zeman, Thermochim. Acta, 31 (1979) 269.
8 S. Zeman, Thermochim. Acta, 41 (1980) 199.
9 S. Zeman, Thermochim. Acta, 49 (1981) 219.
10 S. Zeman, M. Dimun and S. Truchlik, Thermochim. Acta, 78 (1984) 181.
11 G. Lengellé, J. Duterque, J. Godon and J. Trubert, J. Propuls. Power, in press.
12 B.N. Kondrikov, V.M. Raikova and B.S. Samsonov, Fiz. Goreniya Vzryva, 9 (1973) 84.
13 R.J. Karpowicz and T.B. Brill, Appl. Spectrosc., 37 (1983) 79.
14 D.G. Patil and T.B. Brill, Combust. Flame, 87 (1991) 145.
15 C. Trinquecoste, M. Rey-Lafon and M.T. Forel, J. Chim. Phys., 72 (1975) 689.
16 C.F. Melius, in S. Bulusu (Ed.), Chemistry and Physics of Energetic Materials, Kluwer Academic Publishers, Dordrecht, The Netherlands, 1990, p. 21.
17 T.B. Brill and Y. Oyumi, J. Phys. Chem., 90 (1986) 2679.
18 Y. Oyumi, A.L. Rheingold and T.B. Brill, Prop. Explos. Pyrotech., 12 (1987) 1.
19 J.E. Huheey, Inorganic Chemistry, 3rd edn., Prentice Hall, New York, 1983.
20 Y. Oyumi and T.B. Brill, Combust. Flame, 65 (1986) 313.

Thermal Decomposition of Energetic Materials 65. Conversion of Insensitive Explosives (NTO, ANTA) and Related Compounds to Polymeric Melon-Like Cyclic Azine Burn-Rate Suppressants

G. K. WILLIAMS, S. F. PALOPOLI, and T. B. BRILL*
Department of Chemistry, University of Delaware, Newark, DE 19716

Selected triazole, tetrazole, triazine, tetrazine, furazan, and acyclic backbone compounds are shown by IR spectroscopy to convert to polymeric, melon-like, cyclic azine residues upon heating to $T \geq 500°C$. These compounds include the insensitive explosives 3-nitro-1,2,4-triazol-5-one (NTO), 3-amino-5-nitro-1,2,4-triazole (ANTA), and nitroguanidine. The melon-like residue could suppress the burn rate if these compounds are formulated into solid rocket propellants. The IR-active gaseous products from thermolysis are determined as a function of pressure and are related to the atom connectivity in the parent molecules.

INTRODUCTION

During thermal decomposition of explosives and propellants, exothermic release of gaseous products ensues. However, several insensitive energetic and related nonenergetic materials not only liberate gaseous products, but produce definable polymers that are thermally quite stable [1–4]. These polymer-forming compounds potentially have a special place in the propulsion field as additives to solid propellants to suppress the burn rate, enhance combustion stability, decrease the temperature sensitivity, and induce plateau burning.

Diaminofurazan (DAF) and diaminoglyoxime (DAG) are examples of such compounds. They suppress the burning rate and enhance plateau burning of AP/HTPB/Al composite propellants in the 1700–2100 psi range [5]. The specific impulse remains unchanged. DAF and DAG have been proposed to function as burn rate suppressants by transiently forming thermally stable cyclic azine polymers resembling poly[(8-amino-1,3,4,6,7,9,9b-heptaazaphenylene-2,5-diyl)imino], which is commonly called melon, in the superficial reaction layer of the burning surface [3]. Figure 1 shows the reaction stages employing limiting formulas. This idealized reaction scheme has been presented in various ways for cyanamide and dicyandiamide [6–15], and explains why dicyandiamide is also a burn rate suppressant [16]. Melon is thermally stable up to at least 700°C [11, 14]. Therefore, a melon-like residue can accumulate transiently on the burning surface, and retard the mass transfer from the condensed phase to the gas phase and affect the heat transfer from the gas phase to the condensed phase.

In this article, many additional compounds are shown to transform to melon-like cyclic azine polymers, while also liberating low-molecular-weight gaseous products. This implies that the transformation in Fig. 1 is relatively facile provided that a few connectivity requirements are met in the parent molecule. The current results highlight a systematic approach to discovering new potential burn-rate suppressants for solid rocket propellants and possible flame retardants.

EXPERIMENTAL

The compounds of interest in this study are solids at room temperature and are shown in Fig. 2. All triazoles, melamine (MEL), ammeline (AMN), ammelide (AMD), nitroguanidine (NQ), and 5-ATZ were purchased from Aldrich Chemical Co. Sources of other samples were

*Author to whom correspondence should be addressed.

0010-2180/94/$7.00

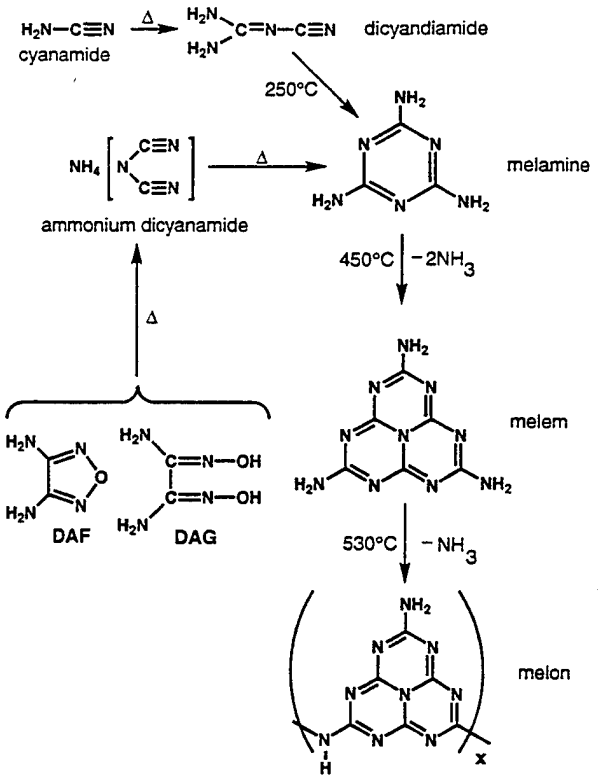

Fig. 1. Limiting formulas in the conversion of selected compounds to highly thermally stable melon-like cyclic azine polymers.

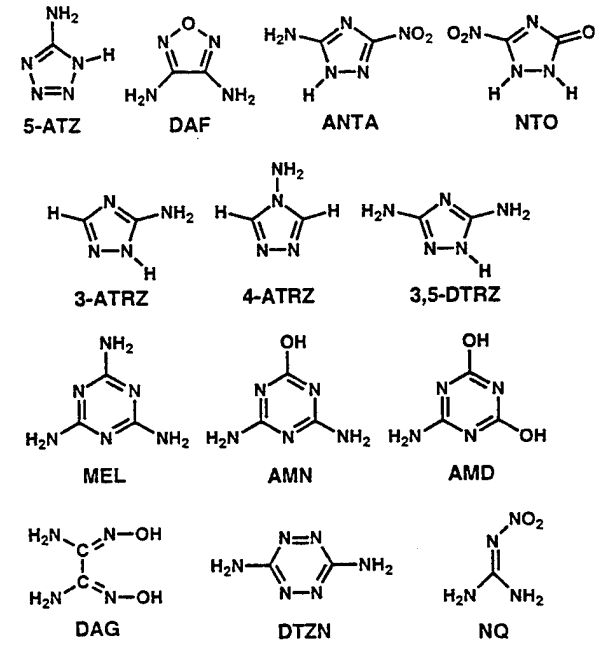

Fig. 2. Compounds found to thermolyze to melon-like cyclic azine polymers when heated above 400°C.

the following: Michael Coburn, Los Alamos National Laboratory (NTO), Phillip Pagoria, Lawrence Livermore National Laboratory (ANTA), Rodney Willer, Thiokol Corp. Elkton, MD (DAF and DAG), and Robert Schmitt, SRI International (DTZN).

Gaseous products of decomposition were determined in a cell described elsewhere [17, 18]. Approximately 1 mg of sample was heated at 150°–300°C s^{-1} on a nichrome ribbon filament to 450°C under a pressure of 1–55 atm Ar. Elevated Ar pressure was usually necessary to reduce volatilization of the parent compound. IR spectra of the gaseous products that appear about 3 mm above the surface were recorded in near real-time by using a Nicolet 60SX FTIR spectrometer set to record ten scans per second at 4 cm^{-1} resolution. When two or more IR active gaseous products were detected, their relative concentrations were determined by using the scaling factor of a characteristic absorbance that is based on the absolute absorbance [19] of each product. The scaling factor of the 2240 cm^{-1} absorbance of HNCO, for which absolute intensity measurements have not been made, was assumed to be 1.5. This value is about midway between the factors for the same mode of N_2O and CO_2, and is reasonable because of the similar structure and bonding in the heavy atom portion of the isoelectronic series HNCO, CO_2, and N_2O.

IR spectra (32 coadded scans) of the solid residues that form upon heating the compounds in Fig. 2 were recorded as pressed KBr pellets at 2 cm^{-1} resolution. The IR spectral study of a film of NTO supported between two NaCl plates was conducted with a cell that is discussed elsewhere [20].

DSC and TGA (DuPont Instruments 910 and 951, respectively) were employed for controlled programmed heating of samples in an Ar atmosphere.

FORMATION OF MELON-LIKE POLYMERS

A yellow-brown residue remained on the nichrome filament after heating each of the compounds in Fig. 2 at 150°–300°C s^{-1}. The mass of the residue was usually less than 20% of the original sample mass. However, as re-

vealed by Fig. 3, a similar residue is obtained from heating the sample much more slowly by TGA or DSC. Therefore, Fig. 4 shows the infrared spectra of the residues formed by programed heating of 1–2 mg of sample at 10°C m^{-1} in a crimped aluminum DSC pan to 600°–650°C. The structures of the polymers obtained at the lower heating rates are, not surprisingly, better organized than those formed during very rapid heating, which results in better quality IR spectra.

All of the residues in Fig. 4 resemble that of melamine (MEL), or, as indicated by Fig. 5, the residues from ammeline (AMN) and ammelide (AMD). The 650–1900 cm^{-1} frequency range shown involves mostly coupled ring absorptions. The pendant groups on the azine rings can be purely $-NH_2$, $=NH$, $-OH$, or $C=O$ groups or random combinations of these groups. Figure 6 shows the infrared absorptions in the hydrogen-to-heavy-atom stretching region arranged for convenience of display. Generally, $-NH_2$ and $-OH$ stretching modes lie in the 3100–3600 cm^{-1} range. Hydrogen-bonding influences the intensity, width, and

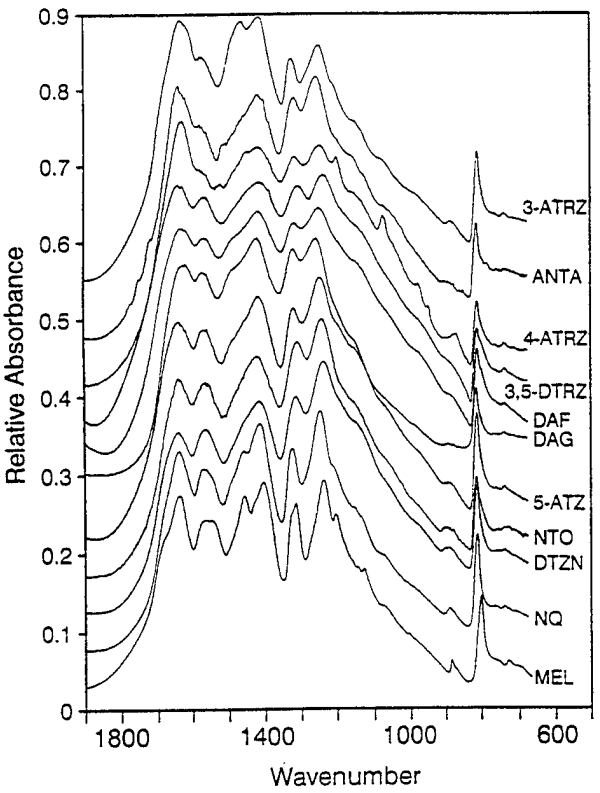

Fig. 4. IR spectra of the coupled ring mode region of the residues obtained by heating compounds in Fig. 2 by DSC to 600–650°C. KBr pellets were employed.

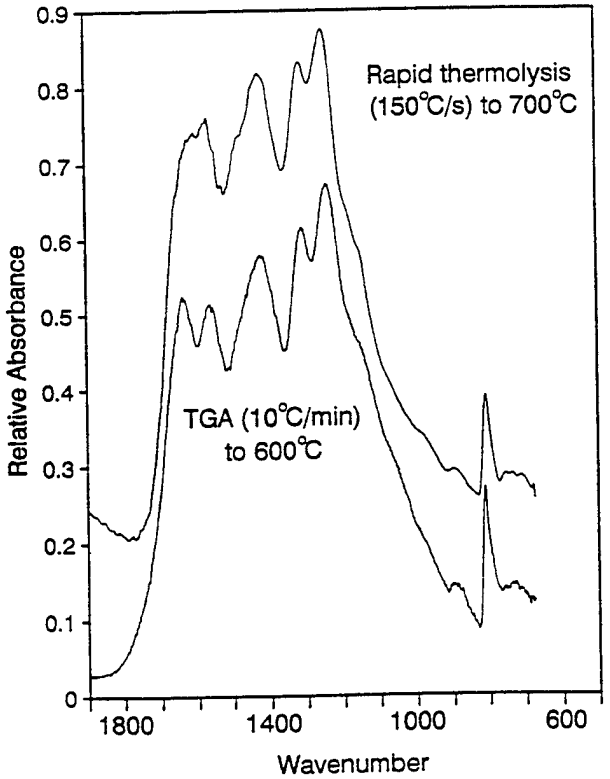

Fig. 3. The mid-IR spectrum of the residue from NTO formed at 10°C m^{-1} and 150°C s^{-1}.

frequency of these absorbances. According to Fig. 6, a variety of pendant groups are probably present.

With regard to the propensity of the residues in Fig. 4 to modify combustion, we are aware that only DAG, DAF, and NQ have been tested. All suppress the burn rate of solid rocket propellants. The fact that each compound in Fig. 2 forms a melon-like thermolysis product upon fast thermolysis suggests that the remaining compounds are *potential* burn rate suppressants. Not included in Fig. 2 are ureas [21, 22] and guanidines [23], some of which are known to form melamine, melem, and melon upon heating. Because the pyrolysis process at the surface of a burning propellant is very complex, none of these compounds are guaranteed to suppress the burn rate of a solid propellant. Confirmation under actual combustion conditions is necessary. Several of the compounds in Fig. 2 are insensitive explosives (NTO, ANTA, and NQ) and may produce sufficient energy upon decomposition in the surface reaction zone to interfere with the

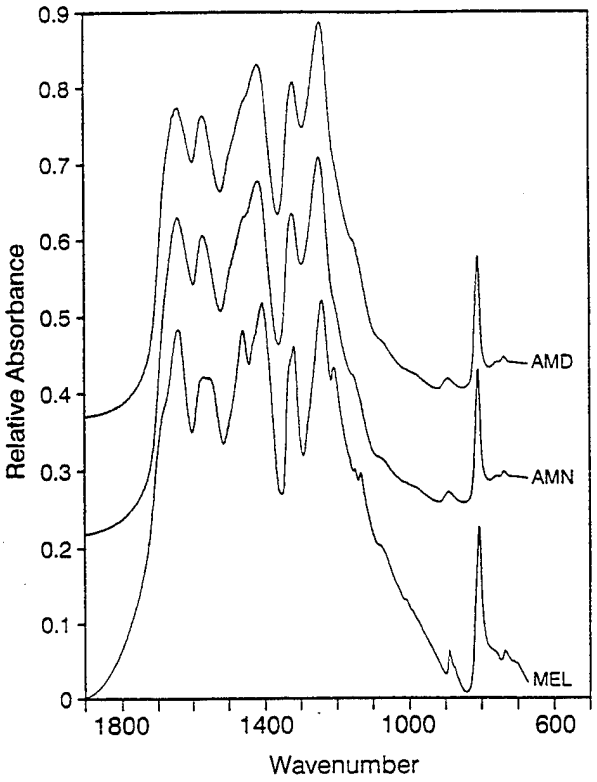

Fig. 5. The IR spectra of residues in KBr pellets from melamine, ammeline, and ammelide treated equivalently to those in Fig. 4.

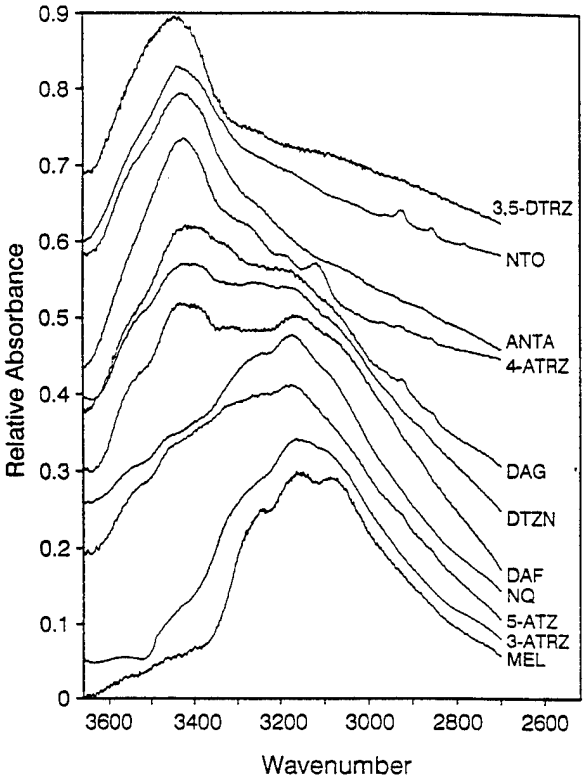

Fig. 6. The H-to-heavy atom stretching region of the pyrolytic residues from compounds in Fig. 2 showing the probability that a variety of pendant groups ($-NH_2$, OH, etc.) occur in the cyclic azine polymers.

proposed alteration in heat and mass transport resulting from the formation of azine-like residues.

The conversion of the compounds in Fig. 2 to the melon-like residue by the sequence shown in Fig. 1 cannot occur by the same pathway in all of the compounds.In fact, only 3-ATRZ and possibly 3,5-DTRZ appear to form melem on the way to melon according to the IR spectrum (*vide infra*). For the remaining compounds, spectral features of melem are absent even though a melon-like polymer eventually forms. Most of the compounds in Fig. 2 contain the "cyanamide-like" H_2N-C-N linkage, but this linkage is not required to form the melon-like residue, as 4-ATRZ and NTO prove. On the other hand, the H_nH-C-N ($n = 1, 2$) connectivity is present in all of the compounds. Given that $-NH_2$ can be replaced by $-OH$ or other groups in the melon-like polymers, the connectivity of overriding importance may simply be the carbodiimide-like $-N=C(R)-N=$ linkage in the parent molecule.

DECOMPOSITION CHARACTERISTICS OF INDIVIDUAL COMPOUNDS

The rapid thermal decomposition characteristics of 5-ATZ [4], DAG [3], DAF [3], and NQ [24] are given elsewhere. MEL, AMN, and AMD follow the scheme in Fig. 1. The remaining compounds in Fig. 2 are described further here. Even though few gaseous products form from most of the compounds and those observed are generally thermodynamically stable, they frequently are understandable from the atomic connectivity in the parent molecule [4]. N_2 is undoubtedly formed, but is not IR active.

NTO

3-Nitro-1,2,4-triazol-5-one (NTO) is a high-performance, relatively insensitive explosive [25, 26] whose properties have been described [27, 28]. Despite its relatively recent identity as an explosive, contradictory data about its decomposition products and kinetics have already

appeared. A primary kinetic deuterium isotope effect was detected [29], suggesting that the N–H bond cleaves in the rate determining step of thermal decomposition. Species involving H-atom transfer were identified in photochemical and thermochemical decomposition of NTO in acetone and TNT solutions [29]. On the other hand, C–NO_2 bond homolysis leading to NO_2 (or HONO) has been proposed to be the initial degradation reaction by laser-induced MS and EI-MS, although very little NO_2(g) was detected [30]. The very small quantity of NO_2(g) was rationalized to be the result of absorption of NO_2 on the chemically deactivated fused silica column used to separate the mass spectrometer from the sample chamber. NO_2, CO_2, and N_2O were reported to be prominent when NTO is heated at 10°C m^{-1} in an IR cell [31]. In another study employing similar conditions, H_2O, NO, CO_2, CO, and N_2O were found, but NO_2 was not [32]. However, NO_2 was detected after 1 h. The decomposition of NTO that has been exposed to x-ray and UV radiation and examined by x-ray photoelectron spectroscopy (XPS) is consistent with the loss of NO_2, reduction of $-NO_2$ to $-NO$, and loss of NO [33].

In summary, three studies propose that C–NO_2 homolysis is a major reaction [30, 31, 33], but a large amount of NO_2 was reported in only one of these studies [31]. A fourth study reports that NO_2(g) forms as a secondary product from oxidation of NO [32]. The oxidant was not identified. Cleavage of the NH bond is proposed to be the rate-determining step [29].

In this article we have determined the pressure dependence of the relative concentrations of the initially detected, IR-active gaseous products from NTO heated at 300°C s^{-1} to 450°C in Ar. This result does not answer detailed questions about the decomposition mechanism, but does show that NO_2(g) or HONO(g) do not form initially in quantities detectable by IR spectroscopy. Figure 7 summarizes the results. NO dominates below 1 atm. At higher pressure, the gaseous products are forced to remain longer in contact with the residue and the hot zone [34]. This environment enhances secondary reactions and results in formation of the more stable products (e.g., CO_2) and degradation of the more reactive

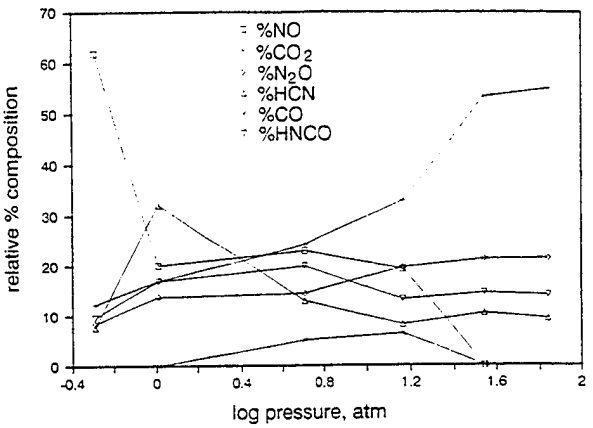

Fig. 7. The relative concentrations of the initially detected IR active gaseous products (excluding H_2O) from pyrolysis of NTO at 300°C s^{-1} to 450°C. The static pressures of Ar in the cell are shown.

products (e.g., NO). Absorbances indicative of a small amount of NO_2(g) appeared after several minutes in accordance with the observation of Rothgery et al. [32]. It would appear that C–NO_2 homolysis to produce NO_2(g) is not a primary thermolysis reaction of NTO under the conditions employed.

Generation of a solid residue during thermal decomposition of NTO in the 220°–350°C range has been noted [29, 32, 33]. By XPS this residue was suggested to be 1,2,4-triazol-3-one (TO) [33], where the $-NO_2$ group of NTO is replace by H. However, the IR spectrum of the residue is reported *not* to be that of TO [32], even though the elemental composition is correct for TO ($C_2H_3N_3O$). In the present study, IR spectra were recorded of a film of neat polycrystalline NTO that was thinly spread between NaCl plates. The plates were heated at 5°C m^{-1} from 25°–320°C. At about 220°C, the spectra began a gradual, but marked, change. The residue at 320°C is insoluble in organic solvents. The absorbances do not match those shown in Figs. 4 and 6 and is not readily identifiable. However, further heating of the film produces the spectral characteristics of melon shown in Fig. 4. More detailed analyses of the kinetics [35] and mechanism [36] of decomposition of NTO are underway.

ANTA

The gaseous products from rapid thermal decomposition of 3-amino-5-nitro-1,2,4-triazole

(ANTA) [37] were determined by rapidly pyrolyzing 1 mg under different pressures of Ar. Figure 8 summarizes the results. Sublimation of ANTA occurs at all pressures. However, the gaseous products and the insensitivity to pressure in the lower pressure range indicate that extensive degradation also occurs in the condensed phase. The formation of NH_3 at high pressure is attributable to the deamination polymerization in Fig. 1. By DSC and TGA, two or possibly three overlapping stages of decomposition occur between 210°C and 240°C. The residue that remains at 600°C is melon-like as indicated by the IR spectra in Figs. 4 and 6.

3-ATRZ

3-Amino-1-hydrogen-1,2,4-triazole is not energetic, but forms the melon-like residue upon slow and fast thermolysis. To reduce sublimation 3-ATRZ was heated at 300°C s^{-1} to 450°C under 45 atm of Ar. A yellowish solid residue and a 9 : 1 NH_3/HCN gaseous product ratio resulted. A small amount of NH_2CN is also detected. Undoubtedly some N_2 also forms but is not detected by IR spectroscopy. The yellowish residue produces the IR spectra shown in Fig. 9, which closely resembles that of melem. Further heating of this melem-like residue in Fig. 9 to 600°C converts it to the melon-like residue shown in Fig. 4. The excess of NH_3 over HCN in the product gases can be attributed to the selective release of NH_3 in the polymerization process (Fig. 1).

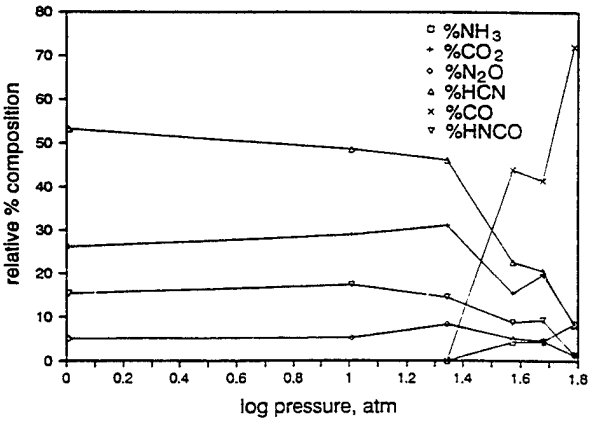

Fig. 8. The relative concentrations of the initially detected IR active gaseous products (excluding H_2O) from pyrolysis of ANTA at 300°C s^{-1} to 450°C. The static pressures of Ar in the cell are shown in each case.

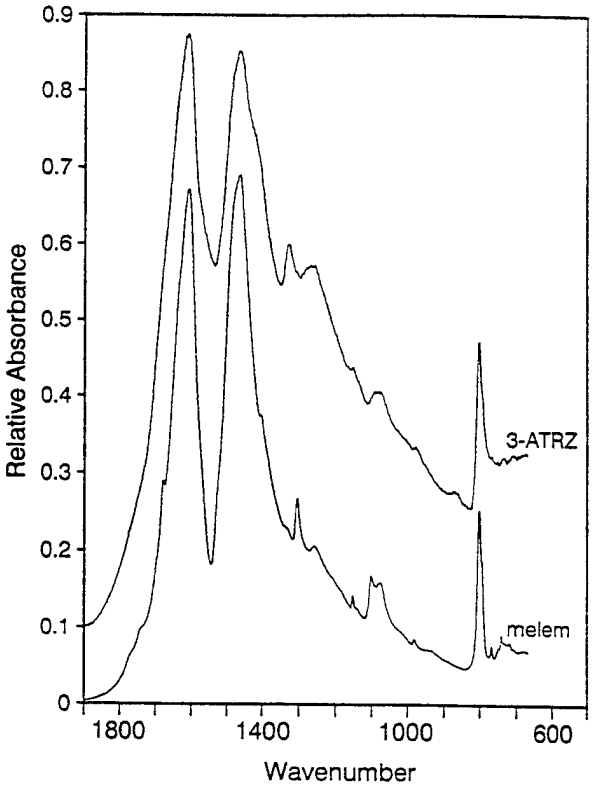

Fig. 9. The IR spectrum of KBr pellets of melem and the residue of 3-ATRZ from heating 3-ATRZ to 450°C.

4-ATRZ

Heating of 4-ATRZ at 300°C s^{-1} under 33 atm of Ar produces NH_3 and HCN in a 1 : 1 ratio along with NH_2CN. The smaller NH_3/HCN concentration ratio compared to 3-ATRZ is attributable to the fact that 4-ATRZ is structurally suited to eliminate HCN upon degradation of the ring. NH_2CN forms even though no NH_2–C–N linkage exists in 4-ATRZ, which indicates that rearrangements involving the position of the $-NH_2$ group might occur during thermal decomposition of the condensed phase. A melon-like residue forms at high temperature (Fig. 4).

3,5-DTRZ

Upon heating of 3,5-DTRZ at 300°C s^{-1} to 450°C under 33 atm Ar, NH_3 and HCN are liberated in an 8.5 : 1.5 ratio along with NH_2CN. The conversion of 3,5-DTRZ to the melon-like residue possibly occurs through a melem-like product in a sequence discernable by IR spectroscopy of the residue (Fig. 10). A

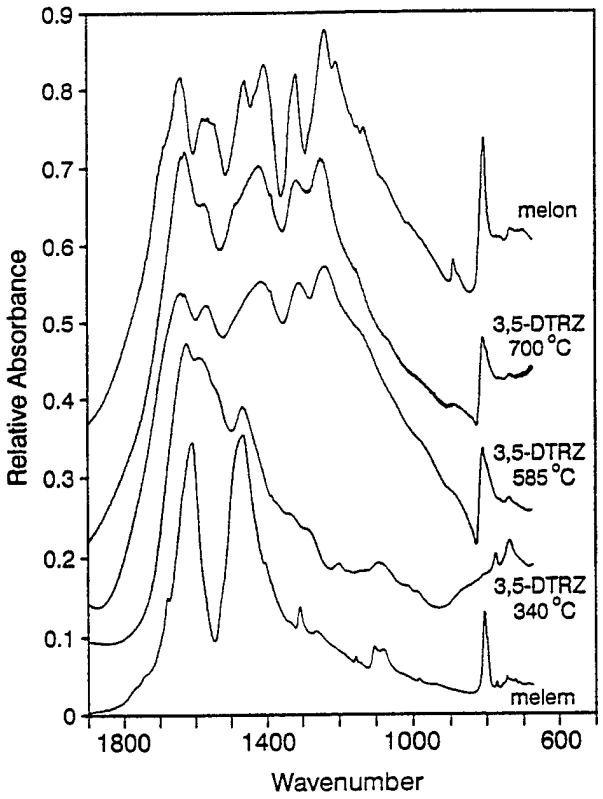

Fig. 10. The IR spectrum of KBr pellets of melem, melon, and the residue from heating 3,5-DTRZ to three different temperatures. 3,5-DTRZ appears to convert to a melon-like product through a melem-like intermediate.

mixture of mostly melem-like residue with some melon-like residue is present at 340°C, where approximately 60% of the sample mass has volatilized. By 585°C the residue is mostly melon-like, but the pendant groups (Fig. 6) are different. NH_3(g) is generated as melon forms.

DTZN

3,6-Diaminotetrazine liberates no IR active gaseous products upon heating at 300°C s^{-1} to 450°C under 33 atm Ar. Instead, sublimation of DTZN occurs and a yellow-brown residue of melon-like polymer remains on the filament. The two cyanamide-like connectivities of DTZN are well-suited for polymerization according to Fig. 1. However, IR inactive N_2 must also be liberated during this process.

We are grateful to the Thiokol Corporation and the Air Force Office of Scientific Research, Aerospace Sciences for financial support of this work. We thank Michael Coburn, Phillip Pagoria, Robert Schmitt, and Rodney Willer for compounds used for these studies; and E. M. Kurian for allowing citation of work in advance of publication.

REFERENCES

1. Davis, T. L., and Abrams, A. J. J., *Proc. Am. Acad. Arts Sci.* 61:437–457 (1926).
2. Volk, F., *Prop. Explos. Pyrotech.* 10:139–146 (1985).
3. Stoner, C. E., Jr., and Brill, T. B., *Combust. Flame* 83:302–308 (1991).
4. Gao, A., Oyumi, Y., and Brill, T. B., *Combust. Flame* 83:345–352 (1991).
5. Willer, R. L., Chi, M. S., Gleeson, B., and Hill, J. C., Thiokol Corp. U.S. Patent 5071495, 1991.
6. Finkel'shtein, A. I., *Opt. Spectrosc.* 6:17–19 (1959).
7. May, H., *J. Appl. Chem.* 9:340–344 (1959).
8. Finkel'shtein, A. I., *J. Gen. Chem.* 31:1046–1048 (1961).
9. Khorosheva, V. V., and Finkel'shtein, A. I., *Russ. J. Phys. Chem.* 36:554–556 (1962).
10. Finkel'shtein, A. I., and Spiridonova, N. V., *Russ. Chem. Rev.* 33:400–405 (1964).
11. Finkel'shtein, A. I., and Spiridonova, N. V., *J. Org. Chem. USSR* 1:602–605 (1965).
12. Simkina, L. A., Finkel'shtein, A. I., and Gal'perin, V. A., *Zavod. Lab.* 39:287–290 (1973).
13. van der Plaats, G., Soons, H., and Snellings, R., in *Proceedings of the Second European Symposium on Thermodynamic Analysis* (D. Dollimore, Ed.), Heyden, London, 1981, pp. 215–218.
14. Costa, L., and Camino, G., *Journ. Calorim. Anal. Therm. Thermodyn. Chim.* 17:213–216 (1986).
15. Costa, L., and Camino, G., *J. Therm. Anal.* 34:423–429 (1988).
16. Roberts, J. A., and Mangum, M. G., Air Force Rocket Propulsion Laboratory, AFRPL-TR-84-038, Sept. 1984.
17. Oyumi, Y., and Brill, T. B., *Combust. Flame* 62:213–224 (1985).
18. Cronin, J. T., and Brill, T. B., *Appl. Spectrosc.* 41:1147–1151 (1987).
19. Brill, T. B., *Prog. Energy Combust. Sci.* 18:91–116 (1992).
20. Karpowicz, R. J., and Brill, T. B., *Appl. Spectrosc.* 37:79–81 (1983).
21. Schmidt, A., *Monatsh. Chem.* 99:664–671 (1968).
22. Medikhanov, D. G., Korobochkin, V. P., and Shehep-tkin, A. A., *VINITI* 356–82 (1982). CA 98:160056z.
23. Smolka, A., and Friedick, A., *Monatsh. Chem.* 10:86 (1889).
24. Oyumi, Y., Rheingold, A. L., and Brill, T. B., *Prop. Explos. Pyrotech.* 12:46–52 (1987).
25. Becuwe, A., FR. Patent 2584066A1, June 28, 1985.

26. Lee, K. Y., Chapman, L. B., and Coburn, M. D., *J. Energet. Mat.* 2:27–33 (1987).
27. Chapman, L. B., *Ninth Symp. (Int.) Detonation*, Portland, OR, 1989, pp. 1001–1007.
28. Becuwe, A., and Delclos, A., *Ninth Symp. (Int.) Detonation*, Portland, OR, 1989, pp. 1008–1013.
29. Menapace, J. A., Marlin, J. E., Bruss, D. R., and Dascher, R. V., *J. Phys. Chem.* 95:5509–5517 (1991).
30. Östmark, H., Bergman, H., Åqvist, G., Langlet, A., and Persson, B., *Sixteenth International Pyrotechnics Seminar*, Jönköping, Sweden, June 24–28, 1991, pp. 874–886.
31. Prabhakaran, K. V., Naidu, S. R., and Kurian, E. M., *Thermochim. Acta* (in press).
32. Rothgery, E. F., Audette, D. E., Wedlich, R. C., Csejka, D. A., *Thermochim. Acta* 185:235–243 (1991).
33. Beard, B. C., and Sharma, J., *J. Energet. Mat.* 7:181–196 (1989).
34. Oyumi, Y., and Brill, T. B., *Combust. Flame* 68:209–216 (1987).
35. Brill, T. B., Gongwer, P. E., and Williams, G. K. (submitted).
36. Williams, G. K., and Brill, T. B. (in press).
37. Lee, K. Y., and Storm, C. B., LA-11907-MS, Los Alamos National Laboratory, October, 1990.

Received 27 September 1993; revised 19 January 1994

Reprinted from The Journal of Physical Chemistry, 1994, 98.

Thermal Decomposition of Energetic Materials. 66. Kinetic Compensation Effects in HMX, RDX, and NTO

T. B. Brill,* P. E. Gongwer, and G. K. Williams

Department of Chemistry, University of Delaware, Newark, Delaware 19716

Received: January 27, 1994; In Final Form: August 21, 1994®

Widely different Arrhenius parameters have been published for thermal decomposition of HMX (octahydro-1,3,5,7-tetranitro-1,3,5,7-tetrazocine), RDX (1,3,5-trinitrohexahydro-*s*-triazine), and NTO (3-nitro-1,2,4-triazol-5-one). Evaluation of these data reveals that an approximately linear relationship exists between ln A and E_a for each compound irrespective of the phase. This kinetic compensation effect accounts for and unifies most of the differences in the reported rates. The range of data is qualitatively attributable to differences in the sample characteristics and experimental conditions. All E_a−ln A sets lying on or close to the compensation regression line consistently account for the rate of thermal decomposition under the conditions reported. E_a−ln A sets not lying on or near the compensation regression line represent a different process or are incorrect. The kinetic compensation effect provides a rational method to select Arrhenius parameters to describe the global thermal decomposition rate of an explosive.

Introduction

Global Arrhenius parameters for thermal decomposition of nitramines in the condensed and gas phase have been used in models of propellant combustion[1,2] and thermal explosion.[3] The reliance that is placed on these global kinetic measurements emphasizes the importance of knowing their origin and validity. To tackle this problem, we chose three energetic materials for which extensive rate data are available. These are octahydro-1,3,5,7-tetranitro-1,3,5,7-tetrazocine (HMX), 1,3,5-trinitrohexahydro-*s*-triazine (RDX), and 3-nitro-1,2,4-triazol-5-one (NTO).

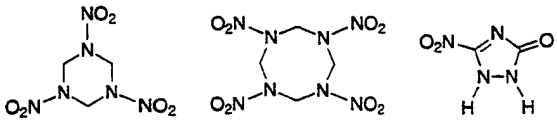

Discussion and evaluation of selected rate data and the resulting Arrhenius parameters for HMX and RDX have been given by Schroeder,[4] Dubovitskii and Korsunskii,[5] and Boggs.[6] Wide discrepancies have been noted, but with comparatively little explanation. No previous analysis of the NTO data has appeared.

From the compilation of the decomposition rate data for HMX, RDX, and NTO, a kinetic compensation effect is apparent, which has not been discussed previously. The kinetic compensation effect refers to the fact that under a variety of conditions an approximately linear relationship exists between the preexponential factor, ln A, and the apparent activation energy, E_a, that are determined for a process from the Arrhenius equation (1).[7,8]

$$\ln k = \ln A - E_a/RT \tag{1}$$

Ln A and E_a for a solid or melt-phase process do not necessarily have the same meaning as ln A and E_a from homogeneous kinetics.[9] They should be viewed primarily as variational parameters of the overall process as opposed to a specific reaction. When ln A and E_a are linearly related, the compensation parameters a and b are defined by eq 2 for all measurements.[7,8,10]

$$\ln A = aE_a + b \tag{2}$$

The compensation effect was first described in the kinetics of dehydration of C_2H_5OH on Cu catalysts[7] and was subsequently observed in many other heterogeneous catalytic[8,10] and solid phase reactions, such as thermal decomposition of $CaCO_3$[11,12] and $MgCO_3$.[13] In effect, an increase in E_a does not cause the expected decrease in the reaction rate because A increases to compensate for E_a. For homogeneous reactions and processes in solution at similar temperatures, the compensation effect is also frequently observed.[14] It is manifested by the constancy of ΔG^* as defined by eq 3 from absolute rate theory and contributes to the existence of linear free energy relationships. Equations 2 and 3 are closely related.[12] As E_a increases, an offsetting increase in ΔS^* occurs.

$$\Delta G^* = E_a - T\Delta S^* \tag{3}$$

The kinetic compensation effect for thermal decomposition of HMX and RDX spans the gas, melt, and solid phases. NTO has primarily been investigated in the solid phase. Recognizing the existence of the compensation effect helps reconcile the large discrepancies among the reported Arrhenius parameters for these compounds. Although the physical and chemical meanings of Arrhenius parameters for heterogeneous processes are uncertain,[9] the origin of the discrepancies and validity of individual data sets can be assessed by the compensation effect as a single, general, chemical phenomenon.

Global Kinetics of Thermal Decomposition

Explanation of selected thermal decomposition measurements of HMX, RDX, and NTO is informative before placing these results on a common footing. The discussion in this article is intended to be general and is not specific to the explosive or physical properties of HMX, RDX, or NTO. For example, bulk HMX and RDX are relatively sensitive to shock and impact[15] and liquefy before or during rapid decomposition, whereas bulk NTO is quite insensitive[16] and decomposes from the solid phase.

* Corresponding author.
® Abstract published in *Advance ACS Abstracts,* November 1, 1994.

0022-3654/94/2098-12242$04.50/0

TABLE 1: Apparent Arrhenius Parameters for Thermal Decomposition of HMX

predominant phase	E_a, kcal/mol	ln A/s^{-1}	T, °C	ref	method and comments[a]
solid	13	5.8	245−270	17	MS; NO formation
solid	18.5	11.5	245−270	17	MS; N_2, N_2O, CO, CO_2 formation
solid	22.9	17.0	253−264	18	DTA
solid	25.9	19.5	229−269	19	DTA; 35 atm, N_2
solid	27	43.8	185−280	20	derivatographic
solid	35.1	26.5	229−269	19	ITGA; 1 atm N_2
solid	36	24.9	150−170	21	EG; β-HMX
solid	37.9	27.8	176−230	22	EG
solid	38	30	220−245	17	MS; CH_2O formation
solid	41	29	180−210	23	EG; α-HMX
solid	41.2	33	185−280	20	derivatographic
solid	44.7	36.6	229−269	19	nonisothermal DTA; 4 mg
solid	44.8	36.0	229−269	19	nonisothermal DTA; 5 mg
solid	46	36.8	220−245	17	MS; N_2, N_2O, CO, CO_2 formation
solid	48.8 ± 3.3	45.6 ± 2.3	166−194	24	IR; $\beta \rightarrow \delta$-HMX transition
solid	49	39.1	229−269	19	ITGA; 1 atm air
solid	49.7	39.3	229−269	19	ITGA; 1 atm O_2
solid	50	39.5	237−279	25	DTA; ignition delay
solid	61.8	54.3	264−275	18	DTA
solid	63	53	220−245	17	MS; NO formation
solid	66.4	55.4	245−257	18	DTA
solid	67	57.6	180−210	23	EG, β-HMX
melt	47.1	42.1		4	"best estimate"
melt	50	41.4	261−278	26	MS flow reactor
melt	51.3	43.3	270−286	27	IDSC
melt	52.7 ± 2	45.4	271−314	28	EG
melt	64.7	56.3	274−284	29	IDSC
gas	32.1	30.4	230−250	23	EG
gas	32.5	28.8	248−383	30	VLPP
gas	38 ± 2.8	27.75 ± 1.2	245−275	31	EG
gas	39.6	32.6	205−280	32	EG
gas	46.2	37.8		33	thermochemical kinetics estimate
gas	52.9	46.5	273−286	34	DSC

[a] MS = mass spectrometry, DTA = differential thermal analysis, ITGA = isothermal thermogravimetric analysis, EG = evolved gas (manometric), IDSC = isothermal differential scanning calorimetry, and VLPP = very low pressure pyrolysis.

HMX. Numerous rate measurements have been published for the early stage of thermal decomposition where the rate increases with temperature. In the later stage the rate decreases with increasing temperature. The early-stage rate expression usually is close to first order. With time, a sigmoidal shape frequently develops in the kinetic curve because autocatalysis takes place as the reaction proceeds. Unfortunately, there are many reports of E_a values without corresponding A factors. E_a or ln A alone has limited value for describing the decomposition process or comparing measurements of rates. Therefore, Table 1 lists only solid, melt, and gas phase measurements of HMX in which the values of E_a and ln A are both reported. This compilation is not necessarily comprehensive. Division of these studies according to phase is somewhat arbitrary because more than one phase is frequently present during the measurement. The realistic error in E_a is 1−5 kcal/mol, although the error is frequently not reported. Figure 1 is a plot of the Arrhenius parameters in Table 1. These data conform well to a single regression line, considering that many workers and techniques are represented. Only one measurement ($\ln k = 43.8 - 27000/RT$)[20] is clearly out of line. Hereinafter, the value of E_a will be used to identify a specific measurement in Table 1.

The range of E_a is 13−67 kcal/mol in Table 1. The lower limit of 13 kcal/mol was determined by mass spectral measurement of the amount of NO that forms when solid HMX is heated in a vacuum.[17] The upper limit of 67 kcal/mol was determined from the pressure rise during the initial 0.1% of decomposition of HMX when heated in the 180−210 °C range.[23] However, much larger values of E_a have been reported without giving the corresponding values of ln A, i.e., 120,[26] 146,[35] 177,[18] 180−210,[36] 228 ± 24,[37] and 256[18] kcal/mol. Chemical significance is occasionally attached to these large values of E_a,[26,38] but to do so requires that their strong dependence on the working conditions (*vide infra*) and Arrhenius anomalies near the melting point[36] be disregarded. The Arrhenius parameters in Table 1 are now considered by phase.

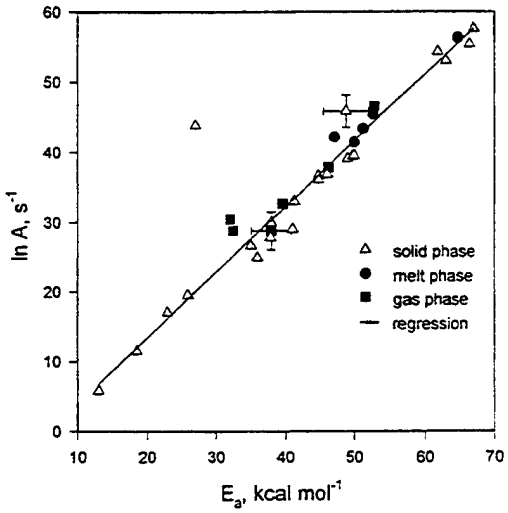

Figure 1. Kinetic compensation plot for thermal decomposition of HMX (Table 1) showing the linear regression line.

The five global gas-phase measurements and one thermochemical estimate yield E_a values of 32−53 kcal/mol. The decomposition process is proposed to be unimolecular and first order.[31] Given the presumably homogeneous reaction conditions, it is reasonable to assume that E_a is dominated by scission of the weakest bond, which are the N−NO_2 bonds. However, with one exception the experimentally determined E_a values are lower than the thermochemical kinetic estimate[33] in Table 1

TABLE 2: Apparent Arrhenius Parameters for Thermal Decomposition of RDX

predominant phase	E_a, kcal/mol	ln A/s^{-1}	T, °C	ref	method[a]
solid	24.7	11.3	43−103	46	NO chemiluminescence
solid	39.5	26.9	130−180	23	EG
solid	41.5	33.4		21	ignition
solid	45.5 ± 2	40.75 ± 1.6	177−200	47	
solid	52	44	150−197	22	EG
melt	28.6	24.4		48	DTA
melt	47.1	42.1	>207	49	DSC
melt	47.5 ± 2	42.6	213−299	28	EG
melt	47.8	43	207−299	4	"best estimate"
melt	47.9	43.1	205−222	50	IDTA
melt	48.7	44.3	207−227	51	GC
melt	49.5	47.9	197−267	52	DTA
melt	50.1 ± 1.95	45.3 ± 2.1	206−252	48	DSC[b]
melt	52.1	47.4	218−242	48	DSC
gas	30	27.1	165−247	4	"best estimate"
gas	30	26.9	170−190	23	EG
gas	30.7	26.9	170−190	32	EG
gas	34.1	31.1	208−256	34	DSC
gas	34.2	31.1	210−255	28	EG
gas	35.1	31.1	170−200	32	EG
gas	40.4 ± 3	36.8 ± 4.6	175−202	31	EG

[a] EG = evolved gas (manometry), DSC = differential scanning calorimetry, IDTA = isothermal differential thermal analysis, and GC = gas chromatography. [b] Error bars refer to difference caused by assuming different reaction orders.

and lower than a recent high-level computational estimate[39] of 48 kcal/mol for the N−NO_2 bond energy in HMX. It is possible that most of the measurements of the rate of decomposition of gaseous HMX are affected by wall and secondary reactions, which reduce the value of E_a.[40] It is also known that clustering of HMX molecules occurs in the gas phase even at low pressure,[41] so that isolated molecules are probably not even decomposing. Although the thermochemical kinetic estimate[33] has been criticized,[32] Schroeder[4] regarded it to be a good estimate of the decomposition rate of HMX in the gas phase.

Rate measurements for thermal decomposition of HMX in the melt phase yield values of E_a in the 47−53 kcal/mol range, except for a single value[29] of 64.7 kcal/mol. However, the very large values of E_a mentioned above[18,26,34−37] were all determined at or near the melting point. These large Arrhenius values for HMX can be discounted as resulting from mixed physical−chemical anomalies due to the melting.[36] They do not reflect any of the primary chemical process of thermal decomposition. The range of 47−53 kcal/mol more likely represents the dominance of chemical processes. Therefore, on average E_a(melt) > E_a(gas). Fifer[42] attributed this trend to a cage effect in which homolysis of a bond is followed by a higher percentage of radical recombinations in the melt phase than in the gas phase. Interatomic potentials[43] also affect the structure and stability of the transition states of reactions in the condensed phase. Most combustion models of HMX that include the condensed phase-to-gas phase transition[1,2] have chosen reasonable values of E_a = 46−48 kcal/mol for liquid phase decomposition. However, Fifer[42] has questioned extrapolation of such rates to the combustion regime.

The values of E_a for solid phase decomposition (13−67 kcal/mol) span the entire range of measurements in which E_a and ln A are both reported. One of these rate measurements (ln k = 43.8 − 27000/RT)[20] deviates markedly from the regression line and is probably not correct. The wide range of values is expected based on the factors discussed below that control solid-phase reactions. These factors have less influence on the liquid and gas phases. HMX forms a variety of polymorphs.[43] The rate of the β — δ-HMX solid−solid phase transition[24] is included in Table 1. The fact that this solid−solid phase transition rate lies near the compensation line for thermal decomposition (Figure 1) is an important indication that crystal

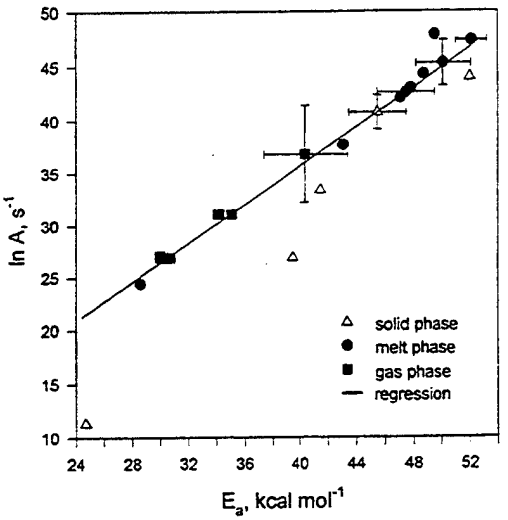

Figure 2. Kinetic compensation plot for thermal decomposition of RDX (Table 2) showing the linear regression line.

variables influence the reaction rate of the solid phase. The effects of different gaseous environments[19] and of sub- and superatmospheric pressures[17,19] have all been probed for their effects on the decomposition rate of the solid phase. The effect of pressure is highly unpredictable. The values of E_a determined below 0.05 atm (13−18 kcal/mol)[17] and at 35 atm (25.9 kcal/mol)[19] are both smaller than those at 1 atm (44.7 kcal/mol).[19] At 35 000 atm, E_a is 120 kcal/mol but decreases to 36 kcal/mol at 65 000 atm.[44] This sawtooth fluctuation of the activation energy with pressure is reminiscent of the behavior of burn rates of several energetic materials with pressure.[45]

RDX. Comments about the general characteristics of thermal decomposition made in the first paragraph above for HMX also apply for RDX. However, fewer measurements have been reported for RDX. A compilation of studies that report both ln A and E_a is given in Table 2. Figure 2 shows that ln A and E_a are essentially linearly related, although the rate data for the solid phase are rather unsatisfactory. The two most aberrant solid phase data points were excluded from the linear regression.

Kinetic studies of thermal decomposition of RDX in the gas phase produce E_a = 30−40 kcal/mol, and the process is reportedly unimolecular and first-order.[28,31] The wide range of

TABLE 3: Arrhenius Parameters for Thermal Decomposition of Solid NTO

E_a, kcal/mol	ln A/s^{-1}	T, °C	ref	method
40.7	26.9	100–137	53	NO chemiluminescence
44.8	38.3	229–246	54	ITGA, Avrami–Erofeev equation
49.3	47.6	195–210	54	IR
50.2	44.5	229–246	54[a]	ITGA
78.1	67.0	220–280	55	HPLC
87.5 ± 1.8	77.8[b]	225–245	56	HPLC
120.4	112.1	266–280	57	DSC

[a] TGA data in ref 54 recalculated using the second-order rate model in ref 56. [b] Calculated from the data given in ref 56.

measured activation energies is reminiscent of HMX, but the average value of the range is about 7 kcal/mol lower than the average for HMX. A slightly smaller A factor is expected for RDX based on statistics, but the N–NO_2 bond energy is similar in HMX and RDX.[39] Therefore, the magnitude of the difference is not expected based on considerations of the isolated molecule but can be attributed to the fact that clustering of HMX molecules in the gas phase occurs to a greater degree than for RDX.[41] Consequently, intermolecular forces can decrease the "gas phase" rate of decomposition of HMX more than RDX.

Because of the lower melting point of RDX (~200 °C) compared to HMX (~283 °C) and the lower rate of decomposition of RDX in the melt phase compared to HMX, a modestly larger number of kinetic studies have been reported for liquid RDX. As with HMX, the rates of decomposition in the melt phase yield E_a values that are larger than those for the gas phase. Also, in line with the trend in the gas phase, the E_a values in the melt phase of RDX are on average smaller than those for HMX.

The apparent Arrhenius parameters for decomposition of solid phase RDX cover the entire range of values. The scatter in the reported values reduces confidence in any interpretation. As is the case with solid HMX, these rate data are affected by many variables that are noted later in this article. However, according to Figure 2, the decomposition rates measured at the two lowest temperatures[23,46] in Table 2 probably do not result from the same process that is operative at higher temperatures. Arrhenius parameters for NTO determined by NO chemiluminescence (*vide infra*) also strongly deviate from the rates measured by all other methods.

NTO. NTO thermally decomposes above about 200 °C from the solid phase. No melting occurs. In addition to the formation of gaseous products, a melonlike, cyclic azine, polymeric residue remains.[58] Table 3 lists the rate measurements reported for the solid phase[53,54,56,57] and in solution.[55] Figure 3 shows that these results display the compensation effect except for 26.9 − 40700/RT, which was determined from NO chemiluminescence[53] and does not appear to originate from the same process that controls the decomposition rate at higher temperatures. The rate constants of Prabhakaran et al.,[54] determined from TGA data and fit to the first-order Avrami–Erofeev equation, were recalculated by us using the second-order kinetic model of Menapace et al.[56] The difference obtained of about 5 kcal/mol gives an indication of the effect when completely different rate expressions are used to analyze the same data. The A factor was not reported by Menapace et al.[56] but is readily determined from their data and is included in Table 3.

Kinetic Compensation Effect for Energetic Materials

With a few exceptions the rates of thermal decomposition of HMX, RDX, and NTO exhibit a single compensation effect for each compound. The quality of the data is insufficient to argue

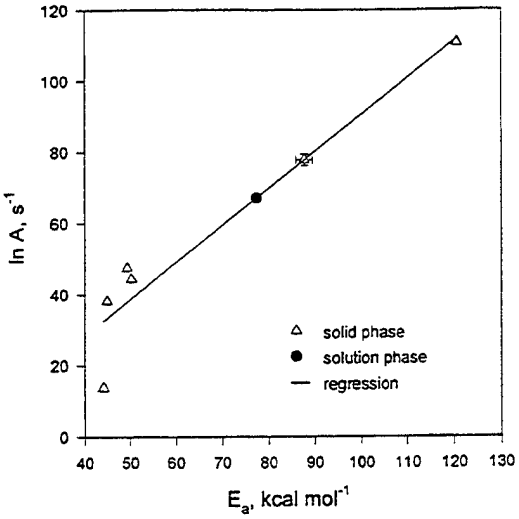

Figure 3. Kinetic compensation plot for thermal decomposition of NTO (Table 3) showing the linear regression line.

TABLE 4: Calculated and Observed Compensation Parameters

	a, mol/(kcal s)				
compound	calcd (=1/RT)	obsd	b (=ln k/s^{-1})	T, K	ref
HMX	0.96 ± 0.04	0.94	−5.4	500–550	this work
RDX	0.96 ± 0.04	0.92	−1.1	500–550	this work
NTO	0.96 ± 0.04	1.03	−13.0	500–550	this work
$CaCO_3$	0.40	0.40	−6.8	1243	12

that each phase produces a different compensation line, so an overall plot for each compound is shown. The sources of the kinetic compensation effect provide insight into the meaning and validity of global measurements of thermal decomposition, at least for HMX, RDX, and NTO.

Before discussing these compounds further, it is important to emphasize that the kinetic compensation effect occurs widely. A striking example is the reversible thermal decomposition of solid $CaCO_3$ to produce CaO and CO_2, which takes place above 925 °C. E_a values of 26–915 kcal/mol and corresponding ln A (s^{-1}) values of 4.6–363 have been obtained and are linearly related.[11,12] Obviously, these values are not connected to a single molecular process.

For any compound exhibiting the compensation effect, a plot of ln A vs E_a yields a set of compensation parameters a and b from eq 2. From eqs 1 and 2, the slope, a, equals 1/RT, where T is a temperature in the range of study.[59] Table 4 gives 1/RT and the observed values of a and b for HMX, RDX, NTO, and $CaCO_3$. Because a reasonably good correlation exists between the calculated and observed slopes, all of the rate data for a given compound that lie on or near the regression line represent legitimate measurements of the global decomposition process. An approximate isokinetic relationship exists among these data. However, the *temperature dependence* of the rate for the global process differs significantly in most of these measurements. The question is, what is the global process that is being measured?

Garn[59] proposed that the compensation effect implies that the same reaction or rate-determining step of the process is being studied but that the governing parameters of the process change. For thermal decomposition of heterogeneous phases, the global values of E_a and ln A cannot be assumed to represent a specific reaction or process unless the rate measurements are backed up by molecular-level observations.[60,61] For thermal decomposition of the solid phase the overall rate is dominated by nucleation and growth of the reaction sites in each crystal.

Microscopic reaction sites in crystals of RDX have been identified.[62] The rate of nucleation and growth varies from crystal to crystal because it depends on the relative "concentration" of corners, edges, and faces on the exterior of the crystals and the number and characteristics of defects in the interior. The rate of reaction at a corner site is expected to be faster than at a face. The existence of multiple types of reaction sites in crystals, each with its own characteristic rate, can explain why the global Arrhenius parameters are sample-dependent.[7,8,63,64] The important roles that the nucleation and growth rates play in determining the overall decomposition rate of solid HMX are emphasized by the resemblance of the $\beta \rightarrow \delta$-HMX polymorphic phase transition rate[24] to the decomposition rates of HMX in Figure 1. Different rates of decomposition have been observed for the polymorphs of HMX.[17,23,65,66]

Compounding the microscopic differences in the distribution and growth of reaction sites in the solid phase of explosives is the effect on the rate of differences in the working conditions. The following, partly interdependent, variables influence the global reaction rate: sample mass,[12,67] particle size,[20] sample configuration,[68] heating rate (rate of heat transfer),[12] self-heating of the sample,[28] characteristics of the surrounding atmosphere,[19,69-73] shape and material of construction of the sample holder,[74] and method[48,75] (also see NTO section above) and subtle errors[8] in the data reduction. Taken together, the crystal and working condition variables can produce a huge number of E_a–ln A pairs for the rate of solid phase decomposition. Therefore, it can be stated with some confidence that all of the E_a–ln A pairs in Tables 1–3 that lie on or close to the regression lines in Figures 1–3 are valid and correct *for the specific characteristics of the sample and measurement used.* It is impossible to state that any of these E_a–ln A pairs is the true intrinsic rate of thermal decomposition for HMX, RDX, or NTO.

The pathways of slow decomposition of solid HMX[76,77] and RDX[78,79] are extremely complex because many parallel reactions occur. Although less is known about NTO, the same situation is likely to exist based on the fact that a solid residue forms in addition to gaseous products.[58] Consequently, the association of the global Arrhenius parameters for thermal decomposition of solid HMX, RDX, or NTO with a specific reaction or process, although occasionally done, is a strong oversimplification.

Given the overriding dependence of the rate of thermal decomposition of the solid phase on the crystal and working conditions, it is surprising that the rates for the solid, liquid, and gas phases have similar compensation parameters. The slope parameter a is determined primarily by the temperature, but the intercept parameter b, which has the units of rate, need not be the same for all phases. Unfortunately, the quality of the published Arrhenius data is not sufficient to detect small phase-dependent differences, if they exist. It might even be considered surprising that the rates for the gas phase and, possibly, the liquid phase exhibit a compensation effect at all. This is because reactions in these phases should be more homogeneous than in the solid phase. Therefore, E_a and ln A values might be more closely associated with a specific reaction or process and be tightly clustered. The fact that a compensation effect occurs in the liquid and gas phases, much like the solid phase, indicates that these rates, too, are affected by the working conditions of the measurement, although their closer clustering suggests that they are less affected than the solid phase. A contributing factor to scattering of the decomposition rates for the liquid and gas phases is that multiple phases can still be present. For instance, it is nearly impossible to eliminate the vapor phase contribution from a liquid phase rate determination. Wall reactions are difficult to eliminate in many gas phase measurements.

For the nominally homogeneous gas and liquid phases, eq 3 indicates that the energies and entropies of activation for decomposition can compensate for one another when different measurements are compared. Because ΔS^* and E_a are both positive for HMX,[44,80] they can indeed compensate for one another as the conditions of the reaction or process are changed.

A practical question is whether any of the measured E_a–ln A pairs can be used with confidence to describe the thermal decomposition behavior of HMX, RDX, or NTO. Because of the compensation effect, the answer is that any E_a–ln A pair lying on or near the regression line, including unmeasured values, is justifiable *provided the same temperature range is maintained.* Concern about the choice of values[2] is unnecessary. However, it is risky to extrapolate these rates to other temperature ranges, such as exist during combustion and explosion. We note that the burn rate of HMX has been calculated qualitatively by using E_a and ln A from DTA data and the pyrolysis law.[25] However, because of the kinetic compensation effect, many other E_a–ln A pairs can successfully predict the burn rate within the error limits of the surface temperature and burn rate measurements.

Facts and Possible Uses of the Compensation Effect

1. Global kinetic measurements of thermal decomposition of HMX, RDX, and NTO are strongly affected by sample characteristics and the experimental conditions. They reflect the rate of the overall process as opposed to a specific reaction.
2. E_a and ln A usually compensate for one another when correctly performed measurements are compared over a similar temperature range. The overall rates by these measurements are similar and, thus, valid for conditions employed.
3. E_a–ln A pairs not lying on the regression line of the compensation plot represent a different process or are not correct.
4. Extrapolation of validly measured decomposition rates in one temperature range to another temperature range, such as from the range of slow decomposition to the range of combustion or explosion, produces widely different predictions of the rate.
5. The compensation effect enables ln A to be estimated when only E_a is published, provided the measurement was made in the same temperature range.
6. The phase dependence of the global rate of decomposition of HMX and RDX provides a rational method to scale the rate of a specific reaction of these molecules from one phase to another when the rate in only one phase is known.

Acknowledgment. We are grateful to the Air Force Office of Scientific Research, Aerospace Sciences, for support of this work on F49620-94-1-0053. The support of the Army Research Office on Contract DAAL03-92-G-0118 through Pennsylvania State University is gratefully acknowledged.

References and Notes

(1) (a) Ben-Reuven, M.; Caveny, L. H.; Vichnevetsky, R. J.; Summerfield, M. *Sixteenth Symposium (International) Combustion*; The Combustion Institute: Pittsburgh, PA, 1976; pp 1223–1233. (b) Beckstead, M. W.; Derr, R. L.; Price, C. F. *Thirteenth Symposium (International) Combustion*; The Combustion Institute: Pittsburgh, PA, 1970; pp 1047–1056. (c) Cohen, N. S.; Lo, G. A.; Crowley, J. C. *AIAA J.* **1985**, *23*, 276–282. (d) Miller, M. S. *Combust. Flame* **1982**, *46*, 51–73. (e) Li, S. C.; Williams, F. A.; Margolis, S. B. *Combust. Flame* **1990**, *80*, 329–349.

(2) Mitani, T.; Williams, F. A. *Twenty-First Symposium (International) Combustion*; The Combustion Institute: Pittsburgh, PA, 1986; pp 1965–1974.

(3) Zinn, J.; Mader, C. L. *J. Appl. Phys.* **1960**, *31*, 323–328.
(4) Schroeder, M. A. *Seventeenth JANNAF Combustion Meeting*, CPIA Publication 329; Sept 1980; Vol. II, pp 493–508.
(5) Dubovitskii, F. I.; Korsunskii, B. L. *Russ. Chem. Rev.* **1981**, *50*, 958–978.
(6) Boggs, T. L. In *Fundamentals of Solids-Propellant Combustion*; Kuo, K. K., Summerfield, M., Eds.; *Prog. Astronaut. Aeronaut.* **1984**, *90*, 121–175.
(7) Constable, F. H. *Proc. R. Soc. London* **1925**, *A108*, 355–378.
(8) Cremer, E. *Adv. Catal.* **1955**, *7*, 75–91.
(9) Garn, P. D. *Thermochim. Acta* **1979**, *28*, 185–187.
(10) Cremer, E. *Z. Phys. Chem.* **1929**, *A144*, 231–242.
(11) Zsakó, J.; Artz, H. E. *J. Therm. Anal.* **1974**, *6*, 651–656.
(12) Gallagher, P. K.; Johnson, D. W., Jr. *Thermochim. Acta* **1976**, *14*, 255–61.
(13) Dollimore, D.; Rodgers, P. F. *Thermochim. Acta* **1979**, *30*, 273–280.
(14) Leffler, J. E.; Grunwald, E. *Rates and Equilibria of Organic Reactions*; John Wiley and Sons: New York, 1963; pp 315–342. Barkley, I. M.; Butler, J. A. V. *Trans. Faraday Soc.* **1938**, *34*, 1445–1454.
(15) Storm, C. B.; Stine, J. R.; Kramer, J. F. In *Chemistry and Physics of Energetic Materials*; Bulusu, S., Ed.; Kluwer Academic: Dordrecht, The Netherlands, 1990; pp 605–639.
(16) Lee, K. Y.; Coburn, M. D. Los Alamos Report LA-10302-MX, 1985.
(17) Suryanarayana, B.; Graybush, R. J. *Proceedings of Thirty-Ninth Congress Industrial Chemistry*; Brussels, Belgium; 1966; pp 1–4.
(18) Kimura, J.; Kubota, N. *Prop. Explos.* **1980**, *5*, 1–8.
(19) Kraeutle, K. J. *Eighteenth JANNAF Combustion Meeting*; CPIA Publication 347; Oct 1981; Vol. II, pp 383–394.
(20) Medvedev, A. I.; Sakovich, G. V.; Konstantinov, V. V. *Conference on Kinetics and Mechanism of Chemical Reactions in the Solid State*; Novosibirsk, 1977; Part 1, p 163 (quoted in ref 5).
(21) Klimenko, G. K. *Combust. Explos.* **1977**, 585.
(22) Maksimov, Yu. Ya. *Tr. Mosk. Khim. Technol. Inst. im. D. I. Mendeleeva* **1967**, *53*, 73–84.
(23) Belyayeva, M. S.; Klimenko, G. K.; Babaytseva, L. T.; Stolyarov, P. N. *Fifth All Union Symposium on Combustion and Detonation*; Sept 1977; pp 47–50 (quoted in ref 5).
(24) Brill, T. B.; Karpowicz, R. J. *J. Phys. Chem.* **1982**, *86*, 4260–65.
(25) Lengellé, G.; Duterque, J. R.; Gordon, J. C.; Trubert, J. F. *J. Propuls. Power*, in press.
(26) Goshgarian, B. B. AFRPL-TR-78-76, Edwards AFB, CA, Oct 1978.
(27) Rogers, R. N. *Thermochim. Acta* **1972**, *3*, 437–447.
(28) Robertson, A. J. B. *Trans. Faraday Soc.* **1949**, *45*, 85–93.
(29) Power, R. J. Personal communication cited in ref 6.
(30) McMillen, D. F.; Barker, J. R.; Lewis, K. E.; Trevor, P. L.; Golden, D. M. SRI Project PYU-5787, June 1979.
(31) Maksimov, Yu. Ya.; Apol'kova, V. N.; Braverman, O. V.; Solov'ev, A. I. *Russ. J. Phys. Chem.* **1985**, *59*, 201–4.
(32) Burov, Yu. M.; Nazin, G. M. *Kinet. Catal.* **1982**, *23*, 5–10.
(33) Shaw, R.; Walker, F. E. *J. Phys. Chem.* **1977**, *81*, 2572–2576.
(34) Rogers, R. N.; Daub, G. W. *Anal. Chem.* **1973**, *45*, 596–600.
(35) Takaira, K.; Okazaki, K. M.S. Thesis, National Defense Academy, 1974 (quoted in ref 18).
(36) Hall, P. G. *Trans. Faraday Soc.* **1971**, *67*, 556–562.
(37) Rogers, R. N.; Morris, E. D. *Anal. Chem.* **1966**, *38*, 412–414.
(38) Farber, M. B. *Mass Spectrom. Rev.* **1992**, *2*, 137–152.
(39) Melius, C. F. In *Chemistry and Physics of Energetics Materials*; Bulusu, S., Ed.; Kluwer Academic: Dordrecht, The Netherlands, 1990; pp 21–78.
(40) Samoilenko, N. G.; Vinokurov, A. A.; Abramov, V. G.; Merzhanov, A. G. *Russ. J. Phys. Chem.* **1970**, *44*, 22–24.
(41) Campana, J. E.; Doyle, Jr., R. J. *J. Chem. Soc., Chem. Commun.* **1985**, 45–6.
(42) Fifer, R. A. In *Fundamentals of Solid-Propellant Combustion*; Kuo, K. K., Summerfield, M., Eds.; *Prog. Astronaut. Aeronaut.* **1984**, *90*, 177–237.
(43) Brill, T. B.; Reese, C. O. *J. Phys. Chem.* **1980**, *84*, 1376–1380.
(44) Piermarini, G. J.; Block, S.; Miller, P. J. *J. Phys. Chem.* **1987**, *91*, 3872–3878.
(45) Foltz, M. F. *Prop. Explos. Pyrotech.* **1993**, *18*, 210–216. Rice, S. F.; Foltz, M. F. *Combust. Flame* **1991**, *87*, 109–122.
(46) Olson, D. B.; Gill, R. J. Presented at the Eastern Section Meeting of the Combustion Institute, Clearwater Beach, FL, 1984.
(47) Unpublished work by G. K. Adams cited in ref 6.
(48) Rogers, R. N.; Smith, L. C. *Thermochim. Acta* **1970**, *1*, 1–9.
(49) Rogers, R. N. *Thermochim. Acta* **1974**, *9*, 444–446.
(50) Oyumi, Y. *Prop. Explos. Pyrotech.* **1988**, *13*, 42–47.
(51) Rauch, F. C.; Fanelli, A. J. *J. Phys. Chem.* **1969**, *73*, 1604–1608.
(52) Miles, K. K. M.S. Thesis, Navy Postgraduate School, Monterey, CA, March 1972.
(53) Östmark, H.; Bergman, H.; Åqrist, G.; Langlet, A.; Persson, B. *Sixteenth International Pyrotechnics Seminar*; Jönköping, Sweden, June 1991; pp 874–886.
(54) Prabhakaran, K. V.; Naidu, S. R.; Kurian, E. M. *Thermochim. Acta*, in press.
(55) Oxley, J. C.; Zhou, Z.; Smith, J. L.; McKenney, R. L. *Proceedings of the ADPA International Symposium on Energetic Materials Technology*; March 21–24, 1994; pp 155–165.
(56) Menapace, J. A.; Marlin, J. E.; Bruss, D. R.; Dascher, R. V. *J. Phys. Chem.* **1991**, *95*, 5509–5517.
(57) Yi, X.; Hu, R.; Wang, X.; Fu, X.; Zhu, C. *Thermochim. Acta* **1991**, *189*, 283–296.
(58) Williams, G. K.; Palopoli, S. F.; Brill, T. B. *Combust. Flame* **1994**, *98*, 197–204.
(59) Garn, P. D. *J. Thermal Anal.* **1973**, *7*, 475–478.
(60) Patil, D. G.; Brill, T. B. *Combust. Flame* **1991**, *87*, 145–151.
(61) Patil, D. G.; Brill, T. B. *Thermochim. Acta* **1994**, *235*, 225–230.
(62) Burov, Y. M.; Nazin, G. M. *Khim. Fiz.* **1984**, *3*, 1126–1130.
(63) Sosnovsky, H. M. C. *J. Chem. Phys. Solids* **1959**, *10*, 304–310.
(64) Shannon, R. D. *Trans. Faraday Soc.* **1964**, *60*, 1902–1913.
(65) Selig, W. *Explosivstoffe* **1969**, *17*, 201–202.
(66) Burov, Yu. M.; Manelis, G. B.; Nazin, G. M. *Dokl. Akad. Nauk SSSR* **1984**, *5*, 1110–1113.
(67) Lukin, A.; Roginskii, S. Z. *Acta Physicochim. URSS* **1932**, *2*, 385–396.
(68) Batten, J. J.; Murdie, D. C. *Aust. J. Chem.* **1970**, *23*, 749–755.
(69) Batten, J. J. *Aust. J. Chem.* **1971**, *24*, 945–954.
(70) Batten, J. J. *Aust. J. Chem.* **1971**, *24*, 2025–2029.
(71) Palopoli, S. F.; Brill, T. B. *Combust. Flame* **1991**, *87*, 45–60.
(72) Nikolaev, A. V.; Lobvinenko, V. A.; Gorbatcher, V. M. *J. Thermal Anal.* **1974**, *6*, 473–479.
(73) Kishore, K. *Prop. Explos.* **1977**, *2*, 78–81.
(74) Keattch, C. J. *An Introduction to Thermogravimetry*; Heyden & Sons: London, 1969; p 21.
(75) Fatemi, N.; Whitehead, R.; Price, D.; Dollimore, D. *Thermochim. Acta* **1986**, *104*, 93–100.
(76) Behrens, Jr., R. *J. Phys. Chem.* **1990**, *94*, 6706–6718.
(77) Behrens, Jr., R.; Bulusu, S. *J. Phys. Chem.* **1991**, *95*, 5838–5845.
(78) Behrens, Jr., R.; Bulusu, S. *J. Phys. Chem.* **1992**, *96*, 8877–8891.
(79) Behrens, Jr., R.; Bulusu, S. *J. Phys. Chem.* **1992**, *96*, 8891–8897.
(80) Lee, E. L.; Sanborn, R. H.; Stromberg, H. C. *Fifth Symposium (International) on Detonation*; Pasadena, CA, 1970; pp 331–42.

Reprinted from The Journal of Physical Chemistry, 1995, 99.

Surface Chemistry of Burning Explosives and Propellants

T. B. Brill,* H. Arisawa, P. J. Brush, P. E. Gongwer, and G. K. Williams

Department of Chemistry, University of Delaware, Newark, Deleware 19716

Received: July 14, 1994; In Final Form: November 23, 1994[⊗]

Rates and pathways of the reactions and processes at the surface of burning energetic materials, such as explosives and propellants, are very difficult to measure experimentally. A "snapshot" simulation of the surface reaction zone is captured by a thin layer of material heated rapidly to temperatures characteristic of the burning surface. By the use of T-jump/FTIR spectroscopy, kinetics and heat changes can be determined during this event, and the early-stage chemistry can be assembled from the gaseous products of decomposition. Results for ammonium nitrate, poly(butadiene) polymers, hydrazinium nitroformate, and octahydro-1,3,5,7-tetranitro-1,3,5,7-tetrazacine (HMX) illustrate progress in this field.

Introduction

Determining rates and pathways of specific reactions at the surface of a burning solid is a chemistry nightmare. A very steep temperature gradient exists which causes many parallel, multiphase reactions to occur over a short linear dimension. Heat and mass transport, thermophysical properties, and reaction characteristics become intimately mixed. It is no surprise that relatively little is known about the chemistry at the surface of a burning solid. However, as transport and kinetic codes to describe combustion become increasingly sophisticated, the demand has increased for experimental details about the surface reaction zone.

The compounds receiving the most attention in our work have been energetic materials in which the fuel and oxidant functionalities are initially built into the molecule. Upon thermolysis, fuel and oxidant molecules are released, react exothermically, and sustain combustion. Because of the complexity of these processes at the surface, determination of the rates and pathways of reactions has necessitated development of new techniques, such as T-jump/FTIR spectroscopy; employment of nonconventional methods of data analysis; and adaptation to the interface between chemistry and mechanical engineering. Chemistry at a burning surface can now be outlined in general terms. Results and methods of analysis are illustrated by using recent studies of ammonium nitrate (AN), hydrazinium nitroformate (HNF), octahydro-1,3,5,7-tetranitro-1,3,5,7-tetrazacine (HMX), and various poly(butadiene) polymers.

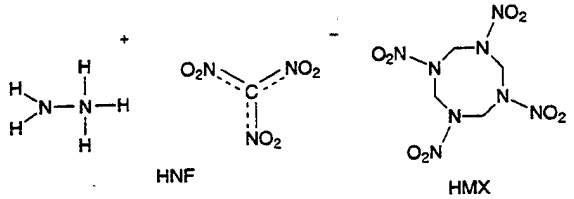

HNF HMX

Historical Perspectives

Pioneering ideas about the surface reaction zone of a solid propellant or explosive were published in this journal by prominent chemists of the midcentury.[1-3] Renowned research in this field also emerged from the former Soviet Union by Semenov,[4] Zel'dovich,[5] and Belyaev,[6] to mention a few. As many chemists turned toward the chemistry and kinetics in the gas phase and flames, fundamental advancements in the combustion of solids, particularly solid rocket propellants, came largely from engineering research.

Numerous philosophical, analytical, and computational models have been devised with the objective of predicting the characteristics of monopropellant and composite propellant combustion. Lacking experimental data about the surface chemistry and acknowledging its physical complexity, the surface reaction zone was envisioned as an infinitely thin, superficial boundary layer that is a source of reactants for the flame zone at a single Arrhenius-type rate. Description of the near-field flame structure was primarily the focus of such models as the granular diffusion flame model of Summerfield et al.;[7] the models of Beckstead, Derr, and Price (BDP);[8] Ben-Reuven et al.,[9,10] as updated by Cohen et al.,[11] Ermolin et al.,[12,13] and Hatch;[14] some of the models of Williams et al.;[15,16] and the CHEMKIN-based model of Melius.[17] However, the surface zone has long been recognized to have a major role in the combustion characteristics and is emphasized particularly in the descriptions of Merzhanov,[18] Strunin and Manelis,[19] Li et al.,[20] and Huang et al.[21] Many workers now agree that 70–90% of the heat from the propellant is released in the interfacial gas-condensed phase region,[7,8,11,15,22] at least to 10–20 atm pressure. Consequently, detailed information is needed about this complicated layer if accurate predictions about the combustion behavior of propellants and explosives are to be achieved.

What Is the Burning Surface?

Pictorializing the burning surface presents some real and semantic problems. Alexander et al.[23] illustrated the complexity by using a figure attributed to Kuo. The real problems mostly arise when defining and parameterizing the equations that describe dynamic, interfacial, microscopic, physical, and chemical processes. In this regard Li et al.[20] and Huang et al.[21] analyzed the two-phase surface zone with considerable care.

From the point of view of chemistry, the surface of a burning solid propellant consists of a thin layer where much of the

* Corresponding author.
⊗ Abstract published in *Advance ACS Abstracts,* January 1, 1995.

0022-3654/95/2099-1384$09.00/0

formulation pyrolyzes by parallel, sequential, and/or concerted steps to fuel and oxidizer molecules, which then engage in secondary exothermic reactions. The thickness of this surface zone depends on the temperature, pressure, and ingredients. The burning surface of HMX and RDX (the six-membered ring homolog of HMX) is liquid during combustion at pressures below 67 atm.[24,25] The surfaces of ammonium perchlorate and HNF are liquid below 50[26] and 70 atm,[27] respectively. In all cases the liquid layer becomes thinner with increasing pressure because the temperature gradient produced by exothermicity of the surface multiphase and near-field gas-phase reactions becomes very steep.[28] The shape of this one-dimensional thermal wave is defined by the thermophysical properties of the material coupled with the mass, momentum, energy, and species conservation equations.[29]

While physical concepts are able to describe the shape of the thermal wave, the surface reaction zone is a complex, finite, chemical entity. Even though the temperature gradient is large at the surface and becomes larger with increasing pressure, the thermal wave still penetrates many unit cell distances into the monopropellant crystal. For example, a surface reaction zone thickness of 1 μm corresponds to roughly 100 unit cell lengths of a crystal of HMX or RDX. Hence, the disappearance of an obvious liquid layer at high pressure does not necessarily signal the end of multiphase chemistry at the surface.

The surface reaction layer does not refer solely to solid- or liquid-phase pyrolysis reactions of the formulated propellant components. Neither does it refer solely to homogeneous gas-phase reactions next to the surface. A more general and accurate description is that of a heterogeneous (or two-phase) zone that includes developing voids and/or bubbles with nanoscopic and microscopic dimensions.[20,21] On the vapor side, the surface boundary is physically rough and dynamically changing owing to the microscopic gasification dynamics. Nominally gas-phase reactions can occur within the multiphase zone and in the near field of the disintegrating surface. Therefore, the operative thickness of the surface zone from the point of view of chemistry is somewhat larger than simply the thickness of the melt-foam layer.

The acute issue is how to determine the rates and pathways of the main reactions in the interfacial surface zone during combustion where the physical dimensions are on the order of microns, the shapes and positions of reaction sites are rapidly changing, and at least two phases and a steep temperature gradient are present. It is unlikely that the detail possible with single-phase, unimolecular, decomposition measurements will ever be available for the burning surface. On the other hand, a "snapshot" simulation of the surface is a film of material heated at a high rate to the temperature present at the burning surface. These conditions are achieved by T-jump/FTIR spectroscopy, which was developed for these studies. By using this method, progress has been made toward identifying gaseous products that are formed at the temperatures present at the surface during steady combustion. In turn, these products help to identify reaction schemes in the surface zone.

T-Jump Simulation of the Burning Surface

The concept of T-jump/FTIR spectroscopy[30,31] is illustrated in Figure 1. Approximately 200 μg of material is thinly spread on the center of a polished Pt ribbon filament. The filament is arranged inside of a gas cell so that the IR beam of a rapid-scanning FTIR spectrometer (Nicolet 800, 60SX, or 20SXC) passes about 3 mm above the surface. The cell is purged with Ar and pressurized at any desired pressure up to 70 atm. By using a high-gain, fast-response power supply (CDS Analytical)

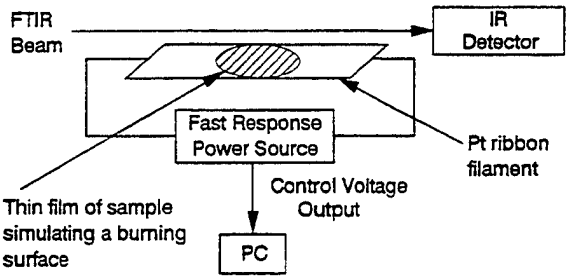

Figure 1. Essential features of T-jump/FTIR spectroscopy to achieve a "snapshot" simulation of a burning surface.

the filament and sample are heated at a high rate and then held at a chosen temperature in the 100−700 °C range for the duration of the experiment. The relationship between the applied voltage and the resulting filament temperature was determined for all experimental conditions by using the melting points of Aldrich Chemical Co. standards.

Although 2000 °C s^{-1} is the filament heating rate, the sample is able to heat at worst at about 200 °C s^{-1} and at best at about 600 °C s^{-1} to the set temperature because of limitations in the rate of heat transfer.[31] Consequently, we disregard data at $\leq$0.5 s because the thermal characteristics of the filament−sample interface are in a highly transient stage. After this time, the characteristic thermal diffusion time, which is the time required for one of the film faces to sense 60% of the temperature change at the other, is about 25 μs[31a] in this experiment, which is much faster than the data collection rate. Once equilibrated, the set temperature is known to at least $\pm$2 °C. As a result, the small changes in control voltage applied to the filament can be used to track the endothermic and exothermic events of the sample. An exotherm produces a sharp spike in the control voltage trace which marks the time to exotherm. A kinetic analysis is possible with these data. Transmission IR spectra of the gas products are recorded every 100 ms at 4 cm^{-1} resolution simultaneously with the control voltage measurement. These data can also indicate the reaction rate and outline the chemistry taking place within the simulated surface reaction zone.

Three concerns arise about this approach. First, the configuration of the experiment is not the same as burning propellant in that the sample is heated from the underside by the filament rather than the top side by the near-surface primary flame reactions. As the reactions accelerate in the experiment, however, a thin gas layer can briefly develop between the steady heat source of the filament and the material. In this sense the configuration of heat source to reactive gas layer to sample in the T-jump experiment resembles the configuration of flame to reactive gas layer to sample for the propellant burning. Second, during steady combustion of a propellant, a back-pressure of gaseous products is present. To simulate this condition in the "snapshot" T-jump experiment, the internal pressure in the cell is raised by adding Ar gas. Diffusion of the gaseous matter does, therefore, occur against a large pressure resistance. Third, it would be useful to know whether connections exist between rapid heating of a film and steady combustion of a bulk energetic material. In fact, the rate of mass loss from these mesoscopic samples at fast heating rates is essentially the same as it is from the burning bulk material at the same pressure.[32−36]

On balance we know that the laboratory simulation of the burning surface by rapidly heating a film cannot be an exact replication of combustion, but considerable effort has been made to be close to that needed for current propellant modeling efforts.

The majority of our past work, in which rapid heating methods and rapid-scan FTIR spectroscopy are combined, was directed at understanding reaction pathways[37−39] and structure/

decomposition relationships of bulk energetic materials. Considerable attention is now being given to determining rates for various processes.

Arrhenius Description of the Burning Surface

The rates of diffusion, vaporization, nucleation, and reaction and the methods of measurement and analysis all contribute to the Arrhenius parameters for the surface reaction zone. This broad view of Arrhenius parameters as simply process parameters is usually necessary for heterogeneous reactions.[37] Equation 1 describes the temperature dependence of the rate of

$$d\alpha/dt = (1 - \alpha)^n A e^{-E_a/RT} \quad (1)$$

conversion, $d\alpha/dt$. With the foregoing precaution in mind, the terms "activation energy" (E_a), "prefactor" (A), and "order of the process" (n) are retained but do not necessarily have the same meaning as in homogeneous-phase kinetics,[34,40] where the rate of change of concentration is usually determined. The inability to identify the mole in the units (kJ mol^{-1}) of E_a for many heterogeneous processes arises from the fact that the units appear as a result of the gas constant R. A concentration term is frequently absence in the rate measurement of a heterogeneous process.

Two apparent activation energies for surface processes must be distinguished. These are the surface activation energy and the chemical activation energy. The surface activation energy, E_s, is described by the pyrolysis law 2. Measured linear regression rates, $\dot{r}$, at various surface temperatures, T_s, determine the value of E_s. Surface regression to which eq 2 applies is

$$\dot{r} = A_s e^{-E_s/RT_s} \quad (2)$$

zeroth-order because fresh reactant replaces gasified products at a constant rate. Diffusion, vaporization, and reaction rates admix in E_s making the association of E_s with a particular reaction a risky adventure. First, the rate law for the controlling chemical reactions, such as homolyses of specific bonds in the surface reaction zone, is likely to be predominantly first order, which makes the Arrhenius parameters for regression and bond homolysis not directly comparable. Second, starting with Merzhanov and Dubovitskii,[41] a number of authors[28,42] have shown that $\dot{r}^2$ is related to the Arrhenius parameters of bulk-phase chemical decomposition. Equation 3 shows this relationship for many propellants, where T_0, d, and C_p are the initial temperature, thermal diffusivity, and specific heat of the propellant, respectively. Q is the heat released in the surface layer. According to eqs 2 and 3, $E_s < E_a$.

$$\dot{r}^2 = \frac{dRT_s^2 A e^{-E_s/RT_s}}{E_a(T_s - T_0 - Q/2C_p)} \quad (3)$$

Indeed, the values of E_s are usually small[43] compared to the strength of the weakest bond in energetic molecules and the global Arrhenius parameters for decomposition of HMX and RDX[44] that are derived from DSC, TGA, and manometry.

Kinetics from the Increase in Total Absorbance. The use of the total absorbance of the gaseous products from a bulk sample to obtain the rate of decomposition is illustrated with ammonium nitrate (AN). AN is the most extensively used energetic component of explosives. Several stoichiometric reactions account for the amount and identity of gaseous products and the accompanying heat changes during rapid pyrolysis of AN.[45] The rate of formation of the IR-active products from AN, which has been T-jumped to the temperature range of the burning surface, can be measured from the

TABLE 1: Scaling Factors to Convert Absorbances to Relative Concentrations

product	frequency, cm^{-1}	multiplicative factor[a]
CO_2	2349 (R)	1.0
N_2O	2224 (R)	1.86
CO	2143 (P)	21.4
NO	1903 (R)	32.1
HNO_3	1709	8
NO_2	1621	2
$HC(NO_2)_3$	1605	1.88
NH_3	968 (Q)	5

[a] Converts absorbance intensity of equal partial pressures of gases to concentration relative to CO_2.

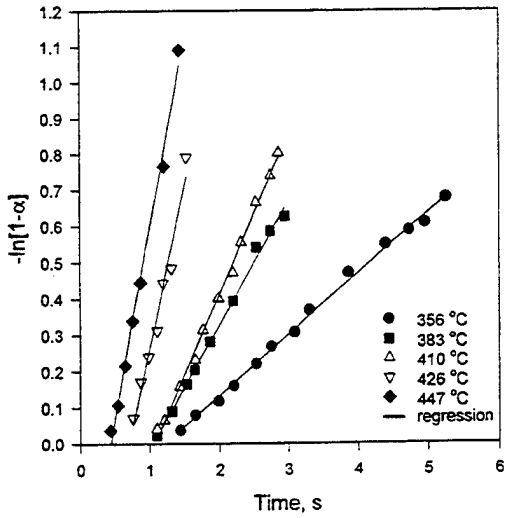

Figure 2. Rate constants for the growth of gas products from NH_4NO_3 during the initial 5−50% of decomposition.

absorbances by rapid-scan FTIR spectroscopy. The absorbances of N_2O, NO, NO_2, HNO_3, NH_3, and NH_4NO_3 (aerosol) were converted to concentration changes by using the scaling factors in Table 1. These factors are based on the absolute absorbance of each species.[39,46] However, the absolute absorbance of AN(aerosol) is unknown. Moreover, the intrinsic IR absorptivity of AN(aerosol) may be affected by Rayleigh scattering. Rayleigh scattering could occur to some extent because the base line slope of the MCT detector output suggests that the particle diameter is smaller than the mid-IR wavelengths. With these concerns in mind, the absolute absorbance of $\nu_3(NO_3^-)$ at 1360 cm^{-1} was arbitrarily assigned a scaling factor of unity, which is equivalent to that of CO_2. This value is plausible in light of the fact that the NO_3^- asymmetric stretch strongly absorbs in all nitrate salts. However, as a result of this choice, AN(aerosol) formation has an important role in the regression rate of the surface. A test of the sensitivity of the kinetic constants to this assumption is mentioned below.

The conversion to gaseous products, α, was determined from $\alpha = A_t/A_{max}$. (A_t is the total IR absorbance at time t, and A_{max} is the final total absorbance.) In Figure 2 the quantity $-\ln(1 - \alpha)$ is plotted against time from each temperature. The respective values of k are determined from regions of linearity according to eq 4. The nonzero intercepts when $\alpha = 0$ result

$$-\ln(1 - \alpha) = kt + c \quad (4)$$

from the finite heat-up time discussed in the T-jump experimental description above. Values of ln k are then plotted vs $1/T$ in Figure 3 from which the Arrhenius parameters $E_s = 75 \pm 5$ kJ mol^{-1} and ln A (s^{-1}) $= 13.1 \pm 0.8$ are determined. E_s compares with independent estimates of 42−63 kJ mol^{-1} by

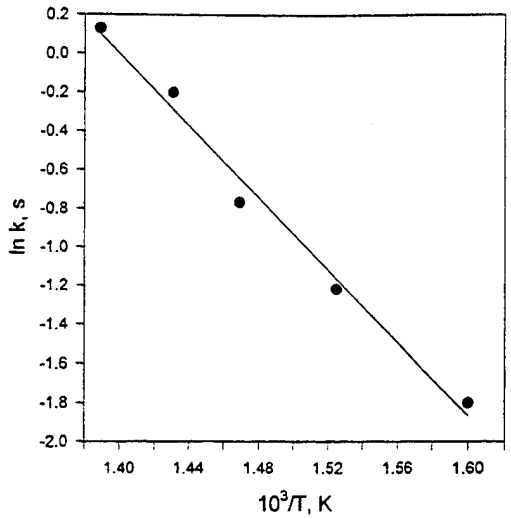

Figure 3. Arrhenius plot of the rates for NH_4NO_3 in Figure 2.

Beckstead[43] from the temperature sensitivity of the burn rate and about 50 kJ mol^{-1} from Chaiken,[47] when his data are corrected for a more realistic surface temperature.[48]

The value of E_s is relatively insensitive to the assumed scaling factor of unity for NH_4NO_3 (aerosol). The fact that N_2 and H_2O are present but not included in the quantitation procedure also has a minor effect on E_s. The addition of N_2 and H_2O or modest changes in the AN scaling factor merely increase the value of k proportionally at each temperature while maintaining the slope in the Arrhenius plot. The prefactor has not been obtained previously for surface regression of AN, and we note that the value of ln A is, unlike E_s, quite sensitive to the method of analysis. A change in the scale factor for the absorbance of AN(aerosol) and the absence of H_2O and N_2 in the quantitation procedure vertically shifts the line in Figure 3. ln A is sensitive to this shift and, therefore, contains some error. More adjustment of ln A than E_s is justifiable in combustion modeling.

Kinetics by the Increase in Specific Absorbances. Aside from their effectiveness as fuel binders in solid propellants, poly(butadiene) rubber polymers are widely known for their thermosetting coating properties, resiliency, and ability to imitiate natural rubber. Hydroxyl-terminated poly(butadiene) (HTPB) and poly(butadiene–acrylic acid–acylonitrile) copolymer (PBAN) are well-known in solid propellant formulations. PBAN is the binder fuel in the solid boosters of the Space Shuttle. The solid fuel ramjet and the Ariane employ HTPB. Small differences among binders have surprisingly large effects on the combustion characteristics of composite propellants.[49,50] With the exception of one recent spectroscopic analysis,[35] previous attempts to describe the kinetics and mechanisms of fast thermal decomposition of propellant binders do not involve direct chemical interrogation.[51] Many gaseous products are liberated at low heating rates which can be detected by IR and mass spectrometry.[52–54] Much more needs to be learned, especially about the kinetics of formation of individual gaseous products at high heating rates and high temperatures.

Careful absorbance measurements on known concentrations of pure hydrocarbon gases provide absolute concentrations of the products from these polymers. The rate of growth of a specific absorbance during fast thermolysis gives the rate of formation of each product. The results for 1,3-butadiene, 4-vinyl-1-cyclohexene (cyclized dibutadiene), and a previously undiscussed fragment, *trans*-2-butene, illustrate the behavior of thin films of HTPB and PBAN that have been rapidly heated to set temperatures in the 460–600 °C range by T-jump/FTIR spectroscopy. Zeroth-order kinetics best describe the absorbance

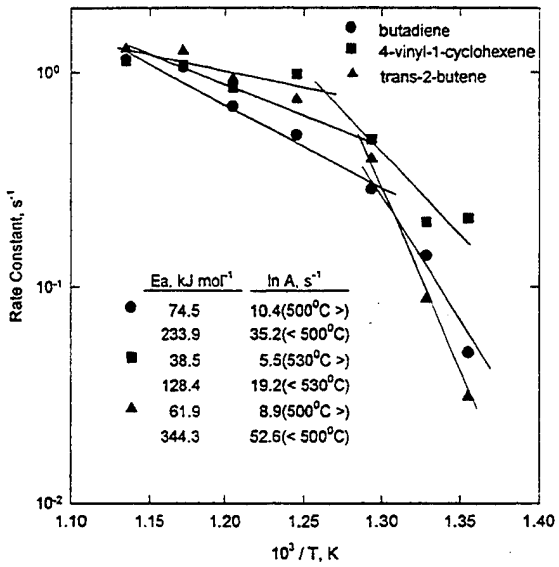

Figure 4. Arrhenius parameters for three products of HTPB.

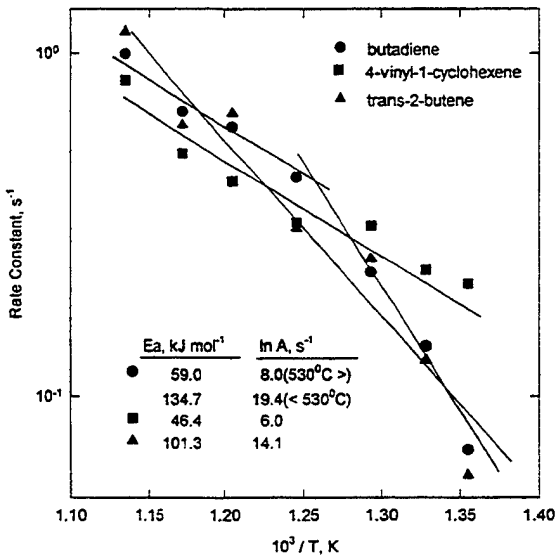

Figure 5. Arrhenius parameters for three products of PBAN.

increases during approximately 10–100% decomposition. Figures 4 and 5 are Arrhenius plots for HTPB and PBAN, respectively. The rates of evolution of all three products from HTPB change markedly at 500–530 °C. The magnitude of the Arrhenius constants suggests that chemical processes are emphasized below 500 °C, while diffusion plays a major role above 530 °C. For PBAN, butadiene evolution exhibits a rate change at about 515 °C, while *trans*-2-butene and 4-vinyl-1-cyclohexene do not.

These high-temperature, high-rate pyrolysis results are in progress and are stimulating because not only can depolymerization kinetics and possible pathways be extracted but also the rates of generation of individual reactants for the primary flame zone can be determined at pressures and temperatures relevant to combustion. The latter measurement is essential for detailed combustion modeling of solid propellants that contain polymeric binder fuels.

Kinetics by the Time to Exotherm. Hydrazinium nitroformate (HNF) is of interest as an oxidizer for environmently "clean" rocket propellants. The rate of formation of the gaseous products from molten HNF is too rapid to employ the conventional FTIR absorbance increase to indicate the decomposition rate. Instead, a kinetic method was used that is based

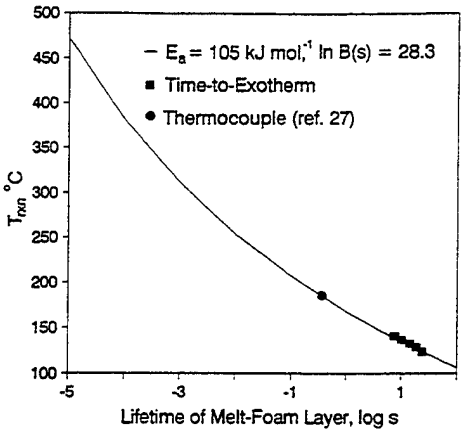

Figure 6. Global kinetics (eq 7) of the melt-foam layer of HNF. Experimental data points are shown. Extension to higher temperature covers the surface temperatures characteristic of deflagration.

on the time to exotherm (t_x) after rapid heating to set temperatures in the 130−140 °C range.[55] This temperature range was chosen because the time before detection of the release of heat is determined primarily by the rate of heat buildup in the sample as opposed to the rate of heat transfer to the filament sensor.[30,31] HNF melts at 123 °C, and rapid decomposition occurs in several seconds above this temperature. Assuming "adiabatic" conditions, eq 5[56] provides the apparent

$$\ln t_x = E_a/RT + \ln B \tag{5}$$

activation energy, E_a. Experimental measurements of t_x yield $E_a = 105$ kJ mol^{-1} and ln B (s) = 28.3. However, the intercept, B, is not the conventional Arrhenius preexponential factor, A, but is approximately related to A by eq 6.[57] The heat capacity, C_p, and the heat of reaction, Q, are unknown for melt-foam HNF, making eq 6 only an estimate. If C_p is assumed to be

$$A = C_pRT^2/QBE_a \tag{6}$$

similar to that of AN (1.7 J g^{-1} °C^{-1})[58] and Q is taken to be 75 kJ (this value of Q is reasoned below), then eq 6 yields ln A (s^{-1}) = 25.4, when T = 137 °C. The difference between A and $1/B$ is only about an order of magnitude. Such a discrepancy suggests that this approach to obtain the global rate of degradation of the surface foam zone is reasonable. The values of E_a and $1/B$ were, therefore, chosen to give the cumulative decomposition rate of the melt foam layer. They do not refer to a specific reaction or event.

The value E_a = 105 kJ mol^{-1} determined experimentally here for decomposition of the melt-foam layer can be compared to E_a = 180 kJ mol^{-1} given by Koroban et al.[59] for solid HNF. The trend of E_a(solid) > E_a(melt) also occurs with other energetic materials, such as HMX and RDX,[44] which makes these E_a values qualitatively consistent.

Several characteristics of the melt-foam layer on the surface of burning HNF are obtained by substituting E_a and $1/B$ into the rearranged form of the Arrhenius eq 7.[60] The lifetime of

$$T_{rxn} = \frac{E_a}{R(\ln A + \ln \Delta t)} \tag{7}$$

the reaction layer, Δt, can be estimated at a given temperature. Figure 6 shows the result. The appropriateness of kinetic constants obtained from the time to exotherm and the resulting predictions from eq 7 and Figure 6 is judged by consistency with the data of McHale and von Elbe[27] obtained by imbedding a thermocouple in burning HNF. At 1 atm they find a lifetime

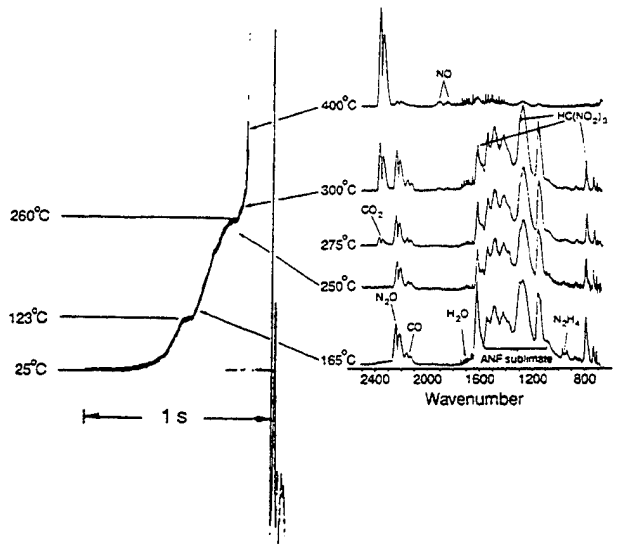

Figure 7. Rapid-scan FTIR spectra of the gaseous products from HNF T-jumped to the temperatures given under 5−7 atm of Ar. These spectra are compared to the thermocouple record of the temperature profile in burning HNF given in ref 27.

of $\Delta t \simeq 0.3$ s and an average temperature of $T \simeq 190$ °C for the melt-foam layer. This $T-\Delta t$ combination lies almost exactly on the rate line in Figure 6. Therefore, reasonable confidence can be placed in these global kinetic constants for HNF. While extrapolation to another temperature range is uncertain, the surface temperatures and residence times during combustion can at least be estimated from Figure 6.

The pathways of thermal decomposition of HNF in the thermal wave representative of combustion can be extracted from T-jump/FTIR data. However, the imbedded thermocouple data[27] for ignited polycrystalline HNF are invaluable to outline the relevant temperature ranges for detailed study. A steady temperature rise is reported for the condensed phase with slope breaks at 123 and 260 °C. Over 25−123 °C, the rise reflects preheating of the solid phase. At about 123 °C, HNF melts and foaming begins due to the generation of gas. The temperature continues to rise to about 260 °C, at which point the rates of gasification and heating accelerate so rapidly that deflagration takes place. This temperature is somewhat below another report of 400 °C for self-ignition of HNF.[61] Taken together, however, these data reveal that the temperature regions of interest in combustion are 123−260 °C, where two-phase foam chemistry occurs, and above 260−400 °C, where deflagration begins.

To outline the chemistry in these ranges, the IR-active gaseous products were determined from HNF that was heated rapidly to set temperatures in the 130−400 °C range under 5−7 atm of Ar.[55] In accordance with the thermocouple data,[27] the extent of chemical transformation was observed to depend distinctively on the set temperature, as illustrated by Figure 7. Identification of the gaseous products required considerable care. $NH_4[C(NO_2)_3]$ (ANF) aerosol, $HC(NO_2)_3$, N_2H_4, N_2O, H_2O, and CO are detected in the 130−260 °C range. These products form predominately in the condensed phase because no stationary flame exists in the T-jump/FTIR experiment. Moreover, HNF aerosol is not detected, so that evaporation of HNF followed by gas phase decomposition is negligible. Instead, HNF decomposes to form ANF, which is described by the idealized limiting reaction 8. This reaction is modestly exothermic by

$$2\text{HNF} \rightarrow 2\text{ANF} + \text{N}_2 + \text{H}_2 \tag{8}$$

−125 kJ mol^{-1} because $\Delta H_f°$ (HNF)[27] = −71 kJ mol^{-1}, while

$\Delta H_f°$ (ANF)[62] = −196 kJ mol^{-1}. The stoichiometry of reaction 8 is speculative to the extent that N_2 and H_2 are IR-inactive. However, Koroban et al.[59] detected appreciable N_2 from slow decomposition of HNF at 70−100 °C. The formation of the additional products (N_2O, CO, H_2O, $HC(NO_2)_3$, and N_2H_4) shows that other reactions of HNF and ANF occur in parallel with reaction 8. First, the formation of N_2H_4(g) and $HC(NO_2)_3$(g) suggests that endothermic dissociation by reaction 9 takes

$$HNF(l) \rightarrow HC(NO_2)_3(g) + N_2H_4(g) \quad (9)$$

place at least to some extent. The heat of dissociation of the HNF is estimated[5] to be 171 kJ mol^{-1}, which is substantially higher than an estimate of the heat of sublimation[62] of ANF of about 105 kJ mol^{-1}. Second, reaction 10 gives the correct stoichiometry in Figure 7 below 260 °C for the thermally more stable products N_2O and CO. Reaction 10 is exothermic by

$$2ANF(l) \rightarrow N_2O + 2CO + 4H_2O + {}^5/_2O_2 + 3N_2 \quad (10)$$

about −360 kJ mol^{-1} of ANF. Taken together reactions 8−10 yield 305 kJ mol^{-1} of HNF. The choice above of Q = 75 kJ for eq 6 assumes that reaction 8 as written and reaction 9 are equally prevalent. The exothermicity of the foam layer is consistent with the temperature rise witnessed by the imbedded thermocouple.[27] Perhaps for this reason, HNF deflagrates at subatmospheric pressures.[27]

Above 260 °C, where a very steep temperature rise occurs in the thermocouple measurement,[27] Figure 7 reveals the formation of CO_2 for the first time. The amount of CO_2 increases with increasing temperature. Because of the large negative heat of formation of CO_2, exothermicity in turn increases with temperature. Above 350 °C, ANF, N_2O, and CO are frequently not detected, and in their place are the products shown in Figure 7 at 400 °C. These products are expected when deflagration dominates. Owing to the very different absolute absorbance values of NO and CO_2 (Table 1), the NO concentration is about twice that of CO_2. A significant quantity of H_2O forms along with a very small amount of N_2O. Neglecting N_2O, reaction 11 accounts for these IR-active products in the approximate amounts observed. This reaction is the most strongly exothermic (−623 kJ mol^{-1}) of reactions 8−11, in accordance with deflagration observed at these temperatures.[27,61]

$$HNF \rightarrow 2NO + CO_2 + 2H_2O + {}^3/_2N_2 + {}^1/_2H_2 \quad (11)$$

Reactions 8−11 are consistent with the products detected through a wide temperature range. In general, they become increasingly exothermic starting from the moderate decomposition rate of molten HNF at 130 °C through the deflagration stage above 350 °C. Thus, these reactions are plausible descriptions of the foam-layer and surface deflagration processes. Obviously, these stoichiometric reactions contain many elementary steps. Most would be very difficult to study in isolation in the melt-foam layer.

Surface Zone Description with Specific Reactions

In the examples above, the rates of all processes in the surface zone are mixed into one overall rate estimate. The frontier of this field is to determine the rates of identified individual reactions or steps. The foregoing discussion emphasizes the severity of this challenge. On the other hand, strategies can be created to circumvent the problem. The following description of the surface chemistry of HMX and RDX illustrates one approach.[63]

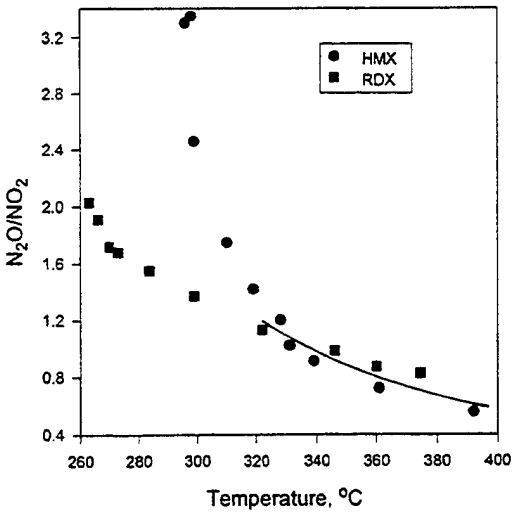

Figure 8. N_2O/NO_2 ratio for HMX and RDX by T-jump/FTIR spectroscopy.

Considerable direct and circumstantial evidence exists that HMX and RDX thermally decompose at high heating rates by two competing branches, (12) and (13).[46,64−71] Reaction 12 is

$$HMX\ (RDX) \rightarrow 4\ (3)\ [N_2O + CH_2O] \quad (12)$$

$$HMX\ (RDX) \rightarrow 4\ (3)\ [HONO + HCN] \quad (13)$$

exothermic by −121 kJ mol^{-1} for RDX.[17] Reaction 13 might be written with other products, such as $NO_2 + H_2CN$ or $NO_2 + HCN + H$, with different resulting heats of reaction. If written as shown, (13) is endothermic[17] by 117 kJ mol^{-1}. When these reactions occur in the bulk phase, we know experimentally that the overall process is approximately thermally neutral and that N_2O and NO_2 do not form at the same rate or time as CH_2O and HCN.[64,65] Although no mechanism is implied by (12) and (13), they do account for most of the initial gaseous products from rapid thermolysis of RDX and HMX. However, (12) and (13) compete differently at each temperature. T-jump/FTIR data are useful to determine the relative roles of (12) and (13) over a wide temperature range. In particular, the ratio of N_2O to NO_2 (HONO) indicates the branching ratio (Figure 8).[64] At lower temperatures, RDX and HMX differ considerably. Above about 320 °C, which is the temperature range of interest for the burning surface,[72−75] HMX and RDX decompose similarly by (12) and (13). If the rate of (12) or (13) is known and the branching ratio in Figure 8 is used, then the rate of the other reaction can be estimated. For simplicity, only HMX will be discussed here, but the analysis also applies for RDX.

The rate-determining step of reaction 13 is probably N−NO_2 homolysis, which is the first step during rapid thermal decomposition.[70] A simple estimate of this rate is obtained from thermal decomposition of dimethylnitramine. Six mostly gas-phase measurements and one thermochemical kinetics estimate of this rate are available.[76−81] These data do not agree, but the occurrence of a kinetic compensation effect (Figure 9) suggests that many of these measurements are biased by such factors as differences in experimental conditions, wall reactions, and secondary homogeneous reactions.[44] The thermochemical kinetics estimate[78] and the recent measurement by Lloyd et al.[77] are approximately the average of these data. The rate given by Lloyd et al.[77] was used to represent N−NO_2 homolysis in (13). For statistical reactions the value of A for

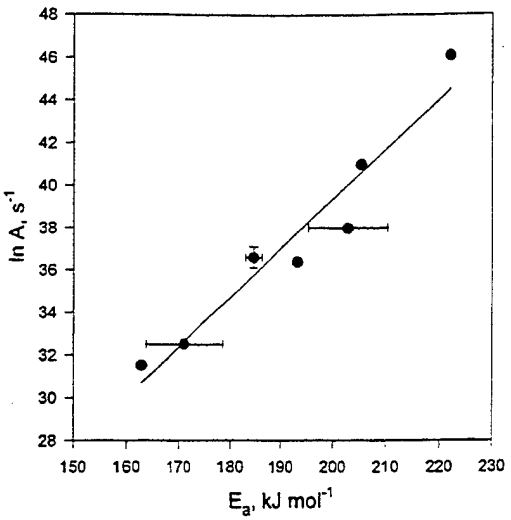

Figure 9. Plot of all Arrhenius data for dimethylnitramine thermal decomposition showing that a kinetic compensation effect exists.

HMX was increased by 4, yielding eq 14 (the units of E_a are kJ mol^{-1}).

$$k_{13} = 10^{16.5} \exp(-184/RT) \quad s^{-1} \tag{14}$$

N_2O and CH_2O form in reaction 12 by a multistep process. No simple secondary nitramine is known to yield only N_2O and CH_2O in order that the rate can be determined. However, the rate can be estimated from the rate of reaction 13 (eq 14) and the temperature dependence of the N_2O/NO_2 concentration ratio in Figure 8. The N_2O/NO_2 ratio should closely track k_{13}/k_{12} because N_2O and NO_2 are unique to reactions 12 and 13. By fixing the rate of (13) according to eq 14, the "best fit" Arrhenius constants for reaction 12 can be determined by curve fitting the ratio in Figure 8. Equation 15 results. This rate roughly

$$k_{12} = 10^{13.0} \exp(-144/RT) \quad s^{-1} \tag{15}$$

compares with those of primary nitramines which decompose to N_2O, an aldehyde, and H_2O.[82] For example, methylenedinitramine[83] has E_a = 148 kJ mol^{-1} and $A = 10^{15.6}$ s^{-1}, while ethylenedinitramine[84] yields E_a = 127 kJ mol^{-1} and $A = 10^{12.8}$ s^{-1}.

Equations 14 and 15 define the initial distribution of products from reactions 12 and 13 for HMX at least up to about the temperature of the burning surface. The pressure dependence of these rates is expected to be small because the reactions occur primarily in the condensed phase. However, the product distribution is affected indirectly by pressure because T_s changes with pressure. The products of (12) and (13) are the main reactants for the primary flame zone and, through their secondary chemistry, are a powerful source of heat. One of these reactions is discussed next.

According to T-jump/FTIR spectroscopy, a strongly exothermic secondary process in the molten film of HMX coincides with formation of NO, H_2O, and CO[63,64] and the decrease in the CH_2O and NO_2 concentrations. This is consistent with the occurrence of reaction 16. This reaction can also be balanced

$$CH_2O + NO_2 \rightarrow CO + NO + H_2O \quad (\Delta H = -186 \text{ kJ mol}^{-1}) \tag{16}$$

by using additional products, such as (17),[10] which gives a different value of ΔH. Reaction 17 differs from (16) by further oxidation of CO by NO_2. The product stoichiometry of (17) is

$$5CH_2O + 7NO_2 \rightarrow 3CO + 2CO_2 + 7NO + 5H_2O \tag{17}$$

most consistent with T-jump/FTIR spectroscopy.[63] Previous thermolysis[46,85] and controlled atmosphere studies[86] are consistent with (16) and (17). Because of the design of the T-jump/FTIR experiment, exothermicity will not be detected unless a large heat transfer coefficient exists between the sample and the filament.[30] This condition exists only if (16) and (17) appear as part of the two-phase zone as opposed to only the near-field gas phase. Several mass spectral and optical determinations, as well as computational schemes, of the gaseous products in the near field during combustion of HMX and RDX qualitatively support reactions 12, 13, 16, and 17.[11-14,17,66-68,69,87]

In practice, quantitative specifics of reactions 12, 13, 16, and 17 are difficult to obtain when they occur in the two-phase region. Reaction 16 is second-order in the gas phase,[88] but the reported rates disagree.[88-90] Greatest confidence can probably be placed in the kinetic measurements in Lin et al.[88] (eq 18),

$$k_{16} = 8.02 \times 10^2 T^{2.77} \exp(-28.9/T) \quad \text{cm}^3 \text{ mol}^{-1} \text{ s}^{-1} \tag{18}$$

because of the wide temperature range over which their mechanistic model seems to apply. Still, these kinetics were determined for the gas phase. The rate is likely to be different when (16) takes place in the condensed phase or at the gas–liquid interface. It is important to have the phase dependence of the rate, which is unknown at this time. For scaling of these rates by phase, the following systematic approach can be used. If the plausible assumption is made that the mechanism of reaction 16 is similar in the gas, liquid, and gas–liquid interfacial regions, then a kinetic compensation effect should exist in the Arrhenius parameters for these regions.[44] That is, the values of E_a and ln A can be increased or decreased pairwise so that a particular isokinetic temperature is maintained, but the rate for other temperatures or in other phases becomes different. Reaction 16 could be expected to have a value of E_a up to 30% larger in the liquid state compared to the vapor state, based on comparison with the global kinetics of decomposition of HMX and RDX.[44] ln A would scale upward as well to compensate.

Finally, the pressure dependence of reaction 16 has not been determined. The effect of pressure on a reaction depends on the change of the volume of activation in the rate-determining step.[91] This step in reaction 16 is transfer of H from CH_2O to NO_2,[88] which is likely to have a small volume of activation and, thus, small pressure dependence. However, in the surface reaction zone, reactions 16 and 17 take place as part of a multiphase layer in which CH_2O and NO_2 continuously form by reactions 12 and 13 and deplete by (16) and (17). In this case, the process is pressure dependent because the density of CH_2O and NO_2 in the control volume of the surface and near-field gaseous reaction zones[92] is higher at elevated pressure. Such a pressure dependence can be likened to hydrodynamic control. It is easiest to account for this effect of pressure on the rate by using the perfect gas law. Equation 19 results but overestimates the influence of high pressure.

$$k = (AP/RT)e^{-E_a/RT} \tag{19}$$

We now bring reactions 12, 13, and 16 together into a chemical description of the burning surface of HMX.[63] The rearranged version of the Arrhenius eq 7 is especially helpful for visualizing combustion and explosion chemistry.[60] For a pressure-dependent process, such as occurs for reaction 16, eq 7 is modified with eq 19. Of course, the effect at high pressure is given only qualitatively. Figure 10 is a plot of eq 7 for

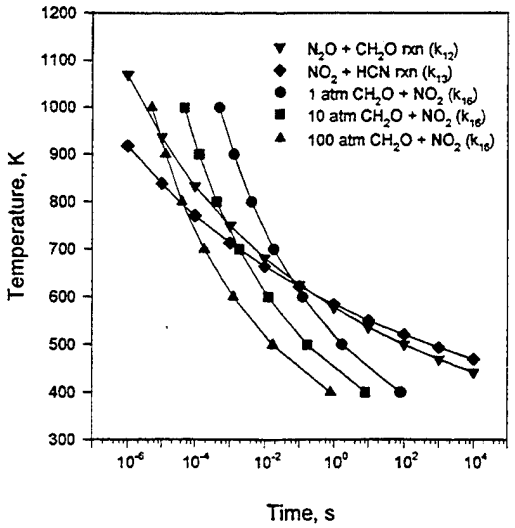

Figure 10. Composite Arrhenius plot of the two decomposition branches of HMX and the heat generation reaction. This a plot enables residence times and temperatures to be predicted considering only the chemistry.

reactions 12 and 13 of HMX. Reaction 16 is also plotted using eq 7 modified by eq 19. Focusing on reactions 12 and 13 first, (12) is faster than (13) at temperatures below about 600 K. Above 600 K, reaction 13 is faster. Extrapolation of these rates to higher temperatures is dubious, but they are probably reasonable to about 800 K, which is in the range of the burning surface temperature. At this temperature, reaction 13 clearly dominates in accordance with flash pyrolysis data.[70] The decomposition process of HMX and RDX becomes increasingly endothermic to the extent that reaction 13 dominates.

The secondary exothermic reaction 16 is the source of heat to sustain (12) and (13). Therefore, this exothermic reaction must occur at a faster rate than (12) or (13) for a given temperature; otherwise, the decomposition of HMX will cease. The behavior of reaction 16 at 1, 10, and 100 atm is shown in Figure 10. The reaction time for decomposition via (12) and (13) must be longer than (to the right of) the reaction time for (16), in order for (16) to be the source of heat. The temperature at which the secondary exothermic reaction is complete sets an upper limit on T_s in this simple description of the heterophase surface zone. Reading from Figure 10, the temperature required for completion of reactions 12 and 13 first, and then followed by (16) at 1 atm is about 620 K, and the residence time for complete reaction is about 100 ms. At 10 atm the surface temperature is roughly 710 K, and the residence time is about 1 ms. At 100 atm the surface temperature predicted from reaction 16 is about 800 K. This temperature is reasonable in that it is near the upper end of thermocouple measurements of the surface temperature of burning HMX as a function of pressure.[72-75]

Conclusion

As heat and mass transport and chemical kinetics computer codes become increasingly sophisticated, the little that we really know about the condensed phase and surface chemistry during combustion becomes glaring. Although some of the new data described herein have sufficient detail for incorporation into computational models, progress in the condensed-phase description lags well behind the gas-phase description. However, the fact that it has now become possible to make FTIR spectroscopic determinations of gaseous products from rapid, controlled heating of small samples, which at least outline some of the decomposition pathways and give some rate data relevant to combustion, is a step ahead in this complex field.

Acknowledgment. We are grateful to the Air Force Office of Scientific Research, Aerospace Sciences and Engineering, for support of this work on F49620-94-1-0053, and the Pennsylvania State University on Army Research Office Contract DAAL-92-G-0118.

References and Notes

(1) Wilfong, R. E.; Penner, S. S.; Daniels, F. *J. Phys. Colloid Chem.* **1950**, *54*, 863–872.
(2) Rice, O. K.; Ginell, R. *J. Phys. Colloid Chem.* **1950**, *54*, 885–917.
(3) Parr, R. G.; Crawford, Jr., B. L. *J. Phys. Colloid Chem.* **1950**, *54*, 929–954.
(4) Semenov, N. N. *Z. Phys.* **1928**, *42*, 571–582.
(5) Zel'dovich, Ya. B. *J. Exp. Theor. Phys. USSR* **1942**, *12*, 498–524.
(6) Belyaev, A. F. *Acta Phys. Chem. URSS* **1938**, *8*. 763–772.
(7) Summerfield, M.; Sutherland, G. S.; Webb, M. J.; Taback, H. J.; Hall, K. P. *Solid Propellant Rocket Research*; Academic Press: New York, 1960; pp 141–182.
(8) Beckstead, M. W.; Derr, R. L.; Price, C. F. *Proc. 13th Symp. (Int.) Combust.* **1970**, 1047–1056.
(9) Ben-Reuven, M.; Caveny, L. H.; Vichnevetsky, R. J.; Summerfield, M. *Proc. 16th Symp. (Int.) Combust.* **1976**, 1223–1233.
(10) Ben-Reuven, M.; Caveny, L. H. *AIAA J.* **1979**, *19*, 1276–1285.
(11) Cohen, N. S.; Lo, G. A.; Crowley, J. C. *AIAA J.* **1985**, *23*, 276–282.
(12) Ermolin, N. E.; Korobeinichev, O. P.; Kuibida, L. V.; Fomin, V. M. *Fiz. Gor. Vzy.* **1986**, *22*, 54–64.
(13) Ermolin, N. E.; Korobeinichev, O. P.; Kuibida, L. V.; Fomin, V. M. *Fiz. Gor. Vzy.* **1988**, *24*, 21–29.
(14) Hatch, R. L. *24th JANNAF Combust. Mtg., CPIA Publ. 476* **1987**, *I*, 383–391.
(15) Guirao, C.; Williams, F. A. *AIAA J.* **1971**, *9*, 1345–1356.
(16) Mitani, T.; Williams, F. A. *Proc. 21st Symp. (Int.) Combust.* **1986**, 1965–1974.
(17) Melius, C. F. *Chemistry and Physics of Energetic Materials*; Bulusu, S., Ed.; Kluwer: Dordrecht, The Netherlands, 1990; pp 51–78.
(18) Merzhanov, A. G. *Combust. Flame* **1969**, *13*, 143–156.
(19) Manelis, G. B.; Strunin, V. A. *Combust. Flame* **1971**, *17*, 69–78.
(20) Li, S. C.; Williams, F. A.; Margolis, S. B. *Combust. Flame* **1990**, *80*, 329–349.
(21) Huang, T. H.; Thynell, S. T.; Kuo, K. K. 30th JANNAF Combust. Mtg., Monterey, CA, Nov. 1993.
(22) Zenin, A. A. *Prog. Astronaut. Aeronaut.* **1992**, *143*, 197–231.
(23) Alexander, M. H.; Dagdigian, P. J.; Jacox, M. E.; Kolb, C. E.; Melius, C. F.; Rabitz, H.; Smooke, M. D.; Tsang, W. *Prog. Energy Combust. Sci.* **1991**, *17*, 263–296.
(24) Taylor, J. W. *Combust. Flame* **1962**, *6*, 103–107.
(25) Parr, T. P.; Hanson-Parr, D. M. *26th JANNAF Combust. Mtg., CPIA Publ. 529* **1989**, *I*, 27–37.
(26) Boggs, T. L.; Derr, R. L.; Beckstead, M. W. *AIAA J.* **1970**, *8*, 370–372.
(27) McHale, E. T.; von Elbe, G. *Combust. Sci. Technol.* **1970**, *2*, 227–237.
(28) Kubota, N. *Prog. Astronaut. Aeronaut.* **1984**, *90*, 1–52.
(29) Kuo, K. K. *Principles of Combustion*; John Wiley: New York, 1986.
(30) Brill, T. B.; Brush, P. J.; James, K. J.; Shepherd, J. E.; Pfeiffer, K. J. *Appl. Spectrosc.* **1992**, *46*, 900–911.
(31) (a) Shepherd, J. E.; Brill, T. B. *Proc. 10th Int. Symp. Detonation*, in press. (b) Thynell, S. T.; Gongwer, P. E.; Brill, T. B. 31st JANNAF Combustion Meeting, Sunnyvale, CA, Oct 1994.
(32) Timken, M. D.; Chen, J. K.; Brill, T. B. *Appl. Spectrosc.* **1990**, *44*, 701–706.
(33) Chen, J. K.; Brill, T. B. *Combust. Flame* **1991**, *85*, 479–488.
(34) Chen, J. K.; Brill, T. B. *Combust. Flame* **1991**, *85*, 157–168.
(35) Chen, J. K.; Brill, T. B. *Combust. Flame* **1991**, *85*, 217–232.
(36) Brill, T. B.; Patil, D. G.; Duterque, J.; Lengellé, G. *Combust. Flame* **1993**, *95*, 183–190.
(37) Brill, T. B. *Chemistry and Physics of Energetic Materials*; Bulusu, S., Ed.; Kluwer: Dordrecht, The Netherlands, 1990; pp 255–276, 277–326.
(38) Brill, T. B. *Anal. Chem.* **1989**, *61*, 897A–904A.
(39) Brill, T. B. *Prog. Energy Combust. Sci.* **1992**, *18*, 91–116.
(40) Garn, P. D. *Thermochim. Acta* **1979**, *28*, 185–187.
(41) Merzhanov, A. G.; Dubovitskii, F. I. *Proc. USSR Acad. Sci.* **1959**, *129*, 153–156.

(42) Lengellé, G. *AIAA J.* **1970**, *8*, 1989–1996.
(43) Beckstead, M. W. *26th JANNAF Combust. Mtg., CPIA Publ. 529* **1989**, *4*, 255–286.
(44) Brill, T. B.; Gongwer, P. E.; Williams, G. K. *J. Phys. Chem.* **1994**, *98*, 12242–12247.
(45) Brill, T. B.; Brush, P. J.; Patil, D. G. *Combust. Flame* **1993**, *92*, 178–186.
(46) Oyumi, Y.; Brill, T. B. *Combust. Flame* **1985**, *62*, 213–224.
(47) Chaiken, R. F. *Combust. Flame* **1959**, *3*, 285–300.
(48) Beckstead, M. W. Personal communication, 1992.
(49) Cohen, N. S.; Fleming, R. W.; Derr, R. L. *AIAA J.* **1974**, *12*, 212–218.
(50) Miller, R. R.; Stacer, H. L.; Goshgarian, B. *19th JANNAF Combust. Mtg., CPIA Publ. 366* **1982**, *II*, 67–79.
(51) See review by: Beck, W. H. *Combust. Flame* **1987**, *70*, 171–190.
(52) Tamura, S.; Gillham, J. K. *J. Appl. Polym. Sci.* **1978**, *22*, 1867–1884.
(53) Thomas, T. J.; Krishnamurthy, V. N.; Nandi, U. S. *J. Appl. Polym. Sci.* **1979**, *24*, 1797–1808.
(54) Rama Rao, M.; Radhakrishnan, T. S. *J. Polym. Sci.* **1981**, *19*, 3197–3208.
(55) Williams, G. K.; Brill, T. B. *Combust. Flame*, in press.
(56) Merzhanov, A. G.; Abramov, V. G. *Prop. Explos.* **1981**, *6*, 130–148.
(57) Zinn, J.; Mader, C. L. *J. Appl. Phys.* **1960**, *13*, 323–328.
(58) Dobratz, B. M. *LLNL Explosives Handbook, UCRL-52997* **1981**, 6–12.
(59) Koroban, V. A.; Smirnova, T. I.; Bashirova, T. N.; Svetlov, B. S. *Tr. Mosk. Khim.-Technol. Inst. im. D. I. Mendeleeva* **1979**, *104*, 38–44.
(60) Brill, T. B.; James, K. J. *J. Phys. Chem.* **1993**, *97*, 8759–8763.
(61) Johnson, H.; Oja, P. D. U.S. Patent 3,213,609; Oct 26, 1965. *CA* 86:P116121y.
(62) Miroshnichenko, E. A.; Lebedev, Yu. A.; Apin, A. Ya. *Russ. J. Phys. Chem.* **1967**, *41*, 791–792.
(63) Brill, T. B. *J. Propul. Power*, in press.
(64) Brill, T. B.; Brush, P. J. *Philos. Trans. R. Soc. London* **1992**, *339*, 377–385.
(65) Brill, T. B.; Brush, P. J.; Patil, D. G.; Chen, J. K. *Proc. 24th Symp. (Int.) Combust.* **1992**, 1907–1914.
(66) Fetherolf, B. L.; Liiva, P. M.; Litzinger, T. A.; Kuo, K. K. *28th JANNAF Combust. Mtg., CPIA Publ. 573* **1991**, *II*, 379–386.
(67) Trubert, J. F. *AGARD/PEP Mtg. Smokeless Prop., AGARD C.P.* **1985**, *391*.
(68) Korobeinichev, O. P.; Kuibida, L. V.; Orlov, V. N.; Tereshchenko, A. G.; Kutsenogii, K. P.; Mavliev, R. A.; Ermolin, N. E.; Fomin, V. M.; Emel'yanov, I. D. *Mass-Spectrom. Khim. Kinet.* **1985**, 73–93.
(69) Hanson-Parr, D. M.; Parr, T. 30th JANNAF Combust. Mtg. Nov 1993.
(70) Botcher, T. R.; Wight, C. A. *J. Phys. Chem.* **1993**, *97*, 9149–9153; **1994**, *98*, 5441–5444.
(71) Morgan, C. U.; Beyer, R. A. *Combust. Flame* **1979**, *36*, 99–101.
(72) Parr, D. M.; Parr, T. P. *20th JANNAF Combust. Mtg. CPIA Publ. 383*, **1983**, *I*, 281–291.
(73) Lengellé, G.; Duterque, J. AGARD/PEP Mtg. Smokeless Prop., AGARD C.P. 391, 1985.
(74) Mitani, T.; Takahasi, M. *West St. Sec. Combust. Inst. Spring Mtg.* **1988**, *3C*-050, 161–163.
(75) Kubota, N.; Sakamoto, S. *19th Int. Conf. ICT* **1988**, *65*–1 to 65–12.
(76) Korsunskii, B. L.; Dubovitskii, F. I. *Dokl. Akad. Nauk SSR* **1964**, *155*, 402–404.
(77) Lloyd, S. A.; Umstead, M. E.; Lin, M. C. *J. Energ. Mater.* **1985**, *3*, 187–210.
(78) Shaw, R.; Walker, F. E. *J. Phys. Chem.* **1977**, *81*, 2572–2576.
(79) McMillen, D. F.; Barker, J. R.; Lewis, K. E.; Trevor, P. L.; Golden, D. M. *SRI-Project PYU-5787*; Stanford Research International: Menlo Park, CA, 1979.
(80) Oxley, J. C.; Hiskey, M.; Naud, D.; Szekeres, R. *J. Phys. Chem.* **1992**, *96*, 2505–2509.
(81) Flournoy, J. M. *J. Chem. Phys.* **1962**, *36*, 1106–1107.
(82) Oyumi, Y.; Brill, T. B. *Combust. Flame* **1987**, *67*, 121–126.
(83) Tobin, M. C.; Fowler, J. P.; Hoffman, H. A.; Sauer, C. W. *J. Am. Chem. Soc.* **1954**, *76*, 3249–3253.
(84) Robertson, A. J. B. *Trans. Faraday Soc.* **1948**, *44*, 677–682.
(85) Cosgrove, J. D.; Owen, A. J. *Combust. Flame* **1974**, *22*, 13–18.
(86) Palopoli, S. F.; Brill, T. B. *Combust. Flame* **1991**, *87*, 45–60.
(87) Parr, T. P.; Hanson-Parr, D. M. *Prog. Astronaut. Aeronaut.* **1992**, *143*, 261–324.
(88) Lin, C. Y.; Wang, H. I.; Lin, M. C.; Melius, C. F. *Int. J. Chem. Kinet.* **1990**, *22*, 455–482.
(89) Pollard, F. H.; Wyatt, R. M. H. *Trans. Faraday Soc.* **1949**, *45*, 760–767.
(90) Fifer, R. A.; Holmes, H. E. *16th JANNAF Combust. Mtg., CPIA Publ. 308* **1979**, *II*, 35–50.
(91) LeNoble, W. J. *Prog. Phys. Org. Chem.* **1967**, *5*, 207–330.
(92) Oyumi, Y.; Brill, T. B. *Combust. Flame* **1987**, *68*, 209–216.

JP941796P

Chapter 4

Chemistry of a Burning Propellant Surface

Thomas B. Brill

1. INTRODUCTION

Combustion of energetic solids is the basis of rocket propulsion for space exploration and military technologies. Accurate models of combustion that contain chemical and fluid-mechanical details are greatly needed because atmospheric contamination and cost considerations limit ground-based testing. International disarmament treaties mandate disposal of stockpiled energetic materials. However, conventional disposal methods, such as open-pit burning and detonation, are increasingly restricted by environmental regulations. Description of the gaseous emission products frequently must be given before combustion is authorized. Manipulation of the combustion process may be necessary. Hence, combustion processes must be understood and predicted with ever greater accuracy.

Of the many chemistry issues that are important during the combustion of energetic solids, two are foremost in our laboratory. One program is focused on determining chemical details of the thin heterophase reaction zone on the surface of a burning energetic material. Identification of the early reaction steps and the first strongly exothermic reaction enables many characteristics of combustion to

THOMAS B. BRILL • Department of Chemistry, University of Delaware, Newark, Delaware 19716.

Combustion Efficiency and Air Quality, edited by István Hargittai and Tamás Vidóczy. Plenum Press, New York, 1995.

be understood and predicted. For instance, this knowledge makes it possible to couple the chemistry and transient characteristics of the near-surface flame zone to the condensed-phase processes. With the aggressive push toward "clean-burning" rocket propellant formulations (e.g., nonaluminized propellants and HCl-free exhaust), chemical details about the surface reaction zone must be incorporated into models that predict the performance and stability of the combustion process.

In a second program the relationship of the molecular structure and composition of the oxidizer or monopropellant to the gaseous products released upon fast thermolysis is being developed for a variety of energetic compounds. Such an understanding helps open the door to rational design of burn rate modifiers and new energetic molecules, whose combustion characteristics are predictable. Several advances in these two thrust areas are overviewed in this chapter.

2. EXPERIMENTAL APPROACHES

The chemical details of the surface reaction zone and near-surface, gas-phase reaction zone cannot be determined spectroscopically with the flame present because the most reactive species are consumed too rapidly. Moreover, the surface reaction zone is spatially very thin, has a steep temperature gradient, contains multiple phases, and may require three dimensions for an accurate description.

An alternate approach to gain the desired chemical description of the burning surface is to simulate the conditions, but in a manner that enables employment of spectroscopic diagnostics. For example, a small, thinly spread mass of sample in contact with a responsive heat source provides a snapshot view of the surface reaction zone. An outline of the chemical sequences is obtained from near-real-time spectroscopic monitoring of the gaseous products released from the surface and simultaneous measurement of the heat flow by a thermocouple or the resistance of the filament. Use of a cool, nonreactive atmosphere in the cell quenches the gaseous products as they form and enables them to be detected. The small amount of sample reduces the chance for ignition or explosion. The two methods of heating are ramp and temperature jump and are illustrated in Fig. 1.

Extensive description of the fast thermolysis/Fourier transform infrared (FTIR) experiments has been given by Oyumi and Brill (1985a), Cronin and Brill (1987), and Brill *et al.* (1992a). Figure 2 shows the design of the cell. The anti-reflection-coated 1.25-cm-thick × 2.5-cm diameter ZnSe windows are held in a 7.5-cm diameter aluminum cylinder by brass end caps. ZnSe was used because it is transparent in the mid-IR portion of the spectrum. It also has high tensile strength so that operation is possible at high pressure. The cell was designed to withstand a static internal pressure of 330 atm but is used primarily in the 0.1–60-atm range.

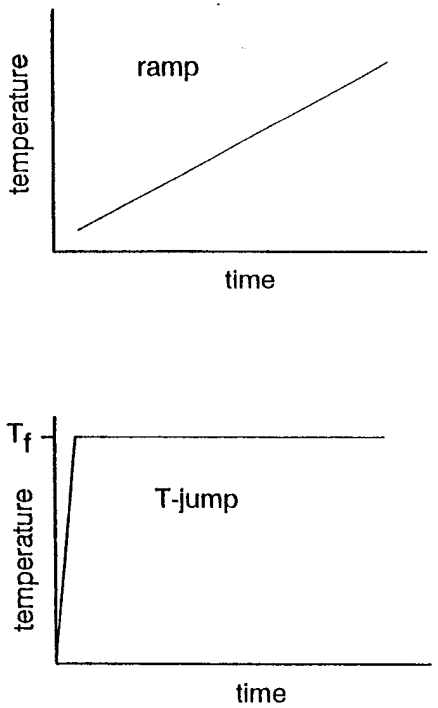

Figure 1. The two modes of fast thermolysis used for simulating surface pyrolysis conditions during combustion of a bulk material.

2.1. Fast Thermolysis by Ramp Heating

For the ramp heating mode in Fig. 1, the heater filament is a slightly creased nichrome IV ribbon (2.5 × 0.6 × 0.012 cm) supported on pressure-tight, electrical feed-through insulators. Although studies have not been conducted on a wide range of compounds, examination of compounds that are expected to be especially sensitive to catalysis by metals revealed little dependence of the thermolysis products on the filament material (Cronin and Brill, 1988). Typically, 1–2 mg of sample (solid, liquid, or a mixture) is heated on the filament by using a constant-voltage–variable-current controller. This method of heating has special value in the ramp-heating experiments whose results are described in Sections 3.2 and 4. In principle, any reasonable heating rate of the sample could be achieved, but 100–400°C/s is used because the spectral collection rate does not separate processes at higher heating rates. A static pressure of argon gas in the cell was set as desired in the 0.1–60-atm range.

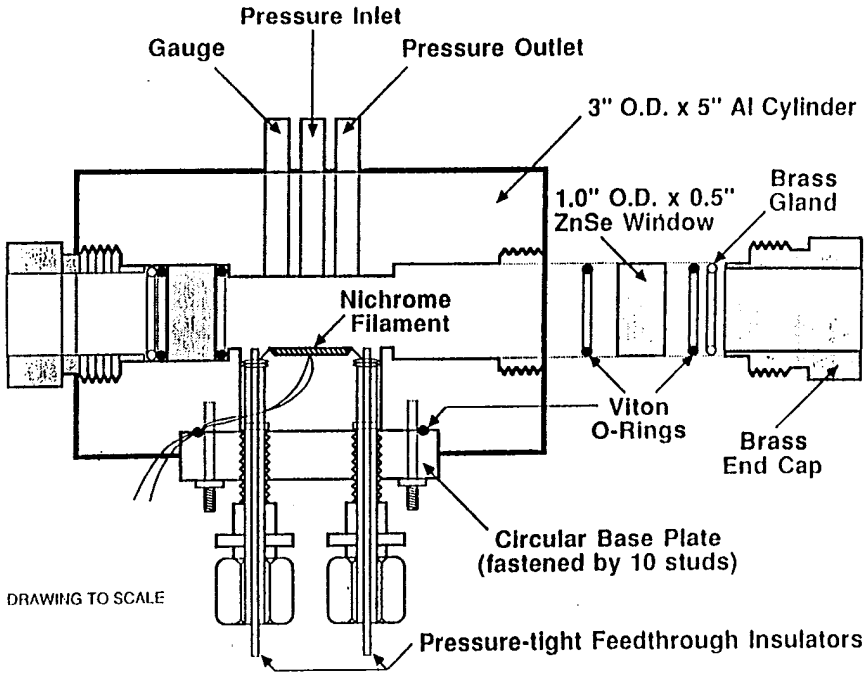

Figure 2. A cross-sectional drawing of the cell used for FTIR spectroscopy determination of the gaseous products from rapid thermolysis of solids and liquids.

2.2. Fast Thermolysis by Temperature Jump

The second mode of heating a sample is by temperature jumping the sample to a constant chosen temperature. T-jump/FTIR spectroscopy (Brill *et al.*, 1992a) permits isothermal decomposition studies to be performed on an approximately 200-μm-thick film of sample at temperatures up to 200°C above the onset of the conventionally accepted thermal decomposition temperature. This condition simulates the conditions that are present in the condensed phase in the heterophase reaction zone at the burning surface. Such studies require heating at a very high rate (e.g., 2000°C/s) to a high final filament temperature, T_f, and then holding at T_f for a period of time while monitoring the near-surface gas products and the heat flow. Since T_f can be set near the burning surface temperature, chemistry relevant to the surface zone during combustion is learned.

In experiments involving fast heating to a high temperature, the efficiency of heat transfer from the heat source to the sample is important, as is the ability of the heater circuit to respond to the endothermic and exothermic events taking place in

the sample (Shepherd and Brill, 1993). The time of each thermal change is matched with the spectra to reveal the sequence of events that take place during decomposition at T_f. Because much of the slower "cooking" chemistry is bypassed by rapid heating, the products and their relative concentrations indicate how the various decomposition reaction branches of a bulk material depend on temperature.

The thinness of the filament on which about 200 μg of sample is spread helps optimize the heat transfer and the responsiveness of the filament to temperature changes (Brill *et al.*, 1992a; Shepherd and Brill, 1993). A Pt filament replaces the nichrome filament shown in Fig. 2. A commercial pyroprobe controller (CDS Instruments) gives excellent heating control (Brill *et al.*, 1992a). The heating rate dT/dt and T_f of the Pt filament can be controlled independently. Furthermore, the endothermic and exothermic events can be sensed by observing the control voltage of the heater circuit. A positive deflection in the control voltage represents an endotherm whereas a negative deflection represents an exotherm.

Because of the value of collecting IR spectra at high temporal resolution (50–100 ms), the rapid-scan mode of an FTIR spectrometer (e.g., Nicolet 800, 60SX, or 20SXB) was used for all studies. With the beam focused several millimeters above the filament surface, the IR-active gas products from the fast-heated sample are detected in near real time. No significant change of pressure in the cell occurred due to the evolved gases because of the small sample size. If smoke or an aerosol with particle diameters less than 50 μm forms during thermolysis, wavelength-dependent dispersion causes the baseline to slope downward from short to long wavelength. However, the gas product concentrations still can be calculated in most cases. In all experiments the relative concentrations of the gas products compared to CO_2 were obtained from the effective width factors and absolute intensities of noninterfering absorbances for each product (Brill, 1992).

3. "CLEAN-BURNING" ROCKET PROPELLANTS

Interest is growing in oxidizers that might replace ammonium perchlorate (AP) in solid propellants. Upon combustion, AP liberates HCl and H_2O, forming an environmentally undesirable plume of HCl(aq). Nucleation of H_2O into droplets by HCl contributes to a prominently visible signature. These detracting features have rekindled interest in ammonium nitrate (AN) as an oxidizer. Unfortunately, AN has a low surface temperature and a low burn rate. The decomposition chemistry of AN is largely responsible for the low energy release. For example, two major decomposition reactions of AN, represented by Eqs. (1) and (2), are endothermic and mildly exothermic, respectively.

$$NH_4NO_3 \rightarrow NH_3(g) + HNO_3(g) \quad (1)$$

$$NH_4NO_3 \rightarrow N_2O + 2H_2O \quad (2)$$

The decomposition of AN can be compared with that of ammonium dinitramide (ADN), $NH_4[N(NO_2)_2]$ (Brill *et al.*, 1993a). Unlike AN, ADN decomposes very rapidly and is potentially a good propellant ingredient. Part of the additional energy release is attributable to the higher heat of formation of ADN [−35 kcal/mol (Swett, 1992)] compared to that of AN (−78 kcal/mol). Beyond this difference, the chemical reactions that cause ADN to decompose very exothermically are not obvious because the gas products from rapid thermolysis of ADN are similar to those of AN. Both compounds liberate HNO_3, NH_3, N_2O, NO_2, NO, H_2O, and N_2, although the mole fractions differ somewhat. As will be described below, the sequential chemistry leading up to the first large exothermic reaction of AN and ADN can be deduced by using T-jump/FTIR spectroscopy.

The fast decomposition sequence of HMX and RDX will also be presented below. HMX and RDX are well established as minimum-smoke, high-energy solid propellant ingredients. The sequential decomposition chemistry of these compounds and the first highly exothermic reaction in the surface zone are revealed by T-jump/FTIR spectroscopy.

3.1. The Chemistry of the Burning Surface Reaction Zone

The use of a sample thinly spread on the Pt foil filament described in Section 2 enables the burning surface to be simulated.

3.1.1. Ammonium Nitrate and Ammonium Dinitramide

Although pure AN will not burn at 1 atm, a sample can be driven by the T-jump method to a temperature that is at or above the measured surface temperature of AN burning at 25 atm (300–350°C) (Whittaker and Barham, 1964). Figure 3 shows the gas products and thermal response of a 200-μg mass film of AN heated at 2000°C/s to 383°C and held at 383°C. The concentration data in this plot are based on the scaled growth of the IR absorbance values for each product. The superposition of several stoichiometric reactions is indicated. Of course, many elementary steps are embedded in each of these stoichiometric reactions, but they are not determinable by T-jump/FTIR spectroscopy.

The first event is rapid endothermic melting of AN, as indicated by the upward deflection in the difference control voltage trace. The control voltage decreases upon completion of melting during the initial 0.5–1 s. The process turns markedly endothermic again at about 1 s. This second endothermic event corresponds to the appearance and growth of AN aerosol. AN aerosol forms from the endothermic dissociation of AN and desorption to $HNO_3(g) + NH_3(g)$, followed by recombination of NH_3 and HNO_3 in the gas phase (Table I, reaction A). Only

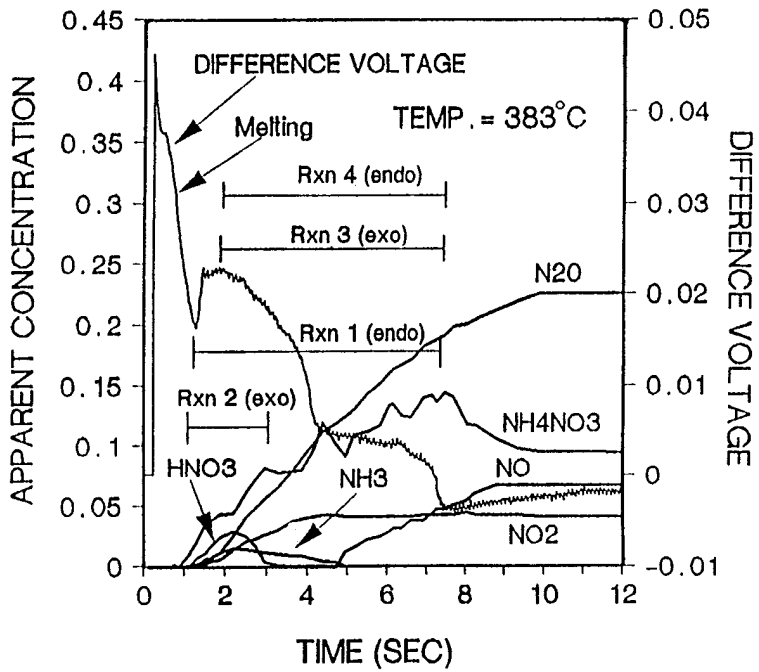

Figure 3. Gaseous products and heat changes of NH_4NO_3 (AN) at 383°C under 1 atm of Ar. The reactions are given in Scheme 1.

the endothermic first step of reaction A is included in the value of ΔH given for reaction A because the second step occurs in the cooler region of the cell away from the filament. Hence, the exothermic second step is not sensed by the filament. However, a white smoke of AN aerosol is visually observed. Despite the continuation of reaction A throughout the decomposition process as evidenced by the growth of the AN aerosol concentration, the decomposition process becomes less endothermic again at about 2 s. H_2O (not quantified) and excess HNO_3 form at this time, which is consistent with the occurrence of reaction B (Table I). This reaction is known, and its enthalpy has been deduced (Federoff, 1960). It is exothermic and would reduce the overall endothermicity of the decomposition process, as is found.

The process becomes still less endothermic from 2 to 4 s as the amount of HNO_3 diminishes. However, N_2O grows rapidly in concentration through this time, suggesting that the exothermic reaction C plays an increasingly important role. However, there is evidence of yet another reaction that occurs in parallel as indicated by the appearance of NO_2 and the eventual decrease in exothermicity again between 4 and 6 s. Also, NO, whose IR absorbance is very small, probably

Table I. Proposed Reactions That Account for the Products of High-Temperature Decomposition of NH_4NO_3 (AN) in Fig. 3

		Approx ΔH (kcal)
A.	$4[NH_4NO_3(l) \rightarrow HNO_3(g)+NH_3(g) \rightarrow NH_4NO_3(\text{solid aerosol})]$	4 (44)[a]
B.	$3[5NH_4NO_3(l) \rightarrow 2HNO_3 + 4N_2 + 9H_2O]$	3 (−35)
C.	$5[NH_4NO_3(l) \rightarrow N_2O + 2H_2O]$	5 (−13)
D.	$4NH_4NO_3(l) \rightarrow 2NH_3 + 3NO_2 + NO + N_2 + 5H_2O$	81
A–D.[b]	$28NH_4NNO_3(l) \rightarrow 6HNO_3 + 3NO_2 + NO + 2NH_3 + 5N_2O + 13N_2 + 42H_2O + 4NH_4NO_3(\text{aerosol})$	87

[a]ΔH for the desorption step only (see text).
[b]Gives the approximate IR-active gas product ratios at 2 s for AN at 383°C (Fig. 3).

forms earlier than is indicated in Fig. 3. Reaction D (Kaiser, 1935) accounts for these observations. Its endothermicity is superimposed on the exothermicity of reaction C and results in a leveling of the control voltage trace (heat flow is balanced) at 4–7 s. Reaction D is also a source of NH_3, which appears as a product for a much longer time than does HNO_3.

The multiplicative factors of the reactions in Table I were determined by the need to match the approximate relative concentrations of the gas products at a time when all of the reactions contribute. The concentrations at 2 s were chosen. The stoichiometry of the net reaction in Table I approximates that found at 2 s in Fig. 3. The enthalpy of the net reaction is slightly endothermic as written.

The formation of NH_3 and NO_2 by reaction D raises the possibility that the process could become exothermic when confined by pressure. The reaction of NH_3 and NO_2 becomes rapid and exothermic in the 330–530°C range (Rosser and Wise, 1956; Bedford and Thomas, 1972). However, significant generation of heat requires confinement to enhance the concentration of NH_3 and NO_2 in the hot zone around the condensed phase.

Figure 4 shows the decomposition process of a 200-μg film of AN heated at 2000°C/s to 415°C under 33 atm of Ar. The concentrations are shown in relative percentages throughout so that the behavior early in the decomposition process can be clearly seen. The melting endotherm initially dominates. The heats of reactions A–D leading to the formation of AN aerosol, N_2O, HNO_3, NH_3, and NO_2 are overall endothermic until 1.5 s. At this time the concentrations of NH_3 and NO_2 formed by reaction D drop markedly, and this drop is accompanied by an exotherm which suggests that the following reaction occurs:

$$2NH_3 + 2NO_2 \rightarrow N_2O + N_2 + 3H_2O \quad (3)$$

ΔH is about −148 kcal for this reaction as written. Under pressure, this nominally gas-phase reaction could occur in the heterogeneous gas-condensed phase (e.g.,

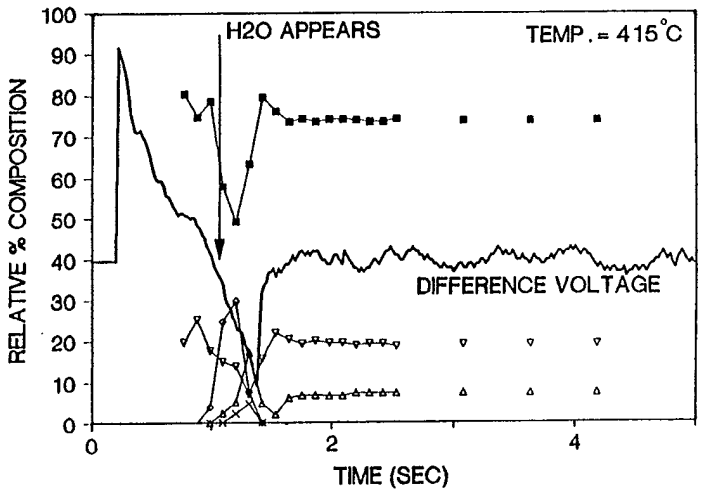

Figure 4. Gaseous products and heat changes of NH_4NO_3 (AN) at 415°C under 33 atm of Ar. △, NO_2; ◇, HNO_3; ×, NH_3; ■, N_2O; ▽, NH_4NO_3.

bubbles and voids) and contribute to the condensed-phase heat balance under combustion conditions.

The thermal decomposition behavior of bulk ADN is very different from that of AN despite the fact that similar gas products are formed upon rapid decomposition. Figure 5 shows T-jump/FTIR data for a 200-μg film of ADN heated at 2000°C/s to 260°C. This temperature compares with a preliminary surface temperature measurement of burning ADN of about 300°C (Fetherolf and Litzinger, 1992), which is surprisingly similar to that of AN. At the onset of decomposition, gas products form and, in contrast to the findings for AN, sharp exothermicity occurs instantly. The first detected products are mostly HNO_3, NH_3, and N_2O in roughly similar amounts. Minor quantities of NO_2, AN, and H_2O are also present in the initial spectrum.

The formation of HNO_3, NH_3, and N_2O in comparable amounts at the beginning suggests the presence of branch A in Table II. This mildly endothermic reaction may have a role during slow decomposition at lower temperatures. It appears to be a minor branch during rapid heating, especially because it does not account for the major heat release that is experimentally observed.

Branch B of Table II is proposed to dominate under rapid thermolysis conditions. Reaction a of branch B is dissociation of ADN to produce NH_3 and $HN(NO_2)_2$. $HN(NO_2)_2$ is not detected and probably homolyzes in the condensed phase at high temperature by reaction b to NO_2 and $HNNO_2$. Reactions a and b are endothermic. Because relatively large quantities of NH_3 and NO_2 occur early in branch B, much heat can be generated by reaction k in the gas phase near the

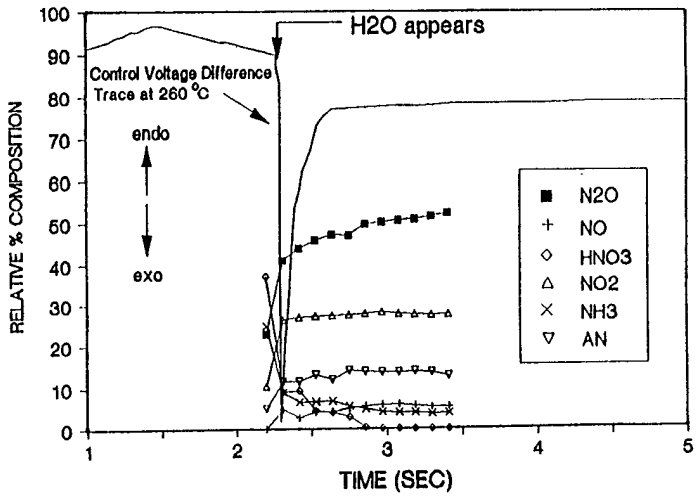

Figure 5. Gaseous products and heat changes of $NH_4[N(NO_2)_2]$ (ADN) at 260°C under 1 atm of Ar.

surface or even as part of the heterogeneous gas–liquid zone at the surface. The high exothermicity is evident in the large control voltage deflection at 2.3 s and provides the energy to complete the decomposition process very rapidly. Some NH_3 and NO_2 remain unreacted because they escape to the cooler atmosphere. Reactions c–h are plausible subsequent steps for decomposition of $HNNO_2$, but they are not determined by T-jump/FTIR spectroscopy. They are simply proposed as reasonable sources of stable products in the quantities detected. The net reaction i of branch B is mildly exothermic. Combining branches A and B yields the exothermic reaction j. Adding some gas-phase recombination of NH_3 and HNO_3 (reaction m) to account for the observed AN solid aerosol yields reaction n, whose stoichiometry approximates the experimentally observed gas product ratios observed at 2.5 s in Fig. 5. Reaction n is strongly exothermic largely because of reaction k, which is the reaction of NH_3 with NO_2.

For both AN and ADN, the exothermic $NH_3 + NO_2$ reaction appears to dominate the heat release stage. In the case of AN, the exotherm occurs only under a large applied pressure and is accompanied by a drop in the amounts of NH_3 and NO_2 that appear in the gas phase. Although the reaction of NH_3 with NO_2 appears to be responsible for this exotherm, the amount of NH_3 and NO_2 is smaller for AN than for ADN, and, therefore, much less heat is generated.

The rapid decomposition process of ADN is strongly exothermic early in the reaction scheme. This behavior is consistent with the ease of formation of a large amount of NH_3 and NO_2 in the early decomposition steps. Because the reaction of

Table II. Proposed Reactions Responsible for the Gases Released by $NH_4[N(NO_2)_2]$ (ADN) during High-Rate Pyrolysis

		Approx ΔH (kcal)
Branch A[a]		
	$3\{NH_4[N(NO_2)_2] \rightarrow NH_3 + HNO_3 + N_2O\}$	3(+11.5)
Branch B		
a.	$9\{NH_4[N(NO_2)_2] \rightarrow NH_3 + HN(NO_2)_2\}$	
b.	$9[HN(NO_2)_2 \rightarrow NO_2 + HNNO_2]$	
c.	$6[HNNO_2 \rightarrow N_2O + OH]$	
d.	$2[HNNO_2 + OH \rightarrow 2NO + H_2O]$	
e.	$HNNO_2 + NO \rightarrow NO_2 + HNNO$	
f.	$HNNO + OH \rightarrow N_2O + H_2O$	
g.	$3\{NH_3 + OH \rightarrow H_2O + NH_2\}$	
h.	$3[NH_2 + NO \rightarrow N_2 + H_2O]$	
i.[b]	$9NH_4[N(NO_2)_2] \rightarrow 6NH_3 + 7N_2O + 10NO_2 + 9H_2O + 3N_2$	−49
j.[c]	$12NH_4[N(NO_2)_2] \rightarrow 9NH_3 + 10N_2O + 10NO_2 + 9H_2O + 3N_2 + 3HNO_3$	−14
k.	$4NH_3 + 4NO_2 \rightarrow 3N_2 + 2NO + 6H_2O$	−309
l.[d]	$12NH_4[N(NO_2)_2] \rightarrow 5NH_3 + 10N_2O + 6NO_2 + 15H_2O + 2NO + 6N_2 + 3HNO_3$	−323
m.[e]	$2NH_3 + 2HNO_3 \rightarrow 2NH_4NO_3$(aerosol)	
n.[f]	$12NH_4[N(NO_2)_2] \rightarrow 3NH_3 + 10N_2O + 6NO_2 + 15H_2O + 2NO + 6N_2 + HNO_3 + 2NH_4NO_3$	−323

[a]Assumes ΔH_f(ADN) = −35 kcal/mol, and $\Delta H[HNO_3(g)]$ = −33 kcal/mol.
[b]Sum of reactions a–h.
[c]Sum of branches A and B.
[d]Sum of reactions j and k.
[e]Occurs in the gas phase away from surface so reaction m is not included in ΔH.
[f]Sum of l and m gives the approximate gas-phase stoichiometry at the end of the exotherm (Fig. 5).

NH_3 and NO_2 can dominate early and produces a large amount of heat, the overall decomposition and gasification process occurs at a much high rate for ADN than AN. Therefore, for both AN and ADN the reaction of NH_3 with NO_2 is implicated as the main source of heat when the pure material is decomposed at high temperature. For AN, this reaction only becomes important under confinement, such as by the application of pressure.

3.1.2. Nitramines

Nitramines, such as HMX and RDX (Scheme 1), are especially important as minimum-smoke, high-energy explosive and propellant ingredients. The decom-

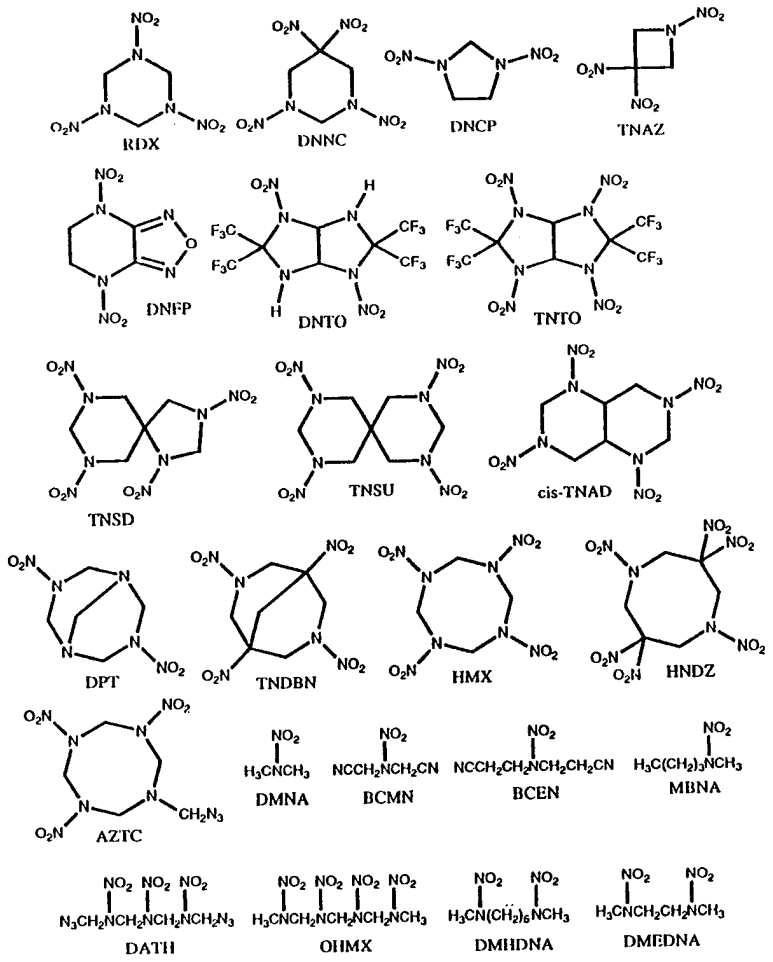

Scheme 1

position processes of HMX (Brill and Brush, 1992) and RDX (Brill *et al.*, 1992b) are similar, and so only HMX will be described.

Figure 6 shows T-jump/FTIR data for a thin film of HMX heated at 2000°C/s to 298°C and then held isothermally while IR spectra of the near-surface gas products are recorded. The global decomposition branches represented by the following reactions occur for bulk RDX and HMX:

$$HMX \rightarrow 4(NO_2 + HCN + H) \quad (4)$$

$$HMX \rightarrow 4(N_2O + CH_2O) \quad (5)$$

Reactions (4) and (5) imply that N_2O and NO_2 should form simultaneously with CH_2O and HCN. This is not found at any temperature studied. Rather, N_2O and

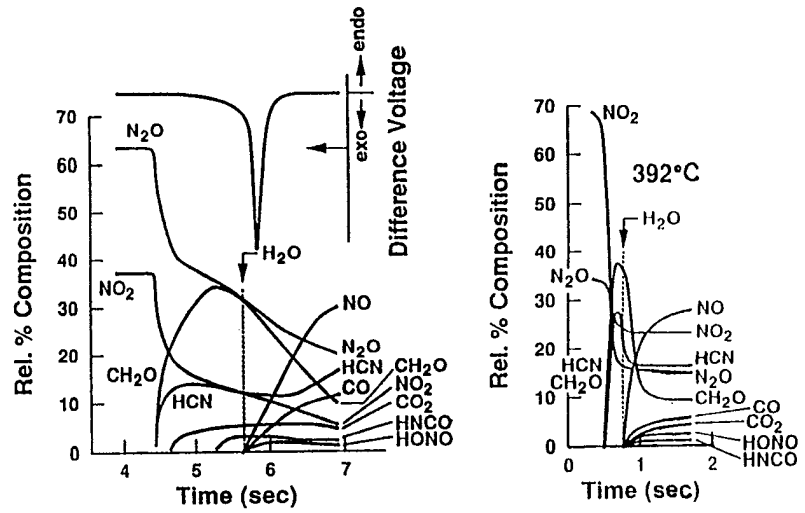

Figure 6. Gaseous products and heat changes of HMX at 298°C (left) and products at 392°C (right) under 2.5 atm of Ar.

NO_2 appear before CH_2O and HCN, which form from the residue left by elimination of N_2O and NO_2. This residue is a mixture of products like hydroxymethylformamide and acetamide (Cosgrove and Owen, 1974; Kimura and Kubota, 1980; Karpowicz and Brill, 1984; Behrens, 1990), which decompose and delay the release of CH_2O, HCN, and HNCO (Behrens, 1990; Palopoli and Brill, 1991).

The growth of the total IR absorbance of the products accelerates between 4.0 and 5.5 s despite the constant heat flow from the filament, which implies that autocatalysis occurs in this stage of decomposition of HMX and RDX. Moreover, the control voltage trace in Fig. 6 reveals only mild exothermicity between 4 and 5.5 s when reactions (4) and (5) dominate. Thus, these reactions release little energy in the condensed phase.

A sharp exotherm develops at 5.5 s. The following secondary reaction appears to be responsible because CH_2O and NO_2 are consumed as NO, CO, and H_2O appear:

$$5CH_2O + 7NO_2 \rightarrow 7NO + 3CO + 2CO_2 + 5H_2O \quad (6)$$

Figure 6 shows that more NO than CO forms, in accordance with reaction (6). Reaction (6) is highly exothermic as written ($\Delta H = -320$ kcal), and, by the large exotherm in Fig. 6, it is the main source of heat in the heterogeneous condensed-phase and near-surface gas-phase reaction zone. These conclusions also apply at 392°C (Fig. 6) except that the time scale is compressed. Hence, this description of

the decomposition of HMX at 298°C applies as well at the surface reaction zone temperature (350–400°C) during combustion. However, the branching ratio of reactions (4) and (5) depends on temperature and favors reaction (4) at higher temperature (Brill and Brush, 1992).

3.2. Structure/Decomposition Relationships among Nitramines

As noted in Section 3.1.2, nitramines are an important class of compounds which produce high energy and minimum smoke on combustion. The decomposition products NO_2, NO, HONO, and N_2O can function as oxidizers in the heterophase surface zone and the primary and secondary flame zone, while CH_2O and HCN are fuels in the surface and the flame zone. However, the relative amounts of these fuel and oxidizer molecules depend on the structure and composition of the parent molecule. This relationship has been developed from fast thermolysis/FTIR spectroscopy in which ramp heating is employed. The relative concentrations of the initially detected gas products are useful to achieve this description.

3.2.1. Formation of NO_2

The formation of NO_2 by reaction (4) is important for nitramine combustion because NO_2 is an oxidizer in the primary (near surface) flame zone. It seems plausible that the length of the N–N bond in secondary nitramines might be an important factor in the tendency of the N–N bond to homolyze and liberate NO_2. It is necessary to draw these conclusions from rapidly heated samples and to detect the species in rapidly recorded FTIR spectra (e.g., at 50–100-ms intervals). Otherwise, secondary reactions of NO_2 obliterate the relationship of the NO_2 concentration to the structure of the parent molecule. However, even simple homolysis of the N–N bond in the condensed phase is, overall, a complicated process. Intermolecular activity possibly occurs. At the very least, some of the NO_2 must diffuse through and desorb from the heterogeneous environment before it is detected. The most severe complication would be if N–N bond homolysis followed or competed with another decomposition route, such that the initial N–N bond distance is no longer the controlling factor. If this were the case, then structure–decomposition relationships involving NO_2 formation would be disguised.

The crystal structures of nitramines are needed for this comparison. Fortunately, many are available. In Fig. 7 (Brill and Oyumi, 1986a; Oyumi *et al.*, 1987a) the average N–N bond distance for a series of secondary nitramines, R_2NNO_2, is plotted versus the average asymmetric $-NO_2$ stretching frequency from the IR spectrum. The compound identities are given in Scheme 1. A reasonably good relationship exists between these two parameters, suggesting that

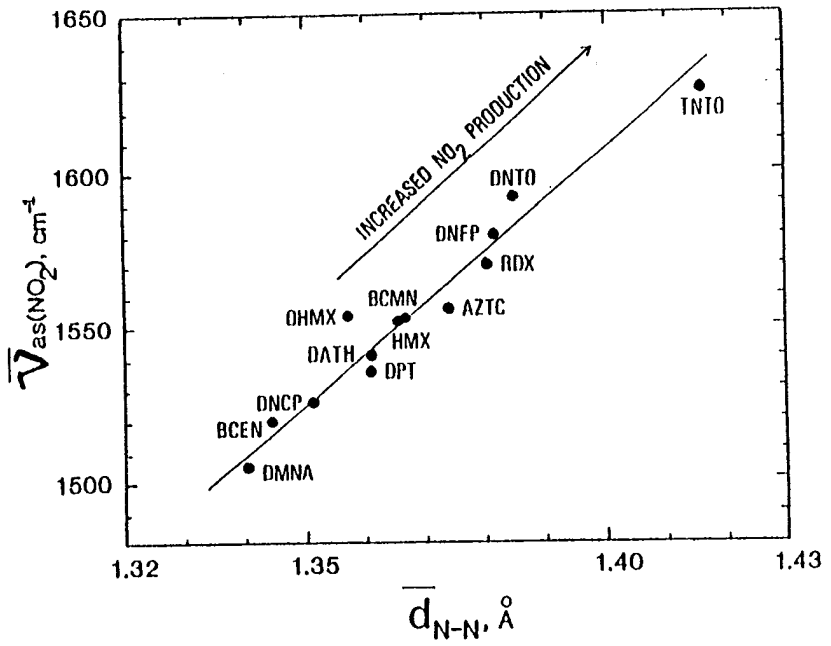

Figure 7. The average asymmetric $-NO_2$ stretching frequency plotted against the average N–NO_2 bond distance for selected secondary nitramines. The compounds on the right release a large amount of NO_2(g) upon fast thermolysis.

the force constant of $-NO_2$ stretching greatly depends on the amount of electron density that the $-NO_2$ group shares with the adjacent N–N bond. From fast thermolysis of these compounds, it is found that NO_2(g) is the dominant, initially detected product for compounds toward the right side of this plot. NO_2 was either not detected or was detected as a less abundant product from compounds on the left side. Thus, long N–N bonds favor N–N scission during fast thermolysis. With reasonable confidence, one can predict the amount of NO_2 that is likely to be generated by fast thermolysis of a secondary nitramine from its IR spectrum or its crystal structure.

Although several exceptions exist to the structure/reactivity relationship for NO_2(g) generation (Oyumi and Brill, 1988), it is encouraging that most secondary nitramines thermolyze in the condensed phase in a systematically predictable way. Thermal reactions in the neat condensed phase are complex, but the correlation above gives hope for uncovering and refining patterns that can be applied in practice to propellant ignition and explosives initiation.

3.2.2. Formation of HONO(g)

Closely related to NO_2 formation is the formation of HONO. At least one additional process, that of H· transfer, is required before HONO(g) is detected from nitramine decomposition. Kinetic modeling indicates that HONO formation plays a role in the N–N bond fission process (Melius and Binkley, 1986). The formation of HONO has been invoked in many previous studies of nitramines to rationalize the formation of other products, but HONO itself was very rarely detected prior to fast thermolysis/FTIR spectroscopy studies (Brill and Oyumi, 1986b). HONO is a reactive and, thus, transient molecule that is not observed without rapid heating and near-real-time product detection.

After examination of a large number of nitramines heated at 145–180°C/s under 1 atm of Ar, it was discovered that the initial relative percent composition of HONO(g) depends strongly on the composition of the parent secondary nitramine (Brill and Oyumi, 1986b). In one instance, HONO represented nearly 60% of the initially detected gaseous products. A qualitative relationship was discovered between the ratio of the number of H atoms to NO_2 groups in the parent molecule and the initial percentage of HONO in the gas products. The relationship is shown in Fig. 8. The leveling off at the higher H/NO_2 values is attributable to dilution of the HONO by other gases. Qualitative insight into the processes by which

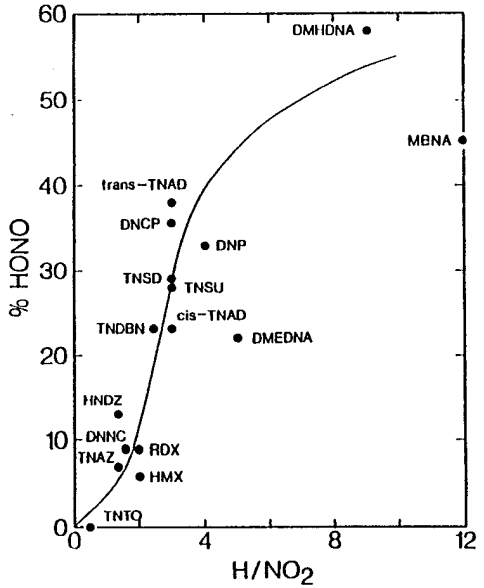

Figure 8. The percentage of HONO in the quantified gaseous products after thermolysis of secondary nitramines compared to the H/NO_2 ratio in the parent molecule.

HONO is formed from the condensed phase is contained in the pattern of Fig. 8. The concentration of HONO must depend on the adventitious encounter of H· and NO_2· (or an NO_2· source) in the condensed phase. Statistically increasing this chance for contact (the H/NO_2 ratio) enhances the HONO concentration. Determination of the molecularity, the nature of the transition state, and any other aspects of the reaction mechanism is beyond extension of these condensed-phase results. Many species could liberate H·, but it is interesting to note that C–H bond fission has been proposed to be rate determining in nitramine decomposition (Shackelford *et al.*, 1985; Bulusu *et al.*, 1986) and combustion (Shackelford, 1987). H_2O assists in HONO formation in the condensed phase (Melius *et al.*, 1991), but the pattern in Fig. 8 would still need to be accommodated if this were the case. Compounds producing the largest amount of HONO are not the ones expected to produce the largest amount of H_2O because of their low oxygen content. Also, the four- and five-center concerted reactions, whose connectivities are shown in Scheme 2 and which could be important in the gas phase (Shaw and

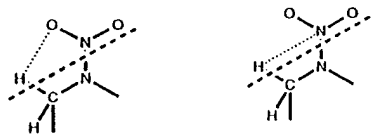

Scheme 2

Walker, 1977), do not appear to dominate in the condensed phase. If they did, only a $-CH_2-$ fragment adjacent to the nitramine would be required to produce HONO. All nitramines having this linkage should produce the same amount of HONO, which they do not.

The most plausible explanation for HONO formation in the condensed phase remains the chance contact between H· and NO_2·, possibly with H_2O as a catalyst. In keeping with this notion, steric crowding of H and NO_2 groups in a molecule enhances the initial HONO concentration (Brill and Oyumi, 1986b). It is interesting to note that if the H/NO_2 ratio is calculated using only the H atoms from secondary carbon atoms ($-CH_2-$), the fit is slightly more linear, as shown in Fig. 9. This suggests that $-CH_2-$ groups in these molecules may be somewhat more efficient H· sources than $-CH_3$ groups. Nitramines having only tertiary carbon atoms (≡CH) do not produce HONO (Brill and Oyumi, 1986a; Oyumi *et al.*, 1987a).

3.2.3. Formation of N_2O(g)

As noted in Section 3.1.2, the relative role of reactions (4) and (5) is temperature dependent for a given compound. A few secondary nitramines are found to liberate a large quantity of N_2O compared to NO_2 or HONO (Brill *et al.*,

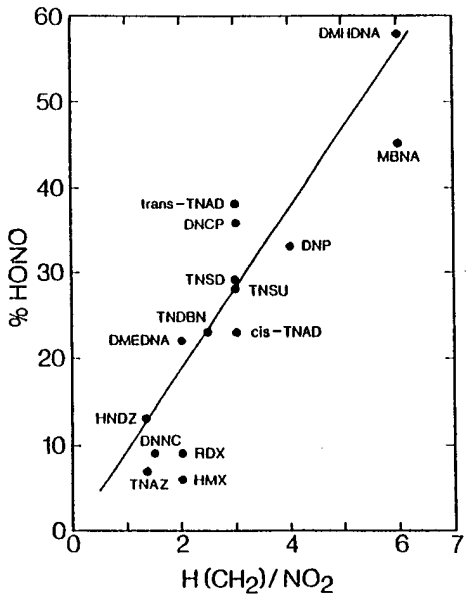

Figure 9. The plot equivalent to Fig. 8 but using only H from the $-CH_2-$ groups in the H/NO_2 ratio.

67

1984; Oyumi and Brill, 1985a; Oyumi *et al.*, 1986a, 1987b,c). Conversely, other nitramines generate N_2O as only a few percent of the total gaseous products (Brill and Oyumi, 1986b; Oyumi and Brill, 1985b; Oyumi *et al.*, 1985, 1986b), while still others produce no N_2O at all (Oyumi *et al.*, 1987a; Oyumi and Brill, 1988).

All of the compounds liberating N_2O have in common a $-CH_2-$ group straddled by two nitrogen atoms, i.e., $-(NO_2)NCH_2N(NO_2)-$. This feature appears to be the only structural requirement for N_2O formation by a secondary nitramine.

Three secondary nitramines that liberate virtually all of their nitramine nitrogen atoms as N_2O are AZTC (Brill *et al.*, 1984), DPT (Oyumi *et al.*, 1986a), and DATH (Oyumi *et al.*, 1987b). The N–N bond distances in these compounds (1.355–1.375 Å) suggest that the abundance of gaseous NO_2 and N_2O should be competitive based on the observations in Section 3.2.1. NO_2 and N_2O appear together at temperatures slightly above the decomposition point of DATH, but N_2O dominates around the decomposition point. The observation that these molecules produce little or no NO_2 at the decomposition temperature emphasizes that the balance of the multiple decomposition pathways is easily shifted in nitramines by the temperature and structure. Both DATH and AZTC produce HN_3 (and no doubt N_2) initially. Thus, the azide group begins the thermolysis reaction. By either radical or electron-pair migration, the backbone tends toward depolymerization in preference to N–N bond homolysis. During depolymerization, oxygen must transfer, but the data do not indicate how. Possibly the same type of reaction in DPT is initiated by the homolysis of a C–N bond in the $-CH_2-$ group bridging the non-nitrated amine groups.

3.2.4. Formation of $CH_2O(g)$

Formaldehyde is an important fuel in the primary flame of nitramines. As we have just noted that a $-CH_2-$ group straddled by two nitramine groups appears to be important, if not required, to produce N_2O from a pure secondary nitramine compound, a logical implication is that transfer of an oxygen atom from the NNO_2 group, perhaps to the adjacent $-CH_2-$ group, liberates CH_2O along with N_2O. $H\cdot$, H^+, $OH\cdot$, or H_2O could assist in lowering the barrier of this oxygen transfer reaction. While DPT, AZTC, and DATH do indeed have this unit and liberate a large amount of CH_2O along with N_2O, several compounds do not follow this simple pattern with respect to CH_2O formation. DNCP and most bicyclonitramines (Brill and Oyumi, 1986b) have the $-(NO_2)NCH_2N(NO_2)-$ unit but liberate no CH_2O. Reasonable explanations exist. DNCP has an unusually thermally stable five-membered ring (Oyumi and Brill, 1988), so that $N-NO_2$ homolysis is the preferred decomposition route. The bicyclonitramines are strong HONO generators (Brill and Oyumi, 1986b). Loss of NO_2 and the removal of H atoms to form HONO could interfere with the tendency to form CH_2O.

The notion that CH_2O and N_2O form simultaneously during the condensed-phase decomposition of nitramines should be discarded. As illustrated in Section 3.1.2, in experiments using T-jump/FTIR spectroscopy and simultaneous thermogravimetry coupled with modulated beam mass spectrometry (Behrens, 1987), N_2O [and NO_2 (Brill and Brush, 1992)] was found to reach the gas phase distinctly ahead of CH_2O and HCN. CH_2O is retained in the condensed phase as part of a nonvolatile residue that decomposes more slowly than the parent nitramines decompose.

4. MODIFICATION OF BURNING RATES

The difficulty of accelerating the burning rate of RDX and HMX by the use of additives and catalysts has stimulated much research and discussion (Schwartz *et al.*, 1984). In principle, potential burn rate modifiers could be intelligently identified with knowledge of (1) the rate-determining decomposition reactions in the condensed and the gas phase and (2) the dominant heat-generating reactions in the near-surface gas phase and surface regions. From the results described in Section 3.1.2, it is easy to reconcile why the burn rates of nitramine-containing propellants are difficult to modify. A dominating early heat generation reaction of

many nitramines is experimentally revealed to be reaction (6) (Brill and Brush, 1992; Brill *et al.*, 1992b, 1993b). Note, however, that the reactants CH_2O and NO_2 of reaction (6) are themselves products of the two separate decomposition branches of RDX and HMX, reactions (4) and (5). If either reaction (4) or (5) were accelerated at the expense of the other, then the burn rate of the nitramine would be unlikely to increase significantly. Both reactions must be about equally prevalent to provide the reactants for reaction (6). Therefore, strategies for greatly accelerating the burning rate of nitramines must either completely alter the decomposition mechanism or be based on additives that accelerate the rate of both reactions (4) and (5) without altering the branching ratio. For these reasons, it is not surprising that acceleration of the burning rate of a nitramine propellant is difficult.

Burn rate modification research in our laboratory has emphasized *suppression* of fast-burning propellants, such as ammonium perchlorate-based composite propellants. In principle, the approach is applicable to any solid rocket propellant. The concept is to form a thin layer of a relatively thermally stable material on the surface of the propellant during combustion. This notion evolved from studies of the mechanism (Stoner and Brill, 1991) by which DAF and DAG (Scheme 3)

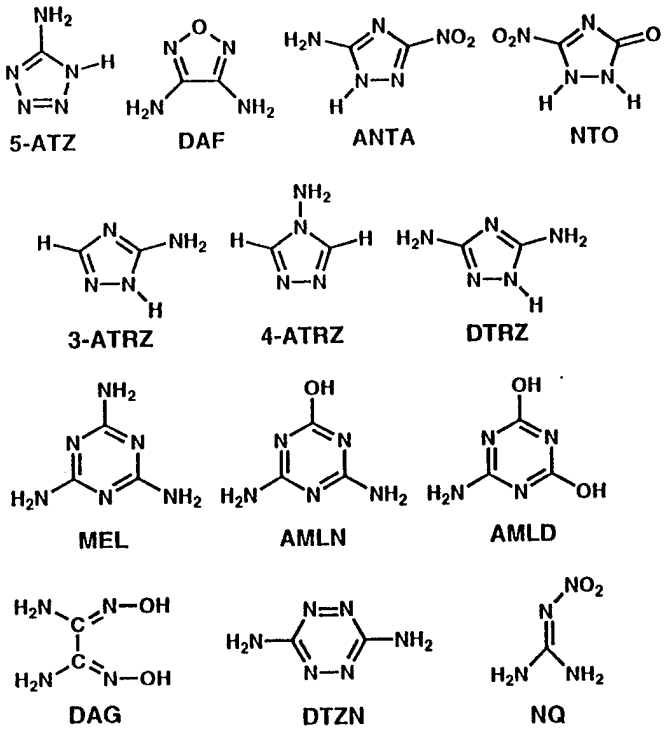

Scheme 3

suppress the burn rate of ammonium perchlorate-based composite propellants (Willer *et al.*, 1991). Upon thermal decomposition, DAG and DAF form high-molecular-weight, thermally stable, cyclic azines in addition to low-molecular-weight gaseous products (Stoner and Brill, 1991). The cyclic azines melem and melon (Scheme 4) appear to form from DAG and DAF via the ammonium

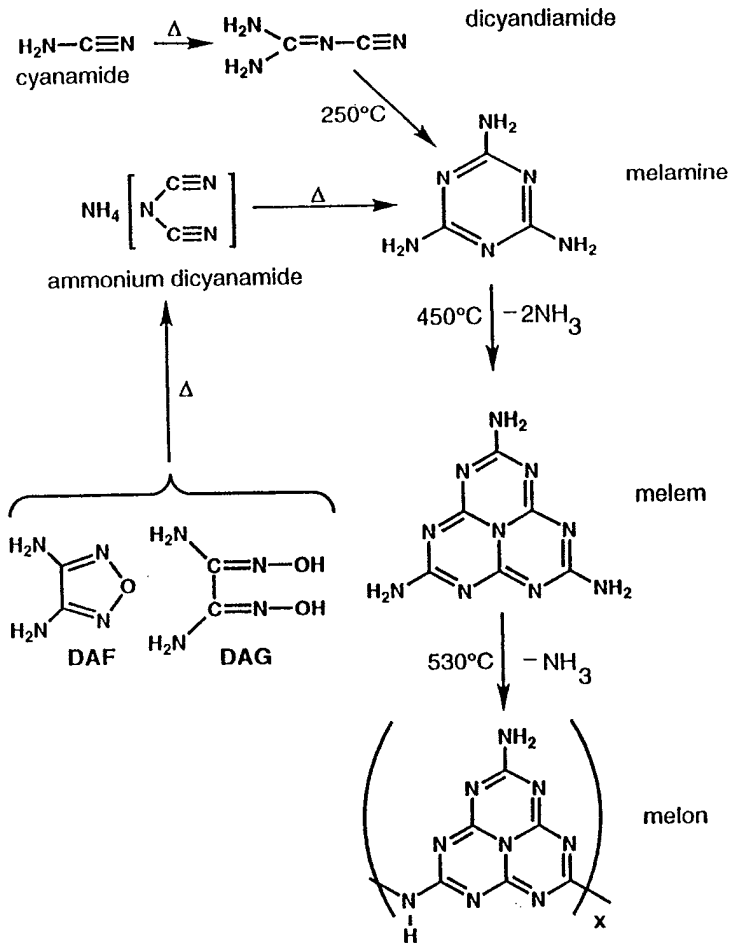

Scheme 4

dicyanamide intermediate. Melon is stable up to at least 650°C. Melon could transiently accumulate on the burning surface and suppress the regression rate by retarding the mass transfer from the condensed phase to the gas phase, and retarding the heat transfer from the flame zone to the reacting heterogeneous condensed phase (Stoner and Brill, 1991).

It has long been known that cyanamide dimerizes to dicyandiamide (Scheme 4) and, upon heating, cyclizes to melamine, melem, and melon (Bann and Miller, 1958). Nitroguanidine (NQ) is known to form melamine upon heating (Stals and Pitt, 1975; Volk, 1985; Lee and Back, 1988). The observation that DAG and DAF react similarly (Stoner and Brill, 1991) suggested that the presence of a NH_2–C–N linkage in the parent molecule might lead to thermally stable cyclic azines. Subsequently, 5-ATZ, which possesses this linkage, was found to produce NH_2CN(g) and a solid residue upon heating (Gao *et al.*, 1991). The residue has an IR spectrum characteristic of melon. In fact, as shown in Fig. 10, all of the compounds in Scheme 3 form a melon-like solid residue when heated above about 400°C (Williams *et al.*, 1994). The NH_2–C–N linkage is present in each of these molecules except for two. NTO only possesses the NH–C–N linkage, implying that H atom migration occurs to produce the NH_2–C–N linkage in the decomposition scheme. 4-ATRZ lacks the NH_n–C–N linkage altogether, which implies

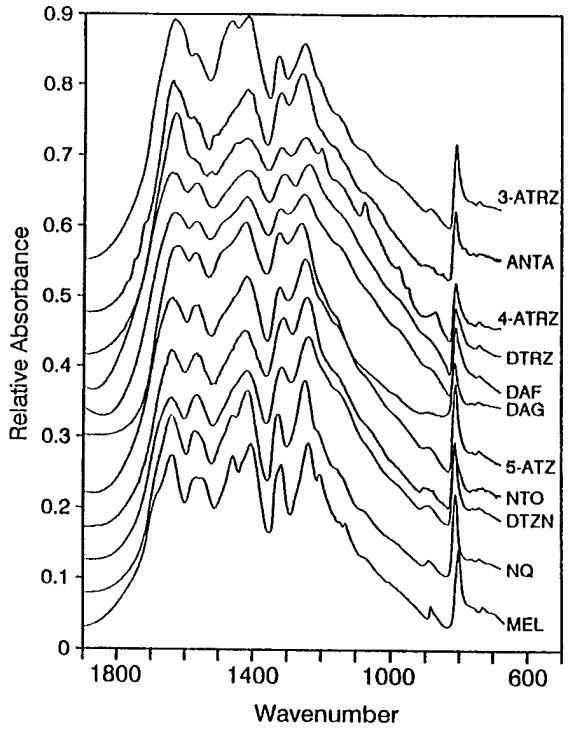

Figure 10. The IR spectra in the ring mode region of compounds (Scheme 5) that upon heating to 600–650°C form residues which are melon-like cyclic azines (Scheme 6).

that relocation of the $-NH_2$ group onto a carbon atom must occur in the decomposition scheme.

The compounds in Scheme 3 are probably "the tip of the iceberg" as potential suppressants of the burn rate of solid propellants by the mechanism of formation of cyclic azines. The presence of the NH_2–C–N unit enhances the chance of formation of cyclic azines but is not a necessary condition.

Information about rapid pyrolysis processes at the surface of energetic and nonenergetic materials provides considerable insight into how solids burn and how burning can be controlled. In turn, these details stimulate design criteria and models based on experimental fact, as opposed to empirical supposition, that improve combustion performance and control.

ACKNOWLEDGMENTS. The students referenced in this chapter have performed the experimental work that is summarized: Peter Brush, Dilip Patil, Aiming Gao, Yoshio Oyumi, Charles Stoner, and Graylon Williams. I am grateful for financial support from the Air Force Office of Scientific Research, Aerospace Sciences Directorate, and Thiokol Corporation.

REFERENCES

Bann, B., and Miller, S. A., 1958, Melamine and derivatives of melamine, *Chem. Rev.* **58**:131–172.

Bedford, G., and Thomas, J. H., 1972, Reaction between ammonia and nitrogen dioxide, *J. Chem. Soc., Faraday Trans. 1*, **1972**:2163–2170.

Behrens, R., 1987, Simultaneous thermogravimetric modulated beam mass spectroscopy and time-of-flight velocity spectra measurements: Thermal decomposition mechanisms of RDX and HMX, in *Chemical Propulsion Information Agency Publication*, Vol. 476, Part 1, pp. 333–342.

Behrens, R., 1990, Thermal decomposition of energetic materials: Temporal behaviors of the rates of formation of the gaseous pyrolysis products of the condensed-phase decomposition of HMX, *J. Phys. Chem.* **94**:6706–6718.

Brill, T. B., 1992, Connecting the chemical composition of a material to its combustion characteristics, *Prog. Energ. Combust. Sci.* **18**:91–116.

Brill, T. B., and Brush, P. J., 1992, Condensed phase chemistry of explosives and propellants at high temperature: HMX, RDX and BAMO, *Philos. Trans. R. Soc. London Ser. A* **339**:377–385.

Brill, T. B., and Oyumi, Y., 1986a, Thermal decomposition of energetic materials 10. A relationships of molecular structure and vibrations to decomposition: Polynitro-3,3,7,7-tetrakis(trifluoromethyl)-2,4,6,8-tetraazabicyclo[3.3.0]octanes, *J. Phys. Chem.* **90**:2679–2682.

Brill, T. B., and Oyumi, Y., 1986b, Thermal decomposition of energetic materials 17. A relationship of molecular composition to HONO formation: Bicyclo and spiro tetranitramines, *J. Phys. Chem.* **90**:6848–6853.

Brill, T. B., Karpowicz, R. J., Haller, T. M., and Rheingold, A. L., 1984, A structural and Fourier transform infrared spectroscopy characterization of the thermal decomposition of 1-(azidomethyl)-3,5,7-tetrazacyclooctane, *J. Phys. Chem.* **88**:4138–4143.

Brill, T. G., Brush, P. J., James, K. J., Shepherd, J. E., and Pfeiffer, K. J., 1992a, T-Jump/FTIR spectroscopy: A new entry into the rapid, isothermal pyrolysis chemistry of solids and liquids, *Appl. Spectrosc.* **46**:900–911.

Brill, T. B., Brush, P. J., Patil, D. G., and Chen, J. K., 1992b, Chemical pathways at a burning surface, in *Twenty-Fourth Symposium (International) on Combustion*, pp. 1907–1914, The Combustion Institute, Pittsburgh.

Brill, T. B., Brush, P. J., and Patil, D. G., 1993a, Thermal decomposition of energetic materials 58. Chemistry of ammonium nitrate and ammonium dinitramide near the burning surface temperature, *Combust. Flame* **92**:178–186.

Brill, T. B., Patil, D. G., Lengellé, G., and Duterque, J. R., 1993b, Thermal decomposition of energetic materials 63. Surface reaction zone chemistry of simulated 1,3,5,5-tetranitrohexahydropyrimidine (DNNC or TNDA) compared to RDX, *Combust. Flame* **95**:183–190.

Bulusu, S., Weinstein, D. I., Autera, J. R., and Velicky, R. W., 1986, Deuterium kinetic isotope effect in the thermal decomposition of 1,3,5-trinitro-1,3,5-triazacyclohexane and 1,3,5,7-tetranitro-1,3,5,7-tetrazacyclooctane: Its use as an experimental probe for their shock-induced chemistry, *J. Phys. Chem.* **90**:4121–4126.

Cosgrove, J. D., and Owen, A. J., 1974, The thermal decomposition of 1,3,5-trinitro hexahydro-1,3,5-triazine (RDX)—part II: Effects of the products, *Combust. Flame* **22**:19–22.

Cronin, J. T., and Brill, T. B., 1987, Thermal decomposition of energetic materials 26. Simultaneous temperature measurements of the condensed phase and rapid-scan FTIR spectroscopy of the gas phase at high heating rates, *Appl. Spectrosc.* **41**:1147–1151.

Cronin, J. T., and Brill, T. B., 1988, Thermal decomposition of energetic materials 29. The fast thermal decomposition characteristics of a multicomponent material: Liquid gun propellant 1845, *Combust. Flame* **74**:81–89.

Federoff, B. T. (ed.), 1960, *Encyclopedia of Explosives and Related Items*, Vol. 1, Picatinny Arsenal, Dover, New Jersey, p. A3111.

Fetherolf, B. L., and Litzinger, T. A., 1992, Penn State University, personal communication.

Gao, A., Oyumi, Y., and Brill, T. B., 1991, Thermal decomposition of energetic materials 49. Thermolysis routes of mono- and diaminotetrazoles, *Combust. Flame* **83**:345–352.

Kaiser, R., 1935, The explosiveness of ammonium nitrate, *Angew. Chem.* **48**:149–150.

Karpowicz, R. J., and Brill, T. B., 1984, *In situ* characterization of the melt phase of RDX and HMX by rapid-scan FTIR spectroscopy, *Combust. Flame* **56**:317–325.

Kimura, J., and Kubota, N., 1980, Thermal decomposition of HMX, *Prop. Explos.* **5**:1–8.

Lee, P. R., and Back, M. H., 1988, Kinetic studies of the thermal decomposition of nitroguanidine using accelerating rate calorimetry, *Thermochim. Acta* **127**:89–100.

Melius, C. F., and Binkley, J. S., 1986, Thermochemistry of decomposition of nitramines in the gas phase, in *Twenty-First Symposium (International) on Combustion*, pp. 1953–1963, The Combustion Institute, Pittsburgh.

Melius, C. F., Bergan, N. E., and Shepherd, J. E., 1991, Effects of water on combustion kinetics at high pressure, in *Twenty-Third Symposium (International) on Combustion*, pp. 217–223, The Combustion Institute, Pittsburgh.

Oyumi, Y., and Brill, T. B., 1985a, Thermal decomposition of energetic materials 3. A high-rate, *in situ*, FTIR study of the thermolysis of HMX and RDX with pressure and heating rate as variable, *Combust. Flame* **62**:213–224.

Oyumi, Y., and Brill, T. B., 1985b, Thermal decomposition of energetic materials 4. High-rate, *in situ*, thermolysis of four, six, and eight membered, oxygen-rich, *gem*-dinitroalkyl cyclic nitramines, TNAZ, DNNC and HNDZ, *Combust. Flame* **62**:225–231.

Oyumi, Y., and Brill, T. B., 1988, Thermal decomposition of energetic materials 28. Predictions and results for nitramines of Bis-imidazolidinedione: DINGU, TNGU and TDCD, *Prop. Explos. Pyrotech.* **13**:69–73.

Oyumi, Y., Brill, T. B., and Rheingold, A. L., 1985, Thermal decomposition of energetic materials 7. High-rate FTIR studies and the structure of 1,1,1,3,6,8,8,8-Octanitro-3,6-diazaoctane, *J. Phys. Chem.* **89**:4824–4828.

Oyumi, Y., Brill, T. B., and Rheingold, A. L., 1986a, Thermal decomposition of energetic materials 9. Polymorphism, crystal structures and thermal decomposition of polynitroazabicyclo[3.3.1]nonanes, *J. Phys. Chem.* **90**:2526–2533.

Oyumi, Y., Rheingold, A. L., and Brill, T. B., 1986b, Thermal decomposition of energetic materials 16. Solid-phase structural analysis and the thermolysis of 1,4-dinitrofurazano[3,4-*b*]piperazine, *J. Phys. Chem.* **90**:4686–4690.

Oyumi, Y., Rheingold, A. L., and Brill, T. B., 1987a, Thermal decomposition of energetic materials 18. Bis(cyanomethyl)nitramine and bis(cyanoethyl)nitramine, *Prop. Explos. Pyrotech.* **12**:1–7.

Oyumi, Y., Rheingold, A. L., and Brill, T. B., 1987b, Thermal decomposition of energetic materials 19. Unusual condensed phase and thermolysis properties of a mixed azidomethyl nitramine: 1,7-Diazido-2,4,6-trinitro-2,4,6-triazaheptane, *J. Phys. Chem.* **91**:920–925.

Oyumi, Y., Brill, T. B., and Rheingold, A. L., 1987c, Thermal decomposition of energetic materials 20. A comparison of the structure properties and thermal reactivity of an acyclic and cyclic tetramethylenetetranitramine pair, *Thermochim. Acta* **114**:209–225.

Palopoli, S. F., and Brill, T. B., 1991, Thermal decomposition of energetic materials 52. On the foam zone and surface chemistry of rapidly decomposing HMX, *Combust. Flame* **87**:45–60.

Rosser, W. A., and Wise, H., 1956, Gas phase oxidation of ammonia by nitrogen dioxide, *J. Chem. Phys.* **25**:1078–1079.

Schwartz, W. W., Askins, R. E., and Flanigan, D. A., 1984, Nitramine Combustion, Report AFRPL TR-84-012, Air Force Rocket Propulsion Laboratory, Edwards AFB, California, April.

Shackelford, S. A., 1987, *In situ* determination of exothermic transient phenomena: Isotopic labelling studies, *J. Phys.* **48**(C4):193–207.

Shackelford, S. A., Coolidge, M. B., Goshgarian, B. B., Loving, B. A., Rogers, R. N., Janney, J. L., and Ebinger, M. H., 1985, Deuterium isotope effects in condensed-phase thermochemical decomposition reactions of octahydro-1,3,5,7-tetranitro-1,3,5,7-tetrazocine, *J. Phys. Chem.* **89**:3118–3126.

Shaw, R., and Walker, F. E., 1977, Estimated kinetics and thermochemistry of some initial unimolecular reactions in the thermal decomposition of 1,3,5,7-tetrazacyclooctane in the gas phase, *J. Phys. Chem.* **81**:2572–2576.

Shepherd, J. E., and Brill, T. B., 1993, Interpretation of time-to-explosion tests, in *Tenth International Symposium on Detonation*, Office of Naval Research, in press.

Stals, J., and Pitt, M. J., 1975, Investigations of the thermal stability of nitroguanidine below its melting point, *Aust. J. Chem.* **28**:2629–2640.

Stoner, C. E., and Brill, T. B., 1991, Thermal decomposition of energetic materials 46. The formation of melamine-like cyclic azines as a mechanism for ballistic modification of composite propellants by DCD, DAG and DAF, *Combust. Flame* **83**:302–308.

Swett, M., 1992, Naval Weapons Center, China Lake, California, personal communication.

Volk, F., 1985, Determination of gaseous and solid decomposition products of nitroguanidine, *Prop. Explos. Pyrotech.* **10**:139–146.

Whittaker, A. G., and Barham, D. C., 1964, Surface temperature measurements on burning solids, *J. Phys. Chem.* **68**:196–199.

Willer, R. L., Chi, M. S., Gleeson, B., and Hill, J. C., 1991, DAG and DAF in propellants based on ammonium perchlorate, U.S. Patent 5,071,495.

Williams, G. F., Palopoli, S. F., and Brill, T. B., 1994, Thermal decomposition of energetic materials 66. Thermal conversion of insensitive explosives and related compounds to polymeric cyclic azine flame retardants, *Combust. Flame* **98**:197–204.

Thermal Decomposition of Energetic Materials 67. Hydrazinium Nitroformate (HNF) Rates and Pathways under Combustionlike Conditions

G. K. WILLIAMS AND T. B. BRILL*
Department of Chemistry, University of Delaware, Newark, DE 19716

Hydrazinium nitroformate (HNF), $N_2H_5[C(NO_2)_3]$, holds promise as a clean-burning, high-energy oxidizer for solid rocket propellants. By using T-jump/FTIR spectroscopy, the thermal decomposition process is outlined in the 130°–400°C range, which includes surface melt/foam formation and self-ignition events. Reaction regimes containing evaporation, conversion to $NH_4[C(NO_2)_3]$, and progressive decomposition into CO_2, CO, N_2O, NO, and H_2O are observed. Based on the products these reaction regimes become increasingly exothermic at higher temperature. Decomposition induction-time kinetics (E_a = 25 kcal/mol, ln $B(s)$ = 25.3) of the melt/foam layer were determined from time-to-exotherm data and give reasonable agreement with the measured combustion characteristics.

INTRODUCTION

Hydrazinium nitroformate (HNF) is a high-energy oxidizer that holds promise in part because it does not contain chlorine. While its value as the oxidizer in high burn-rate, high I_{sp}, and thixotropic propellants has long been recognized [1–3], recent expanded efforts to develop high-energy, clean-burning propellants have revived interest in HNF.

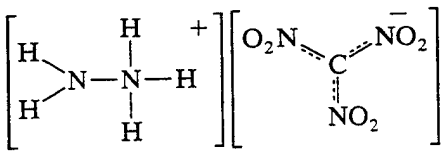

HNF

Extensive hydrogen bonding influences the packing of the HNF crystal lattice [4] and contributes to an acceptable density of 1.86–1.89 g/ cm^3. Reasonably low hygroscopicity and satisfactory thermal stability are important additional properties of HNF. Consideration has been given to compatability issues and the kinetic stability of HNF [5]. The thermal decomposition rate of solid HNF in the 70°–100°C range along with suggested reaction pathways have been given by Koroban et al. [6]. Building on this information about the lower temperature and heating rate range, an investigation of the changes in the vibrational spectrum of HNF over the 25°–125°C range is presented in this article.

While the thermal decomposition characteristics of HNF below 125°C may be useful to understand the slow cook-off behavior, the decomposition rate and pathways of HNF at high heating rates and high temperatures are needed to describe the combustion process. The melt/ foam layer on the burning surface is of paramount interest. The description given here of this zone was obtained by using T-jump/ FTIR spectroscopy [7] at temperatures up to 400°C, which is a reported self-ignition temperature of HNF [2]. The IR-active gaseous products formed as a function of temperature outline the decomposition process, while the times-to-exotherm enable introduction rate parameters to be estimated. These parameters reproduce temperature-time characteristics of burning HNF extracted from thermocouple measurements by McHale and von Elbe [8].

EXPERIMENTAL

Materials

A sample of HNF dissolved in H_2O was supplied by Dr. P. A. O. G. Korting of APP/TNO, The Netherlands. H_2O was removed under vacuum, the sample recrystallized from methanol, and the resulting damp powder dried at 10^{-4} torr. The yellow polycrystalline powder melted at 123°C. Ammonium nitroformate (ANF), $NH_4[C(NO_2)_3]$, was prepared by adapt-

* Corresponding author.

0010-2180/95/$9.50
SSDI 0010-2180(94)00283-X

COMBUSTION AND FLAME 102: 418–426 (1995)

ing the procedure for $K[C(NO_2)_3]$ [9] to the NH_4^+ salt. To 1 mL of 15 M NH_4OH (0.012 mol) dissolved in 2 ml ethanol was added 1 g of $C(NO_2)_4$ (Aldrich) (0.005 mol). Evaporation of the solution yielded yellow crystalline ANF which was dried at 10^{-4} torr. Colorless $HC(NO_2)_3$ was prepared from $C(NO_2)_4$ as described elsewhere [9].

Vibrational Spectroscopy

IR spectra of neat solid phase compounds were recorded by burnishing the sample onto an NaCl plate and coadding 32 spectra at 2 cm^{-1} resolution. Figure 1 shows the mid-IR spectrum of HNF. When HNF was heated between two IR-transparent plates, such as BaF_2 or NaCl, the film physically migrated on the surface of BaF_2, but not NaCl. Therefore, spectral changes induced by temperature were determined for HNF on the NaCl plates. The spectrum of $HC(NO_2)_3(g)$ was obtained by vaporizing solid $HC(NO_2)_3$ from a warm nichrome filament housed in a sealed gas cell [10].

The Raman spectrum of a solid HNF packed into an NMR tube was recorded on a Nicolet 910 FT-Raman spectrometer and is shown in Fig. 2. Excitation at the 1.06-μm wavelength by a 300-mW diode-pumped Nd-YAG laser proved invaluable because of the yellow color of HNF. Such a sample rapidly discolors when excited by a visible wavelength laser.

Gaseous thermal decomposition products originating from the bulk phase were determined by T-jump/FTIR spectroscopy [7]. An approximately 200-μg sample of HNF was

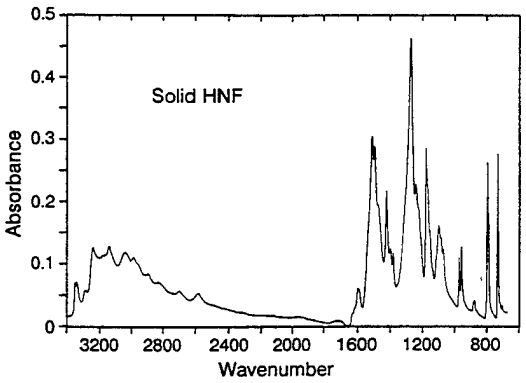

Fig. 1. IR spectrum of dry solid HNF.

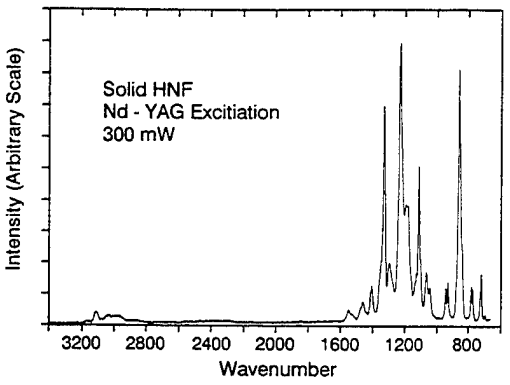

Fig. 2. FT-Raman spectrum of dry solid HNF.

thinly spread on the center segment of a polished Pt ribbon filament that was arranged inside of a gas cell. The cell was purged with Ar and pressurized to the desired value. By using a high-gain, fast-response power supply (CDS Analytical), the filament and sample were heated rapidly and then held at the set temperature for the duration of the experiment. Although 2000°C/ s is the filament heating rate, the sample is only able to heat at about 600°C/ s to the set temperature in the 140°–400°C range because of limitations in the rate of heat transfer. Once the set temperature is reached, the filament control voltage rapidly responds to hold the sample isothermally at the set temperature. This control voltage was extracted to track the endothermic and exothermic events of the sample. By subtracting the control voltage when the sample is present from the control voltage of the bare filament when the sample is absent, an exotherm is revealed as a sharp negative spike in the difference voltage trace. This spike marks the time-to-exotherm at a given temperature. Figure 3 shows these exotherms for 200-μg samples of HNF. Four data points were taken at each temperature and were reproducible to ± 0.4 s. These data enable a kinetic analysis to be made. Simultaneously, transmission FTIR spectra (Nicolet 800, 10 scans/ s, 4 cm^{-1} resolution) were recorded of the gaseous products that became frozen by the cool Ar atmosphere. The sequence of liberation and relative abundances of these products outline the chemical processes of the developing multiphase film of material. No flame is created in this experiment because the objective is to identify the

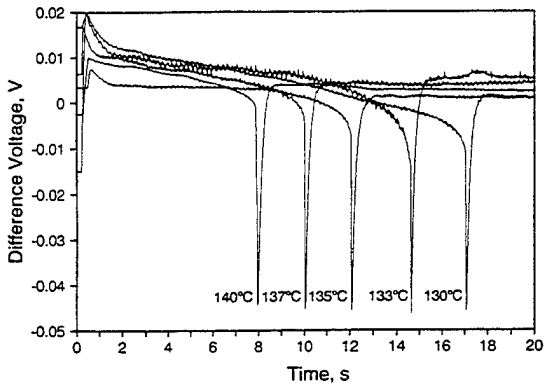

Fig. 3. The control voltage difference traces (bare filament voltage minus sample-filament voltage) showing the time-to-exotherm following T-jump heating to the temperature shown.

molecules that leave the surface at surface temperatures relevant to combustion. The IR beam is focused about 3 mm from the surface to maximize the overall absorbance and minimize the thermal lens effect of the hot filament. The observation volume at the onset of decomposition is about 10 mm^3.

An important concern is whether the platinum surface catalyzed decomposition, particularly because it is well-known that Pt catalyzes decomposition of N_2H_4 [11]. In fact, it has been suggested that any transition metal having an incomplete d shell electron configuration can strongly catalyze N_2H_4 decomposition, whereas metals with d^0 or d^{10} configurations are not catalytic [12]. Hence, Pt with a $5d^96s^1$ configuration is cause for concern. On the other hand, Au with a $5d^{10}6s^1$ configuration should not be (and is not) catalytic toward N_2H_4. To evaluate whether the gaseous products described herein are affected by catalyis, a comparison was made of the gaseous products from Pt and Au filaments at the same pressure and temperature. No detectable differences occurred in the products or their concentrations. In particular, the same amount of N_2H_4(g) was produced by the Pt and Au surfaces. We are, therefore, confident that surface catalysis does not influence any of the results presented herein.

Differential scanning calorimetry was conducted in a sealed Al pan on a DuPont Instruments 910 DSC. Thermogravimetric analyses were made on samples of 1.25 mg mass in a 20 mL/min Ar flow with a DuPont Instruments 951 TGA.

SPECTRA AND DECOMPOSITION OF SOLID HNF

The crystal structure of HNF at −160°C reveals that $N_2H_5^+$ ions are hydrogen-bonded to neighboring $C(NO_2)_3^-$ ions [4]. Two crystallographically independent and structurally different formula units are contained in the unit cell. One of the $N_2H_5^+$ ions is staggered while the other is eclipsed. The CN_3 framework of both $C(NO_2)_3^-$ ions is planar, but these propeller-shaped ions have N_2C-NO_2 dihedral angles between 4° and 74°. Figure 1 shows that the absorbance IR spectrum of dry solid HNF burnished onto an NaCl plate. Figure 2 shows the Raman spectrum of neat solid HNF. The IR and Raman frequencies and suggested assignments are given in Table 1 [13–15]. Given the structural complexity of solid HNF, splittings of the group vibrational modes are ex-

TABLE 1

IR and Raman Frequencies of Neat Solid NHF[a]

IR	Raman	
2578–3350 m[b]	2950–3350 w[c]	N–H str.
1615 w, sh	1618 w	NH_3^+ def.
1595 w	1595 w	
1512 s	1522 w	NO_2 antisym. str.
1496 s		
1474 m, sh	1463 m	
1421 m		NH_3^+ bend
1396 w	1385 s	
1380 w	1345 m	
1271 s	1276 s	NO_2 sym str. and
1241 m	1237 s	NH_2 rock
1177 s	1166 w, sh	NH_3^+ wag
1153 w, sh	1151 s	
1098 m	1099 m	N–C–N asym. str.
1084 m, sh	1075 m	
1069 m	1075 m	
971 m	968 m	N–N str.
955 m	954 m	
879 w	879 s	$C-NO_2$ in-phase str.
872 w		
794 s	793 m	NO_2 bend
788 w, sh	785 m	
734 s	731 m	

[a] s = strong, m = medium, w = weak, sh = shoulder
[b] A broad envelope containing 13 resolvable absorbances
[c] A broad envelope containing 6 resolvable bands

pected. The breadth and complexity of the N–H stretching modes results from extensive hydrogen bonding, which produces coupling and Fermi resonance. HNF has been reported to be stable at 77°C for 40 h [3], however the $N_2H_5^+$ absorbances of HNF were found in the present work to change slightly in this temperature range. Most notably the doublet at 955–971 cm^{-1} assigned to N–N stretching [16] reversibly broadened to a single absorbance which suggests an increase in torsional disorder. Such an event frequently accompanies a first-order solid-solid phase transition. However, no change in enthalpy was observed by DSC through this temperature range, implying that either the occurrence of rotational disorder is thermally neutral or that the phase transition is second-order.

The wide range of $N_2C–NO_2$ dihedral angles found for $C(NO_2)_3^-$ ions is consistent with the fact that the barrier to rotation of the $-NO_2$ groups is only 0.3–0.8 kcal/mol [17]. Therefore, the 1400–1550 cm^{-1} region containing $-NO_2$ antisymmetric stretching strongly depends on the counter ion in $C(NO_2)_3^-$ salts [18]. This fact aids assignment of absorbances from gaseous species evolved upon rapid heating of HNF (*vide infra*).

When solid HNF is partially confined between two NaCl plates and heated to the temperature range of decomposition, all of the IR absorbances are observed to decrease at about the same rate. According to the IR spectrum the only solid product is NH_4NO_3. There is no evidence for formation of ANF as an intermediate of this solid-phase conversion, which contrasts with the proposal of Koroban et al. [6] that ANF forms during slow decomposition of the solid at 70°–100°C. The absence of ANF in the present study cannot be attributed to our inability to detect it. ANF was synthesized and is clearly distinguishable from other products in both the solid and vapor phases by IR spectroscopy. It was found here to be an important product formed at the high heating rates and discussed later. However, the formation of NH_4NO_3 from HNF without evidence of ANF may result from the fact that H_2O is a gaseous product of HNF and, when in the presence of the NaCl surface, is retained by dissolving some of the NaCl. Ionic reaction pathways leading preferentially to AN should be favored by the presence of an H_2O–NaCl solution. NH_4NO_3 was not detected in any other experiments performed on HNF in this study. However, it was found that heating of a sample of ANF at 1°C/min by TGA produced a two-step weight loss. The first step centered at 112°C corresponded to decomposition/sublimation of ANF, while the second step centered at 170°C corresponded to decomposition/sublimation of NH_4NO_3. Consequently, solid ANF thermally decomposes to solid NH_4NO_3 along with gaseous products under these conditions.

Combustion-like Decomposition

Of considerable interest in combustion of HNF are the rates and mechanisms of decomposition in the thermal wave at the surface of the deflagrating material. Fortunately, imbedded Pt/Pt–Rh thermocouple data are available that outline the relevant temperature ranges [8]. For example, polycrystalline HNF at 0.7 TMD (1.3 g/cm^3) ignited at 1 atm in an open-ended glass tube produces a steady temperature rise in the condensed phase with slope breaks at 123° and 260°C. Over 25°–123°C, the rise reflects preheating of the solid phase. At about 123°C, HNF melts and foaming begins due to the generation of gas. Burning HNF is reported to have a melt layer on the surface even at elevated pressure in a window bomb [8]. The temperature continues to rise to about 260°C at which point the rates of gasification and heating accelerate so rapidly that deflagration occurs. This temperature is somewhat below the value of 400°C given elsewhere for self-ignition of HNF [2]. Nevertheless, these thermocouple data indicate that the temperature regions of special importance to combustion are 123°–260°C, where two-phase foam chemistry occurs, and above 260°–400°C where combustion events dominate.

To outline the chemistry in these ranges, the IR-active gaseous products were determined from a 200-μg sample of HNF thinly spread on the Pt filament and heated rapidly to set temperatures in the 130°–400°C range. In accordance with the thermocouple data, the extent of chemical transformation was observed to

depend distinctively on the set temperature, as is illustrated by Fig. 4. Identification of the gaseous products required considerable care and is discussed next before describing general reactions.

IR Spectra of Gaseous Products

The composite IR spectrum of the gaseous products from rapid heating of HNF to temperatures of 130°–400°C is highly congested with absorbances. For example, Fig. 5 shows the 700–2500 cm^{-1} region when HNF is heated to 165° under 5 atm Ar. This spectrum is representative of those obtained at 130°–260°C under pressures of 1–10 atm Ar. Gaseous N_2O, CO, and H_2O are readily identified. Because the absolute IR absorbances of these molecules differ, the multiplicative factors [19] in Table 2 were used to scale the absorbances to concentrations relative to CO_2. The presence of $HC(NO_2)_3$(g) was confirmed by the close match of absorbances with those of an authentic sample of $HC(NO_2)_3$(g) in Fig. 5. To the list in Table 2 can now be added the factor for $HC(NO_2)_3$ in tetrachloroethane solution, which was determined by Popov and Shlyapochnikov [13] by integrating the intensity of $\nu_{as}(-NO_2)$ at 1605 cm^{-1}. It is doubtful that the intensity of this absorbance changes significantly from the solution to the gaseous phase. The observed absorbance intensity of 35000 cm^{-2} L mol^{-1} converts to 1431 cm^{-2} atm^{-1}. This absolute absorbance closely resembles the value of 1419 cm^{-2} atm^{-1} for ν_3 of NO_2(g) [20]. Thus, the multiplicative factor of 1.88 converts the intensity of 1605 cm^{-1} absorbance of $HC(NO_2)_3$ to concentration when the 2349 cm^{-1} absorbance of CO_2(g) is set at 1.0. N_2H_4(g) was identified from the N–N stretching doublet at 966 and 933 cm^{-1}. The absolute absorbance of this mode was not found in the literature. Because of its reactivity, N_2H_4 is detected for only about 0.3 s at the onset of decomposition.

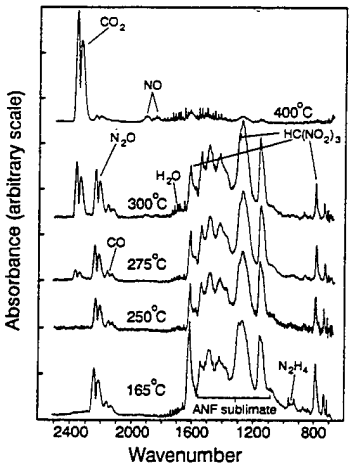

Fig. 4. The gaseous products liberated by 200 μg of HNF heated at about 600°C/s to the temperature shown under 5–7 atm Ar. Strong dependence on temperature is observed.

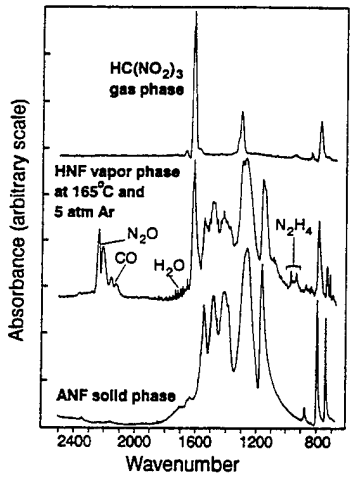

Fig. 5. Assignments of the nontrivial absorbances in the gas phase above a fast-heated sample of HNF.

The remaining absorbances in Fig. 5 are assigned to ANF based on the close match with an authentic sample of ANF. The amount of ANF was not established, but by comparison

TABLE 2

Scaling Factors Needed to Convert Equal Partial Pressures of Gases from Absorbance Intensiy[a] to Concentration

Product	Frequency cm^{-1}	Multiplicative Factor[b]
CO_2	2349(R)	1.0
N_2O	2224(R)	1.86
CO	2143(P)	21.4
NO	1903(R)	32.1
$HC(NO_2)_3$	1605(ν_{as})	1.88

[a] Branch or assignment given parenthetically.
[b] Scaling factor to convert absorbance intensities to relative concentrations when CO_2 is set at 1.0.

of Figs. 1 and 5, the absorbances clearly do not match those of HNF, so that simple sublimation is not an important event.

Finally, Koroban et al. [6] employed a nonspecific product of stoichiometry CNO_2H_3 to balance the decomposition reaction of HNF. CH_3NO_2 and N-hydroxylformamide, HC(O)N(OH)H, are plausible products having this stoichiometry. The existence of these two compounds was ruled out in the case of CH_3NO_2 by comparison of the IR spectrum of the decomposition gases to an authentic sample of CH_3NO_2(g), and in the case of an amide by the absence of a C=O stretch at 1675–1715 cm^{-1}. Koroban et al. [6] also employ $CH_2(NO_2)_2$ and HNO_2 as products in decomposition reactions. $CH_2(NO_2)_2$ has a distinctive IR absorbance [13] at 830 cm^{-1}, which is absent in Fig. 5. HONO is readily observed during rapid decomposition of nitramines [21], but was not detected here for HNF. Consequently, at fast heating rates we are unable to confirm many of the proposed complete reactions of HNF given before for the 70°–100°C range, and conclude that $CH_2(NO_2)_2$, HNO_2, and CNO_2H_3 are present in low steady-state quantity, if they are present at all.

PRODUCTS AT 123°–260°C

Rapid decomposition of HNF was investigated in the 130°–260°C range under static Ar pressure of 5–7 atm. As was shown by Figs. 4 and 5, ANF aerosol, $HC(NO_2)_3$, N_2H_4, N_2O, H_2O, and CO are detected in the gaseous phase. The formation of these products occurs predominately in the condensed phase because no stationary flame exists in the T-jump/FTIR experiment. Moreover, HNF aerosol is not detected, so that evaporation of HNF followed by gas decomposition is negligible. Instead, HNF decomposes to form ANF, which is understandable from the idealized limiting reaction 1:

$$2HNF \rightarrow 2ANF + N_2 + H_2. \quad (1)$$

This reaction is exothermic by −30 kcal/mol of HNF because ΔH_f° (HNF) = −17 kcal [8], while ΔH_f° (ANF) = −47 kcal/mol [22]. The stoichiometry of reaction 1 is speculative to the extent that N_2 and H_2 are not IR-active. However, Koroban et al. [6], detected appreciable N_2 from slow decomposition of HNF at 70°–100°C. The formation of additional products (N_2O, CO, H_2O, $HC(NO_2)_3$, and N_2H_4) clearly indicates that other reactions of HNF and ANF occur in parallel with reaction 1. First, the formation of N_2H_4(g) and $HC(NO_2)_3$(g) suggests that reaction 2 takes place to some extent, but that recombination as gaseous or aerosol HNF does not occur:

$$HNF(l) \rightarrow HC(NO_2)_3(g) + N_2H_4(g) \quad (2)$$

The endothermic heat of dissociation of HNF is estimated to be 41 kcal/mol [6], which is substantially higher than an estimate of the heat of sublimation of ANF of about 25 kcal/mol [22]. The low absorbance by N_2H_4 compared with $HC(NO_2)_3$ can be accounted for by the fact that (a) the $N_2H_5^+$ absorbances in Fig. 4 are generally less intense than those of $C(NO_2)_3^-$, and (b) some of the $HC(NO_2)_3$(g) in Fig. 5 could result from dissociative evaporation of ANF. However, no NH_3(g) was detected suggesting that any NH_3 formed is consumed quickly by secondary reactions. Finally, by using the absolute absorbance values of N_2O and CO in Table 2 and the measured intensities in Fig. 5, reaction 3 involving ANF matches the stoichiometry in Fig. 5 below 260°C.

$$2ANF(l) \rightarrow N_2O + 2CO + 4H_2O + 5/2O_2 + 3N_2. \quad (3)$$

This reaction is exothermic by about −86 kcal/mol of ANF. Taken together reactions 1–3 yield 73 kcal/mol of HNF. Exothermicity in the foam layer is qualitatively consistent with the temperature rise witnessed by an imbedded thermocouple [8]. Perhaps for this reason, HNF sustains self-deflagration at subatmospheric pressures [8].

PRODUCTS AT 260°C AND HIGHER

According to Figs. 4 and 5, the IR-active gaseous products from decomposition of HNF strongly depend on the temperature to which the sample is heated. Above 260°C, where a very steep temperature rise occurs according to the thermocouple measurement [8], Fig. 4

reveals formation of CO_2 for the first time. The amount of CO_2 increases with increasing temperature. Because of the large negative heat of formation of CO_2, exothermicity in turn increases with temperature. Above 350°C, ANF, N_2O, and CO are frequently not detected and in their place are the products shown in Fig. 4 at 400°C. These products are those expected when deflagration dominates. Owing to the substantially different absolute absorbance values of NO and CO_2 (Table 2), the NO concentration is about twice that of CO_2. A significant quantity of H_2O forms along with a very small amount of N_2O. Neglecting N_2O, reaction 4 accounts for these IR-active products in the approximate amounts observed.

$$\mathrm{HNF} \rightarrow 2\mathrm{NO} + \mathrm{CO_2} + 2\mathrm{H_2O} + 3/2\mathrm{N_2} + 1/2\mathrm{H_2} \quad (4)$$

This reaction is the most strongly exothermic (−149 kcal/mol) of reactions 1–4, in qualitative accordance with the trend from decomposition to ignition reported in other studies at these temperatures [2, 8]. The products of reaction 4 are not in thermodynamic equilibrium concentrations that exist at the theoretical adiabatic flame temperature [8]. Further reaction at higher temperature is expected.

Reactions 1–4 are consistent with the products detected through a wide temperature range. They generally become increasingly exothermic from the moderate decomposition rate of molten HNF at 130°C to the deflagration stage above 350°C. Thus, these reactions are plausible semiglobal descriptions of the foam layer and surface deflagration processes. Obviously, these stoichiometric reactions contain many elementary steps. Most of these steps would be difficult to study in isolation in the melt/foam layer. Therefore, kinetic measurements over a wide temperature range reflect the composite rates of many reactions. Kinetic considerations are now addressed.

KINETICS OF THE SURFACE MELT / FOAM LAYER

During burning of HNF at pressures at least below 90 atm, a foam layer covers the surface [8]. As occurs for many other energetic materials, the burning rate of HNF has a positive pressure exponent. As the temperature gradient increases with increasing pressure, the melt/foam layer decreases in thickness. Other oxidizers, such as ammonium perchlorate (AP) [23], HMX [24], and RDX [25], also possess a molten surface layer during combustion at pressures below 65 atm. This layer plays a major role in controlling the combustion characteristics of AP, HMX, and RDX, and the same is probably true of HNF.

Ideally, the rates of specific reactions in the multiphase surface reaction zone would be measured isothermally at a series of temperatures. In practice, isothermal conditions are nearly impossible to achieve for a reacting bulk energetic material, because heat is released rapidly as the decomposition reactions proceed. Although the overall rate of decomposition of the melt/foam phase of HNF describes the composite process, even this rate can be difficult to measure for HNF because the process accelerates rapidly following melting. In place of specific rates of reactions, the kinetic constants based on the times-to-exotherm (t_x) after heating the sample at about 600°C/s to specific set temperatures in the 130°–140°C range were extracted from Eq. 5 based on conservation of heat energy [26]:

$$-\lambda \nabla^2 T + \rho C_p (dT/dt) = \rho Q A e^{-E_a/RT} \quad (5)$$

The induction time before the release of heat is determined primarily by the rate of heat build-up in the sample as opposed to the rate of heat transfer [27] in this temperature range. λ is the thermal diffusivity of HNF, ρ is the density, and C_p is the heat capacity. Assuming zeroth-order Arrhenius heat generation under quasi-adiabatic conditions, Eq. 5 reduces to [28]

$$\ln t_x = E_a/RT + \ln B \quad (6)$$

and provides the apparent activation energy, E_a. The individual experimental measurements of t_x shown in Fig. 3 yield $E_a = 25$ kcal/mol and $\ln B(s) = 28.3$. However, the intercept, $\ln B$, is not the conventional Arrhenius preexponential factor, A, but is approximately related to A by Eq. 7. C_p and Q are not known for melt/foam HNF making the use of Eq. 7

rather approximate. If C_p is assumed to be similar to that of AN (0.4 cal/ g°C) [30], then the remaining unknown

$$A \simeq \frac{C_p R T^2}{Q B E_a} \tag{7}$$

is Q. Because of the competition of reactions 1 and 2 in this temperature range, fixing the value of Q is tenuous. If for example, $Q = 19$ kcal, i.e., reactions 1 and 2 as written are assumed to be equally prevalent, then Eq. 7 yields $\ln A(s^{-1}) = 25.4$, when $T = 137$°C.

The values of E_a and $1/B$ give the cumulative decomposition rate of the melt/foam layer based on the induction time. They do not refer to a specific reaction or event. The value E_a = 25 kcal/mol determined experimentally here for decomposition of the melt/foam layer can be compared to $E_a = 43$ kcal/mol given by Koroban et al. [6], for solid HNF. The trend of E_a(solid) > E_a(melt) is also found for other energetic materials, such as HMX and RDX [31], which makes these E_a values qualitatively consistent.

Several characteristics of the melt/foam layer on the surface of burning HNF can be obtained by substituting E_a and B into the rearranged form of the Arrhenius Eq. 8 [32]:

$$T_{rxn} = \frac{E_a}{R(\ln \Delta t - \ln B)} \tag{8}$$

The life time of the reaction layer Δt, can be estimated at a given temperature. Figure 6 shows the result. The appropriateness of kinetic constants based on the times-to-exotherm and the resulting predictions from Eq. 8 and Fig. 6 is judged by the consistency with the thermocouple measurements of burning HNF given by McHale and von Elbe [8]. At 1 atm, they report that the melt/foam layer has a lifetime $\Delta t \simeq 0.3$ s and an average temperature of $T \simeq 190$°C. This T–Δt combination lies almost exactly on the line of Fig. 6.

Induction-time kinetics and semiglobal reactions in the melt/foam layer of HNF have been obtained by the use of T-jump/FTIR data. Because of the complexity of the process, remarks about rates and pathways are necessarily qualitative, but not necessarily speculative. A connection exists between regions where the chemistry is clearly changing and thermal and combustion transitions are reported.

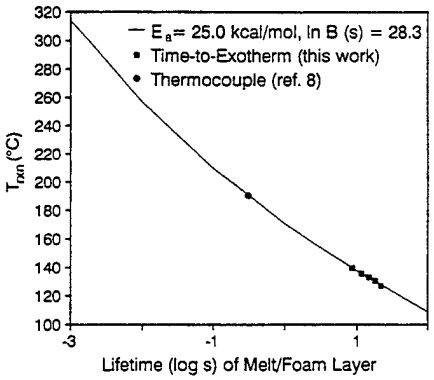

Fig. 6. Induction-time kinetics (Eq. 8) of decomposition of the melt/foam phase of HNF over the temperature range for moderately slow decomposition into the rapid decomposition-ignition stage. Experimental data points are shown.

We are grateful to Dr. P. A. O. G. Korting for supplying HNF and to the Air Force Office of Scientific Research, Aerospace Sciences (F49620-94-1-0053), ESTEC, and the Netherlands Agency for Aerospace Programs for financial support.

REFERENCES

1. Godfrey, J. N., U.S. Patent 3,196,059, July 20, 1965, CA 63:P8113g.
2. Johnson, H., and Oja, P. D., U.S. Patent 3,213,609, Oct. 26, 1965, CA 64:P3276d.
3. Lovett, J. R., U.S. Patent 3,378,594, April 16, 1968, CA 68:P116121y.
4. Dickens, B., *J. Res. Natl. Bureau Stds.* 74A:309–318 (1970).
5. Jago, W. H., U.S. Patent 3,307,985, March 7, 1967, CA 67:P4516d.
6. Koroban, V. A., Smirnova, T. I., Bashirova, T. N., and Svetlov, B. S., *Tr.-Mosk. Khim.-Tekhnol. Inst. im. D. I. Mendeleeva*, 104:38–44 (1979).
7. Brill, T. B., Brush, P. J., James, K. J., Shepherd, J. E., and Pfeiffer, K. J., *Appl. Spectrosc.* 46:900–911 (1992).
8. McHale, E. T., and von Elbe, G., *Comb. Sci. Tech.* 2:227–237 (1970).
9. Maslak, P., and Chapman, Jr., W. H., *J. Org. Chem.* 55:6334–6347 (1990).
10. Oyumi, Y., and Brill, T. B., *Combust. Flame*, 62: 213–224 (1985)
11. Maurel, R., Menezo, J. C., and Barrault, J., *J. Chim. Phys.* 70:1221–1226 (1973).

12. Ederstein, I. J., and Glassman, I., *Am. Rocket. Soc., Liquid Rockets and Propellants*, L. E. Bollinger, Ed., *Prog. Astronaut. Rocketry*, Vol. 2, (1960), pp. 351–386.
13. Popov, E. M., and Shlyapochnikov, V. A., *Opt. Spectrosc.* 15:174–178 (1963)
14. Schettino, V., and Salmon, R. E., *Spectrochim. Acta.* 30A:1445–1450 (1974).
15. Milićev, S., and Maček, J., *Spectrochim. Acta* 41A: 651–655 (1985).
16. Durig, J. R., Bush, S. F., and Mercer, E. E., *J. Chem. Phys.* 44:4238–4247 (1966).
17. Levin, A. A., Mikhailov, V. K., and Krapokovskii, G. M., *Mezhmol. Vzaimodeistwie Konform. Mol. Tezisy Dokl. Vses. Simp., 3rd*, 77–78 (1976).
18. Slovetskii, V. I., Erashko, V. I., and Orlova, M. K., *Izv. Akad. Nauk SSSR, Ser. Khim.* 6:1221–1226 (1970).
19. Brill, T. B., *Prog. Ener. Combust. Sci.* 18:91–116 (1992).
20. Devi, V. M., Fridovich, B., Jones, G. D., Snyder, D. G. S., Das, P. P. , Flaud, J.-M., Camy-Peyret, C., and Rao, K. N., *J. Mol. Spectrosc.* 93:179–195 (1982).
21. Brill, T. B. and Oyumi, Y., *J. Phys. Chem.* 90:6848–6853 (1986).
22. Miroshnichenko, E. A., Lebedev, Yu. A., and Apin, A., Ya., *Russ. J. Phys. Chem.* 41:791–792 (1967).
23. Boggs, T. L., Derr, D. L., and Beckstead, M. W., *AIAA J.* 8:370–372 (1970).
24. Parr, T. P. and Hanson-Parr, D. M., *Proc. 26th JANNAF Mtg.* CPIA Publ. 529, Vol. I, 1989, pp. 27–37.
25. Taylor, J. W., *Combust. Flame* 6:103–107 (1962).
26. Frank-Kamenetskii, D. A., *Acta Physicochem. URSS* 10:365–370 (1939)
27. Shepherd, J. E., and Brill, T. B., *Tenth Symposium (International) on Detonation*, in press.
28. Merzhanov, A. G. and Abramov, V. G., *Prop. Explosives* 6:130–148 (1981).
29. Zinn, J. and Mader, C. L., *J. Appl. Phys.* 31:323–328 (1960).
30. Dobratz, B. M., *LLNL Explosives Handbook*, UCRL-52997, March 16, 1981, p. 6–12.
31. Brill, T. B., Gongwer, P. E., and Williams, G. K., *J. Phys. Chem.*, 99:12242–12247 (1994).
32. Brill, T. B., and James, K. J., *J. Phys. Chem.* 97: 8759–8763 (1993).

Received 24 May 1994; revised 14 December 1994

Multiphase Chemistry Considerations at the Surface of Burning Nitramine Monopropellants

T. B. Brill

Reprinted from

Journal of Propulsion and Power

Volume 11, Number 4, Pages 740–751

AIAA

A publication of the
American Institute of Aeronautics and Astronautics, Inc.
370 L'Enfant Promenade, SW
Washington, DC 20024-2518

JOURNAL OF PROPULSION AND POWER
Vol. 11, No. 4, July–August 1995

Multiphase Chemistry Considerations at the Surface of Burning Nitramine Monopropellants

Thomas B. Brill*
University of Delaware, Newark, Delaware 19716

The surface reaction zone of a solid propellant is increasingly acknowledged as imparting major, if not dominant, characteristics to combustion. An overview of this evolving issue is given. Chemistry considerations associated with the multiphase surface layer of the nitramine monopropellants HMX and RDX are discussed critically. These include global rates, specific decomposition and exothermic reactions, evaporation, and surface temperatures. A chemistry description is offered that involves the competition of two decomposition branches and one strongly exothermic reaction. Based simply on rationally derived reaction rates, reasonable deductions may be made about the surface temperature and reaction-zone thickness during combustion of HMX and RDX.

I. Introduction

CONCERNS about cost, safety, performance, and ecology have stimulated a march to develop new, high-energy, clean-burning solid rocket propellants. Important departures from past practices are likely to define these efforts. In particular, expanded computational models that predict the combustion behavior may reduce the need for live testing on an exhaustive matrix of ingredients. Acceptance of these combustion models rests on their ability to imitate the observed performance. A great deal of work remains before such reliability is realized. Research that has brought us to the present understanding of conventional solid propellants is a useful guide for future strategies.

An impressive array of chemical and physical details about the gas-phase domain of combustion has been developed and refined by the research community.[1] Recently, the two-phase surface reaction zone of a solid propellant has been physically modeled in considerable detail.[2,3] These important advancements remain limited to some extent by uncertainties about the pathways and rates of specific controlling chemical reactions, especially in the condensed phase and where nonsteady combustion is concerned. The fact is that it is enormously difficult to make the necessary experimental measurements on the very thin surface reaction zone, even assuming a one-dimensional combustion wave and a homogeneous monopropellant. However, some of the chemical processes in the surface zone can be outlined by experimental simulation experiments.[4–6]

The opinions and descriptions in this article center on the chemistry and the important role of the surface reaction zone of the nitramine monopropellants RDX and HMX, although

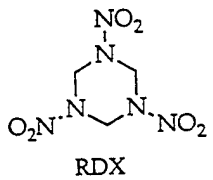

RDX

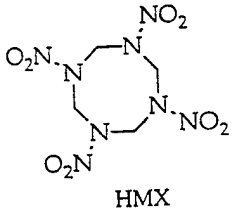

HMX

other materials are mentioned for perspective. The analysis applies primarily to combustion of the homogeneous monopropellant component of the solid rocket propellant.

Received June 16, 1994; revision received Nov. 9, 1994; accepted for publication Dec. 2, 1994.

*Professor of Chemistry, Department of Chemistry.

II. What is the Surface Reaction Zone?

The concept of a surface zone in which chemical reactions take place during combustion is an old one. For example, it was conceptualized in 1950 in publications on double-base propellants.[7–9] Pictorializing the surface zone presents a few problems, some real and some semantic. Alexander et al.[1] illustrate the complexity of the problem by using a figure attributed to Kuo. The real problems mostly arise when defining and solving the equations that properly describe dynamic, interfacial, microscopic, physical, and chemical processes. In this regard Li et al.[2] and Huang et al.[3] analyzed the two-phase zone with considerable care. A simpler and more conventional approach is to define the surface reaction zone as an infinitely thin (superficial) boundary layer from which evaporation and/or decomposition products magically appear.

From the point of view of chemistry, the surface of a burning solid propellant consists of a thin layer in which much of the formulated materials pyrolyze to fuel and oxidizer molecules, which then engage in secondary exothermic reactions. The thickness of this surface reaction zone depends on the temperature, pressure, and formulated ingredients. For example, the surface of HMX and RDX is liquid during combustion at pressures below 67 atm.[10,11] The surface of ammonium perchlorate (AP) is liquid below 50 atm.[12] The liquid layer becomes thinner with increasing pressure because the thermal (or combustion) wave produced by surface multiphase reactions and near-field gas-phase reactions becomes extremely steep.[13] The shape of the one-dimensional combustion wave is defined by the thermophysical properties coupled with the mass, momentum, energy, and species conservation equations.[14] In a simpler approach, Zenin[15] has proposed several generalized equations to govern the surface temperature and heat release in the condensed phase of double-base propellants.

While physics can describe the shape of the combustion wave, the surface reaction zone is a complex, finite, physicochemical entity. Even though the temperature gradient is large at the propellant surface and becomes larger with increasing pressure, the thermal wave still penetrates many unit-cell distances into the repeating lattice of the crystalline monopropellant. For example, a surface reaction zone thickness of 1 μm corresponds to roughly 100 unit-cell lengths of the crystal of HMX or RDX. Hence, the disappearance of an obvious liquid layer at high pressure does not necessarily signal the end of condensed-phase chemistry at the surface.

The surface reaction layer does not refer solely to solid- or liquid-phase pyrolysis reactions of the formulated propellant components. Neither does it refer solely to homogeneous gas-

phase reactions next to the surface. A more general and accurate description is that of a heterogeneous (or two-phase) zone that includes developing voids and/or bubbles with nanoscopic and microscopic dimensions.[2,3] On the vapor-phase side, the surface boundary is physically rough and dynamically changing owing to the microscopic gasification dynamics. Nominally gas-phase reactions can occur within the multiphase zone and in the near field of the disintegrating surface. Therefore, the operative thickness of the surface reaction zone from the point of view of chemistry is somewhat larger than simply the thickness of the melt layer. However, at least for AP, Hermance[16] had to assume a surface area that is much larger than observed[12] to achieve satisfactory agreement with the characteristics of combustion. Although this detail of Hermance's model seems unreasonable, the ill-defined heterogeneous depiction of the surface is chemically attractive. It enables changes in temperature and pressure to define the changes in species concentrations that are associated with the surface layer. For RDX, Li et al.[2] found that the two-phase surface model and infinitely thin surface model gave similar results in their description of combustion. The distinction between these two models depended largely on the volatility of propellant components.

Finally, the term "melting" is loosely used to describe the formation of the liquid layer on the surface of burning RDX and HMX. However, melting is better reserved for the equilibrium first-order phase transition between the solid and liquid states. To a lesser degree in the case of RDX and a greater degree in the case of HMX,[17] decomposition occurs simultaneously with the change of state. The terms "progressive melting" or simply "liquefaction" more soundly describe this event.[17-20]

III. Evolving View of the Importance of the Surface Reaction Zone

Of course, models of the combustion of solid propellants contain assumptions based on necessity and wisdom at the time. Evolution of conventional wisdom occurs because of subsequent experimental data and the increase in computational power. Throughout this article, limitations of assumptions are occasionally noted. This is done in the spirit of stimulating thought rather than criticism.

Rather than review combustion models, which has been done expertly elsewhere,[21-27] the focus of this section is to mention whether and how the surface reaction zone has been incorporated. Historically, extensive research and modeling of solid-rocket-propellant combustion was developed in the context of the contribution of the gas phase. In the views of Lewis and von Elbe[28] and Zeldovich,[29] the combustion mechanism was dominated by the gas phase. Belyaev[30] experimentally observed that evaporation followed by gas-phase reaction occurred during combustion of an explosive. Heat from the gas phase was believed to sustain pyrolysis of the surface. This viewpoint, in which gas-phase control was widely accepted, profoundly influenced many subsequent approaches to modeling of steady combustion. It is certainly fair to say that combustion characteristics of highly volatile energetic materials will be overwhelmingly dominated by gas-phase chemistry. However, a wealth of experimental and computational evidence has appeared since these early reports, which reveals that the 1–50-μm-thick surface reaction zone and the ill-defined phase transition to the very near-field gaseous state are major factors or even dominate in determining the combustion characteristics of most solid propellants and their energetic components.

A brief description of several efforts to model the combustion of homogeneous and heterogenous propellants places the present state of understanding of the surface zone into context. Among the pioneering descriptions of the near field during combustion of solid propellants were the works of Rice and Ginnell,[7] Parr and Crawford,[8] and Wilfong et al.,[9] the latter of whom developed their ideas in 1941.[22] A sequence of primary and secondary reactions of homogeneous double-base propellants was proposed to account for the surface gasification and the dark zone of the flame against the surface. Heterogeneous propellants were tackled in the granular diffusion flame (GDF) model of Summerfield and co-workers.[31,32] Experimental observations and theoretical work revealed a nonturbulent gaseous zone of up to 1 mm thickness against the surface of an AP composite propellant, and that most of the heat is released within about 100 μm of the surface. Heterogeneity of the surface and the release of heat at the surface were introduced by Hermance[16] in a refinement of the GDF model. This model can certainly be cited as one that sets the stage for incorporation of a finite surface reaction layer into combustion modeling. Subsequent models of Beckstead et al.[12,33,34] and Guirao and Williams[35] both concluded that 70–75% of the heat of AP is released in the condensed-phase surface zone. However, the absence of experimental details about chemistry prompted emphasis to be placed on the transport and spatial aspects of combustion as opposed to the chemical reaction sequences. In fact, the surface zone was set aside in many subsequent descriptions of solid propellant combustion in favor of attention to flame structure. For example, the model of Beckstead et al.,[12,33,34] (BDP) generalized an approach for modeling flame structure and emphasized the major role played by the surface temperature. The petite ensemble model of Glick[36] statistically refined the flame structure according to the effect of different particle sizes of the oxidizer in a composite propellant. The effects of particle size on the combustion characteristics were also refined.[37] Miller attempted to formulate a general model of homogeneous propellant combustion based on a single-step process in each phase.[38]

More recently, models of solid propellant combustion have incorporated multistep kinetics and heat release. The majority of these models retain the simplicity of an infinitely thin surface zone that is merely a source of reactants for the gaseous flame zone. Examples of this approach are summarized first. While such models might be considered to originate from the early descriptions of double-base propellants,[7-9] the model of Guirao and Williams[35] describing the combustion of AP also stands out as a pioneering effort. They incorporate a global decomposition rate for the condensed phase, but specific gas-phase reactions. Subsequent models of AP combustion[39,40] make use of more complex gas-phase reaction schemes, some of which are controversial.[41] An attempt to refine several aspects of the surface zone chemistry of AP has been made.[42] Models of the combustion of HMX and RDX with specific reaction kinetics have been presented.[24,43-52] Widely differing numbers of reactions and species are included in these models, however, many aspects of the gas-phase chemistry have been experimentally verified. In particular, mass spectrometry, in which a quartz microprobe is inserted into the flame to sample the species, is especially useful.[53-55]

The expanding effort to model physicochemical details of the surface reaction layer foretells how its role has become recognized. Reactions involving this heterophase layer are now considered by many workers to play a significant role in controlling the burning rate. The weight of experimental evidence for this belief is growing. Many studies indicate that most of the heat comes from exothermic processes in a thin surface layer and not from the far-field gas phase.[12,15,33-35,56,57] Relevant, but perhaps less convincing, studies are of burn-rate enhancement, which suggest that most of the action occurs in the condensed phase.[58,59]

Although early work on double-base propellants did stress the importance of the surface reaction zone,[7-9], detailed descriptions of the process came later in the articles by Merzhanov[60] and Strunin and Manelis[61] on AP. Combustion models[2,12,33-35,62-64] on nitramines incorporate a finite surface layer in which a global rate of decomposition is assumed. Huang

et al.[3] have used specific reactions in the surface layer as discussed in Sec. V. A major fraction of the heat is released in the surface layer in most models developed by Williams and coworkers[2,35,62] and by Beckstead and coworkers.[12,33-45] Cohen et al.[47] updated the gas-phase kinetics in the model of Ben-Reuven et al.,[63,64] and concluded that most of the heat is released by HMX within 10 μm of the surface. This distance is within the control volume that defines the multiphase zone of a burning surface. Along the same lines Zenin[15] found that 80–90% of the heat is released in the condensed phase during combustion of nitrocellulose. In none of these models or experiments is there an implication that the gas phase can be ignored. The main point is that both the condensed phase and the gas phase must be modeled to achieve truly accurate predictions.

The partitioning of the heat between the condensed phase and gas phase depends on pressure and the formulation of the propellant. In modeling efforts, the relative contributions of each phase depend on the assumptions and parameters chosen. In this article, the focus is on the role played by the rates of several specific chemical reactions in the surface zone of a solid propellant under conditions representative of combustion. This component is but one of the important aspects of the total description of combustion of the solid propellant.

IV. Surface Reaction Zone: Description with Global Rates

Global Arrhenius parameters for the surface reaction zone are best viewed as giving only the temperature dependence of the overall process. This definition is broader than process control by the chemical kinetics alone.[65] Equation (1) is the well-known Arrhenius equation for describing the temperature dependence of the rate of conversion, $d\alpha/dt$. With the foregoing precautionary comment in mind, the terms

$$\frac{d\alpha}{dt} = (1 - \alpha)^n A e^{-E_a/RT} \tag{1}$$

activation energy E_a, prefactor A, and order of the process n will be retained.

Two types of global Arrhenius parameters for surface processes must be distinguished. These are the surface activation energy and the chemical activation energy. The surface activation energy E_s is obtained from the pyrolysis law (2). Measured linear regression rates $\dot{r}$ at various surface temperatures T_s define the value of E_s. Surface regression to which Eq. (2) applies is a zero-order process because fresh

$$\dot{r} = A_s e^{-E_s/RT_s} = aP^b \tag{2}$$

reactant replaces gasified products at a constant rate.

Diffusion, vaporization, and reaction rates all contribute to the value of E_s. In fact, Eq. (2) applies over only limited pressure ranges where the pressure exponent b remains constant. Nevertheless, surface activation energies have occasionally been mentioned in the same context as chemical activation energies,[66,67] such as bond-breaking steps or bimolecular reactions. It is risky to equate E_s and E_a. First, the rate law for the rate-controlling chemical reactions, such as homolyses of specific bonds in the surface reaction zone, is likely to be predominately first-order, which makes the Arrhenius parameters for regression and bond homolysis not directly comparable. Second, the contributions of transport and chemical rates are mixed in E_s. Third, starting with Merzhanov and Dubovitskii,[68] a number of authors[13,69] have shown that the square of the linear regression rate is related to the Arrhenius parameters of bulk-phase chemical decomposition. Equation (3) shows this relationship for many propellants, where T_0 is the initial temperature, d is the thermal diffusivity, Q is the heat released in the surface layer T_s^2 and C_p is the heat capacity.

$$\dot{r}^2 = \frac{dRT_s^2 A e^{-E_a/RT_s}}{E_a(T_s - T_0 - Q/2C_p)} \tag{3}$$

According to Eq. (3), $E_s \propto E_a/2$. In practice, the values of E_s are indeed usually small[70] compared to the strength of the weakest bond in energetic molecules and the global Arrhenius parameters for decomposition of HMX and RDX[71] that are derived from differential scanning calorimetry (DSC), thermogravimetric analysis (TGA), and manometry. Equation (3) has a better chance to predict burn rates than Eq. (2) when the gas and condensed phases are coupled. Other aspects of Eq. (2) are mentioned by Zanotti et al.[72]

The global rates referred to in the title of this section are of the second kind, namely decomposition rates extracted from Eq. (1) by measuring the rate of heat release, pressure increase, or weight decrease. A compilation of published Arrhenius parameters (E_a, A) for slow thermal decomposition of HMX and RDX in the solid, liquid, and vapor phases reveals poor agreement, irrespective of the phase.[71] For HMX, $22E_a$ values for the solid phase cover 13–67 kcal/mol. Six values for the liquid phase are E_a = 47–65 kcal/mol, and six values for the vapor phase are E_a = 32–53 kcal/mol. For all but one case, the differences among E_a values are compensated by differences in A, so that the plot of E_a vs $\ln A$ produces an approximately straight line.[71] As a result, the rates of decomposition are roughly the same over the temperature range of measurement. In effect, all of the E_a-$\ln A$ combinations on this regression line legitimately describe the rate of decomposition. The wide range of E_a values is caused by differences in the sample characteristics and the experimental conditions. However, extrapolation of the rates from these E_a-$\ln A$ pairs to another temperature range, such as the one that exists during combustion, gives wildly different predictions.

Several models of combustion of HMX and RDX make use of global rates of decomposition in the liquid and/or gas phases.[2,38,45,47,50,62-64] The values usually chosen lie in the experimentally determined range for slow decomposition, but Mitani and Williams[62] expressed concern about the fact that the Arrhenius parameters required for their model are at the low end of this experimental range. Because of the compensation effect, their choice of values is not cause for concern. Any E_a-$\ln A$ pair lying on the compensation line, whether measured or not, is a legitimate representation of the rate at some particular set of conditions.[71] There is no single intrinsically "correct" global rate of decomposition of bulk phase HMX or RDX because the determined values depend on the sample characteristics and working conditions.[71] Therefore, in combustion models containing these global rates, the E_a-$\ln A$ pair should be viewed as an adjustable parameter along the compensation line, as opposed to a parameter that is fixed by the "correct" rate of decomposition. No one can take issue with the E_a-$\ln A$ combination as long as it resides along the compensation line.

V. Surface Reaction Zone: Description with Specific Reactions

Rather than using phase-dependent global rates of thermal decomposition, many authors of combustion models have employed the rates of specific reactions of the parent molecule and its products. This approach is ultimately preferable to using only phase-dependent global rates because it enables more accurate refinements to be made on the effects of temperature and pressure. Several aspects of this approach are heuristic, which stimulates suspicions and contrary opinions. For example, a critical evaluation[41] of previous gas-phase reaction schemes for combustion of AP[35,39,40] revealed unreasonable assumptions in each case and motivated development

of yet another scheme.[41] Similar uncertainty exists with RDX and HMX, and will no doubt arise in efforts to describe combustion of the next generation of energetic materials.

A. Thermolysis Reactions of HMX and RDX

The thermal decomposition pathways of RDX and HMX in the condensed phase have become much better defined in recent years.[73] Significant differences exist between reactions that occur at lower temperature/heating rate conditions[74-78] and those at higher temperature/heating rates.[4-6,79,80]

Many combustion models now incorporate the kinetics of specific reactions beginning with decomposition of HMX or RDX. Essentially two schemes have been used. Scheme I [Eqs. (4) and (5)] was the first:

$$HMX(g) \rightarrow 4/3NO_2 + 4/3N_2O + 2N_2 + 4CH_2O \quad (4)$$

$$HMX(l) \rightarrow NO + 3N_2O + 1/2N_2 + 4CH_2O \quad (5)$$

The exothermic reaction (4) in Scheme I appears to have been adopted from the decomposition data of Suryanarayana and Graybush[81] and Cosgrove and Owen,[82,83] which were obtained in the lower temperature/heating rate regime. Reaction (4) has been employed in many combustion models, such as those of Ben Reuven et al., for RDX[63] and HMX[64]; Ermolin et al.,[49] for RDX; Mitani and Williams[62] and Kubota and Sakamoto[84] for HMX. Ben-Reuven et al., use reaction (5) in Scheme I as well for the liquid phase. Scheme I is difficult to accept for the combustion regime because it fails to account for the high level of HCN and the low level of N_2 at the burning surface of RDX found by quartz microprobe mass spectrometry[53-55]:

$$HMX(RDX) \begin{cases} \nearrow\ 4(3)\ (CH_2O + N_2O) & (6) \\ \searrow\ 4(3)\ (HCN + HONO) & (7) \end{cases}$$

Scheme II [Eqs. (6) and (7)] is another decomposition pathway that states that rapid thermolysis of HMX and RDX occurs by two competing branches represented by (6) and (7). The formalism for reaction (7) varies, i.e., the products might also be written as $H_2CN + NO_2$ or $H\cdot + NO_2 + HCN$. When written as shown, reaction (6) is exothermic (-29 kcal/mol), whereas (7) is endothermic ($+28$ kcal/mol) by about the same energy.[51] Scheme II is more attractive than Scheme I because it has experimental support in the gaseous products that are liberated during combustion[53-55] and from a film of HMX or RDX when heated at a high rate to temperatures in the range of the burning surface.[5,80,85] This latter experiment is described later in this article. Scheme II has been adopted in several models of nitramine combustion, many of which predated experimental verification. For example, Price et al.[43] incorporated a portion of Scheme II into the BDP description of nitramine flame structure. However, their proposed temperature dependence of several products of reactions (6) and (7) was opposite that determined subsequently by experiment.[5] More recent models and descriptions[3,46,50,51,86,87] employ (6) and (7), and where used, (6) and (7) appear to be given the correct temperature dependence.

Scheme II cannot be verified directly with a burning solid propellant because the surface reaction zone is spatially very thin and positionally transient, possesses a steep temperature gradient, and has a mixture of phases. Although optical spectroscopy of the gaseous phase close to the surface has been achieved,[88-90] the critical near field at ≤ 20 μm from the surface has not been probed. Therefore, laboratory simulation experiments have been invented[80,91,92] to try to outline the major chemical processes. A reasonably well-controlled technique is T-jump/FTS-IR spectroscopy, in which a "snapshot" experimental simulation of the surface reaction layer is attempted.[91] This technique has been discussed and modeled sufficiently,[91-93] and so only a brief description will be given here. A thin *Pt* ribbon filament is used to heat a film of material of about 200 μg mass at $dT/dt = 2000$ K/s to a constant temperature representative of the surface during steady combustion. This set temperature is maintained while the gaseous products evolve into the cool surrounding atmosphere of an inert gas. These products are monitored several mm above the surface in near real-time by rapid-scan (50–100 ms/scan) FTS-IR spectroscopy. The sequence of formation and identity of the products outline the thermal decomposition pathway of the simulated surface layer. These products react in the multiphase surface zone, the dark zone, and the luminous flame. The change of the control voltage across the *Pt* filament is measured simultaneously and indicates the sequential endothermicity and exothermicity of this simulated surface reaction layer.

T-jump/FTS-IR spectra of pyrolyzed bulk samples of HMX[5] and RDX[85] verify the essential details of Scheme II, at least to the 25 atm and 700 K limits of study. Consonant with Scheme II, the initially detected thermolysis products are NO_2 and N_2O, whereas the formation of CH_2O and HCN is slightly delayed. The overall process is approximately thermally neutral. A second important finding is that the concentration ratio of N_2O/NO_2 depends on the set temperature.[5] The pattern is shown in Fig. 1. Thus, reaction (6) is favored at lower temperature, whereas reaction (7) is favored at high temperature. This trend is corroborated by lower temperature-lower heating rate experiments, which show that N_2O and CH_2O are among the major products.[77] N_2O is also detected in the cooler subsurface by IR-fiber optic interrogation of a burning propellant composed mostly of RDX.[94] Conversely, high heating rate experiments on HMX, such as those of Morgan and Beyer,[4] reveal H_2CN and NO_2, while those of Botcher and Wight[6] on RDX reveal that NO_2 is the only nitrogen oxide cleaved from RDX. The concentration of NO_2 is maximum near the surface of RDX according to uv-visible absorption and planar laser-induced fluorescence (PLIF) measurements at 1 atm by Hanson-Parr and Parr.[95] Despite the qualitative agreements among products, there is no absolute proof that Scheme II is complete. For example, a small amount of CO_2 appears early in the T-jump/FTS-IR measurements,[5] and a

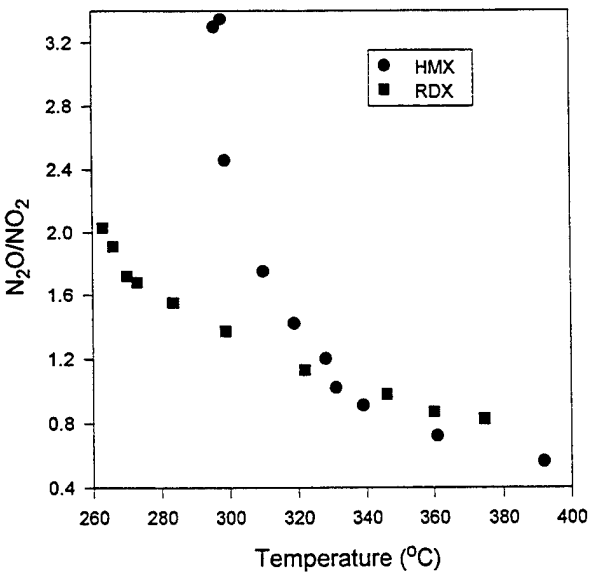

Fig. 1 Experimental N_2O/NO_2 ratio after 10 s at 5 atm Ar from T-jump/FTIR spectroscopy of HMX and RDX at the temperatures shown. The ratios above 320°C were used and taken to be the same for RDX and HMX within experimental accuracy.

larger amount is found in the time-of-flight (TOF) mass spectrometry data of Fetherolf et al.[55]

Going beyond Scheme II by dividing reactions (6) and (7) into a series of verifiable elementary steps in the multiphase zone of the combustion wave will be very difficult. The fact that N_2O and NO_2 do not even appear simultaneously with CH_2O and HCN is an indication that each product in Scheme II forms by a different step.[5,75,85] Also, substantial evidence is available that H-atom transfer occurs in the rate-determining step of burning RDX and HMX.[96] These facts all indicate that many chemical details are imbedded in this semiglobal description. However, the semiglobal nature of Scheme II must be retained if the combustion description is to rest mostly upon experimental evidence rather than conjecture.

In summary, Scheme II appears to play a major role in the thermal decomposition of the liquid and vapor phases of RDX and HMX at pressures above 1 atm. Competition of Scheme II with several other lesser abundant reactions is not rigorously ruled out. The competition between reactions (6) and (7) in Scheme II depends on temperature, as revealed by Fig. 1. However, Scheme II is approximately thermally neutral so that reactions that generate heat to sustain (6) and (7) must be determined. Several plausible reactions, one of which has been experimentally indicated to involve the interfacial zone, are considered next.

B. Heat Generation Reactions of HMX and RDX

Because Scheme II is experimentally observed to produce little heat,[5] secondary reactions among the products of reactions (6) and (7) must provide the heat to sustain pyrolysis. These reactions can occur in the bulk phase, in bubbles, and on the near-field gaseous side of the surface. Several plausible secondary reactions are considered here: $CH_2O + NO_2$, $CH_2O + N_2O$, and $HCN + NO_2$. The relative merits of these reactions can be specified by spectroscopic observation and kinetic modeling.

1. $CH_2O + NO_2$

By T-jump/FTS-IR spectroscopy, the strong exotherm during decomposition of the molten film of HMX and RDX coincides with the formation of NO, H_2O, and CO.[5,85] CH_2O and NO_2 simultaneously diminish, which is consistent with the occurrence of reaction (8):

$$CH_2O + NO_2 \rightarrow CO + NO + H_2O \ (\Delta H = -44 \text{ kcal/mol}) \quad (8)$$

This reaction can also be balanced by using additional products as shown in (9)[64] and (10),[87] with somewhat different resulting values of ΔH. Reaction (9) differs from (8) by further oxidation of CO by NO_2. Reaction (10) is unsatisfying chemically because it is like (8), except that CO is oxidized by H_2O. The product stoichiometry of (9) is most consistent with T-jump/FTS-IR spectroscopy[5]:

$$5CH_2O + 7NO_2 \rightarrow 3CO + 2CO_2 + 7NO + 5H_2O \quad (9)$$

$$2CH_2O + 2NO_2 \rightarrow CO + CO_2 + 2NO + H_2O + H_2 \quad (10)$$

Previous thermolysis[80,82] and controlled atmosphere studies[97] are consistent with (8) and (9). Because of the design of the T-jump/FTS-IR experiment, exothermicity will not be detected unless a large heat transfer coefficient exists between the sample and the filament.[91] This condition exists only if (8) and (9) occur as part of the two-phase zone as opposed to only the near-field gas phase. Several mass spectral and optical determinations of the gaseous products in the near field during the combustion of HMX and RDX qualitatively support Scheme II and reactions (8) and (9).[48,49,53-55,95] For example, the large quantity of NO can be attributed to (8) and (9), while the large quantity of HCN and the large HCN/N_2O ratio in the near-field gaseous regime[47-49,51,53-55,88] are consistent with dominance of reaction (7) over (6) and the occurrence of reactions (8) and (9). The consensus of modeling efforts on HMX and RDX has also been that reactions (8) and (9) play a crucial role in the surface and near-field gaseous zones.[46,50,51,63,64,84,87]

In practice, quantitative specifics of reactions (6–9) are difficult to define when they occur in the two-phase region. Reaction (8) is second-order in the gas phase.[98] Sizable differences exist in the reported Arrhenius parameters for (8),[98-100] which are shown in Table 1. None of these experimentally determined rates were used by Cohen et al.,[47] or Kubota[13] in their descriptions. However, greatest confidence can probably be placed in the kinetic measurements by Lin et al.,[98] because of the wide temperature range over which their mechanistic model seems to apply. Still, these kinetics were determined for the gas phase. The rate is likely to be different when reaction (8) takes place in the condensed phase and at the gas-liquid interface. It is important to have the phase dependence of the rate, which is unknown at this time. The following systematic approach is suggested to scale the rate between phases. If the plausible assumption is made that the mechanism of reaction (8) is similar in the gas, liquid, and gas–liquid interfacial regions, then a kinetic compensation effect should exist in the Arrhenius parameters for these regions.[71] That is, the values of E_a and $\ln A$ can be increased or decreased pairwise so that a particular isokinetic temperature is maintained, but the rate at other temperatures or in other phases becomes different. Reaction (8) could be expected to have up to roughly 30% larger Arrhenius parameters in the liquid state than in the vapor state, based on comparison with the global kinetics of decomposition of HMX and RDX.[71]

Finally, the pressure dependence of reaction (8) has not been determined. The effect of pressure on a specific chemical reaction depends on the change of the volume of activation in the rate determining step. This step in the bimolecular reaction (8) is the transfer of H from CH_2O to NO_2,[98] which is likely to have a small volume of activation and, thus, small pressure dependence. However, in the surface reaction zone, reactions (8) and (9) take place as part of a multiphase reaction layer in which CH_2O and NO_2 continuously form according to Scheme II and are depleted by reactions (8) and (9). In this case, the process is pressure-dependent because the density of CH_2O and NO_2 in the control volume of the surface and near-field gaseous reaction zones[102] is higher at elevated pressure. It is easiest to account for the effect of pressure on the rate by using the perfect gas law. Equation (11) results, but overestimates the effect at high pressure. As will be discussed in Sec. VIII, reactions (8) and (9) appear to

Table 1 Arrhenius parameters for exothermic reactions

T, K	A, cc/mol s	E_a, kcal/mol	Reference
	$CH_2O + NO_2$		
>443	10^{12}	19.0	99
1424–1910	$10^{13.1}$	26.7	100
300–2000	$8.02 \times 10^2 T^{2.77}$	13.73	98
	$HCN + NO_2$		
1424–1910	4.9×10^{11}	43.3[a]	100
350–600	1×10^{12}	25.0	101
	$CH_2O + N_2O$		
1424–1910	8.41×10^{11}	27.4[b]	100

[a]Order is reported to be 1.67. [b]Order is reported to be 1.65.

dominate in producing heat, at least at pressures up to 100 atm and temperatures up to 700–800 K:

$$k = (AP/RT)e^{-E_a/RT} \quad (11)$$

2. HCN + NO_2

HCN and NO_2 are increasingly preferred decomposition products of HMX and RDX as the temperature increases (Fig. 1). Consequently, reactions (12) and (13)[103] could contribute extensively at higher temperature:

$$2HCN + NO_2 \rightarrow C_2N_2 + NO + H_2O$$
$$(\Delta H = -33 \text{ kcal/mol}) \quad (12)$$

$$2HCN + 3NO_2 \rightarrow 2CO + 3NO + N_2 + H_2O$$
$$(\Delta H = -132 \text{ kcal/mol}) \quad (13)$$

Substantially different rates have been measured for the exothermic reaction of HCN and NO_2 (Table 1). Because of modeling, the kinetic measurement of He et al.[101] is best-supported.

3. $CH_2O + N_2O$

In a description of nitramine combustion reactions that predated most of the kinetic measurements in Table 1, McCarty[66] suggested an important role for reaction (14). Knowledge about the products of thermal decomposition of HMX and RDX at the time of McCarty's report came primarily from studies at low heating rates and low temperatures in which CH_2O and N_2O are major products:

$$CH_2O + N_2O \rightarrow N_2 + CO + H_2O \ (\Delta H = -74.5 \text{ kcal/mol}) \quad (14)$$

As noted previously, these products are dominated by HCN and NO_2 under combustion-like conditions.[4–6] The only measured rate constant found for reaction (14) (Table 1) is from Fifer and Holmes,[100] but others subsequently assumed very different rates in combustion models, e.g., k (cc/mol·s) = $1.2 \times 10^{13} \exp(-44{,}000/RT)$,[63] and $k = 3.2 \times 10^7 \exp(-16{,}000/RT)$.[41] Several other models of combustion make use of reaction (14).[13,50] When Hatch allowed reaction (14) to dominate, the burning rate of HMX at 67 atm was twice the experimental value.[50] On the other hand, Ben-Reuven et al.[63] discounted the role of reaction (14).

It should be mentioned that Korobeinichev et al.[53] did not believe that reactions (8–14) [especially (8) and (9)] play as large a role in the near field as the reaction of HCN with NO. Since NO is itself a product of many of the secondary exothermic reactions given above, the HCN + NO reaction would belong to a tertiary class of reactions. The conclusions of Korobeinichev et al.[53] were based largely on quartz microprobe mass spectrometry measurements and modeling of the flame zone of RDX. The inability to probe and separate the most reactive species very close to the surface will tend to skew the description of the chemistry toward a farther field, such as the dark zone, where the reaction of HCN and NO could indeed be quite important.

VI. Vaporization of Intact HMX and RDX

The equilibrium vapor pressure P_v above the solid or liquid phase of a pure substance depends on temperature according to the Van't Hoff Eq. (15), where $\Delta H°$ is the standard heat

$$P_v = P_0 e^{-\Delta H°/RT} \quad (15)$$

of vaporization. The heat of vaporization decreases with increasing temperature and reaches zero at the vapor–liquid critical point. This change of ΔH with temperature is not accounted for by (15), which yields a straight line. Consequently, Eq. (16), which parametrically allows for the change of ΔH with temperature, is needed:

$$\Delta H(T) = \Delta H° + aT + bT^2 + cT^3 + \cdots \quad (16)$$

Unfortunately, Eq. (16) has not been parameterized for HMX or RDX.

Measurements of the solid-vapor equilibrium ($\Delta H°_{subl}$) of HMX and RDX[104–108] by Eq. (15) are summarized in Table 2. The vapor pressure for RDX is greater than HMX at a given temperature. No measurements have been reported for the liquid–vapor equilibrium, so that $\Delta H°_{evap}$ is commonly extracted from Eq. (17). $\Delta H°_{melting}$ for RDX is 8.52 kcal/mol, whereas the value for HMX is estimated to be 11.4 kcal/mol[64]:

$$\Delta H°_{evap} = \Delta H°_{subl} - \Delta H°_{melting} \quad (17)$$

The Arrhenius equation for the rate of vaporization [Eq. (1), $n = 0$] has the same form as Eq. (15). Measurements of the rate vaporization of HMX yield E_a = 38 and 22.9 kcal/mol,[109] but no A factor was reported. An estimate of E_a from $\Delta H°_{subl}$ gave E_a = 39.45 kcal/mol,[109] although the reasoning is dubious. Melius estimated $k = 7.5 \times 10^{16} \exp(-22{,}600/RT)$ s^{-1} for the rate of evaporation of RDX in his combustion model.[51] A frequent method to obtain the rate of vaporization has been to use the prima facie similarity of the kinetic Eq. (1) and the thermodynamic Eq. (15) and transfer the variables between them.[62–64] In doing so, the approximation is accepted that liquid–vapor equilibrium exists next to the burning surface. However, this is not quite true under combustion conditions because of the high velocity mass flow away from the surface. Furthermore, as was just noted, the value of ΔH_{evap} changes with temperature. It is only a rough approximation to extrapolate ΔH_{evap} from the lower temperature range of measurement to the higher temperature range of combustion. Melius[51] used the difference between the rate of evaporation and condensation to obtain the burning rate, while Mitani and Williams[62] used vapor pressure as a means to calculate the surface temperature.

The parameters chosen for Eq. (15) and the pressure and temperature dependence assumed for vaporization affect the division of heat between the gaseous and condensed phases. Although this is an important detail, the influence of evaporation is not considered further here because the focus is on the extensive experimental evidence for both chemical reaction and heat release in the surface layer, at least at pressures below 67 atm.

VII. Surface Temperature Measurements

The surface temperature T_s during combustion is most commonly determined by using a microthermocouple imbedded in the material. Various considerations are summarized by

Table 2 Vaporization parameters for RDX and HMX [Eq. (15)]

T, °C	log A, mm Hg	$\Delta H°_{subl}$, cal/mol	Reference
	RDX		
56–98	14.18	31,110	105
56–140[a]	14.4 ± 0.6	31,500 ± 500	108
70–174	16.89	32,080	107
110–138	10.87	26,770	104
	HMX		
97–129	16.18	41,890	105
97–214[b]	17.6 ± 1.9	44,300 ± 700	108
142–206	16.86	38,470	107
188–213	14.95 ± 0.23	38,600 ± 1,000	106

[a]Curve fit of data in Refs. 104 and 105.
[b]Curve fit of data in Refs. 105 and 106.

Zanotti et al.[72] Through limited pressure ranges, changes in the ambient pressure cause approximately parallel changes in the burning rate and T_s by Eq. (2). However, Beckstead noted the poor agreement among the experimentally determined surface temperatures of HMX and the burn rate (Fig. 2).[110] The data of Mitani and Takahashi[111] are the most extensive, but also the most unusual. The lowest regression rates are considerably below the liquefaction temperature of HMX. The temperatures determined by Lengellé and Duterque[112] are consistently higher than those of Kubota and Sakamoto[113] and Parr and Hanson-Parr.[114] Because of the steep temperature gradient at the surface, higher surface temperatures will result if a portion of the flame zone becomes included in the measurement. By excluding the data of Mitani and Takahashi, the three remaining studies are consistent in showing that the surface temperature of burning HMX is in the 650–850 K range at the pressures used. This range is too wide to be of specific value for defining chemical kinetics, but it is qualitatively useful.

Calculated surface temperatures from several combustion models of HMX and RDX are listed in Table 3. The agreement is not much better than in the experimental data, but the expected trend of increasing surface temperature with pressure roughly exists. The lower surface temperatures for RDX compared to HMX have been attributed to the lower heat of vaporization and melting point of RDX.[62]

One might try to estimate the boiling temperature T_b of RDX and HMX from Trouton's rule, Eq. (18). This estimate presumes that RDX and HMX boil without decomposition, which is clearly not true. However, $T_s = T_b$ with this assumption:

$$\Delta H_{evap}/T_b = x \tag{18}$$

It also requires that the value of x be known. For nonpolar liquids, x = 21–22 cal/deg mol. For energetic materials exhibiting some association in the liquid state, x is probably larger. For example, x = 23–32 cal/deg mol for nitroaromatic compounds.[116] A conservative value of x = 30 cal/deg mol was chosen here just to see what Eq. (18) predicts for RDX and HMX. ΔH_{evap} was estimated from Eq. (17) by using the ΔH_{subl} values from Maksimov et al.[108] With these parameters the two additional values of T_s given in Table 3 are obtained. T_s for RDX is on the high side of the reasonable range, whereas T_s for HMX is far too large. These results could be viewed as further evidence that considerable decomposition takes place in the condensed phase of RDX and HMX during combustion, and/or that ΔH_{evap} is smaller in the combustion regime compared to the range in which measurements have been made.

Table 3 Calculated surface temperatures T_s

	T_s, K		
P, atm	RDX	HMX	Reference
0.5	593	—	53
1	549	—	51
1	550	—	115
1	560	680	2
1	690	—	62
1	766	1097	Eq. (18)[a]
20	643	—	51
68	—	874	70
100	630	—	115
100	710	870	2
100	870	—	62

[a]Trouton's rule estimate assuming no reaction in the surface layer and ΔH_{evap} measured at a much lower temperature.

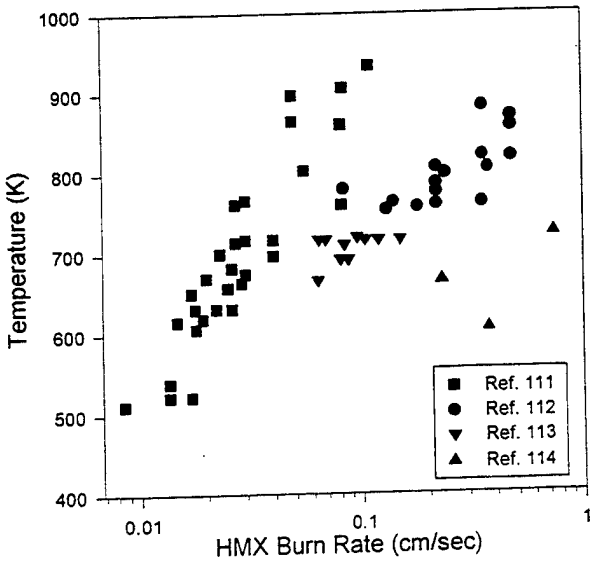

Fig. 2 Surface temperature measurements for HMX.

VIII. Chemical Description of the Surface Reaction Zone

Chemical models of the surface reaction zone, that are couched primarily in experimentally established kinetics, are difficult to validate with measured surface temperatures because of the wide range of available experimental values in Table 3. However, it is possible to estimate the temperature, residence time, and thickness of the surface chemical reaction zone based on kinetics alone. This train of thought concludes this article.

Scheme II and reactions (8–14) frame the chemistry that converts intact HMX and RDX into the heat generation process in the two-phase surface layer defined in Sec. II. The elementary steps, reactive intermediates, and details of homogeneous and heterogeneous processes are not known, but the overall steps can be written to be consistent with the gaseous products detected during simulated and actual combustion. Proceeding on this foundation, reasonable rate constants can be estimated for the decomposition reactions (6) and (7). The rates of (8) and (12), which are strongly exothermic and potentially early stage reactions, then define the fastest rates that are possible at a given temperature and pressure. These predictions can be compared to T_s values in Table 3 for HMX and RDX, and used to estimate the residence time and the surface layer thickness.

A. Rate of Reaction (7)

The rate-determining step of reaction (7) for HMX and RDX is probably N-NO_2 homolysis, which is the first step during rapid thermal decomposition.[6] The simplest way to estimate this rate is by using the rate of thermal decomposition of dimethylnitramine (DMN). Six mostly gas-phase measurements and one estimate of this rate are given in Table 4.[117–122] These data do not agree, but a kinetic compensation effect exists (Fig. 3). The occurrence of the compensation effect suggests bias in the rate measurements which is probably caused by such factors as differences in experimental conditions, wall reactions, and secondary homogeneous reactions.[71] The thermochemical kinetics estimate[119] and the recent measurement by Lloyd et al.[118] are approximately the average of these data. The rate given by Lloyd et al.[118] was chosen here to represent N-NO_2 homolysis. For statistical reasons the value of A was increased by a factor of 3 for RDX, and 4 for HMX yielding (19) and (20):

$$k_7(\text{RDX}) = 10^{16.4} \exp(-44{,}100/RT)\ \text{s}^{-1} \tag{19}$$

$$k_7(\text{HMX}) = 10^{16.5} \exp(-44{,}100/RT)\ \text{s}^{-1} \tag{20}$$

Table 4 Arrhenius parameters for N-NO_2 homolysis of DMN

A, s^{-1}	E_a, cal/mol	Reference
$10^{13.7}$	38,900	117
$10^{14.1}$	40,700 ± 1,800	117
$10^{15.9 \pm 0.2}$	43,700 ± 400	118
$10^{15.8}$	46,200[a]	119
$10^{16.5}$	48,500 ± 1,800	120
$10^{17.8}$	48,100[b]	121
10^{20}	53,100	122

[a]Thermochemical kinetics estimate. [b]In isooctane solution.

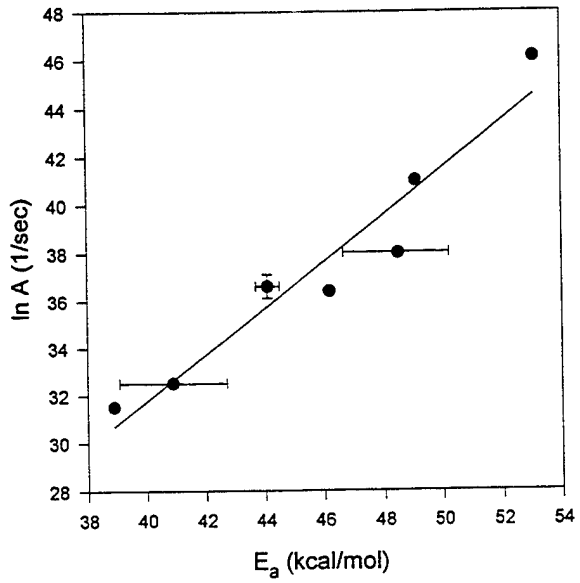

Fig. 3 Kinetic compensation effect that exists in the thermal decomposition rate measurements on dimethylnitramine.

B. Rate of Reaction (6)

N_2O and CH_2O form separately from a complex set of reactions.[5] No simple secondary nitramine is known that forms only N_2O and CH_2O in order that the rate can be determined. However, the rate can be estimated by using the rate of reaction (7) [Eqs. (19) and (20)], and the temperature dependence of the N_2O/NO_2 concentration ratio in Fig. 1. The N_2O/NO_2 ratio should closely track k_7/k_6, because N_2O and NO_2 are unique to reactions (6) and (7). Figure 1 shows that above 330°C, the N_2O/NO_2 concentration ratio for HMX and RDX is the same within experimental error. By fixing the rate of (7) according to Eqs. (19) and (20), the "best fit" Arrhenius constants for reaction (6) can be determined by curve-fitting the ratio in Fig. 1. The rates given by Eqs. (21) and (22) result. These rates broadly agree with those of primary nitramines that thermolyze to N_2O, an aldehyde, and H_2O.[123] Methylenedinitramine[124] affords E_a = 35.4 kcal mol^{-1} and $A = 10^{15.6}$ s^{-1}, while ethylenedinitramine[125] yields E_a = 30.5 kcal/mol and $A = 10^{12.8}$ s^{-1}.

The rates given by Eqs. (19–22) define the initial distribution of products from reactions (6) and (7) for RDX and

$$k_6(\text{RDX}) = 10^{12.9} \exp(-34{,}400/RT)\ s^{-1} \quad (21)$$

$$k_6(\text{HMX}) = 10^{13.0} \exp(-34{,}400/RT)\ s^{-1} \quad (22)$$

HMX at least up to about the temperature of the burning surface. The pressure dependence of these rates is expected to be small because the reactions occur primarily in the condensed phase. However, the product distribution is indirectly affected by pressure because T_s changes with pressure. The products of reactions (6) and (7) are the main reactants for the primary flame zone and are a powerful source of heat.

C. Rates of Primary Exothermic Reactions

As discussed in Sec. V.B., the reaction between CH_2O and NO_2 is indicated by T-jump/FTS-IR spectroscopy to be the first strongly exothermic reaction for RDX and HMX. This reaction can occur in the condensed phase, in bubbles and voids in the liquid layer, and in the gas phase near the surface. Rate measurements of this reaction are summarized in Table 1. However, this nominally gas-phase bimolecular reaction is expected to be sensitive to pressure. Therefore, Eq. (11) was used to describe the contribution of reaction (8).

Although the reaction between HCN and NO_2 [reactions (12) and (13)] was not indicated by T-jump/FTS-IR spectroscopy (no C_2N_2 was observed), HCN and NO_2 become increasingly preferred products as the temperature increases. Consequently, the higher initial concentrations of HCN and NO_2 enhance the potential contribution of (12) and (13) at higher pressure and temperature.

D. Composite Chemistry Description of the Surface Zone

The rearranged version of the Arrhenius Eq. (23) is especially helpful for visualizing combustion and explosion chemistry.[126] The time constant or residence time for essentially complete reaction Δt, rather than the rate constant, can be plotted vs temperature. For a pressure dependent process

$$T_{\text{reaction}} = \frac{E_a}{R(\ln A + \ln \Delta t)} \quad (23)$$

such as the one that occurs with the $CH_2O + NO_2$ and HCN + NO_2 reactions, Eq. (23) is modified with Eq. (11). Of course, the effect at high pressure is given only qualitatively. Figure 4 for HMX is a plot of Eq. (23) for reactions (6) and (7) and reactions (8) and (12) using Eq. (23) modified by Eq. (11). Focusing on reactions (6) and (7) first, (6) is faster than (7) at temperatures below about 600 K. Above 600 K, reaction (7) is faster. Extrapolation of these rates to higher temperatures is dubious, but they are probably reasonable estimates to about 800 K. At this temperature, reaction (7) clearly dominates in accordance with flash pyrolysis data.[6] The decomposition process of HMX and RDX becomes increasingly endothermic to the extent that reaction (7) dominates.

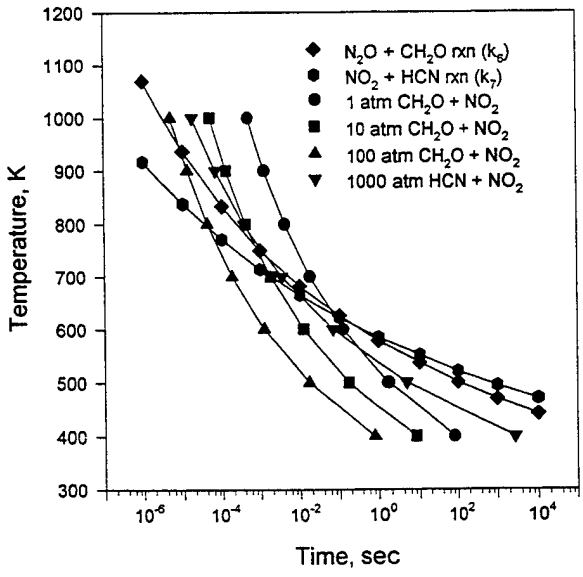

Fig. 4 Plots of Eqs. (11) and (23) for the reactions of HMX indicated. Δt is the residence time of the surface zone at a given temperature T.

Table 5 Predicted surface reaction zone characteristics of HMX and RDX

P, atm	$\dot{r}$, cm/s[a]	T_s,[b] K	Δt,[b] ms	h, μm[c]
1	0.063	~620	100	63
10	0.63	~710	1	6
100	6.3	~800	0.1	6

[a]Reference 113. [b]From Fig. 4. [c]From $\dot{r}$ and residence time [Eq. (24)].

The secondary reactions among the products of (6) and (7) produce the heat needed to sustain (6) and (7). These secondary exothermic reactions must occur at a faster rate than (6) or (7) for a given temperature. Otherwise the decomposition of RDX or HMX will cease. The behavior of the $CH_2O + NO_2$ reaction at 1, 10, and 100 atm is shown. The reaction time of decomposition of HMX and RDX via (6) and (7) must be longer than (to the right of) the $CH_2O + NO_2$ reaction time, in order for $CH_2O + NO_2$ to be the source of heat. The temperature at which the secondary exothermic reaction is complete sets an upper limit on T_s in this simple description of the multiphase surface zone. Reading from Fig. 4, the temperature required for completion of reactions (6) and (7) first, and then followed by (18) at 1 atm is about 620 K, and the residence time for complete reaction is about 100 ms. At 10 atm the surface temperature is roughly 710 K and the residence time is about 1 ms. At 100 atm an interesting situation arises. The surface temperature predicted from the $CH_2O + NO_2$ reaction is about 800 K, at which temperature reaction (7) will greatly dominate (6). In this case the reaction of $HCN + NO_2$ [Eqs. (12) and (13)] might become a significant source of heat. The tentatively known rate of the $HCN + NO_2$ reaction[100] scaled to 1000 atm is shown on Fig. 4. These rates place it slower than the $CH_2O + NO_2$ reaction at the same pressure and temperature. Taken together when driven by completion of these reactions, T_s remains at or below about 800 K. This temperature range is reasonable based on the discussion in Sec. VII.

The thickness of the surface reaction zone h can be estimated from the residence time Δt in Fig. 4. In doing so remember that the surface reaction zone was defined in Sec. II to include both the two-phase liquid layer and the increment of the near-field gas phase that incorporates the microscopic surface roughness. Table 5 summarizes the predicted surface layer thickness for reactions (6), (7), and (8), and burn rate data for HMX from Parr and Parr.[114] Equation (24) was used for these estimates:

$$\dot{r}\Delta t = h \tag{24}$$

The thickness of the surface zone levels out at about 6 μm in the 10–100 atm range, because the burn rate increases and residence time decreases to compensate for one another.

This description of the surface reaction zone is based entirely on the competition of the rates of a few reactions. The approach is offered as a means of evaluating chemical processes that are difficult or impossible to measure directly in a multiphase layer. It would be naive to imply that these reactions can account for every detail. For example, the role of vaporization is currently neglected, as is the assessment of the heat balance from these three reactions. Other secondary and tertiary gas-phase reactions (e.g., NO + HCN) are not included. The rate of $HCN + NO_2$ is still not firmly settled, which adds to further uncertainty about the higher temperature and pressure range. On the other hand, plausible characteristics of the surface layer are predicted by the use of only three competing, experimentally based reactions. Future work remains to refine this description, and to learn more about the changes that take place when an additional component, such as a binder, is present.

Acknowledgments

We are grateful for financial support of this work from the Air Force Office of Scientific Research, Aerospace Sciences, on F49620-94-1-0053, and Pennsylvania State University on Army Research Office Contract DAAL-92-G-0118. Helpful comments by Merrill Beckstead, Stefan Thynell, Charles Wight, and Vigor Yang are appreciated.

References

[1]Alexander, M. H., Dagdigian, P. J., Jacox, M. E., Kolb, C. E., Melius, C. F., Rabitz, H., Smooke, M. D., and Tsang, W., "Nitramine Propellant Ignition and Combustion Research," *Progress in Energy and Combustion Science*, Vol. 17, 1991, pp. 263–296.

[2]Li, S. C., Williams, F. A., and Margolis, S. B., "Effects of Two-Phase Flow in a Model of Nitramine Deflagration," *Combustion and Flame*, Vol. 80, 1990, pp. 329–349.

[3]Huang, T. H., Thynell, S. T., and Kuo, K. K., "Partially Confined Hot Fragment Conductive Ignition: Part I—Modeling," Thirtieth JANNAF Combustion Meeting, Monterey, CA, Nov. 1993.

[4]Morgan, C. U., and Beyer, R. A., "Electron Spin Resonance Studies of HMX Pyrolysis Products," *Combustion and Flame*, Vol. 36, 1979, pp. 99–101.

[5]Brill, T. B., and Brush, P. J., "Condensed Phase Chemistry of Explosives and Propellants at High Temperature: HMX, RDX, and BAMO," *Philosophical Transactions of the Royal Society of London, Series A: Mathematical and Physical Sciences*, Vol. 339, 1992, pp. 377–385.

[6]Botcher, T. R., and Wight, C. A., "Transient Thin Film Laser Pyrolysis of RDX," *Journal of Physical Chemistry*, Vol. 97, 1993, pp. 9149–9153; also "Explosive Thermal Decomposition Mechanism of RDX," *Journal of Physical Chemistry*, Vol. 98, 1994, pp. 5441–5444.

[7]Rice, O. K., and Ginell, R., "The Theory of the Burning of Double Base Rocket Powders," *Journal of Physical and Colloid Chemistry*, Vol. 54, 1950, pp. 885–917.

[8]Parr, R. G., and Crawford, B. L., Jr., "The Physical Theory of Burning of Double Base Rocket Propellants, I," *Journal of Physical and Colloid Chemistry*, Vol. 54, 1950, pp. 929–954.

[9]Wilfong, R. E., Penner, S. S., and Daniels, F., "A Hypothesis for Propellant Burning," *Journal of Physical and Colloid Chemistry*, Vol. 54, 1950, pp. 863–872.

[10]Taylor, J. W., "A Melting Stage in the Burning of Solid Secondary Explosives," *Combustion and Flame*, Vol. 6, 1962, pp. 103–107.

[11]Parr, T. P., and Hanson-Parr, D. M., "Nitramine Flame Structure as a Function of Pressure," *Proceedings of the 26th JANNAF Combustion Meeting*, Vol. I, CPIA Publ. 529, 1989, pp. 27–37.

[12]Boggs, T. L., Derr, R. L., and Beckstead, M. W., "The Surface Structure of Ammonium Perchlorate Composite Propellants," *AIAA Journal*, Vol. 8, 1970, pp. 370–372.

[13]Kubota, N., *Survey of Rocket Propellants and Their Combustion Characteristics*, edited by K. K. Kuo and M. Summerfield, Vol. 90, Progress in Astronautics and Aeronautics, AIAA, New York, 1984, pp. 1–52.

[14]Kuo, K. K., *Principles of Combustion*, Wiley, New York, 1986.

[15]Zenin, A. A., *Thermophysics of Stable Combustion Waves*, Vol. 143, Progress in Astronautics and Aeronautics, AIAA, Washington, DC, 1992, pp. 197–231.

[16]Hermance, C. E., "A Model of Composite Propellant Combustion Including Surface Heterogeneity and Heat Generation," *AIAA Journal*, Vol. 4, 1966, pp. 1629–1637.

[17]Karpowicz, R. J., and Brill, T. B., "In Situ Characterization of the 'Melt' Phase of RDX and HMX by Rapid-Scan FTIR Spectroscopy," *Combustion and Flame*, Vol. 56, 1984, pp. 317–325.

[18]Kraeutle, K. J., "Thermal Decomposition of HMX: Effect of Experimental Conditions and of Additives," *18th JANNAF Combustion Meeting*, Vol. II, CPIA Publ. 347, 1981, pp. 383–394.

[19]Batten, J. J., and Murdie, D. C., "Decomposition of RDX at Temperatures Below the Melting Point," *Australian Journal of Chemistry*, Vol. 25, 1972, pp. 2337–2351.

[20]Hall, P. G., "Thermal Decomposition and Phase Transitions in Solid Nitramines," *Transactions of the Faraday Society*, Vol. 67, 1971, pp. 556–562.

[21]Barrere, M., Jaumotte, A., Venbeke, B. F., and Vandenkerckhove, J., *Rocket Propulsion*, Elsevier, New York, 1960.

[22]Penner, S. S., *Chemical Rocket Propulsion and Combustion Re-*

search, Gordon and Breach, New York, 1962.

[23]Williams, F. A., Barrere, M., and Huang, N. C., "Fundamental Aspects of Solid Propellant Rockets," AGARDograph 116, Technivision, Slough, England, UK, 1969, pp. 395–456.

[24]Beckstead, M. W., and McCarty, K. P., "Calculated Combustion Characteristics of Nitramine Monopropellants," *13th JANNAF Combustion Meeting*, Vol. I, 1976, pp. 57–68.

[25]Kishore, K., "Comprehensive View of the Combustion Models of Composite Solid Propellants," *AIAA Journal*, Vol. 17, 1979, pp. 1216–1224.

[26]Cohen, N. S., "Review of Composite Propellant Burn Rate Modeling," *AIAA Journal*, Vol. 18, 1980, pp. 277–293.

[27]Ramohalli, K. N. R., "Steady State Burning of Composite Propellants Under Zero Cross-Flow Situation," Vol. 90, Progress in Astronautics and Aeronautics, AIAA, New York, 1984, pp. 409–478.

[28]Lewis, B., and Von Elbe, G., "On the Theory of Flame Propagation," *Journal of Chemical Physics*, Vol. 2, 1934, pp. 537–546.

[29]Zeldovich, Ya. B., "Theory of Burning of Powders and of Explosive Substances," *Journal of Experimental and Theoretical Physics (USSR)*, Vol. 12, 1942, pp. 498–524.

[30]Belyaev, A. F., "Combustion of Explosives," *Acta Physical Chemistry URSS*, Vol. 8, 1938, pp. 763–772.

[31]Summerfield, M., Sutherland, G. S., Webb, M. J., Taback, H. J., and Hall, K. P., "Burning Mechanism of Ammonium Perchlorate Propellants," *Solid Propellant Rocket Research*, Academic, New York, 1960, pp. 141–182.

[32]Blair, D. W., Bastress, E. K., Hermance, C. E., Hall, K. P., and Summerfield, M., "Some Problems in Steady-State Burning of Composite Solid Propellants," *Solid Propellant Rocket Research*, Academic, New York, 1960, pp. 183–206.

[33]Beckstead, M. W., Derr, R. L., and Price, C. F., "A Model of Composite Solid Propellant Combustion Based on Multiple Flames," *AIAA Journal*, Vol. 8, 1970, pp. 2200–2207.

[34]Beckstead, M. W., Derr, R. L., and Price, C. F., "The Combustion of Solid Monopropellants and Composite Propellants," *Thirteenth Symposium (International) on Combustion*, The Combustion Institute, Pittsburgh, PA, 1970, pp. 1047–1056.

[35]Guirao, C., and Williams, F. A., "A Model for Ammonium Perchlorate Deflagration Between 20 and 100 Atm," *AIAA Journal*, Vol. 9, 1971, pp. 1345–1356.

[36]Glick, R. L., "On Statistical Analysis of Composite Solid Propellant Combustion," *AIAA Journal*, Vol. 12, 1974, pp. 384, 385.

[37]Condon, J. A., and Osborn, J. R., "The Effect of Oxidizer Particle Size Distribution on the Steady and Non-Steady Combustion of Composite Propellants," Air Force Rocket Propulsion Lab., AFRPL-TR-78-17, Edwards AFB, CA, June 1978; also Miller, R. R., "A Framework for a Totally Statistical Composite Propellant Combustion Model," 19th JANNAF Combustion Meeting, Oct. 1982.

[38]Miller, M. S., "In Search of an Idealized Model of Homogeneous Solid Propellant Combustion," *Combustion and Flame*, Vol. 46, 1982, pp. 51–73.

[39]Ermolin, N. E., Korobeinichev, O. P., Tereshchenko, A. G., and Fomin, V. M., "Kinetic Calculations and Mechanism Definition for Reactions in an Ammonium Perchlorate Flame," *Fizika Goreniya i Vzryva*, Vol. 18, 1982, pp. 180–189.

[40]Sahu, H., Sheshadri, T. S., and Jain, V. K., "Novel Kinetic Scheme for the Ammonium Perchlorate Gas Phase," *Journal of Physical Chemistry*, Vol. 94, 1990, pp. 294, 295.

[41]Cohen, N., "A Review of Kinetic Models of the High Temperature Gas Phase Decomposition of Ammonium Perchlorate," Aerospace Corp., ATR-92(9558)-3, Los Angeles, CA, 1992.

[42]Brill, T. B., Brush, P. J., and Patil, D. G., "Thermal Decomposition of Energetic Materials 60. Major Reaction Stages of a Simulated Burning Surface of NH_4ClO_4," *Combustion and Flame*, Vol. 94, 1993, pp. 70–76.

[43]Price, C. F., Boggs, T. L., and Derr, R. L., "Modeling of Solid Monopropellant Deflagration," AIAA Paper 78-219, Jan. 1978.

[44]Price, C. F., Boggs, T. L., and Derr, R. L., "The Steady-State Combustion Behavior of Ammonium Perchlorate and HMX," AIAA Paper 79-0164, Jan. 1979.

[45]Beckstead, M. W., "A Model for Solid Propellant Combustion," *Eighteenth Symposium (International) on Combustion*, The Combustion Inst., Pittsburgh, PA, 1981, pp. 175–183.

[46]Bizot, A., and Beckstead, M. W., "A Model for HMX Propellant Combustion," *Flame Structure*, edited by O. P. Korobeinichev, Vol. 1, Nauka Siberian Branch, Novosibirsk, USSR, 1991, pp. 230–235.

[47]Cohen, N. S., Lo, G. A., and Crowley, J. C., "Model and Chemistry of HMX Combustion," *AIAA Journal*, Vol. 23, 1985, pp. 276–282.

[48]Ermolin, N. E., Korobeinichev, O. P., Kuibida, L. V., and Fomin, V. M., "Study of the Kinetics and Mechanism of Chemical Reactions in Hexogen Flames," *Fizika Goreniya i Vzryva*, Vol. 22, 1986, pp. 54–64.

[49]Ermolin, N. E., Korobeinichev, O. P., Kuibida, L. V., and Fomin, V. M., "Processes in Hexogene Flames," *Fizika Goreniya i Vzryva*, Vol. 24, 1988, pp. 21–29.

[50]Hatch, R. L., "Chemical Kinetics Modeling of HMX Combustion," *24th JANNAF Combustion Meeting*, Vol. I, CPIA Publ. 476, 1987, pp. 383–391.

[51]Melius, C. F., "Thermochemical Modeling II. Application to Ignition and Combustion of Energetic Materials," *Chemistry and Physics of Energetic Materials*, edited by S. Bulusu, Kluwer, Dordrecht, The Netherlands, 1990, pp. 51–78.

[52]Yetter, R. A., and Dryer, F. L., "RDX Flame Structure," JANNAF Workshop on Kinetics and Related Aspects of Propellant Combustion Chemistry, Langley, VA, Oct. 1992.

[53]Korobeinichev, O. P., et al., "Mass Spectrometric Probe Study of the Flame Structure and Kinetics of Chemistry Reactions in Flames," *Mass-Spectrometry and Chemical Kinetics*, Nauka, Moscow, 1985, pp. 73–93.

[54]Trubert, J. F., "Analysis of the Condensed Phase Degradation Gases of Energetic Binders," AGARD/PEP Specialists' Meeting on Smokeless Propellants, AGARD C. P. 391, Florence, Italy, Sept. 1985.

[55]Fetherolf, B. L., Liiva, P. M., Litzinger, T. A., and Kuo, K. K., "Thermal and Chemical Structure of the Preparation and Reaction Zones for RDX and RDX Composite Propellants," *28th JANNAF Combustion Meeting*, Vol. II, CPIA Publ. 573, Oct. 1991, pp. 379–386.

[56]Kubota, N., "Combustion Mechanisms of Nitramine Composite Propellants," *Eighteenth Symposium (International) on Combustion*, The Combustion Inst., Pittsburgh, PA, 1981, pp. 187–194.

[57]Hsieh, W. H., Li, W. Y., and Yim, Y. J., "Combustion Behavior and Thermochemical Properties of RDX-Based Solid Propellants," AIAA Paper 92-3628, 1992.

[58]Kishore, K., and Gayathri, V., "Chemistry of Ignition and Combustion of Ammonium Perchlorate-Based Propellants," edited by K. K. Kuo and M. Summerfield, Vol. 90, Progress in Astronautics and Aeronautics, AIAA, New York, 1984, pp. 53–119.

[59]Krishnan, S., and Jeenu, R., "Subatmospheric Burning Characteristics of AP/CTPB Composite Propellants with Burning Rate Modifiers," *Combustion and Flame*, Vol. 80, 1990, pp. 1–6.

[60]Merzhanov, A. G., "The Theory of Stable Homogeneous Combustion of Condensed Substances," *Combustion and Flame*, Vol. 13, 1969, pp. 143–156.

[61]Manelis, G. B., and Strunin, V. A., "The Mechanism of Ammonium Perchlorate Burning," *Combustion and Flame*, Vol. 17, 1971, pp. 69–78.

[62]Mitani, T., and Williams, F. A., "A Model for the Deflagration of Nitramines," *Twenty-First Symposium (International) on Combustion*, The Combustion Inst., Pittsburgh, PA, 1986, pp. 1965–1974.

[63]Ben-Reuven, M., Caveny, L. H., Vichnevetsky, R. J., and Summerfield, M., "Flame Zone and Sub-Surface Reaction Model for Deflagrating RDX," *Sixteenth Symposium (International) on Combustion*, The Combustion Inst., Pittsburgh, PA, 1976, pp. 1223–1233.

[64]Ben-Reuven, M., and Caveny, L. H., "Nitramine Flame Chemistry and Deflagration Interpreted in Terms of a Flame Model," *AIAA Journal*, Vol. 19, 1979, pp. 1276–1285.

[65]Brill, T. B., "Structure-Thermolysis Relationships for Energetic Materials," *Chemistry and Physics of Energetic Materials*, edited by S. Bulusu, Kluwer, Dordrecht, The Netherlands, 1990, pp. 277–326.

[66]McCarty, K. P., "HMX Propellant Combustion Studies," Air Force Rocket Propulsion Lab., AFRPL-TR-76-59, Edwards AFB, CA, 1976.

[67]Fifer, R. A., "Chemistry of Nitrate Ester and Nitramine Propellants," edited by K. K. Kuo and M. Summerfield, Vol. 90, Progress in Astronautics and Aeronautics, AIAA, New York, 1984, pp. 177–237.

[68]Merzhanov, A. G., and Dubovitskii, F. I., "On the Theory of Steady State Monopropellant Combustion," *Proceedings of the USSR Academy Sciences*, Vol. 129, 1959, pp. 153–156.

[69]Lengellé, G., "Thermal Degradation Kinetics and Surface Pyrolysis of Vinyl Polymers," *AIAA Journal*, Vol. 8, 1970, pp. 1989–1996.

[70]Beckstead, M. W., "Modeling AN, AP, HMX, and Double-Base Monopropellants," *26th JANNAF Combustion Meeting*, Vol. 4, CPIA Publ. 529, 1989, pp. 255–286.

[71]Brill, T. B., Gongwer, P. E., and Williams, G. K., "Thermal Decomposition of Energetic Materials 66. Kinetic Compensation Effects in HMX, RDX, and NTO," *Journal of Physical Chemistry*, Vol. 98, 1994, pp. 12,242–12,247.

[72]Zanotti, C., Volpi, A., Bianchessi, M., and De Luca, L., "Measuring Thermodynamic Properties of Burning Propellants," Vol. 143, Progress in Astronautics and Aeronautics, AIAA, Washington, DC, 1992, pp. 145–196.

[73]Adams, G. F., and Shaw, R. W., Jr., "Fast Chemical Reactions in Energetic Materials," *Annual Review of Physical Chemistry*, Vol. 43, 1992, pp. 311–340.

[74]Schroeder, M. A., "Critical Analysis of Nitramines Decomposition Data: Product Distributions from HMX and RDX Decomposition," Ballistic Research Lab., BRL-TR-2659, Aberdeen Proving Ground, MD, June 1985.

[75]Behrens, R., Jr., "Thermal Decomposition of Energetic Materials: Temporal Behaviors of the Rates of Formation of the Gaseous Pyrolysis Products from Condensed Phase Decomposition of Octahydro-1,3,5,7-Tetranitro-1,3,5,7-Tetrazocine," *Journal of Physical Chemistry*, Vol. 94, 1990, pp. 6706–6718.

[76]Behrens, R., Jr., and Bulusu, S., "Thermal Decomposition of Energetic Materials 2. Deuterium Isotope Effect and Isotopic Scrambling in Condensed-Phase Decomposition of Octahydro-1,3,5,7-Tetranitro-1,3,5,7-Tetrazocine," *Journal of Physical Chemistry*, Vol. 95, 1991, pp. 5838–5845.

[77]Behrens, R., Jr., and Bulusu, S., "Thermal Decomposition of Energetic Materials 3. Temporal Behaviors of the Rates of Formation of the Gaseous Pyrolysis Products from Condensed Phase Decomposition of 1,3,5-Trinitrohexahydro-s-Triazine," *Journal of Physical Chemistry*, Vol. 96, 1992, pp. 8877–8891.

[78]Behrens, R., Jr., and Bulusu, S., "Thermal Decomposition of Energetic Materials 4. Deuterium Isotope Effects and Isotopic Scrambling (H/D, $^{13}C/^{18}O$, and $^{14}N/^{15}N$) in Condensed Phase Decomposition of 1,3,5-Trinitrohexahydro-s-Triazine," *Journal of Physical Chemistry*, Vol. 96, 1992, pp. 8891–8897.

[79]Axworthy, A. E., Flanigan, D. A., and Gray, J. C., "Interaction of Reaction Kinetics and Nitramine Combustion," Air Force Armament Lab., AFATL-TR-80-58, Eglin AFB, FL, May 1980.

[80]Oyumi, Y., and Brill, T. B., "Thermal Decomposition of Energetic Materials 3. High-Rate, In Situ, FTIR of the Thermolysis of RDX and HMX with Pressure and Heating Rate as Variables," *Combustion and Flame*, Vol. 62, 1985, pp. 213–224.

[81]Suryanarayana, B., and Graybush, R. J., "Thermal Decomposition of 1,3,5,7-Tetranitro-1,3,5,7-Tetrazacyclooctane (HMX): A Mass Spectrometric Study of the Products from β-HMX," *Proceedings of the 39th Congress on Industrial Chemistry*, Supplement 24, 1966, pp. 1–4.

[82]Cosgrove, J. D., and Owen, A. J., "Thermal Decomposition of 1,3,5-Trinitrohexhydro-1,3,5-Triazine (RDX)—Part I: The Products and Physical Parameters," *Combustion and Flame*, Vol. 22, 1974, pp. 13–18.

[83]Cosgrove, J. D., and Owen, A. J., "Thermal Decomposition of 1,3,5-Trinitrohexahydro-1,3,5-Triazine (RDX)—Part II: Effects of the Products," *Combustion and Flame*, Vol. 22, 1974, pp. 19–22.

[84]Kubota, N., and Sakamoto, N., "Combustion Mechanism of HMX," *Propellants, Explosives, Pyrotechnics*, Vol. 14, 1989, pp. 6–11.

[85]Brill, T. B., Brush, P. J., Patil, D. G., and Chen, J. K., "Chemical Pathways at a Burning Surface," *Twenty-Fourth Symposium (International) on Combustion*, The Combustion Inst., Pittsburgh, PA, 1992, pp. 1907–1914.

[86]Edwards, T., "Investigation of Solid Propellant Combustion Chemistry," AIAA Paper 90-0547, Jan. 1990.

[87]Lengellé, G., Duterque, J. R., Gordon, J. C., and Trubert, J. F., "Solid Propellant Steady Combustion-Physical Aspects," *Journal of Propulsion and Power* (to be published).

[88]Parr, T. P., and Hanson-Parr, D. M., "Nonintrusive Diagnostic Techniques for Research on Nonsteady Burning of Solid Propellants," Vol. 143, Progress in Astronautics and Aeronautics, AIAA, Washington, DC, 1992, pp. 261–324.

[89]Stufflebeam, J. H., "CARS Diagnostics for Solid Propellant Combustion Investigations," United Technologies Research Center, R92-957787F, East Hartford, CT, Jan. 1992.

[90]Vanderhoff, J. A., "Species Profiles in Solid Propellant Flames Using Absorption and Emission Spectroscopy," *Combustion and Flame*, Vol. 84, 1991, pp. 73–92.

[91]Brill, T. B., Brush, P. J., James, K. J., Shepherd, J. E., and Pfeiffer, K. J., "T-Jump/FTIR Spectroscopy: A New Entry into the Rapid, Isothermal Pyrolysis Chemistry of Solid and Liquids," *Applied Spectroscopy*, Vol. 46, 1992, pp. 900–911.

[92]Timken, M. D., Chen, J. K., and Brill, T. B., "Thermal Decomposition of Energetic Materials 37. SMATCH/FTIR (Simultaneous Mass and Temperature Change/FTIR) Spectroscopy," *Applied Spectroscopy*, Vol. 44, 1990, pp. 701–706.

[93]Shepherd, J. E., and Brill, T. B., "Interpretation of Time-to-Explosion Tests," *Tenth Symposium (International) on Detonation* (to be published).

[94]Wormhoudt, J., Kebabian, P. L., and Kolb, C. E., "Infrared Fiber-Optic Diagnostic Observations of Solid Propellant Combustion," Aerodyne Research, Inc., ARI-RR-1029, Cheyenne, WY, Oct. 1993.

[95]Hanson-Parr, D., and Parr, T., "RDX Flame Structure and Chemistry," 30th JANNAF Combustion Subcommittee Meeting, Nov. 1993.

[96]Trulove, P. C., Chapman, R. D., and Shackelford, S. A., "Kinetic Deuterium Isotope Effects in the Combustion of Formulated Nitramine Propellants," *Propellants, Explosives, Pyrotechnics*, Vol. 19, 1994, pp. 42–58.

[97]Palopoli, S. F., and Brill, T. B., "Thermal Decomposition of Energetic Materials 52. On the Foam Zone and Surface Chemistry of Rapidly Decomposing HMX," *Combustion and Flame*, Vol. 87, 1991, pp. 45–60.

[98]Lin, C. Y., Wang, H. I., Lin, M. C., and Williams, C. F., "A Shock Tube Study of the $CH_2O + NO_2$ Reaction at High Temperatures," *International Journal of Chemical Kinetics*, Vol. 22, 1990, pp. 455–482.

[99]Pollard, F. H., and Wyatt, R. M. H., "Reactions Between Formaldehyde and Nitrogen Dioxide," *Transactions of the Faraday Society*, Vol. 45, 1949, pp. 760–767.

[100]Fifer, R. A., and Holmes, H. E., "Kinetics of Nitramine Flame Reactions," *Sixteenth JANNAF Combustion Meeting*, Vol. II, CPIA Publ. 308, 1979, pp. 35–50.

[101]He, Y., Liu, X., Lin, M. C., and Melius, C. F., "Thermal Reaction of HNCO with NO_2 at Moderate Temperatures," *International Journal of Chemical Kinetics*, Vol. 25, 1993, pp. 845–863.

[102]Oyumi, Y., and Brill, T. B., "Thermal Decomposition of Energetic Materials 22. The Contrasting Effects of Pressure on the High-Rate Thermolysis of 34 Energetic Compounds," *Combustion and Flame*, Vol. 68, 1987, pp. 209–216.

[103]Melius, C. F., "Theoretical Studies of the Chemical Reactions Involved in the Ignition of Nitramines," *Twenty-fourth JANNAF Combustion Meeting*, Vol. I, CPIA 476, 1987, pp. 359–366.

[104]Edwards, G., "The Vapour Pressure of Cyclotrimethylene Trinitramine (Cyclonite) and Pentaerythritoltetranitrate," *Transactions of the Faraday Society*, Vol. 49, 1953, pp. 152–154.

[105]Rosen, J. M., and Dickenson, C., "Vapor Pressures and Heats of Sublimation of Some High Melting Organic Explosives," *Journal of Chemistry and Engineering Data*, Vol. 14, 1969, pp. 120–124.

[106]Taylor, J. W., and Crooks, R. J., "Vapour Pressure and Enthalpy of Sublimation of 1,3,5,7-Tetranitro-1,3,5,7-Tetraazacyclooctane (HMX)," *Journal of the Chemical Society, Faraday Transactions I*, Vol. 72, 1976, pp. 723–729.

[107]Cundall, R. B., Palmer, T. F., and Wood, C. E. C., "Vapour Pressure Measurements of Some Organic Explosives," *Journal of the Chemical Society, Faraday Transactions I*, Vol. 74, 1978, pp. 1339–1345.

[108]Maksimov, Yu. Ya, Apal'kova, V. N., Braverman, O. V., and Solov'ev, A. I., "Kinetics of Thermal Decomposition of Cyclotrimethylenetrinitramine and Cyclotetramethylene-Tetranitramine in the Gas Phase," *Russian Journal of Physical Chemistry*, Vol. 59, 1985, pp. 201–204.

[109]Kimura, J., and Kubota, N., "Thermal Decomposition Process of HMX," *Propellants and Explosives*, Vol. 5, 1980, pp. 1–8.

[110]Beckstead, M. W., personal communication, Brigham Young Univ., Provo, UT, 1993.

[111]Mitani, T., and Takahasi, M., "Temperature Measurements of Monopropellants Using a Counterflow Burner Method," *Western States Section of the Combustion Institute Spring Meeting*, 3C-050, 1988, pp. 161–163.

[112]Lengellé, G., and Duterque, J., "Combustion de Propergols à Base d'Octogene," *Smokeless Propellant*, AGARD, CP-391, 1986, pp. 8-1–8-17.

[113]Kubota, N., and Sakamoto, S., "Combustion Mechanism of HMX," *Nineteenth International Conference of the ICT*, 1988, pp. 65-1–65-12.

[114]Parr, D. M., and Parr, T. P., "Condensed Phase Temperature Profiles in Deflagrating HMX," *Twentieth JANNAF Combustion Meeting*, Vol. I, CPIA Publ. 383, 1983, pp. 281–291.

[115]Liau, Y. C., and Yang, V., "Analysis of RDX Monopropellant Combustion with Two-Phase Subsurface Reaction," *Journal of Propulsion and Power*, Vol. 11, No. 4, 1995, pp. 729–739.

[116]Maksimov, Yu. Ya., "Vapour Pressures of Aromatic Nitrocompounds at Various Temperatures," *Russian Journal of Physical Chemistry*, Vol. 42, 1988, pp. 1550–1552.

[117]Korsunskii, B. L., and Dubovitskii, F. I., "Kinetics of Thermal Decomposition of N,N'-Dimethylnitramine," *Doklady Akademia Nauk SSSR, (Soviet Physics—Doklady)*, Vol. 155, 1964, pp. 402–404.

[118]Lloyd, S. A., Umstead, M. E., and Lin, M. C., "Kinetics and Mechanism of Thermal Decompositon of Dimethylnitramine at Low Temperatures," *Journal of Energetic Materials*, Vol. 3, 1985, pp. 187–210.

[119]Shaw, R., and Walker, F. E., "Estimated Kinetics and Thermochemistry of Some Initial Unimolecular Reactions in the Thermal Decomposition of 1,3,5,7-Tetranitro-1,3,5,7-Tetraazacyclooctane in the Gas Phase," *Journal of Physical Chemistry*, Vol. 81, 1977, pp. 2572–2576.

[120]McMillen, D. F., Barber, J. R., Lewis, K. E., Trevor, P. L., and Golden, D. M., "Mechanisms of Nitramine Decomposition: Very Low Pressure Pyrolysis of HMX and Dimethylnitramine," Final Rept., SRI-Project PYU-5787, ARO, Menlo Park, CA, June 1979.

[121]Oxley, J. C., Hiskey, M., Naud, D., and Szekeres, R., "Thermal Decomposition of Nitramines: Dimethylnitramine, Diisopropylnitramine, and N-Nitropiperidine," *Journal of Physical Chemistry*, Vol. 96, 1992, pp. 2505–2509.

[122]Flournoy, J. M., "Thermal Decomposition of Gaseous Dimethylnitramine," *Journal of Chemical Physics*, Vol. 36, 1962, pp. 1106, 1107.

[123]Oyumi, Y., and Brill, T. B., "Thermal Decomposition of Energetic Materials 21. The Effect of Backbone Composition on the Products Evolved from Rapid Thermolysis of Linear Nitramines," *Combustion and Flame*, Vol. 67, 1987, pp. 121–126.

[124]Tobin, M. C., Fowler, J. P., Hoffman, H. A., and Sauer, C. W., "The Thermal Decomposition of Methylene Dinitramine," *Journal of the American Chemical Society*, Vol. 76, 1954, pp. 3249–3253.

[125]Robertson, A. J. B., "Thermal Decomposition of Explosives," *Transactions of the Faraday Society*, Vol. 44, 1948, pp. 677–682.

[126]Brill, T. B., and James, K. J., "Thermal Decomposition of Energetic Materials 62. Reconciliation of the Kinetics and Mechanisms of TNT on the Time Scale from Microseconds to Hours," *Journal of Physical Chemistry*, Vol. 97, 1993, pp. 8759–8763.

Reprinted from The Journal of Physical Chemistry, 1995, 99.

Thermal Decomposition of Energetic Materials. 68. Decomposition and Sublimation Kinetics of NTO and Evaluation of Prior Kinetic Data

G. K. Williams and T. B. Brill*

Department of Chemistry, University of Delaware, Newark, Delaware 19716

Received: April 17, 1995; In Final Form: June 8, 1995[⊗]

Seven previously published global kinetic measurements for thermal decomposition of the energetic compound 5-nitro-2,4-dihydro-3*H*-1,2,4-triazol-3-one (NTO) report Arrhenius activation energies ranging from 40.7 to 120.4 kcal/mol. To resolve this large discrepancy, two potentially dominating processes (sublimation and thermal decomposition) were isolated and their kinetics determined. For sublimation $E_a = 25.8$ kcal/mol, ln A (s^{-1}) = 29.2 (isothermal at 0.002 atm); $E_a = 28.6$ kcal/mol, ln A (s^{-1}) = 31.3 (nonisothermal at 0.002 atm). Decomposition kinetics on semiconfined NTO (20 atm pressure) by flash-heating with T-jump/FTIR spectroscopy yield $E_a = 87.1$ kcal/mol and ln A (s^{-1}) = 74.8. From these data and selected, evaluated, previous measurements, the kinetic constants for decomposition alone are $E_a = 78-87$ kcal/mol and ln A (s^{-1}) = 67−78. Smaller values of the Arrhenius parameters reported previously are shown to result predominantly or partly from sublimation.

Introduction

The energetic compound 5-nitro-2,4-dihydro-3*H*-1,2,4-triazol-3-one (NTO) is of interest as an insensitive explosive,[1] a gas

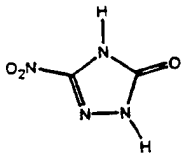

NTO

generator for automobile inflatable restraints systems,[2] and a potential burn-rate modifier.[3] Considerable effort has been expended to characterize the decomposition products by IR spectroscopy,[3] mass spectrometry,[4-6] X-ray photoelectron spectroscopy,[4] and ESR spectroscopy.[7]

While information about the decomposition products of energetic materials is valuable for specifying the reaction pathways, the kinetic constants are essential to describe the burning or explosion process. It is very difficult, however, to acquire these data under such conditions. The rate of decomposition of NTO has been determined in the temperature range of gradual thermal decomposition by IR spectroscopy,[8] thermogravimetric analysis (TGA),[8] differential thermal analysis (DTA),[9] differential scanning calorimetry (DSC),[10] NO chemiluminescence,[6] and by analysis of the concentrations following partial decomposition in a sealed tube.[7,11] The rates obtained by these methods yield activation energies scattered from $E_a =$ 40.7 to 120 kcal/mol. However, when the value of E_a is plotted against its prexponential (ln A) counterpart, most of these pairs produce points that lie on or close to a single line.[12] This coincidence is frequently referred to as the "kinetic compensation effect". That is, an increase in E_a does not reduce the rate correspondingly because of an offsetting increase in the A factor. Consequently, widely scattered values of Arrhenius parameters for a heterogeneous global decomposition process may produce the same rate at a given temperature (i.e., they are isokinetic) but predict very different rates at other temperatures, such as exist during combustion or explosion. This difference in Arrhenius parameters can be attributed to differences in the sample characteristics and experimental conditions.[12] For NTO, however, a pattern has begun to emerge in which the seven reported values of E_a appear to gather into two ranges: 40.7−52 and 78−120 kcal/mol.

In the spirit of reconciling conflicting data on energetic compounds,[12-14] the objective of this article is to resolve the descrepancy in the kinetics of NTO by separately determining the rates of the two dominating global processes, namely, sublimation and thermal decomposition. The outcome is a method to evaluate all of the reported kinetic data for NTO in terms of the process that was actually measured.

Experimental Determination of Kinetic Constants

Samples of NTO were obtained from M. Coburn (Los Alamos National Laboratory) and T. Russell (Naval Research Laboratory). Both samples had been purified and yielded the same results in experimental tests. In all cases, NTO was pulverized in a mortar and pestle and dried overnight at 295 K under 8×10^{-4} atm.

Sublimation rates were determined both isothermally and nonisothermally by thermogravimetry. A circular (15 mm diameter) sample boat was fabricated from 0.025 mm tantalum foil to which a 0.0076 mm diameter chromel wire was attached as a hanger. Each pellet of NTO was prepared by pressing approximately 200 mg of sample in a vacuable KBr die (Wilmad Glass) at 1335 atm for 10 min, while evacuating at 0.002 atm to remove any trapped gas. The resulting well-formed disk of NTO had 1.0 ± 0.1 mm thickness, 13 mm diameter, and a density of about 95% of the theoretical maximum density[15] of 1.92 g/cm^3.

To determine the rate of sublimation under isothermal conditions, the glass housing of the TGA instrument (DuPont Instruments Model 951) designed for low-pressure work[16] was purged with Ar and sealed. A vacuum pump was used to reduce the pressure to 0.002 atm as measured by a McLeod gauge. The desired sample temperature was attained in about 5 min and was held constant for about 120 min. A thermocouple positioned about 1 mm above the surface of the sample monitored the temperature (±0.5 K). Six sets of mass loss data were recorded at temperatures between 407 and 437 K. The

* Correspondence author.
[⊗] Abstract published in *Advance ACS Abstracts*, July 15, 1995.

0022-3654/95/2099-12536$09.00/0

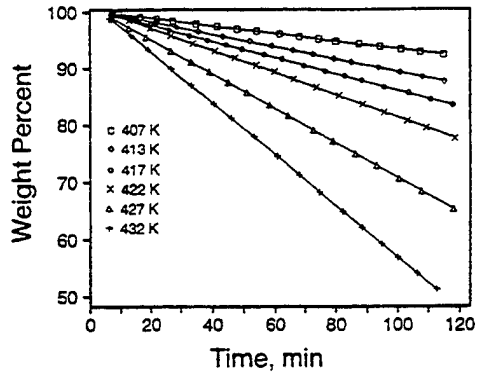

Figure 1. Time dependence of the mass loss due to sublimation of NTO at 0.002 atm and a series of temperatures.

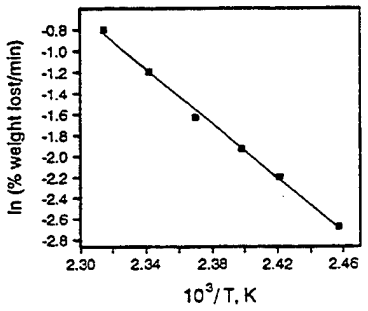

Figure 2. Arrhenius plot for the isothermal rate of sublimation of NTO.

TABLE 1: Arrhenius Parameters for Processes of NTO

E_a (kcal/mol)	ln A (s^{-1})	T, K	method	ref
		Sublimation		
25.8	29.2	407–436	isothermal TGA[a]	this work
28.6	31.1	407–448	nonisothermal TGA[a]	this work
31.1	30.1	453–503	nonisothermal TGA[b] this work	this work
		"Decomposition"		
40.7	26.9	373–410	NO chemiluminescence	6
44.8	38.3	502–519	isothermal TGA	8
49.3	47.6	468–483	IR	8
52.3	47.0[c]	503–523	DTA-TG	9
78.6	67.0	493–553	HPLC, solution	11
87.1	74.8	562–572	T-jump	this work
87.5	77.8[c]	498–553	HPLC	7
120.4	112.1	539–553	DSC	10

[a] At 0.002 atm. [b] At 0.02 atm. [c] Not reported, but derived from the data given.

resulting linear ($R^2 > 0.999$) mass loss vs time plots are shown in Figure 1. The slope of each line is, of course, the zeroth-order rate constant for sublimation, k_s. A plot of ln k_s vs $1/T$ (Figure 2) yields the Arrhenius constants given in Table 1 for isothermal sublimation.

By evacuation of the glass housing, the sublimation rate could be measured at temperatures well below the range where any significant decomposition takes place. To prove this, NTO was heated for 18 h at 423 K in a sealed Al pan in a DSC (DuPont Instruments 910). No thermal events were detected, and the IR spectrum was the same before and after. In addition, the sublimate of NTO had the same IR spectrum as the original sample.

The sublimation rate under nonisothermal conditions was determined by the extent of mass loss at a series of temperatures with a programmed heating rate of 1 K/min to 448 K. The atmosphere surrounding the sample was 0.002 atm Ar. By using the method of Coats and Redfern[17] for a zeroth-order process

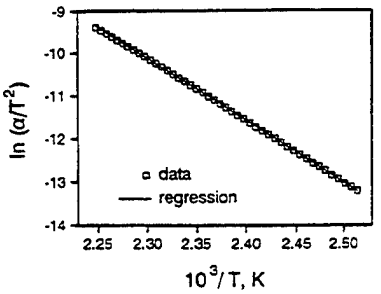

Figure 3. Arrhenius-type plot for the nonisothermal rate of sublimation of NTO using the Coats and Redfern analysis.

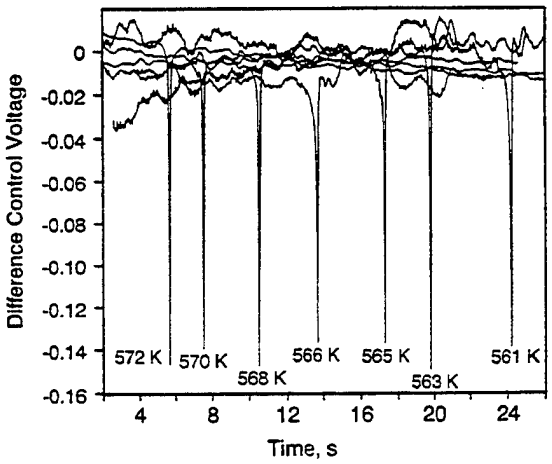

Figure 4. Times-to-exotherm for NTO heated at 600 K/s to the temperatures shown under 20 atm of Ar.

(eq 1), a plot of the left-side term vs $1/T$ yielded a straight line

$$\ln\left(\frac{\alpha}{T^2}\right) = \ln\frac{AR}{\alpha E_a}\left[1 - \frac{2RT}{E_a}\right] - \frac{E_a}{RT} \qquad (1)$$

(Figure 3, $R^2 = 0.999$) whose slope was the activation energy E_a/R. In eq 1, α is the degree of mass loss. By substitution of α at a given temperature into the intercept expression of eq 1, the preexponential factor ln A (s^{-1}) was determined. The Arrhenius constants are given in Table 1. The same experiment was performed at 0.02 atm to test the effect of pressure on the Arrhenius parameters. E_a = 31.1 kcal/mol and ln A (s^{-1}) = 30.1.

The T-jump/FTIR experiment[18] was employed to determine the kinetic constants for decomposition of flash-heated NTO. An approximately 200 μg sample of polycrystalline NTO was thinly spread on a Pt ribbon filament housed inside of a transmission IR spectroscopy cell. The cell was pressurized with 20 atm Ar. By use of a fast-response, high-gain power supply, a filament heating rate of 2000 K/s was obtained. The actual heating rate of the sample was about 600 K/s.[19] The control voltage of the power supply was under precise control so that the chosen set temperature in the 562–572 K range was reached within 1 s and maintained (±0.5 K) for 30 s. The true temperature was determined independently by using melting point standards. The power supply is highly responsive to small heat changes originating in the sample. Monitoring of this control voltage in real-time revealed that endothermic melting followed by rapid exothermic decomposition occurred. The time required to produce an exotherm at a given temperature, once the sample reached the filament temperature (ca. 1.2 s), is shown in Figure 4. These times-to-exotherm are equivalent to the time-to-explosion analyzed by Semenov for a thermal process.[20,21] Equation 2 can be used to determine apparent

$$\ln t_x(\mathrm{s}) = E_a/RT + \ln B \qquad (2)$$

Arrhenius-like constants. A plot of $\ln t_x$ vs $1/T$ (Figure 5) yields the activation energy and intercept (assumed to be $-\ln A$) that are given in Table 1.

IR spectra of the gaseous products from the experiments described above were recorded on a Nicolet 800 FTIR spectrometer. Typically, 10 scan/s, 1 spectrum per file, and 4 cm^{-1} resolution was used. The product identities were useful to verify when sublimation or decomposition was the dominant process.

Evaluation and Discussion of Kinetic Constants for NTO

The two dominant processes occurring in NTO at elevated temperatures are sublimation and decomposition. Curiously, the existence of sublimation of NTO has not been discussed in previous studies. By optimizing the conditions that are preferential to sublimation (i.e., low pressure, moderate temperature), the rate constants specifically for sublimation of NTO were determined for the first time. The values are given in Table 1. The formation of sublimed NTO without detectable solid or gaseous decomposition products was proven by IR spectroscopy.

To isolate the thermal decomposition process from sublimation, the decomposition rate could be measured on confined NTO in a sealed ampule, or NTO could be heated at a high rate to a high temperature under an applied pressure. Since the former method has been used previously,[7,11] the latter method was attempted here. These data are the first flash-heating kinetics for NTO. Although some sublimation was found to occur even under 67 atm of Ar, the decomposition kinetics were emphasized. The similarity of the resulting Arrhenius parameters with those obtained by slowly heating confined NTO[7,11] suggests that the global kinetic processes induced by heating at degrees/min are similar to those at 600 K/s.

All of the available global decomposition kinetics of NTO are summarized in Table 1. It is noteworthy that two ranges of E_a values emerge: 40.7−52 and 78−120 kcal/mol. All of the lower range values were obtained on unconfined NTO, such as by heating on an open pan or matrix. The NO chemiluminescence data[6] will not be discussed further here because the extraordinary sensitivity of the method to tiny quantities of NO makes it difficult to specify the factors responsible for NO production. Therefore, the lower range of E_a values for discussion here will be 45−52 kcal/mol. The values of E_a = 78−120 kcal/mol were all determined on a confined or semiconfined sample, such as in a crimped DSC pan, in a sealed ampule, or by flash-heating under pressure. We were unable to reproduce the DSC-derived value[10] of E_a = 120.4 kcal/mol because the thermal trace was found to double-back on itself as a result of uncontrolled self-heating of the sample. Nevertheless, we retained the reported value for Figure 6, but will exclude it from the discussion.

It is easiest to compare the data in Table 1 by placing them on a single Arrhenius plot (Figure 6). The ranges of E_a for decomposition cluster at 45−52 and 78−87 kcal/mol in the temperature range of measurement (468−553 K). Because the upper range of values was obtained on confined or semiconfined NTO, sublimation kinetics do not contribute significantly. There are undeniable differences in these rates, but the scatter is typical of that found with other materials which exothermically decompose from the condensed phase.[12] Moreover, the process order best matching the data is second in the work of Menapace et al.,[7] first in the work of Oxley et al.,[11] and zeroth in this work. Similar scatter is even observed in the Arrhenius

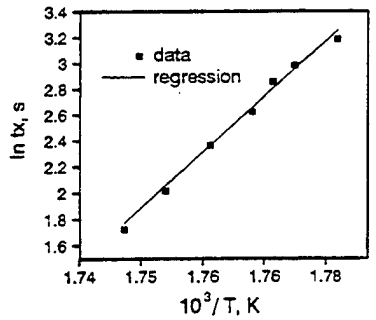

Figure 5. Arrhenius-type plot of the time-to-exotherm for NTO which was T-jumped at 600 K/s to set temperatures under 20 atm of Ar.

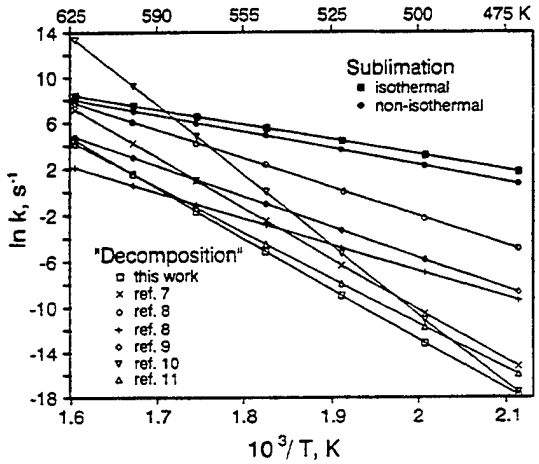

Figure 6. Arrhenius plots for all of the decomposition rate data in Table 1, except those of ref 6 (see text), and the 0.002 atm sublimation kinetics.

constants for first-order decomposition of dimethylnitramine in the gas phase.[22]

On the other hand, the values of E_a in the 45−52 kcal/mol range yield rates that lie between those for sublimation and those for decomposition in the temperature range of measurement. Because these rates were determined on an unconfined sample of NTO, it is probable that they are a mixture of sublimation and decomposition kinetics. A rough estimate of the degree to which sublimation affects these measurements at each temperature can be made by eq 3. In eq 3 $k_m(T)$ is the rate derived

$$k_m(T) = k_d(T) + ak_s(T) \qquad (3)$$

from the previously reported Arrhenius constants with E_a = 45−52 kcal/mol, k_d is the decomposition rate determined by E_a values in the 78−87 kcal/mol range, and k_s is the sublimation kinetics. Our value of k_d and the nonisothermal kinetics of sublimation, k_s, in Table 1 were used. The value of a in eq 3 was adjusted to achieve equality. Therefore, the fraction of the rate attributable to sublimation is $ak_s(T)/k_m(T)$. Figure 7 shows the approximate fraction of sublimation in the "rates of decomposition" previously reported for unconfined NTO. It can be seen that the kinetic constants for decomposition that yield E_a = 45−52 kcal/mol almost entirely represent sublimation of NTO in the lower temperature range and a mixture of decomposition and sublimation at higher temperatures.

It is evident that considerable care must be exercised when determining and interpreting the kinetic constants for decomposition of a volatile energetic compound, such as NTO. In the unconfined state, the kinetic constants may be a mixture of the rates of sublimation and decomposition, the balance of which shifts with changes in the experimental conditions. With

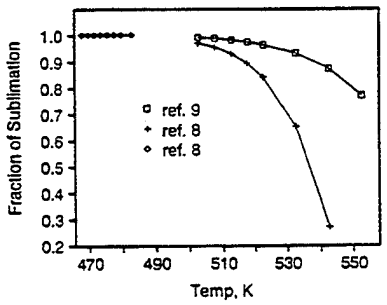

Figure 7. Approximate fraction of sublimation in several reported "rate of decomposition" measurements of unconfined NTO.

appropriate precautions these two dominating processes may be separated and independently investigated. If the thermal decomposition rate of NTO is desired, then the kinetics which yield activation energies in the vicinity of 78−87 rather than 45−52 kcal/mol should be used.

Acknowledgment. We are grateful to the Air Force Office of Scientific Research (NA) for support of this work on F49620-94-1-0053.

References and Notes

(1) Lee, K.-Y.; Coburn, M. D. US Patent 4,733,610, 1988.
(2) Wardle, R. B.; Hinshaw, J. C.; Hajik, R. M. US Patent 4,931112, 1990.
(3) Williams, G. K.; Palopoli, S. F.; Brill, T. B. *Combust. Flame* **1994**, *98*, 197−204.
(4) Beard, B. B.; Sharma, J. *J. Energet. Mater.* **1993**, *11*, 325−344.
(5) Rothgery, E. F.; Audette, D. E.; Wedlich, R. C.; Csejka, D. A. *Thermochim. Acta* **1991**, *185*, 235−243.
(6) Östmark, H.; Bergman, H.; Åqvist, G.; Langlet, A.; Persson, B. *Sixteenth International Pyrotechnics Seminar* Jönköping, Sweden, June, 1991; pp 874−886.
(7) Menapace, J. A.; Marlin, J. E.; Bruss, D. R.; Dascher, R. V. *J. Phys. Chem.* **1991**, *95*, 5509−5517.
(8) Prabhakaran, K. V.; Naidu, S. R.; Kurian, E. M. *Thermochim. Acta* **1994**, *241*, 199−212.
(9) Hara, Y.; Taniguchi, H.; Ikeda, Y. Takayama, S.; Nakamura, H. *Kayaku Gakkaishi* **1994**, *55*, 183−187.
(10) Yi, X; Hu, R; Wang, X.; Fu, X.; Zhu, C. *Thermochim. Acta* **1991**, *189*, 283−296.
(11) Oxley, J. C.; Zhou, Z.; Smith, J. L.; McKenney, R. L. *Proceedings of the ADPA International Symposium on Energetic Materials Technology*; March 21−24, 1994; pp 155−165.
(12) Brill, T. B.; Gongwer, P. E.; Williams, G. K. *J. Phys. Chem.* **1994**, *98*, 12242−12247.
(13) Brill, T. B.; James, K. J. *J. Phys. Chem.* **1993**, *97*, 8752−8758.
(14) Brill, T. B.; James, K. J. *J. Phys. Chem.* **1993**, *97*, 8759−8763.
(15) Lee, K.-Y.; Gilardi, R. *Mater. Res. Soc. Symp. Proc.* **1993**, *296*, 237−242.
(16) Barrall, II, E. M.; Logan, J. A. *Thermochim. Acta* **1974**, *9*, 205−206.
(17) Coats, A. W.; Redfern, J. P. *Nature* **1964**, *201*, 68−69.
(18) Brill, T. B.; Brush, P. J.; James, K. J.; Shepherd, J. E.; Pfeiffer, K. J. *Appl. Spectrosc.* **1992**, *46*, 900−911.
(19) Shepherd, J. E.; Brill, T. B. *10th Int. Symp. Deton.* July, 1993; pp 849−857.
(20) Semenov, N. N. *Z. Phys.* **1928**, *48*, 571−582.
(21) Merzhanov, A. G. *Combust. Flame* **1967**, *11*, 201−211.
(22) Brill, T. B. *J. Propuls. Power* **1995**, *11*, 740−751.

JP9510960

CNF 485

Flash Pyrolysis of Hydroxyl-Terminated Polybutadiene (HTPB) I: Analysis and Implications of the Gaseous Products

H. ARISAWA and T. B. BRILL*
Department of Chemistry, University of Delaware, Newark, DE 19716

Flash pyrolysis of structurally different hydroxyl-terminated polybutadiene polymers (HTPB) was conducted at 600°C/s to constant temperatures in the 450°–609°C range under 2 and 11 atm of applied pressure. T-Jump/FTIR spectroscopy was used. With chemometric procedures based on the entire mid-IR spectrum, 13 gaseous products representing at least 70% of the polymer were identified and quantified. Contrary to previous indications that butadiene and 4-vinyl-l-cyclohexene dominate, the *trans*-butadiene oligomers are major products. These oligomers are probably responsible for smoke formation. The product concentrations are sensitive to the temperature below 500°–530°C and 2 atm Ar, but are relatively insensitive to the temperature above 500°–530°C.

I. INTRODUCTION

HTPB (hydroxyl-terminated polybutadiene) is the most widely used polymeric binder/fuel in solid rocket propellants. Knowledge about the gaseous products and their rates of formation from pyrolysis of HTPB is needed to describe the fuel component of the diffusion flamelets of a composite solid propellant in terms of detailed chemistry. Several research studies have been conducted on thermal decomposition of HTPB under conditions that approximate combustion [1–6], such as at high heating rates and pressure of 1 atm or greater. However, direct determinations of the liberated products and kinetics under these conditions are not in a refined state [5, 6], although more is known about HTPB than any other propellant binder/fuel.

Most gaseous product analyses have been conducted with gas chromatography (GC) and GC-mass spectrometry (MS). These studies have provided much information summarized in Section II about the species formed upon pyrolysis of butadiene polymers (PBD) at relatively low heating rates. Potential shortcomings of these methods are the long delay time between pyrolysis and analysis; the use of conditions different from those during combustion; the extensive heterogeneous, bulk-phase chemistry that occurs before gaseous products form; and the inability to identify the gaseous components beyond determination of their mass or retention time; and emphasis on lower molecular weight products.

Infrared (IR) spectroscopy has rarely been used to characterize the pyrolysis process of PBD. An advantage of IR spectroscopy is that relatively direct measurements are now possible by using a rapid-scanning interferometer. Relatively realistic thermolysis conditions are also available by employing T-jump/FTIR spectroscopy [7]. A possible disadvantage of this approach is that many types gaseous hydrocarbon molecules, which have similar spectral characteristics, are simultaneously liberated from PBD. Therefore, it is impossible to use single wavelength measurements to identify and quantify all of these species simultaneously, as has been achieved in previous research dealing with energetic materials [8, 9]. A new approach was used to circumvent this problem. This is to use absorbance measurements made simultaneously at all mid-IR wavelengths. The result is a spectral series that can be resolved to identify and quantify major hydrocarbon products from pyrolysis of HTPB that are liberated throughout the pyrolysis process. These measurements are made at heating rates, temperatures, and pressures that are more typical of the pyrolysis conditions during combustion than have been used previously. New insights are acquired about the identity of the products that are available to the primary flame zone.

The following companion article addresses kinetic aspects of the formation of the gaseous products which were identified and quantified in this article.

* Corresponding author.

COMBUSTION AND FLAME

Published by Elsevier Science Inc.

0010-2180/96/$15.00
SSDI 0010-2180(96)00253-7

II. PREVIOUS PYROLYSIS STUDIES OF PBD

Many synthetic polybutadiene compounds are known having different relative percentages of *trans*(l), *cis*(m), and vinyl(n) groups, and different degrees of tacticity, terminal groups, and average molecular weight. The general formula for HTPB is shown

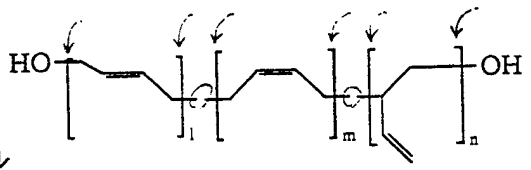

here. The product distribution from pyrolysis of this polymer depends on the microstructure of the polymer [10–15], the temperature [10, 13, 14], and the heat rate [10, 16, 17]. Most of the thermal decomposition studies of PBD before 1987 were reviewed by Beck [18]. Attention will be given here primarily to HTPB because of its dominance as a binder in solid rocket propellant formulations.

A. Low Heating Rates

For heating rates of $\leq 10^2$ deg/min into the decomposition temperature range, the techniques of DSC, TGA, and DTA provide global kinetics and thermochemistry. GC and MS are commonly used to identify the volatile products. The initial chemical event appears to be endothermic *cis-trans* isomerization leading to a 31:69 *cis*:*trans* distribution at 260°C [19]. This step is proposed to take place by H-transfer at 200°–300°C rather than by scission of the C—C double bonds [19]. Others have noted the insolubility of PBD after heating to about 200°C, and attributed this to self-cross-linking reactions [20, 21]. In fact, cross-linking and cyclization reactions are always found when the heating rate is low [6, 12, 14, 16, 20–26]. They dominate the 300°–400°C range and primarily involve the vinyl groups and H-transfer [19–21]. This class of reactions is exothermic overall (950 J/mol [22], 783 J/g [6], 1130–1880 J/g [25]), but the actual value depends upon the heating rate [25] and the structure of the polymer [6]. About 15% of the weight is lost in this stage as a result of vaporization of the cyclized products [6, 12, 22, 25]. The existence of free radicals has been detected [27] or inferred [28–30] in this stage.

Above 400°C, endothermic chain-scission becomes increasingly prevalent [6, 12, 25]. At least 70 volatile products have been registered by GC [13, 17], but most workers report that butadiene and the cyclized dimer of butadiene (4-vinyl-l-cyclohexene) dominate. Other molecules having moderate concentration are 1,3-cyclohexadiene, 1,5-hexadiene, and cyclopentene. Fragments as large as $C_{16}H_{26}$ are detected by GC/MS [13, 31], although $C_{16}H_{28}$ formed by *cis*-1,4-PBD is proposed to be 1,8-dimethylperhydrophenanthrene [10]. The existence of higher molecular weight molecules and smoke is not a developed subject.

B. High Heating Rates

Heating rates of $\geq 10^2$ deg/s into the decomposition temperature range produce pyrolysis reactions more relevant to the combustion process. Unfortunately, the conditions of rapid pyrolysis at high heating rates restrict the details that can be extracted about molecular processes in the bulk phase. The reactions take place in a short time; the regions of distinguishable behavior observed with low heating rates either do not exist or change in relative importance; and the uncertainty in the temperature and reaction rate increases. For all of these reasons the decomposition characteristics of polymers are known to be sensitive to the heating rate [2, 6, 10, 12, 13, 16, 17, 25, 32–34].

At high heating rates, the exothermic cross-linking stage, which is present at low heating rates, is masked by the chain scission stage, if it exists at all [6, 22]. In fact, the overall decomposition process becomes exothermic above 370°C when HTPB is rapidly heated [2]. It has been proposed that exothermicity occurs in the initial step of decomposition [2], but this prospect, which can mainly arise from cyclization, must be balanced against the endothermicity of bond scission in the early steps. There is evidence that the amount of 4-vinyl-l-cyclohexene decreases with increasing temperature [25], while lower molecular weight products, such as butadiene, become more preva-

lent up to 700°C [10], and faster heating rates [12, 17, 22]. Ethylene is found to dominate at 900°C [13], although it is not established whether it formed from PBD or from secondary pyrolysis of other products.

Advances in understanding of the pyrolysis process of HTPB are benefitted by a different approach than has been used previously. In this article, new insights about the liberated products were determined by T-jump/FTIR spectroscopy.

III. T-JUMP/FTIR SPECTROSCOPY APPLIED TO HTPB

The objective of T-jump/FTIR spectroscopy is to combine flash heating of a thin film of sample with near real-time IR spectral detection of the gaseous products that are liberated from the surface [7]. The global heat change of the film is monitored simultaneously with the gaseous products form. The sequence of formation of the gaseous products can frequently be observed. In the case of PBD polymers, all products form simultaneously on the timescale of the experiment, but form at different rates, so that the real-time rate of formation of individual products can be distinguished. The species are discussed in this article and the kinetics are presented in the following article.

A. PBD Samples

The HTPB binder of a solid propellant is cured by the addition of a compound containing -NCO groups, which reacts with the -OH groups of the polymer to produce urethane cross-links. While the curing agent affects the ultimate ballistic properties of the composite propellant [35–38], rapid thermal decomposition studies of the urethane cross-linked HTPB reveal that the urethane bonds are first to cleave and that most of the cross-linking agent vaporizes [6]. The vapor pressure of the cross-linking agent seems to influence the ballistic properties. The remaining HTPB decomposes as though it were an uncurred polymer [6].

Descriptive details of the polymers used are given in Table 1. R45M and BM94 were obtained from Thiokol Corp. *Cis*-1,4-PBD rubber was obtained from Aldrich Chemical Company. The percentage of *cis*, *trans*, and vinyl components was based on IR and ^{13}C NMR spectroscopy [39, 40]. R45M (ARCO, Lot 003097) had an equivalent weight based on the -OH groups of 1300 g/eq. R45M was heated to 60°C under vacuum in a rotary evaporator for 2 h to minimize the H_2O content, and was stored in a desiccator. BM94 and *cis*-1,4-PBD were used without further purification. R45M and BM94 are HTPB polymers, while *cis*-1,4-PBD is methyl-terminated PBD. The high MW of the available *cis*-1,4-PBD limits its comparability to the other polymers. Only a few of its pyrolysis characteristics are given here.

B. Experimental Technique

An approximately 0.2-mg sample of liquid R45M or BM94 was spread as a film having about 100 μm thickness on the center of a Pt ribbon filament. *Cis*-1,4-PBD rubber was used as a solid. By resistance heating, the filament temperature rose at 2000°C/s. However, owing to the heat capacity of PBD, the nominal heating rate of the sample can be as low as 600°C/s to the final temperature [41, 42]. For temperatures in the 450°–609°C range, 0.7–1 s is required to achieve the chosen steady-state temperature (±2°C). The true temperature of the filament for a given voltage setting was determined independently by the use of compounds

TABLE 1

Percentage of *cis*- and *trans*-Butadiene and Vinyl Groups in the PBD Polymers

Sample	Percentage (IR) *cis*	*trans*	vinyl	M.W.	terminal group
R45M	21	57	21	~ 2500	–OH
BM94	32.5	67.5	0	~ 3000	–OH
cis-1,4-PBD	92	6	2	~ 4.5×10^6	$-CH_3$

with standard melting points. This temperature was held for about 19 s. The upper end of this temperature range probably approaches the surface temperature of HTPB during combustion of composite propellant formulations, although the latter temperature is not well defined. Also, the 450°–609°C range was found to contain the important switch between controlling processes of gas generation.

The control circuit of the Pt filament (CDS Analytical) has sufficiently high gain and fast response to sense the heat change of the sample as decomposition occurs. By subtracting the control voltage of the filament with sample present from the voltage trace of the filament with no sample present, a difference voltage trace is generated. When this difference trace has positive inflection, the sample has absorbed heat indicating that endothermic processes dominate. A negative inflection results when exothermic processes dominate. HTPB samples produce a slight negative inflection and are, therefore, net exothermic upon decomposition.

The filament was housed in a gas-tight spectroscopy cell containing ZnSe windows [7]. Simultaneously with flash heating of the film, 4 cm^{-1} resolution IR spectra (4000–600 cm^{-1}) were recorded at 0.17s intervals throughout the process. A Nicolet 20SXC rapid-scan FTIR spectrometer was used. The focal point of the IR beam was located at 0.3 cm above the surface of the film. All pyrolysis experiments were performed in a cool, static, Ar atmosphere so that the products are thermally quenched by the time they reach the detection volume. For R45M, pressures of 2 and 11 atm Ar were used, while 2 atm Ar was used for BM94 and *cis*-1,4-PBD.

C. Products

During flash pyrolysis of HTPB, the products shown in Fig. 1 could be identified. These are estimated to represent about 70% of the original sample. For final filament temperatures of 450°–500°C, a residue, made white in appearance by the presence of bubbles, remains on the filament. This residue represents 5%–10% of the original sample. Between 500° and 580°C, the residue is black and carbonaceous. The

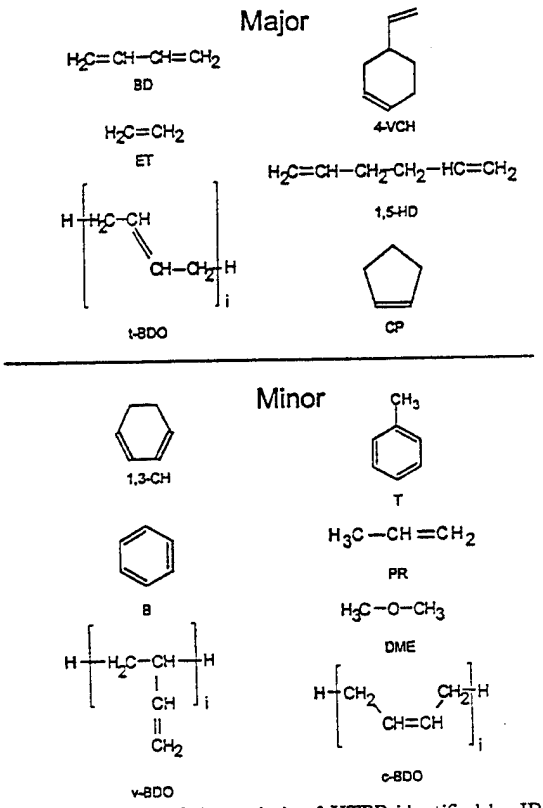

Fig. 1. Products of thermolysis of HTPB identified by IR spectroscopy.

quantity is less than 5% of the original sample. Above 580°C, no residue remained. Apart from the residue and the identified products, a number of unidentified products evolved. Many of these can be ascribed to oligomers of MW greater than 350 and saturated hydrocarbons. However, none of these individual products constitute more than a few percent of the total products. The temperature dependence of these unidentified products is addressed in Section III.E. Nine of the identified products in Fig. 1 have been mentioned in previous studies. The ill-defined nature of the vaporized oligomers required the use of *trans*-2-butene, *cis*-2-butene, and 1-butene to model the classes of compounds consisting of *cis*, *trans*, and vinyl-butadiene oligomers, respectively. The *cis* and vinyl components proved to be absent, so that oligomers based on *trans*-butadiene dominate.

The important role of t-BDO class of products has strong support in the IR absorbance

at 964 cm^{-1}, which is the "*trans*-CH-wag" [43]. This mode is characteristic of all *trans*-olefin compounds, is intense in the IR spectrum, and is rigorously absent in the other products of Fig. 1. We determined that the intensity of 964 cm^{-1} absorbance is, indeed, roughly proportional to the percent of *trans*-butadiene groups by recording the spectrum of a series of phenyl-terminated polybutadiene films in which the percentage of *trans* groups is known and differs (Fig. 2).

Dimethyl ether is tentatively identified by IR modes characteristic of the ether linkage at 1189 and 1174 cm^{-1}. Previously, a small amount of CH_2O was observed [6] from HTPB that had been cross-linked by urethane groups prior to pyrolysis. No -OH IR mode was detected the gas phase previously or now. The presence of a small amount of ether and/or aldehyde groups helps to account for the fate of the -OH group.

D. Quantitation and Data Analysis

Most of the compounds in Fig. 1 have characteristic absorbances in the 600–1100 cm^{-1} range. Therefore, interference makes the single-wavelength measurement of the concentrations (called zeroth-order calibration) impossible. On the other hand, concentrations can be determined for all species simultaneously if every wavelength of the spectrum is used (called first-order calibration). This procedure is described here.

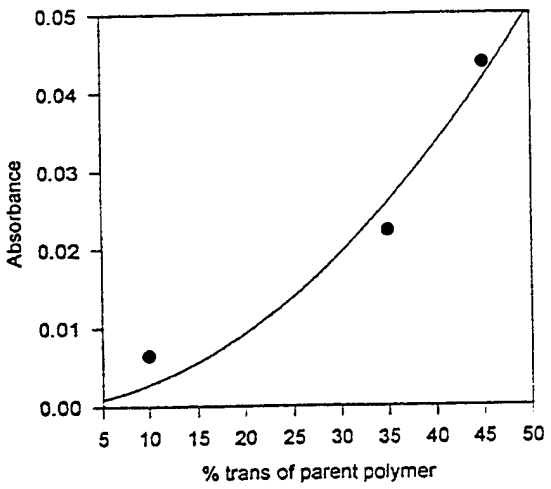

Fig. 2. The relationship of the intensity of the "*trans*-CH-wag" and the percentage of *trans*-butadiene groups in phenyl-terminated PBD.

For each compound in Fig. 1, which is gaseous at 20°C and 1 atm, the relationship between absorptivity and concentration was determined by measuring absorbances across the entire spectrum for a range of partial pressures of the pure gas in Ar. This produces a three-dimensional, generalized matrix relating absorbance, concentration, and wavelength. A plot of this matrix is shown in Fig. 3 for pure ET. To illustrate that this three-dimensional plot has Lambert-Beer characteristics, the relationship between the absorbance at 949 cm^{-1}, which is characteristic of ethylene, and the concentration is shown in Fig. 4. A linear relationship exists. However, we emphasize that the concentration of each compound was determined by interpolation of spectra of which Fig. 3 is illustrative, rather than by Fig. 4.

For the thermolysis products that are liquid at 20°C and 1 atm, the absorptivity-concentration relationship was determined by placing an excess amount of the liquid in the sealed spectroscopy cell and measuring the vapor phase spectrum once vapor-liquid equilibrium existed. This condition required about 6 h to achieve. The equilibrium vapor pressures, P, were calculated for all compounds, except for 1,3-CD, by using Eq. 1. The constants A, B, and C of eq. 1 were taken from Lange [44]. Equation 2 [45] was used to estimate ΔH_v for 1,3-CD, where T_b is

$$\log P = A - \left(\frac{B}{T + C}\right) \tag{1}$$

$$\Delta H_v = KT_b(8.75 + 4576 \log T_b), \tag{2}$$

the boiling point and K is the correlation factor (Table 3.1 of Ref. 45). The vapor pressure of 1,3-CD was then calculated by the Clausius–Clapeyron equation. The ideal equation of state was used to convert the partial pressure to concentration at 1 atm.

The coefficient matrix for the t-BDO family was determined by the absorbance-concentration plot of the simplest component, *trans*-2-butene. This compound has about 5% of the concentration BD based on a GC-MS determi-

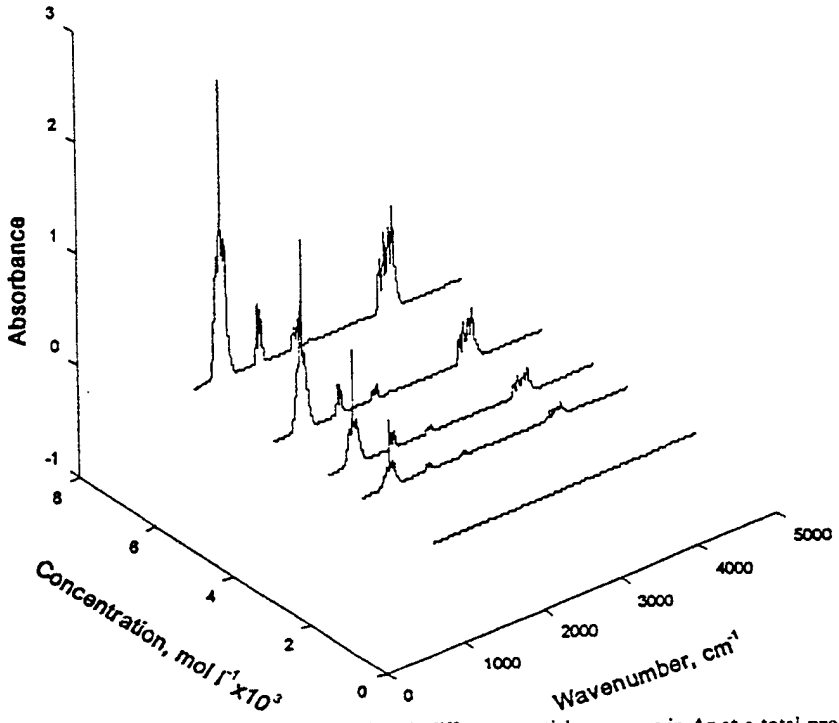

Fig. 3. IR spectrum of ethylene (ET) with different partial pressures in Ar at a total pressure of 2 atm.

nation of the products in the IR cell. Therefore, the higher molecular weight *trans*-butadiene oligomers must be relatively abundant. The method of determining the approximate concentration of t-BDO is given in Section III.F.

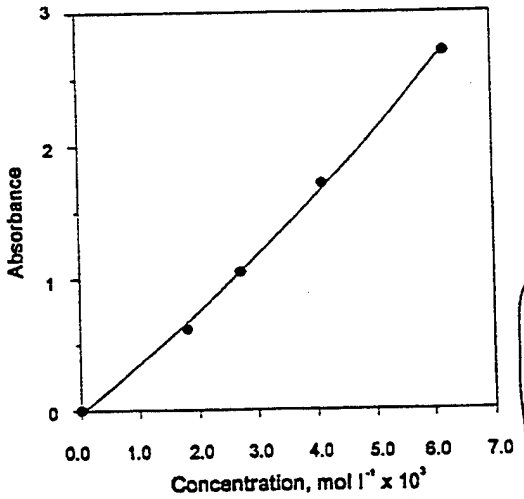

Fig. 4. A Lambert–Beer plot of the 949 cm^{-1} absorbance of ET.

For a time series of IR spectra during pyrolysis, the time dependence of the concentration of each product was calculated by using the non-negative least-squares regression ("nnls", MATLAB ver. 4.0, Mathworks, Inc.) [46]. Equation 3 gives the basic formula subject to the condition that the concentration, c, is ≥ 0:

$$\mathbf{m} = \mathbf{E}\mathbf{c} - \mathbf{r}(t). \quad (3)$$

The coefficient matrix **E** contains the calibration spectra of the thermolysis products, and the vector $\mathbf{r}(t)$ contains the IR spectrum of the thermolysis products at time t. The calculated vector **c** corresponds to the concentration of each product at t. The objective is to minimize **m**. This is achieved in the algorithm by adding or removing a column of coefficients in **E** which corresponds to a particular thermolysis product. Finally, the remaining columns, which have non-negative concentrations and minimize **m**, provide the simultaneous concentrations of the other products at time t.

A practical problem is that the nonnegative

least-squares method is difficult to apply if the spectral baseline changes nonlinearly with frequency. Baseline correction is required for pyrolysis of PBD because smoke particles have an absorption continuum and produce light scattering at shorter wavelengths. This perturbation affects the baseline at longer times, as shown in Fig. 5. The baseline slope becomes larger when pyrolysis is conducted at higher temperatures. The baseline correction of the IR spectrum of a flame has been empirically made with Eq. 4 [47].

$$\kappa_\lambda = \kappa^* C \lambda^{-\beta} \tag{4}$$

κ_λ is the spectral absorption coefficient, κ^* is the molar absorptivity, C is the concentration, λ is the wavelength, and β is characteristic of the material. To avoid the harmful effect of the changing baseline on the calculation of concentration profiles, the spectral range above 1800 cm^{-1} was excluded. Useful spectral information is not lost because C–H modes, which are not sufficiently unique for quantitation, are the only fundamental modes in this range. Below 1800 cm^{-1} the baseline was manually flattened by assuming a first-order polynomial for 1500–1800 cm^{-1}, and a first-order or mixture of first- and second-order polynomials for 620–1400 cm^{-1}. Figure 6 shows the improvement of conditioning the baseline in this fashion. Also shown in Fig. 6 is removal of the 1400–1500 cm^{-1} range where nonspecific C–H modes overlap and interfere.

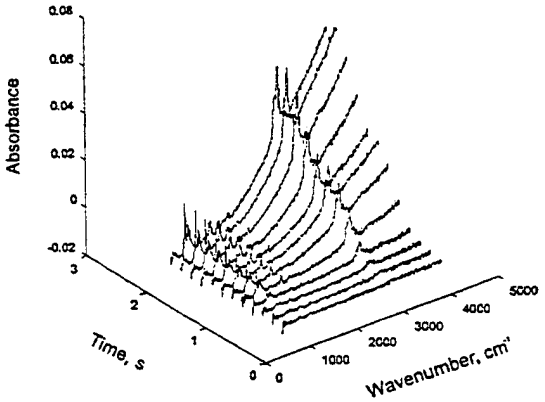

Fig. 5. The IR spectrum of the gas phase above R45M heated at 600°C/s to 500°C in 2 atm Ar.

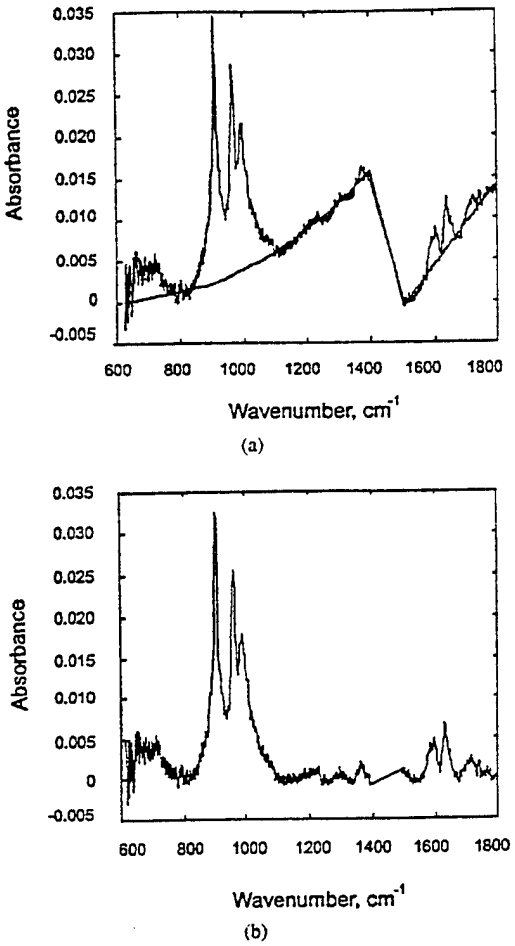

Fig. 6. Truncation and base-line correlation of R45M. (a) Before correction. (b) After correction with first and second-order polynomials.

E. Analysis of Error

The residual between the predicted and observed spectra is an indication of the goodness-of-fit. This residual is determined by the root mean square, Eq. 5:

$$\mathrm{RMS}(t) = \sqrt{\sum_{n=1}^{n} \frac{[\hat{\mathbf{r}}(t) - \mathbf{r}(t)]^2}{n}} \tag{5}$$

$\hat{\mathbf{r}}$ and $\mathbf{r}$ are the predicted and actual spectrum, respectively, at time t. The number of spectral points at t is n. Figure 7 shows that the RMS residual increases with time when the temperature exceeds 500°C. The largest deviation is about 20%. This difference is caused by the

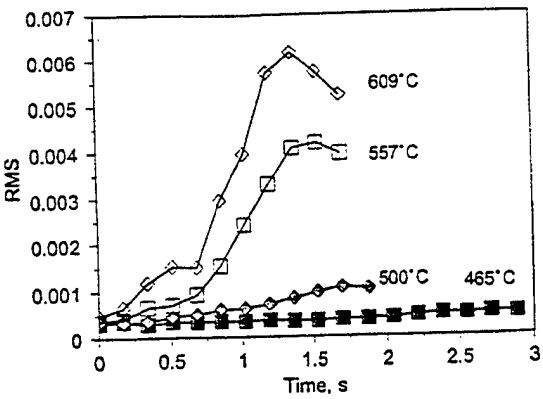

Fig. 7. The goodness of fit of the calculated and observed spectra for R45M at 2 atm Ar represented by the RMS values as a function of temperature.

increased presence of gaseous high MW *trans*-butadiene oligomers and saturated hydrocarbons at higher temperature (*vide infra*), whose IR spectral characteristics are not completely accounted for in the analysis.

F. The Approximate Concentration of *t*-BDO

In analysis described in Section III.D, the *t*-BDO concentration was noted to be related to the intensity of the *trans*-CH-wag. This intensity is, in fact, only the concentration of the total number of *trans* components. Since the oligomers contain multiple *trans* components, the actual concentrations of oligomer molecules is less than this number. In other words, the *trans* component concentration is the sum of the degree of polymerization-weighted concentrations, ΣiC_i, where i is the number of units and C_i is the concentration of *t*-BDO, ΣC_i, from the independent measurement discussed below.

A purely statistical distribution of oligomers might be assumed [48]. However, the distribution of oligomers is clearly non-statistical when the chain length has less than 7 monomer units [31, 49]. Therefore, instead of a purely statistical distribution, an experimental determination of the oligomers distribution and its temperature dependence were obtained by pyrolysis-photoionization mass spectrometry. In this experiment, less than 1 mg of sample was coated on the inside wall of a Pyrex vial. The sample was heated at 100°C/min under 10^{-10} atm. The vaporized products were ionized softly by single photon excitation with coherent vacuum ultraviolet radiation from a Nd:YAG laser system (118 nm or 10.5 eV). Each mass spectrum was the sum of 64 laser shots. While the conditions are not the same as those used in the T-jump/FTIR experiment, they are necessary to take advantage of mass spectroscopy to obtain the vapor oligomer distribution. The experiments were performed on R45M and BM94. Figure 8 shows a mass spectrum of R45M at 554°C, which is representative. Table 2 summarizes the normalized mass ion peak intensities of oligomers for both polymers as a function of temperature. The average degree of polymerization, p, at each temperature in Table 2 is defined by eq. 6 as

$$p = \frac{\Sigma iN_i}{\Sigma N_i} \approx \frac{\Sigma iC_i}{\Sigma C_i}, \qquad (6)$$

where N_i is the normalized peak intensity for chain length i. Calculated values of p up to $n = 6$ center around 3.75 and reveal no systematic dependence on the temperature. Also, there were no differences between the values of p for R45M and BM94. Therefore, an average value of $p = 3.75$ was used to calculate ΣC_i from ΣiC_i. We assumed that this value of p is also relatively independent of pressure based on a study of polyethyleneglycol[50] for which oligomers were available and could be characterized individually. At 1, 2, and 11 atm, the value of p did not change significantly for this polymer.

IV. PRODUCT CHARACTERISTICS

Thirteen gaseous products shown in Fig. 1 were identified from thermolysis of HTPB. These are estimated to represent about 70% of the original polymer mass. Of these thirteen products, six represent 95%–98% of the identified gaseous species. These are highlighted as the "major" products in Fig. 1. The mole fractions of these six major products for R45M and BM94 at 2 atm and R45M at 11 atm are given in Figs. 9–11, respectively, as a function of temperature. The respective weight fractions are given in Table 3. It is apparent that the *trans*-butadiene oligomers (*t*-BDO) are a major

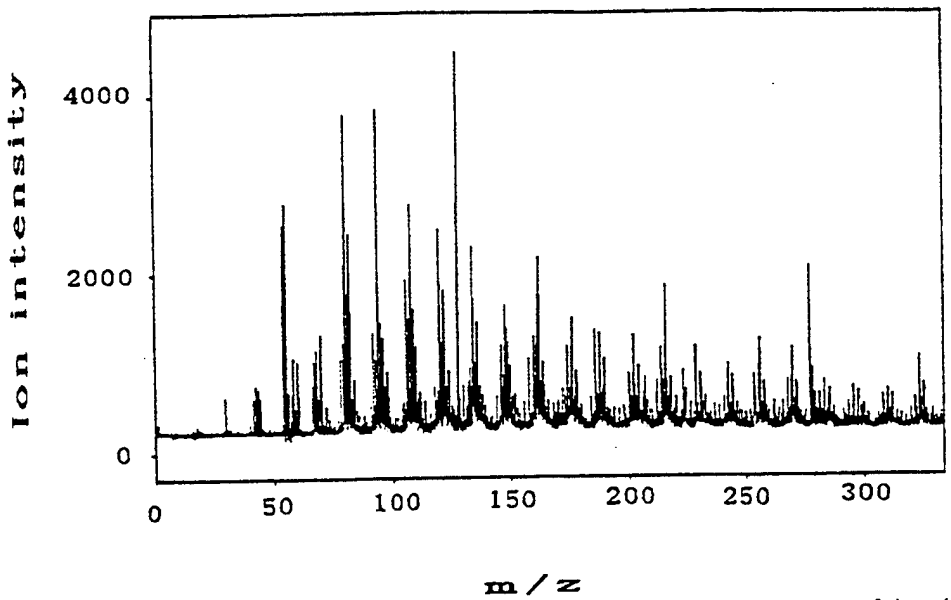

Fig. 8. The t-BDO distribution from vacuum ultraviolet ionization mass spectrometry of the volatile oligomers from R45M at 554°C.

class of products especially when the film is T-jumped to higher temperatures. This result is surprising in light of the studies summarized in Section II, which generally agree that BD and 4-VCH dominate. On the other hand, this result is not especially surprising because *t*-BDO forms from the polymer simply by random scission of the *trans*-butadiene sections and stabilization of the resulting radical by H-transfer. Only one previous study [31] mentions the important role of butadiene oligomers in the gas phase. The probable reason for minimal attention to the higher-molecular-weight products is that most previous studies are not designed to detect them. Also, the heating rate used in our work is faster than that employed by most other studies, which

TABLE 2

Normalized Intensity of *t*-BDO[a]

R45M					BM94				
	Temperature (°C)					Temperature (°C)			
i	466	516	554	620	*i*	466	525	550	615
1	0.07	0.06	0.06	0.06	1	0.10	0.11	0.10	0.09
2	0.10	0.11	0.10	0.08	2	0.10	0.14	0.13	0.12
3	0.31	0.29	0.28	0.28	3	0.32	0.28	0.23	0.24
4	0.21	0.21	0.23	0.22	4	0.17	0.19	0.21	0.18
5	0.16	0.19	0.17	0.20	5	0.16	0.16	0.17	0.18
6	0.15	0.14	0.16	0.16	6	0.15	0.12	0.16	0.19
p[b]	3.71	3.79	3.79	3.82	p[b]	3.66	3.52	3.52	3.83

[a] Ratio of ion current of each mass divided by the total ion current. For each value of i except for $i = 1$ and 2, the mass used was the sum of the intensities for linear $H\text{-}(CH_2CH{=}CHCH_2)_i\text{-}H$ and cyclic $(CH_2CH{=}CHCH_2)_i$.

[b] Average degree of polymerization (see text).

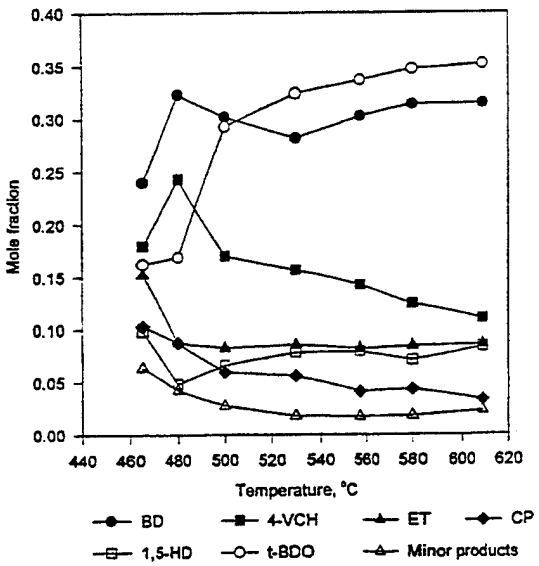

Fig. 9. The temperature dependence of the final concentrations of the major products from R45M at 2 atm Ar.

AU: PLEASE SEE QUERY ON MANUSCRIPT

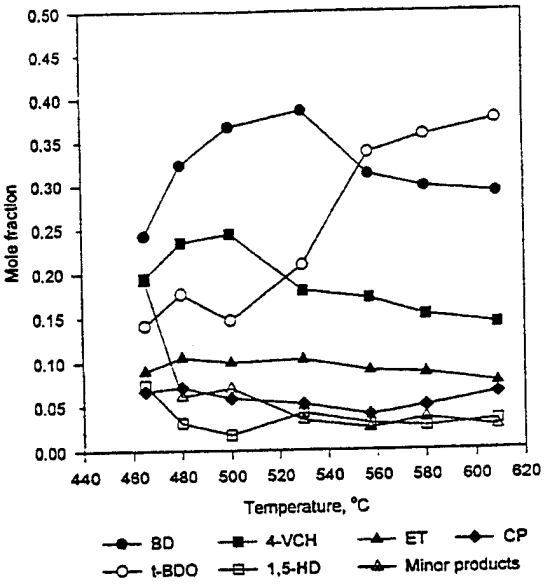

Fig. 10. The temperature dependence of the final concentrations of the major products from BM94 at 2 atm Ar.

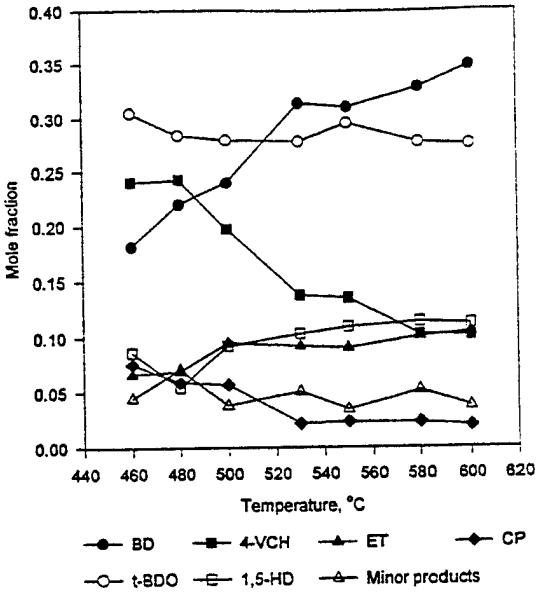

Fig. 11. The temperature dependence of the final concentrations of the major products for R45M at 11 atm Ar.

gives less time for secondary reactions to occur among the primary fragments. It is probable that these higher molecular weight oligomers are responsible for most of the smoke from HTPB and the RMS error trend shown in Fig. 7.

Several significant conclusions about the pyrolysis of HTPB can be drawn from these new insights about the products. In addition, a connection exists between the patterns in Figs. 9–11 and the kinetics discussed in the following companion article.

First, it is obvious that the product concentrations in Figs. 9 and 10 at 2 atm are quite sensitive to the pyrolysis temperature below 500°–530°C. Most previous pyrolysis studies have been conducted in this temperature range and below. Under these conditions heterogeneous bulk-phase processes (*cis-trans* isomerization, cross-linking, cyclization, and chain scission) dominate. Thus, numerous competitive reactions, each having a specific rate constant, combine to produce the products observed, so that it is not surprising that the product concentrations display a complex behavior shown in Figs. 9 and 10. The most important trend is that *t*-BDO increases in concentration at the expense of BD and 4-VCH as temperature increases. That is, cleavage of the polymer into intermediate-size segments accompanied by H-transfer is favored over monomer and dimer formation. On the other hand, when $530 < T < 609$°C, the product concentrations are markedly less sensitive to

TABLE 3

Weight Fractions of the Major Volatile Products from R45M at 2 atm

Compound	Temperature (°C) 465	480	500	530	557	580	609
BD	0.139	0.186	0.145	0.135	0.142	0.150	0.151
4-VCH	0.225	0.282	0.158	0.152	0.135	0.119	0.106
t-BDO	0.382	0.368	0.571	0.591	0.612	0.624	0.634
Et	0.048	0.026	0.022	0.022	0.021	0.021	0.022
1,5-HD	0.072	0.034	0.045	0.048	0.050	0.043	0.051
CP	0.092	0.077	0.045	0.041	0.032	0.031	0.024

ET – (Et)

the pyrolysis temperature. A plausible explanation for this sudden development of insensitivity is that the heterogeneous-phase thermolysis reactions have reached their maximum rate and cease to be especially sensitive to the temperature. This idea is provocative, but has support in the observations of an upper limit on the temperature of thermal decomposition of a polymer. For example, at a heating rate of 5×10^9 deg/s PMMA is found to have a limiting temperature of 715°C [51], whereas at 5×10^4 deg/s, the limiting temperature is 515°C [52]. With the heating rates here for PBD that are more similar to those of the latter study, the crossover occurs near 500°–530°C from temperature sensitivity in product distribution to relative insensitivity. In the following article, the kinetic implications of this crossover are discussed.

Figure 11 shows the mole fractions of products from R45M at 11 atm Ar. *t*-BDO has relatively constant concentration, whereas BD monomer forms at the expense of 4-VCH, the cyclized dimer of BD. In general, a relatively weak temperature dependence of the product concentrations is found. The implication of these product trends at 11 atm is that the control exerted by reactions in the heterogeneous, bulk-phase at lower pressures and temperatures mostly disappears, irrespective of the temperature in the 450°–609°C range. Only the monomer and dimer concentrations are sensitive. The increase in concentration of BD and decrease in concentration of 4-VCH with increasing temperature has been noted by others [10, 25].

Second, the *trans*-butadiene content of the backbone of the parent polymers used here is partly reflected in the mole fraction of *trans*-butadiene groups that vaporize. However, the choice of pyrolysis conditions is important to obtain this result. Figure 12 shows the mole fraction of *trans*-butadiene as a function of temperature for three PBDs. Also shown is percentage of *trans* groups in the parent polymer from Table 1. For $P = 2$ atm, the mole fraction of gaseous *trans*-butadiene groups closely matches the percentage of *trans* groups in R45M and BM94 provided that the temperature exceeds about 650°C. At 11 atm, any temperature in the 450°–609°C produces a

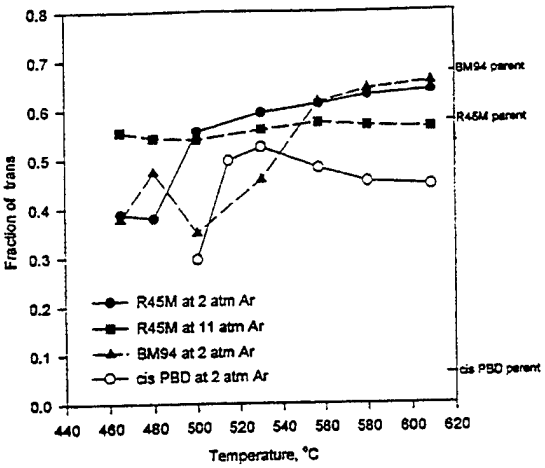

Fig. 12. The mole fraction of *trans*-butadiene group liberated by the three PBD polymers compared to the percentage of *trans*-butadiene linkages in the parent polymer.

good match. On the other hand, the match for *cis*-1,4-PBD is poor, although the mole fraction of gaseous *trans*-butadiene groups is smaller than that from R45M and BM94. A possible explanation for the higher than expected percentage of *t*-BDO from *cis*-1,4-PBD is the occurrence of *cis* → *trans* isomerization during pyrolysis. This isomerization has been observed when bulk PBD is slowly heated [19]. The *trans* conformation was experimentally found to be favored over *cis*, reaching a 70 : 30 ratio at 260°C. Perhaps even under rapid heating conditions of isomerization from *cis* to *trans* occurs, especially when the parent polymer has a high percentage of the *cis*-conformation.

Third, the retention of the *trans*-conformation when gaseous products are liberated implies that the *cis* and vinyl groups are mainly responsible for the other products in Fig. 1. Stereochemically, the *cis*-butene linkage and vinyl group in the backbone of HTPB are already positioned for cyclization [12–14], whereas the *trans*-butene linkage is not. The formation of the $-CH_3$ group that must occur to produce *t*-BDO is reasonable. CH_3- formation has been mentioned in previous studies [14, 19], and proposed to be favored by higher temperatures [14].

The major role that *t*-BDO plays in the gas phase at fast heating rates requires a redistribution of the H/C ratio between the gas phase and the residue. This is because the H/C ratio

69:31

560°C

609°C, not 1609°C

OK

of *t*-BDO is greater than that of HTPB. By elemental analysis, the H/C ratio of the polymers studied here was found to be 1.52–1.53 rather than 1.50 for idealized PBD. If the carbonaceous residue formed at 560°C represents 5% of the original mass, then the required total H/C ratio for the gaseous products is > 1.52–1.53. Indeed, the *t*-BDO series averages H/C > 1.5, whereas the other gaseous products have H/C ≈ 1.5.

Fourth, when the difference control voltage of the Pt filament is recorded during thermolysis, the temperature dependence of the thermal characteristics of the polymer can be sensed. Figure 13 reveals that the polymer consumes heat for the first several seconds mostly because of reorganization of the chains. This is polymer "melting." The negative inflection of the difference voltage trace at the onset of liberation of gaseous products indicates that the pyrolysis process of HTPB is slightly exothermic. Thus, any reaction scheme for R45M or BM94 must account for this exothermicity. ΔH of reaction can be estimated from Hess' Law, where ΔH_f^0 (HTPB) ≈ −770 kcal/mol when the MW is about 5500 [53]. The heats of formation of the products in Fig. 1 are available [44] or are easily calculated. The most abundant products reported in prior studies (BD and 4-VCH) have positive ΔH_f^0. The same is true of most of the minor products. By using these products alone as implied by previous studies, the heat of decomposition of HTPB would be strongly endothermic, which conflicts with the experimental fact in Fig. 13.

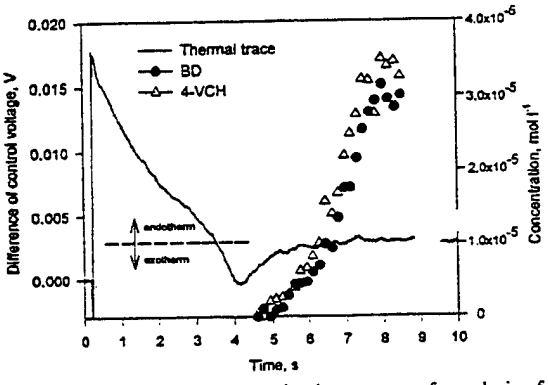

Fig. 13. The difference control voltage trace of pyrolysis of about 200 μg of R45M heated at 600°C/s to 480°C under 2 atm Ar. The rate of growth of BD and 4-VCH is shown.

On the other hand, ΔH_f^0 values of *t*-BDO are negative. The approximate values for *t*-BDO in Fig. 1 (*i* values given parenthetically) are −11.1(1), −27.5(2), −52(3), −77(4) kcal/mol, etc. Because the mole fraction of *t*-BDO becomes substantial, they readily offset the negative ΔH_f^0 of HTPB and produce the slightly exothermic decomposition process that is observed in Fig. 13. Others have found that HTPB decomposes exothermicity when heated at a high rate [2]. As was noted in Section II, the decomposition of HTPB is, on the other hand, endothermic above 400°C, when heated at a low rate. This is one of several significant differences between the low heating rate and fast heating rate decomposition process.

In summary, a new method of IR data analysis for determining the identities and concentrations of products of flash pyrolysis of polymers in near-real time has been devised. Upon application to the solid propellant binder/fuel, HTPB, and important discovery is that oligomers composed of *trans*-butadiene units form with significant concentration at high heating rates, and increase in concentration with increasing temperature. These species probably produce smoke and must be burned in the gas phase. A major change in the pyrolysis characteristics is observed in the 500°–530°C range. Major kinetic differences also appear in this temperature range. These kinetic effects are identified and discussed in the next article.

We are grateful to the Air Force Office of Scientific Research, Aerospace Science and Engineering Directorate, for support of this work on F49620-94-1-0053. R. Wardle supplied the sample of BM94 and S. F. Palopoli provided R45M. Dr. M. V. Johnston and D. Zoller provided the VUV-mass spectral data.

REFERENCES

1. Cohen, N. S., Fleming, R. W., and Derr, R. L., *AIAA J.* 12:212–218 (1974).
2. Bouck, L. S., Baer, A. D., and Ryan, N. W., *Fourteenth Symposium (International) on Combustion.* The Combustion Institute, Pittsburgh, 1973, pp. 1165–1176.
3. Blazowski, W. S., Cole, R. B., and McAlevy, III, R. F., *Fourteenth Symposium (International) on Combustion,* The Combustion Institute, Pittsburgh, 1973, pp. 1177–1186.

4. Hansel, J. G., and McAlevy, III., R. F., *AIAA J.* 4:841–848 (1966).
5. Ericsson, I., *J. Chromatogr. Sci.* 16:340–344 (1978).
6. Chen, J. K., and Brill, T. B., *Combust. Flame* 87:217–232 (1991).
7. Brill, T. B., Brush, P. J., James, K. J., Shepherd, J. E., and Pfeiffer, K. J., *Appl. Spectrosc.* 46:900–911 (1992).
8. Brill, T. B., *Prog. Energ. Combust. Sci.* 18:91–116 (1992).
9. Brill, T. B., in *Chemistry and Physics of Energetic Materials* (S. Bulusu, Ed.), Kluwer, Dordrecht, The Netherlands, 1990, pp. 277–326.
10. Shono, T., and Shina, K., *Anal. Chim. Acta* 56:303–307 (1971).
11. Haeusler, K. G., Schroeder, E., and Wege, F. W., *Plaste Kautsch.* 24:175–179 (1977).
12. Tamura, S., and Gillham, J. K., *J. Appl. Polym. Sci.* 22:1867–1884 (1978).
13. Radhakrishnan, T. S., and Rama Rao, M., *J. Polym. Sci.* 19:3197–3208 (1981).
14. Rama Rao, M., and Radhakrishnan, T. S., *J. Appl. Polym. Sci.* 41:2251–2263 (1990).
15. Rama Rao, M., Sebastian, T. V., Radhakrishnan, T. S., and Ravindran, P. V., *J. Appl. Polym. Sci.* 42:753–766 (1991).
16. Thomas, T. J., Krishnamurthy, V. N., and Nandi, U. S., *J. Appl. Polym. Sci.* 24:1797–1808 (1979).
17. Braun, D., and Canji, E., *Angew. Mackromol. Chem.* 29/30:491–505 (1973).
18. Beck, W. H., *Combust. Flame* 70:171–190 (1987).
19. Golub, M. A., and Gargiulo, R. J., *J. Polym. Sci. Polym. Lett.* 10:41–49 (1972).
20. Schneider, B., Doskocilova, D., Stokr, J., and Svoboda, M., *Polymer* 34:432–436 (1993).
21. Grassie, N., and Heaney, A., *J. Polym. Sci. Polym. Lett.*, 12:89–94 (1974).
22. Brazier, D. W., and Schwartz, D. W., *J. Appl. Polym. Sci.*, 22:113–124 (1978).
23. Coffman, J. A., *Ind. Eng. Chem.*, 44:1421–1428 (1952).
24. McCreedy, K., and Keskkula, H., *Polymer* 20:1155–1159 (1979).
25. Du, T., *Thermochim. Acta* 138:189–197 (1989).
26. Golub, M. A., and Sung, M., *J. Polym. Sci. Polym. Lett.* 11:129–138 (1973).
27. Tkak, A., *J. Polym. Sci. Symp. 57*, 109–120 (1976).
28. van Schooten, J., and Evenhius, J. K., *Polymer* 6:343–359 (1965).
29. Wall, L. A., and Straus, S., *J. Polym. Sci.* 44:313–323 (1960).
30. Simha, R., Wall, L. A., and Blatz, P. J., *J. Polym. Sci.* 5:615–632 (1950).
31. Lattimer, R. P., Harris, R. E., Rhee, C. K., and Schulten, H.-R., *Rubber Chem. Tech.* 61:639–657 (1988).
32. McAlevy III, R. F., and Hansel, J. G., *AIAA J.* 3:244–249 (1965).
33. Cheng, J.-H., Ryan, N. W., and Baer, A. D., *Twelfth Symposium (International) Combustion*, The Combustion Institute, Pittsburgh, 1968, pp. 525–532.
34. Baer, A. D., Hedges, J. H., Seader, J. D., Jayakar, K. M., and Wojcik, L. H., *AIAA J.* 15:1398–1404 (1977).
35. Adams, G. K., Newman, B. N., and Robins, A. B., *Eighth Symposium (International) on Combustion*, Williams & Wilkins, Baltimore, 1962, pp. 693–705.
36. Miller, R. R., Donohue, M. T., and Peterson, J. P., *12th JANNAF Combustion Mtg., CPIA Publ.* 273, Vol. II, Dec. 1975, pp. 371–381. Miller, R. R., Stacer, H. L., and Goshgarian, B. B., *19th JANNAF Combust. Mtg. CPIA Publ.* 366, Vol. II, Oct. 1982, pp. 67–79.
37. Fong, C. W., and Hamshere, B. L., *Combust. Flame* 65:61–69 (1986).
38. Stacer, R. G., Eisele, S., and Eisenreich, N., *Twenty-First International Annual Conference of the ICT*, Karlsruhe, Germany, July, 1990, paper 80.
39. Morero, D., Santambrogio, A., Porri, L., and Ciampelli, F., *Chim. Ind.* 41:758–762 (1959).
40. Kanakavel, M., *Makromol. Chem.* 188:845–854 (1987).
41. Shepherd, J. E., and Brill, T. B., *Tenth Symposium (International) on Detonation*, NSWC, White Oak, MD, ~~in press~~ 1993, pp. 849–855.
42. Thynell, S. T., Gongwer, P. E., and Brill, T. B., *31st JANNAF Comb. Meeting*, Sunnyvale, CA, Oct. 1994.
43. Lin-Vien, D., Colthup, N. B., Fateley, W. G., and Grasselli, J. G., *Handbook of Infrared and Raman Characteristic Frequencies of Organic Molecules*, Academic, New York, 1991.
44. Dean, J. A., Ed., *Lange's Handbook of Chemistry*, 14th ed., McGraw-Hill, New York, 1992.
45. Fishtine, S. H., *Ind. Eng. Chem.* 55:47–56 (1963).
46. Lawson, C. L., and Hanson, R. J., *Solving Least Squares Problems*, Prentice Hall, Englewood Cliffs, NJ, 1974, pp. 158–173.
47. Vernish, P., Puechberty, D., and Mohamed, T., *Combust. Flame* 41:179–186 (1981).
48. Seeger, M., and Gritter, R. J., *J. Polym. Sci. Polym. Chem. Ed.* 15:1393–1402 (1977).
49. Mita, I. in *Aspects of Degradation and Stabilization of Polymers* (H. H. G. Jelinek, Ed.), Elsevier, New York, 1978.
50. Arisawa, H., and Brill, T. B., ~~in press~~ Combust. Flame, Submitted
51. Lee, I. Y. S., Wen, X., Tolbert, W. A., Dlott, D. D., Doxtader, M., and Arnold, D. R., *J. Appl. Phys.* 72:2440–2448 (1992).
52. Shlensky, O. F., Matyukhin, A. A., and Varynshteyn, E. F., *J. Thermal. Anal.* 31:107–115 (1986).
53. Meyer, R., *Explosives*, 3rd ed., VCH Publishers, New York, 1987, p. 357.

Received 11 May 1995; revised 2 November 1995

CNF 486

Flash Pyrolysis of Hydroxyl-Terminated Polybutadiene (HTPB) II: Implications of the Kinetics to Combustion of Organic Polymers

H. Arisawa and T. B. Brill*

Department of Chemistry, University of Delaware, Newark, DE 19716

The first semi-micro kinetics analysis is described for rapid pyrolysis of an organic polymer. T-Jump/FTIR spectroscopy and structurally different hydroxyl-terminated polybutadiene polymers (HTPB) were used. The rates of formation were determined for the six most prevalent volatile products from HTPB heated at 600°C/s to constant temperatures in the 450°–609°C range under 2 and 11 atm of applied pressure. The resulting Arrhenius parameters reveal that mildly exothermic, bulk-phase, heterogeneous decomposition reactions control the rate of gaseous product evolution at $T < 500°–530°C$ under 2 atm Ar. The exact temperature depends on the product and the polymer microstructure. The rate evolution of most of the gaseous products at $T > 500°–530°C$ is controlled by desorption of fragments of the polymer rather than bulk-phase decomposition. When $P = 11$ atm Ar, the formation and desorption of these fragments controls the rate of product of evolution over the entire 460°–600°C range. These individual rate constants combined into a single rate yield macro kinetics of gas evolution from R45M as follows: $E_a = 51$ kcal/mol, ln A $(s^{-1}) = 31$ for 2 atm and 450°–530°C; $E_a = 18$ kcal/mol, ln A $(s^{-1}) = 11$ for 2 atm and 530°–609°C; $E_a = 12$ kcal/mol, ln A $(s^{-1}) = 6.6$ for 11 atm and 460°–600°C. A generalized equation that qualitatively matches for the kinetics of gaseous product evolution as a function of pressure is given.

I. INTRODUCTION

During combustion of a relatively nonenergetic polymeric compound, pyrolysis takes place at the surface which liberates gaseous products into the near-field flame zone. Modeling of the steady and non-steady aspects of the combustion process is benefitted greatly by having the pressure and temperature dependence of the rate of product evolution under relevant conditions. We have undertaken a major effort directed at gaining this insight for important organic polymers.

In the preceding article [1], the methods of acquisition and analysis were described to identify the gaseous products from hydroxyl-terminated polybutadiene (HTPB) which had been flash-heated to temperatures representative of the surface during steady burning. HTPB was chosen from the important category of polybutadiene (PBD) rubber polymers because of its prominence as a binder/fuel in solid rocket propellants and hybrid rockets. T-Jump/FTIR spectroscopy [2] was employed for this work.

In this article, the kinetics of liberation of the six major gaseous products from HTPB were determined individually as a function of pressure and temperature. This work is the first semi-micro kinetic analysis of HTPB. These data can be combined to give a macro kinetic description of the pyrolysis of HTPB at high heating rates.

With the objective of expanding the insights gained in this work to organic polymers in general, an equation was derived which models the experimentally determined temperature and pressure dependence of the gaseous products liberated from flash-pyrolyzed HTPB.

II. PREVIOUS KINETIC INFORMATION

Numerious polybutadiene polymers have been synthesized with a wide variety of properties including different relative percentages of *trans*(l), *cis*(m), and vinyl(n) groups. Figure 1 shows the general structure of the polymer along with the characteristics of the HTPB polymers employed in this study.

*Corresponding author.

COMBUSTION AND FLAME 00:000–000 (1996)

Published by Elsevier Science Inc.

0010-2180/96/$15.00
SSDI 0010-2180(95)0025+5

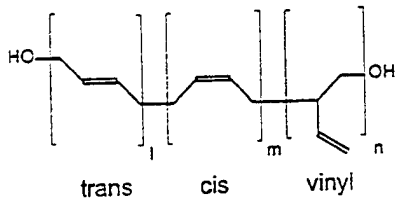

Samples	l	:	m	:	n
R45M:	57		21		21
BM94:	67.5		32.5		0

Fig. 1. The generalized structure of the polybutadiene polymers used for this study.

The techniques of DSC, TGA, and DTA provide global kinetics at heating rates of $\leq 10^2$ deg/min into the decomposition temperature range. The chemical processes that are believed to take place in PBD include endothermic *cis-trans* isomerization [3], exothermic self-cross-linking and cyclization reactions [4–14], and endothermic chain scission reactions [4, 5, 13]. Table 1 summarizes the Arrhenius parameters for the processes that have been presumed to occur in heated PBD. Except for those in Ref. 15, all of these data were acquired at relatively low heating rates of 1°–100°C/min, and either in vacuum or at 1 atm pressure. The relatively poor agreement among these data suggests that the reactions just mentioned occur in parallel. Their balance can be affected by the microstructure of the

TABLE 1

Arrhenius Data for Polybutadiene Polymers at 1-100°C/min Heating Rate

E_a (kcal/mol)	ln A (s^{-1})	T (°C)	Ref.	Comments
		Cis-trans Isomerization		
31 ± 3[a]	—	200–300	3[a]	IR, vacuum
		Cross-linking and Cyclization		
15[a]	—	230	9	IR, vacuum, first order, vinyl groups
18.8[b]	2.5	328–420	4	TGA
27.6 ± 1.6[b]	16.2	350–400	13[b]	TGA
39	—	250	11	Hardening data
		Chain Scission		
37.6[c]	25.6	450–532	15	pyrolysis-GC, BD formation, first order
40.7 ± 3	—	N/A	10	estimate of 4-vinyl-1-cyclohexene formation
42.1[a]	—	362–434	10	DSC
42.8	—	—	16	estimate
46 ± 0.6[b]	22.8	436–470	4	TGA
51.9[a]		350–425	10	TGA
60.0 ± 3.5[a]	—	N/A	10	estimate of BD formation
60.1[b]	17.1	367–407	13	TGA
62	—	380–395	14	weight change
62 ± 4[d]	—	410–500	6	TGA
		Unspecified Processes		
24.5 – 38.5[e]	12.2–20.8	350–550	7	TGA
28[e]	12.8	400–500	18	TGA, order = 0.6 – 1
21.5 – 31.1[b]	8.9–13.8	N/A	19	TGA

[a] 1,4-polybutadiene.
[b] HTPB.
[c] Cis-1,4-polybutadiene; dT/dt = 5000°C/s.
[d] Polybutadiene-acrylonitrile-acrylic acid (PBAN).
[e] Carbonyl-terminated polybutadiene (CTPB).

reactant polymer and the experimental conditions. Perhaps because all of these reactions occur competitively, the decomposition characteristics of polymers are sensitive to the heating rate [4, 5, 7, 20–23, 24—26].

Heating rates of $\geq 10^2$ deg/s into the decomposition temperature range produce pyrolysis reactions relevant to the combustion process. Such conditions restrict the details that can be extracted about kinetics in the bulk phase because the reactions take place in a short time; the regions of distinguishable behavior observed with low heating rates either do not exist or change in relative importance; and the uncertainty about temperature and reaction rate increases. Consequently, much less is known.

The Arrhenius parameters compiled in Table 2 reflect the rate of mass loss, linear regression, or gas generation when various polymers are heated at high rates to high temperatures. The paucity of data for PBD polymers prompts the inclusion of data for several other polymers. With the exception of two studies [15, 24], the values of the apparent activation energy are significantly smaller than those in Table 1 obtained at lower heating rates. The data of Ericsson [15] will be discussed later in this article. The interpretation frequently given for these small values of the Arrhenius parameters is that gasification is controlled by the rate of desorption of species from the surface as opposed to the rate of bond-breaking in the bulk phase [4, 27–31]. However, small values of the activation energy of thermolysis can also arise from partially conjugated polymers, such as HTPB, by taking into account resonance stabilization of the resulting radical [16]. Activation energies as low as 10 kcal/mol are possible for the formation of larger fragments.

In general, the state of understanding of the kinetics of decomposition of PBD is relatively crude despite the existence of many studies by GC, GC-MS, DSC, and TGA. A very rough pattern exists in which the magnitude of the Arrhenius parameters decreases with increasing heating rate. A unifying understanding of the pyrolysis process of HTPB requires a dif-

TABLE 2

Arrhenius Data for Polymer Pyrolysis at Heating Rates > 100°C/s

E_a (kcal/mol)	ln A (s^{-1})	Ref.	Comments
7.8 ± 0.7[a]	7.1 ± 1	4	linear pyrolysis, process order = 2
8.3 ± 1.2[b]	7.1 ± 1	4	linear pyrolysis, process order = 2
10 – 15[b]	—	20	bulk pyrolysis, IR lamp
11.0[c]	—	27	linear pyrolysis, hot plate
37[c]	—	24	linear pyrolysis, gas jet
37.6[d]	25.6	15	pyrolysis GC, BD formation, order = 1
10.5[e]	A = 12.8[f]	28	arc furnace, mass loss
16.7[g]	A = 270[f]	28	arc furnace, mass loss
16.9[b]	A = 299[f]	28	arc furnace, mass loss
2.1 – 8[h]	−4 to −2	29	furnace, $dT/dt \approx 20$°C/s

[a] Hydroxyl-terminated polyethyleneglycoladipate (HTPA).
[b] HTPB.
[c] Polymethylmethacrylate (PMMA).
[d] Cis-1,4-polybutadiene.
[e] Carboxyl-terminated polybutadiene (CTPB).
[f] g/cm² s.
[g] Polybutadiene-acrylonitrile-acrylic acid (PBAN).
[h] cellulose.

ferent approach. In this article, new insights about the kinetics are determined by T-jump/FTIR spectroscopy.

III. KINETIC ANALYSIS OF PRODUCT EVOLUTION BYT-JUMP / FTIR SPECTROSCOPY

The design of the T-jump/FTIR spectroscopy experiments to identify the products of a flash-heated film of polymer in near real-time was described in the preceding article [1]. The six major products were butadiene (BD), 4-vinyl-1-cyclohexene (4-VCH), *trans*-butadiene oligomers (t-BDO), ethylene (ET), 1,5-hexadiene (1,5-HD), and cyclopentene (CP).

A. Method of Analysis

The determination of the rates of formation of these six major products as a function of temperature is a major objective of this work. It was accomplished by measuring the rate of growth of the absorbances of each of these products at different pyrolysis temperatures. Figure 2 shows the IR absorbance data for two of the many products from R45M. Superimposed on these data is the control voltage difference trace of the filament. From similar such plots, the concentration versus time relationships were constructed for each major product. For example, the rates of BD formation from R45M at 2 atm are plotted in Fig. 3.

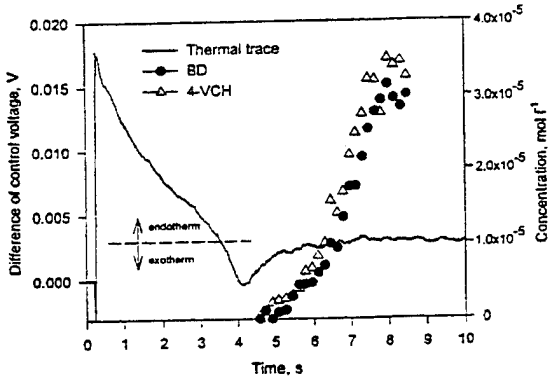

Fig. 2. The difference control voltage trace of pyrolysis of about 200 μg of R45M at 480°C and 2 atm Ar structure the rate of growth of BD and 4-VCH.

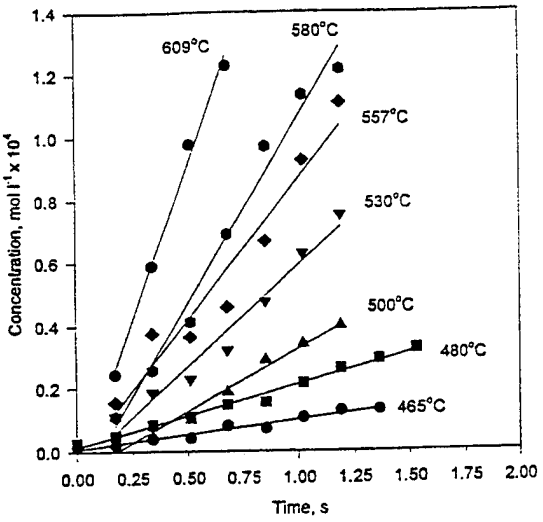

Fig. 3. Rate constants for BD formation from pyrolysis of R45M at dT/dt = 600°C/s to the temperatures shown under 2 atm Ar. Time = 0s corresponds to the first detection of products.

Each slope is the rate constant for generation of BD at the temperature given.

The linearity of the relationships in Fig. 3 indicates a zeroth-order rate expression. This result was found for all products from all of the polymers, and conflicts with the results of Ericsson [15], who determined the rate of BD formation to be first-order when *cis*-1,4-PBD was pyrolyzed at a heating rate similar to that used here. To test the correctness in our work of the zeroth-order behavior for BD formation shown in Fig. 3, the reaction order was analyzed by Guggenheim's method [32]. In Eq. 1, which represents a first-order reaction $dC/dt = -kC$, $\ln(C_{t+\Delta t} - C_t)$ should linearly decrease with time, t:

$$\ln(C_{t+\Delta t} - C_t) = -kt + \ln\left[C_\infty(1 - e^{-k\Delta t})\right] \quad (1)$$

C_∞ is the final concentration and was fixed for convenience at the concentration of the 600°C experiment. The rate constant is k. Figure 4 shows that the function for BD is approximately constant in time which indicates zeroth-order rather than first-order kinetics. In fact, all six major products quantified for each polymer follow zeroth-order kinetics at 2–11 atm and 450°–609°C. The rate constants for

formation of the major products were, therefore, calculated by the zeroth-order eq. 2:

$$\frac{d(C/C_\infty)}{dt} = k \qquad (2)$$

The behavior of Eq. 2 with Ericsson's Arrhenius constants for BD is shown in Fig. 4 for comparison. The discrepancy in the two reported process orders most likely originates from the fact that Ericsson employed a 7-μg sample, whereas we employed about 200 μg. With the larger amount of polymer, the rate of formation of gaseous products depends relatively less on the "concentration" of the parent polymer and thereby favors zeroth-order kinetics. With the smaller sample mass used by Ericsson, the "concentration" of parent polymer becomes a factor. The conditions employed in our work more closely resemble the conditions during steady combustion where the "concentration" of the reactant polymer remains relatively constant during steady pyrolysis.

B. Kinetic Constants at 2 Atm Ar

Figures 5 and 6 are plots of $\ln k$ vs. $1/T$ for R45M and BM94 at 2 atm. The Arrhenius activation energy, E_a, and pre-exponential factor, A, were calculated for the six major gaseous products. New findings are immediately apparent. First, the controlling mechanism of decomposition leading to evolution of most of the gaseous products fundamentally changes in the 500°–530°C range for R45M and at about 500°C for BM94. CP and 1,5-HD from R45M and BM94, respectively, are exceptions in that they exhibit no change of mechanism in the temperature range studied. Second, below the transition temperature the overall magnitude of E_a suggests that chemical reactions in the bulk phase control the decomposition process. The difference between the rate constants for the evolution of individual products is relatively large, which suggests that multiple reactions occur to form each product. Third, above the transition temperature, the magnitude of E_a suggests that bulk phase chemical reactions do not control the process. The difference between the rate constants is comparatively small which implies that similar processes control the rate of formation of all products.

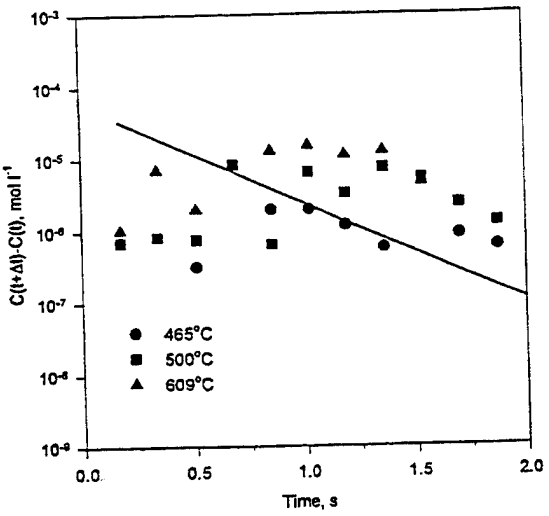

Fig. 4. Analysis of the order of the process by the Guggenheim method showing that zeroth-order applies here. The line is Ericsson's data [15] showing first order.

The chemistry that controls the rate evolution of most of the major products from PBD polymers, when pyrolysis occurs below the transition temperature, results in Arrhenius parameters whose magnitudes are consistent with control by bulk-phase chemical reactions. For example, the observed values of E_a = 38 – 76 kcal/mol not only span the previously reported values in Table 1, but extend nearly to the C—C bond dissociation energy of 83 kcal/mol. It is impossible to assign these Arrhenius parameters to specific reactions, even though they give more detail than has been available previously. Multiple steps involving bond breaking and rearrangements are required before liberation of each species. H-transfer reactions are additionally required to form several products. A wide range of E_a values is understandable from the point of view that the heats of reaction to produce the observed products differ widely. Assuming that E_a roughly parallels ΔH_r for these radical homolysis reactions, the widely different E_a values found are not surprising.

The formation of CP from R45M and 1,5-HD from BM94 is exceptional and is discussed in

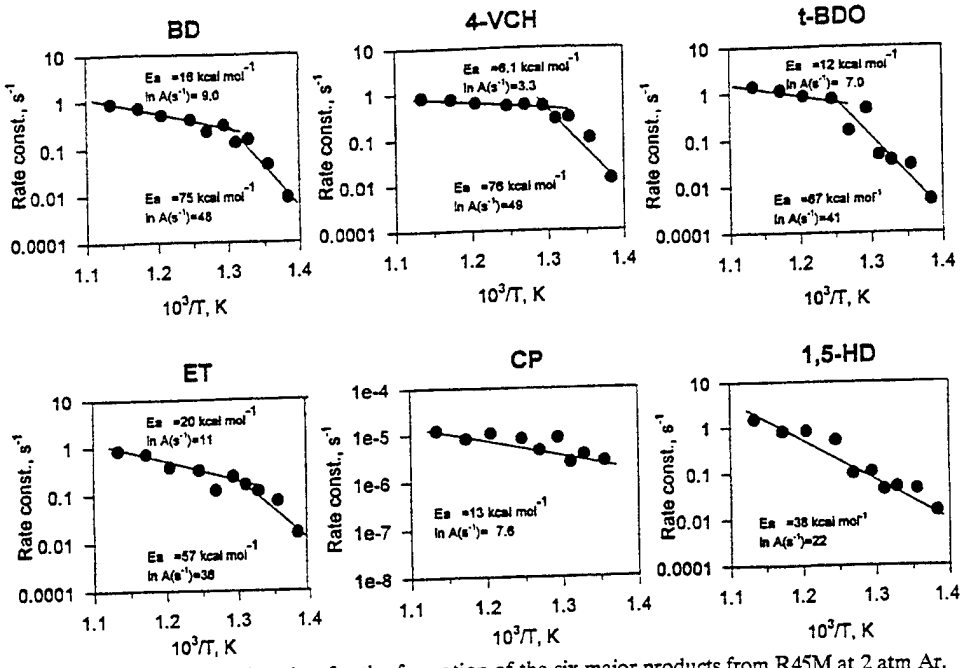

Fig. 5. Arrenhius plots for the formation of the six major products from R45M at 2 atm Ar.

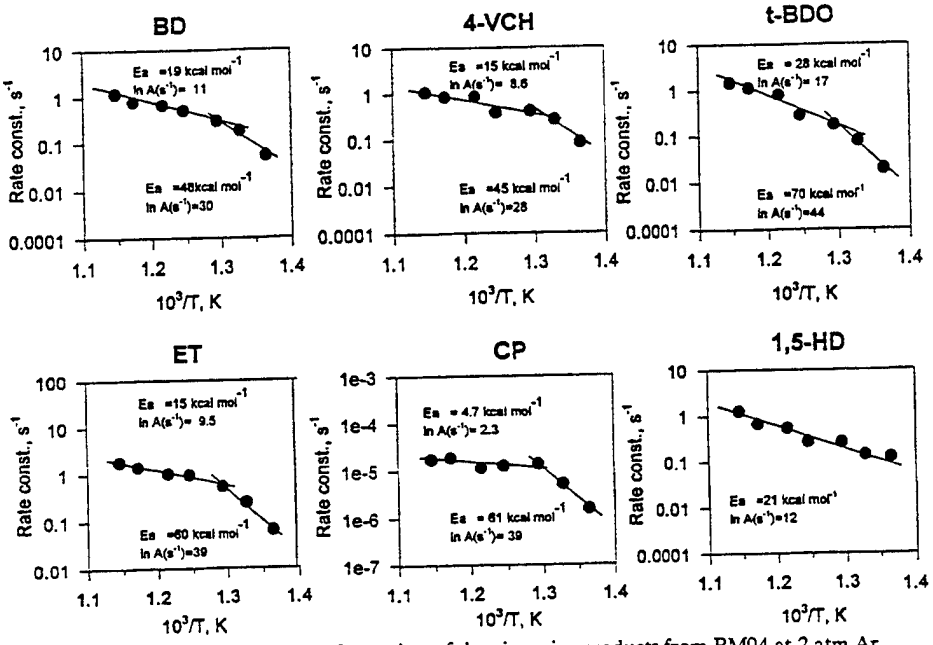

Fig. 6. Arrenhius plots for the formation of the six major products from BM94 at 2 atm Ar.

the following paragraph. Before doing so, we note that the Arrhenius plot for 1,5-HD in Fig. 5 suggests that two regions of behavior might actually exist instead of the single one shown. If this is the case, then the 450°–530°C range yields E_a = 42 kcal/mol and ln A (s^{-1}) = 25, while 530°–609°C produces E_a = 17 kcal/mol and ln A (s^{-1}) = 10. This ambiguity about the kinetics of 1,5-HD is not serious because it is not an abundant product.

Above the transition temperature in Figs. 5 and 6, the Arrhenius parameters are lower. In fact, most are smaller than would be expected for bulk-phase, chemistry-controlled processes. The majority of E_a values are clustered below 16 kcal/mol, and resemble the values given in Table 2 for polymers heated at high rates to high temperatures. The interpretation frequently given for Arrhenius parameters of this magnitude is that heat and mass transport predominately control the rate [2, 27–31]. A logical explanation here is that the rate of desorption of these gaseous species from the surface dominates the rate of gas formation. It is probable that these low values of E_a reflect the combined desorption rate and the formation of resonance-stabilized radicals which lead to the larger molecules that become important at the higher temperatures. CP from R45M and (possibly) 1,5-HD from BM94 are unusual in that the rate of desorption appears to control their evolution throughout the temperature range studied.

The 500°–530°C temperature range, where the transition between bulk-phase chemical reaction control and desorption control occurs, was also notable for the change of product characteristics in the preceding article [1]. In about this temperature range, the switch from strong temperature dependence of the products to weaker temperature dependence occurs. This switch is probably not coincidental and results from the change in the controlling mechanism. As suggested previously [1, 33, 34], the limiting rate of bulk-phase thermal decomposition may be reached in this temperature range. Above this temperature range, the rate of gas evolution is controlled by the rate of desorption rather than bulk-phase decomposition.

C. Kinetic Constants at 11 Atm Ar

Figure 7 shows Arrhenius plots for product evolution from R45M under 11 atm Ar in the

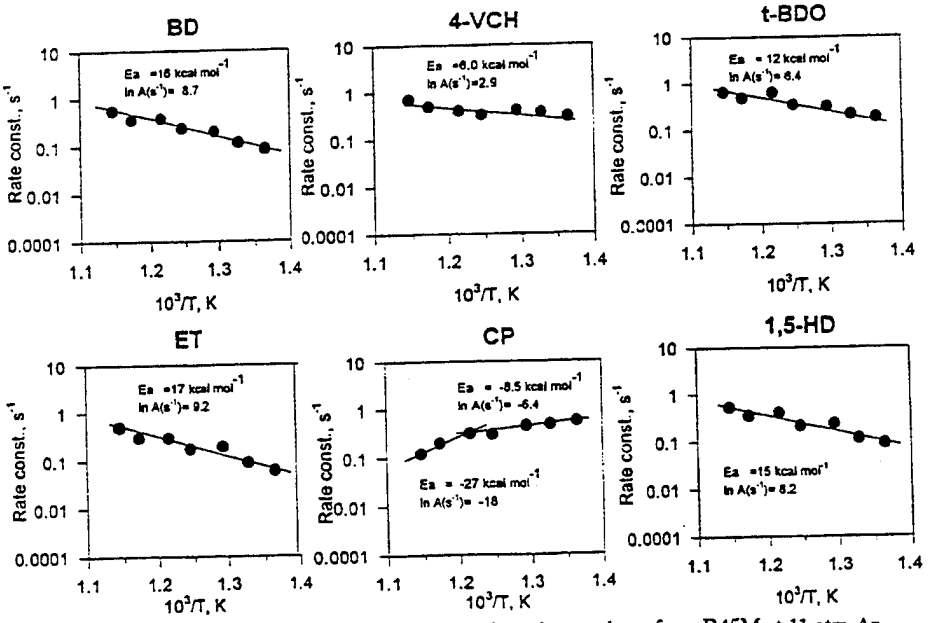

Fig. 7. Arrenhius plots for the formation of the six major products from R45M at 11 atm Ar.

temperature range of 460°–600°C. In all cases, the process shift above 530°C at 2 atm (Figs. 5 and 6) is no longer observed, and the lower range of values of the Arrhenius parameters dominates throughout 460°–600°C. The implication of these results is that at higher pressures the rate of desorption of gaseous products controls the rate of mass loss. It is not necessary to know the detailed pyrolysis reactions in the bulk phase to describe the rate of degradation of PBD.

A curious finding is the anti-Arrhenius behavior of CP from R45M. Many reasons exist for why a process might become slower as the temperature is increased. A plausible explanation with PBD polymers is that the specific reactant that produces CP also produces one or more other products. The CP formation branch could be disfavored at higher pressure and temperature relative to another product. Because CP from BM94 under 2 atm pressure does not exhibit anti-Arrhenius behavior, it is possible that the vinyl group contributes in some way to the anomaly of CP from R45M.

D. Macro Kinetics of Pyrolysis

Pyrolysis of PBD occurs as part of the overall combustion process of a solid propellant. The semi-micro kinetics of evolution of individual products into the flame zone may be needed if the effects of transient pressure and temperature oscillations in the chamber are to be modeled in the surface reaction zone with detailed chemistry. However, the overall rate of degradation of the surface is still needed. In this context, the Arrhenius data in Figs. 5–7 can be combined to give a total rate of product evolution, which, in turn, yields macro kinetic Arrhenius parameters. Figure 8 and Table 3 show these data for R45M at 2 and 11 atm, and BM94 at 2 atm. For pyrolysis at 2 atm, the crossover from chemical reaction control at lower temperatures to desorption control at higher temperatures is apparent. In the lower temperature range the macro kinetic Arrhenius parameters in Fig. 8 span the range of values for chain scission measured at much lower heating rates (Table 1). For pyrolysis at temperatures above the transition temperature

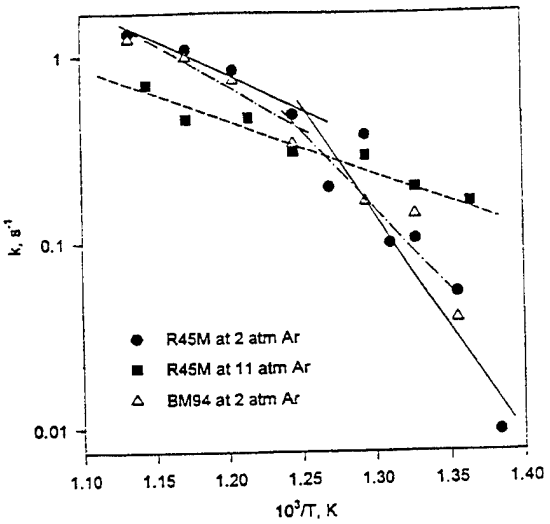

Fig. 8. The macro kinetic Arrhenius parameters for the overall rate of gaseous product formation from R45M and BM94, as determined by combining the data in Figs. 5–7.

at 2 atm and for all temperatures at 11 atm, the Arrhenius parameters fall into the range of control by desorption of products from the surface (Table 2). These findings help to reconcile the literature in this area and provide some insight on how to incorporate polymer pyrolysis kinetics into combustion modeling.

The major kinetic conclusion is that the rate of gas generation and regression of the binder surface during combustion is controlled by the rate of desorption of the gaseous products. The rates of specific pyrolysis reactions of the PBD polymer appear to play a minor role in the rate of product evolution if the temperature is above the 500°–530°C range at 2 atm. As the pressure is raised, this temperature range decreases. Therefore, for the purpose of modeling the binder pyrolysis rate during combustion of solid rocket propellents containing HTPB, the desorption ki-

TABLE 3

Macro Kinetic Arrhenius Parameters for Flash Pyrolysis of HTPB

Sample	Pressure (atm)	Temp (°C)	E_a (kcal/mol)	ln A (s^{-1})
R45M	2	450–530	51	31
BM94	2	465–530	35	21
R45M	2	530–609	18	11
BM94	2	530–609	23	14
R45M	11	460–600	12	6.6

netics involving the higher molecular weight fragments should be employed rather than the bulk-phase chemical decomposition kinetics.

At first sight this statement may seem counterintuitive in that the desorption rate would be expected to be suppressed by increasing the pressure. How could it then become the dominant process at higher pressure? Figure 8 reveals that the rate of desorption is, indeed, decreased by increasing the applied pressure. However, the bulk phase reaction rates are still occurring at a rate faster than desorption in the temperature range used, making desorption rate controlling.

IV. GENERALIZED MODEL OF FLASH PYROLYSIS OF HTPB

Figures 5–8 suggest that the rate of rapid pyrolysis of HTPB is controlled by heterogeneous, bulk-phase, decomposition processes below the 500°–530°C range, but desorption processes control above this range. Pressure clearly influences the temperature at which the crossover between processes occurs. We sought to develop a simple model which accounts for the trends in Figs. 5–8.

Chaiken et al. [27] specified the basis of such a model for PMMA, which was adapted here to account for the effect of pressure. The rate of gas evolution, k, from the polymer surface is given by Eq. 3,

$$k = \theta k_s, \tag{3}$$

where θ is the fraction of desorption sites and k_s is the rate of desorption. Equation 4 applies for steady regression,

$$(k_a c_g + k_d M)(1 - \theta) = \theta k_s N_0, \tag{4}$$

where k_a is the rate of adsorption, c_g is the gaseous product concentration, k_d is the rate of decomposition, M is the concentration of polymer in the bulk phase, and N_0 is the number of desorption sites. θ can be derived from Eq. 4 and substituted into Eq. 3 to yield Eq. 5:

$$k = \left[\frac{k_a n_g + k_d M}{k_s N_0 + k_a c_g + k_d M}\right] k_s. \tag{5}$$

Assuming $k_a \simeq k_s$, Eq. 5 reduces to Eq. 6:

$$k = \frac{k_s c_g + k_d M}{M + c_g + (k_d/k_s)M}, \tag{6}$$

Also, if M is assumed to be constant, then $M = \rho/\mathrm{MW} \simeq N_0$, where MW is the molecular weight, and ρ is the density [27]. Furthermore, $c_g = P/RT_0$ by the perfect gas law. $T_0 = 298$ K because the gases are quenched in our experiment. Substitution for these terms into Eq. 6 yields a generalized description of the rate of gas evolution from the polymer, Eq. 7,

$$k = \frac{(P/RT_0)k_s + (\rho/\mathrm{MW})k_d}{\rho/\mathrm{MW}(1 + k_d/k_s) + P/RT_0}, \tag{7}$$

in which all of the terms can be specified by the experimental methods and data given in this article. $k_d = A_d \exp(-E_d/RT)$ and $k_s = A_s \exp(-E_s/RT)$. By using the Arrhenius parameters given in Table 3 for decomposition and desorption, Fig. 9 shows that the predicted rate of gas evolution from R45M is approximately reproduced by Eq. 7 between 465° and 609°C at the two pressures investigated. Equation 7 might be used to incorporate the rate of binder pyrolysis into the combustion model of a composite propellant. As such, it is useful to see from Fig. 10 that Eq. 7 predicts that desorption rather than decomposition controls the surface

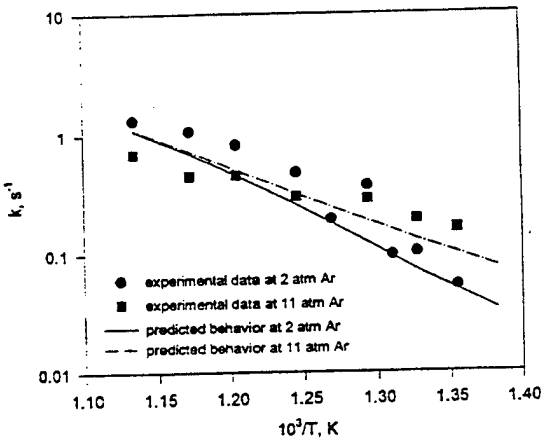

Fig. 9. A comparison of the experimentally determined rates and predicted rates (Eq. 7) of gas product evolution from R45M which was flash pyrolyzed at 600°C/s under two pressures of Ar.

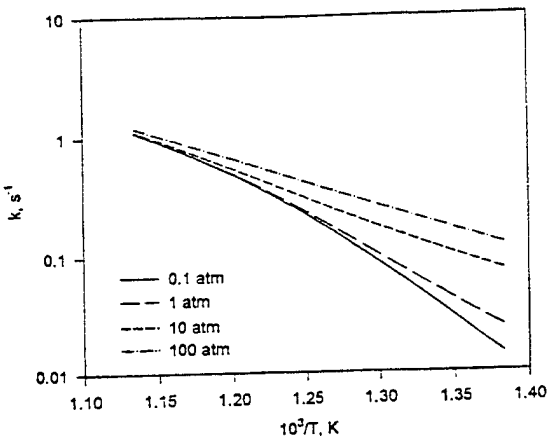

Fig. 10. The predicted pressure dependence of gas evolution from HTPB suggesting that desorption dominates at pressure greater than 10 atm.

regression rate of the binder at pressures typical of those in the nozzled combustion chamber of a solid propellant rocket.

V. CONCLUSIONS

1. The pyrolysis kinetics of PBD compounds are not comparable in the least at low heating rates and high heating rates. The "cooking" reactions that occur when the bulk phase is slowly heated preclude the use of these kinetics for combustion-like problems.
2. In general, bulk-phase pyrolysis reactions dominate the rate of decomposition when dT/dt is deg/min; or with the combination of $dT/dt \geq 10^2$ deg/s, $P \leq 2$ atm, and $T \leq 500°-530°C$. This fact is reflected in the magnitude of the Arrhenius parameters and the high sensitivity of the gaseous product distribution to temperature.
3. In general, the rate of desorption and the formation of higher MW oligomers dominate the rate of gaseous product evolution under the following conditions: $dT/dt \geq 10^2$ deg/s, $P = 2$ atm, and $530 < T < 609°C$; or $dT/dt \geq 10^2$ deg/s, $P \geq 11$ atm, and $T > 460°C$. These conditions cover most that exist during combustion of solid rocket propellants. Thus, for combustion modeling the desorption kinetics of HTPB described herein, rather than the bulk-phase decomposition kinetics, should be employed.
4. The temperature range where the crossover from control by the bulk-phase decomposition rate to control by the desorption rate probably defines the temperature where the maximum rate of bulk-phase pyrolysis reactions is reached. Above this temperature the rate of desorption of larger fragments dominates the rate of gas evolution.
5. The effect of increasing the pressure is to decrease the temperature at which the rate of gas generation is controlled by the rate of desorption. All of the above facts can be incorporated into a single equation which describes the pressure and temperature dependence of the rate of gas evolution from HTPB.

We are grateful to the Air Force Office of Scientific Research, Aerospace Science and Engineering Directorate, for support of this work on F49620-94-1-0053. R. Wardle supplied the sample of BM94 and S. F. Palopoli provided R45M.

REFERENCES

1. Arisawa, H., and Brill, T. B., *Combust. Flame*, preceding article.
2. Brill, T. B., Brush, P. J., James, K. J., Shepherd, J. E., and Pfeiffer, K. J., *Appl. Spectrosc.* 46:900–911 (1992).
3. Golub, M. A., and Gargiulo, R. J., *J. Polym. Sci. Polym. Lett.* 10:41–49 (1972).
4. Chen, J. K., and Brill, T. B., *Combust. Flame* 87:217–232 (1991).
5. Tamara, S., and Gillham, J. K., *J. Appl. Polym. Sci.* 22:1867–1884 (1978).
6. Rama Rao, M., and Radhakrishnan, T. S., *J. Appl. Polym. Sci.* 41:2251–2263 (1990).
7. Thomas, T. J., Krishnamurthy, V. N., and Nandi, U. S., *J. Appl. Polym. Sci.* 24:1797–1808 (1979).
8. Schneider, B., Doskocilova, D., Stokr, J., and Svoboda, M., *Polymer* 34:432–436 (1993).
9. Grassie, N., and Heaney, A., *J. Polym. Sci. Polym. Lett.*, 12:89–94 (1974).
10. Brazier, D. W., and Schwartz, D. W., *J. Appl. Polym. Sci.*, 22:113–124 (1978).
11. Coffman, J. A., *Ind. Eng. Chem.* 44:1421–1428 (1952).
12. McGreedy, K. and Keskkula, H., *Polymer* 20: 1155–1159 (1979).
13. Du, T., *Thermochim. Acta* 138:189–197 (1989).
14. Golub, M. A., and Sung, M., *J. Polym. Sci. Polym. Lett.* 11:129–138 (1973).
15. Ericsson, I., *J. Chromatogr. Sci.* 16:340–344 (1978).
16. Bolland, J. C., and Orr, W. J. C., *Trans. I.R.I.* 21:133–138 (1945).
17. Straus, S., and Madorsky, S. L., *J. Res. NBS* 61:77–81 (1958).
18. Varney, A. M., and Strahle, W. C., *Combust. Flame* 16:1–8 (1971).

cop C

19. Ninan, K. N., and Krishnan, K., *J. Spacecraft Rock.* 19:92–94 (1982).
20. Bouck, L. S., Baer, A. D., and Ryan, N. W., *Fourteenth Symposium (International) on Combustion*, The Combustion Institute, Pittsburgh, 1973, pp. 1165–1176.
21. Shono, T., and Shina, K., *Anal. Chim. Acta* 56:303–307 (1971).
22. Radhakrishnan, T. S. and Rama Rao, M., *J. Polym. Sci.* 19:3197–3208 (1981).
23. Braun, D., and Canji, E., *Angew. Makromol. Chem.* 29/30:491–505 (1973).
24. McAlevy III, R. F., and Hansel, J. G., *AIAA J.* 3:244–249 (1965).
25. Cheng, J.-H., Ryan, N. W., and Baer, A. D., *Twelfth Symposium (International) on Combustion*, The Combustion Institute, Pittsburgh, 1968, pp. 525–532.
26. Baer, A. D., Hedges, J. H., Seader, J. D., Jayakar, K. M., and Wojcik, L. H., *AIAA J* 15:1398–1404 (1977).
27. Chaiken, R. F., Anderson, W. H., Barsh, M. K., Mischuck, E., Moe, G., and Schultz, R. O., *J. Chem. Phys.* 32:141–146 (1960).
28. Cohen, N. S., Fleming, R. W., and Derr, R. L. *AIAA J.* 12:212–218 (1974).
29. Gullett, B. K., and Smith, P., *Combust. Flame*, 67:143–151 (1987).
30. Hansel, J. G. and McAlevy, III, R. F., *AIAA J.* 4:841–848 (1966).
31. Anderson, W. H., Bills, K. W., Mischuck, E., Moe, G., and Schultz, R. O., *Combust. Flame* 3:301–317 (1959).
32. Guggenheim, E. A., *Philos. Mag.* 2:538–543 (1926).
33. Lee, I. Y. S., Wen, X., Tolbert, W. A., Dlott, D. D., Doxtader, M., and Arnold, D. R., *J. Appl. Phys.* 72:2440–2448 (1992).
34. Shlensky, O. F., Matyukhin, A. A., and Varynshteyn, E. F., *J. Thermal Anal.* 31:107–115 (1986).

Received 11 May 1995; revised 2 November 1995

TOWARD QUANTITATIVE THERMODYNAMICS AND KINETICS OF PYROLYSIS OF BULK MATERIALS AT HIGH TEMPERATURE AND PRESSURE

G. K. WILLIAMS and T. B. BRILL
Department of Chemistry and Biochemistry, University of Delaware, Newark, DE 19716

ABSTRACT

An evaluation was made of whether T-jump/FTIR spectroscopy could be used to determine the decomposition kinetics (E_a and ln A) and thermochemical (ΔH_d) constants of an energetic material at high temperature and high heating rate. Polystyrene peroxide was chosen because of its known, simple, decomposition process. The kinetic constants are reasonable for O-O bond homolysis as the rate determining step: E_a = 39 kcal/mol, ln (A, s^{-1}) = 21.5. Significant uncertainty exists, however, in the estimation of ΔH_d.

INTRODUCTION

The experimental heat of reaction and kinetic parameters associated with the thermal decomposition of almost all energetic materials in the bulk state are difficult to obtain. DSC and TGA are common methods to obtain these global parameters. When applied to energetic materials, these techniques suffer several shortcomings. First, in DSC the heat release during thermal decomposition of most energetic materials is so rapid a time lag exists between the reaction and the recording of the response. Second, the decomposition chemistry can be affected by changes in the heating rate, pressure, and average temperature. DSC and TGA apply to relatively slow decomposition which may not be representative of combustion. Of greatest concern to us has been the kinetics and thermodynamics of fast decomposition which is representative of the surface reaction zone during combustion of an energetic material [1,2]. One approach to gain such data is to measure the time to ignition or explosion [3-5]. The desire to learn about species and rates simultaneously prompted development of T-jump/FTIR spectroscopy [6], which simultaneously records thermal events and gaseous decomposition products of a flash-heated material in near real-time. DSC and T-jump/FTIR spectroscopy are similar in that both record electrical requirements for maintaining a programmed temperature, but do so at very different heating rates. The voltage is extracted from T-jump/FTIR whereas DSC records power. This precludes direct calculation of the heat of reaction as in DSC. Therefore, an energetic material was sought with a "one-step," exothermic decomposition mechanism and known heat of reaction. The integrated voltage change in the T-jump/FTIR experiment might be used as a calibration standard to gain thermal data on other energetic materials. Kinetic data might be extracted either from the rate of the voltage change or time-to-exotherm. It would be desirable if the material could be cast as a thin film to maximize sample-to-filament contact for uniform heating.

Polystyrene peroxide (PSP) was chosen because it decomposes exothermally to an equimolar ratio of benzaldehyde and formaldehyde which account for more than 95% of the products. Kishore, et al., [7-11] have studied many aspects of PSP. Pressure or heating rate differences do not appear to change the decomposition mechanism. PSP is easily cast as a film from benzene. The unusually simple decomposition chemistry could also enable comparisons to be made among the kinetic methods of DSC, TGA, and T-jump/FTIR spectroscopy.

in "Decomposition, Combustion and Detonation Chemistry of Energetic Materials," T. B. Brill, T. P. Russell, W. C. Tao and R. B. Wardle, Eds. Materials Research Society, Vol. 418, Pittsburgh, PA 1995.

EXPERIMENTAL AND RESULTS

PSP was prepared by the "equimolar copolymer" procedure [12] and stored at 253 K in the dark. The resulting polymer had a monomodal distribution with weight-average (M_w = 19900) and number-average (M_n = 12400) molecular weights determined by GPC using polystyrene standards and THF solvent. Proton NMR and solid state IR spectra closely matched previous reports [13, 14]. The equimolar ratio of gaseous benzaldehyde and formaldehyde was confirmed in the IR spectrum by integrating ν_8 of benzaldehyde [15] and ν_3 of formaldehyde [16] and establishing the concentrations by the absolute intensity of these modes.

Kinetic Constants

In a typical nonisothermal TGA (DuPont Instruments Model 951) experiment, 16-20 mg of PSP was placed in a open Al pan situated on the hanger of the thermobalance under a flow of Ar, and was heated from ambient temperature to 438 K at 1 K/min. The first derivative of the TGA mass loss curve revealed a single mass loss step. The method of Coates and Redfern [17] was utilized to determine the kinetic parameters for this process. Table 1 gives the Arrhenius activation energy (E_a) in the 345-400 K range.

Nonisothermal DSC experiments were conducted on a DuPont Instruments Model 910 calibrated with an In metal standard. Samples of 5-15 mg were heated at rates of 1-10 K/min in open or hermetically sealed Al pans under a flow of Ar. The method of Barrett [18] was used to calculate the kinetic parameters. The heat of degradation (ΔH_d) of PSP (217±3 cal/g) corresponds to the area, W, of the exotherm. Any fraction, w, of W corresponds to the heat released in a particular time, t. Assuming that the amount of heat evolved is proportional to the number of moles of reacted, then $k = (dH/dt)/(W-w)$ for a first-order reaction. Since the temperature was continually rising, several rate constants are obtained from a single experiment. A plot of ln k vs $1/T$ yields Arrhenius data given in Table 1.

At high heating rates, kinetics were determined by T-jump/FTIR spectroscopy [6]. A Pt ribbon filament was situated inside a gas cell in an Ar atmosphere having a chosen, constant pressure. Detailed heat transfer models of this device are available [19, 20]. To maximize the heat transfer between the Pt ribbon filament and the sample, approximately 200 μg of PSP was cast onto the filament from benzene solution. The filament was placed under 0.10 torr for 10 minutes to remove the benzene. However, no combination of reduced pressure and mild heating could remove all of the benzene as evidenced by the IR spectra collected during thermolysis. By a separate TGA experiment, approximately 10% of the mass deposited on the filament remained as benzene after pumping. Because of the chemical inertness of C_6H_6, none of the kinetic features of the exotherms discussed below can be attributed to C_6H_6. Since pressure differences of 1-60 atm had no apparent effect on the decomposition of PSP, all T-jump/FTIR experiments were conducted at 1 atm Ar. A high-gain, fast-response power supply heated the Pt filament at 2000 K/s to a predetermined temperature. The power supply rapidly adjusted the power requirements to maintain the final temperature of the filament at a constant value during the experiment. An exothermic event required a decrease (negative deflection) in the voltage (V) necessary to maintain the filament at the set temperature. This control voltage was stored at 50 points/s during the experiment. As shown in Figure 1, there is a generally decreasing value of the control voltage throughout the experiment because of convective heat loss to the surrounding Ar atmosphere. Superimposed on this profile are the thermal events of PSP.

Table 1. Arrhenius Constants for PSP

Method	T, K	E_a [a]	ln (A, s^{-1})
TGA	345-400	21.5	----
DSC	362-396	27.5	32.4
DSC[b]	405-415	32.5[c]	----
T-jump	435-451	38.9	45.9
TTX	430-440	19.5	21.5

[a] kcal/mol [b] Data from reference 8
[c] Reaction order changes from 2 at 405 K to 1.2 at 415 K .

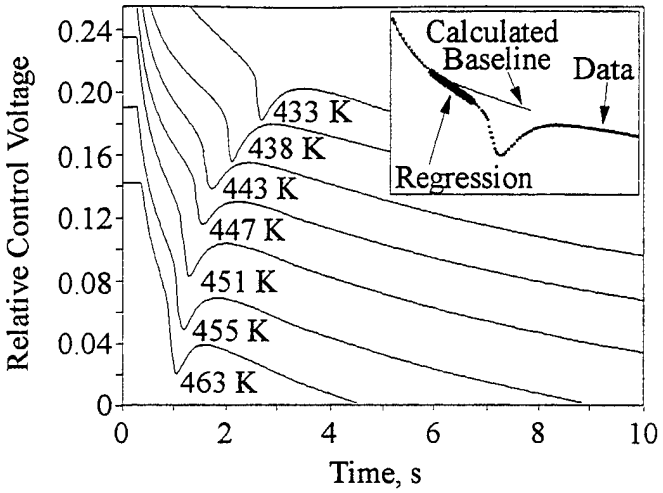

Figure 1. Difference control voltage traces for PSP from T-jump/FTIR.

Figure 1 reveals a gradual release of heat prior to the main exothermic event. A similar, possibly related, sequence was observed in several of the DSC thermograms (Figure 2), although only a single mass loss step was observed by TGA. By IR spectroscopy, formaldehyde and benzaldehyde appear in the gas phase concurrently with the onset of heat release, and they rise rapidly in concentration at the strongly exothermic point.

The activation energy of the initial step of heat release was determined in the T-jump experiment by adapting Rogers' method [21] of using DSC data to obtain rate data. PEAKFIT software was used to calculate the baseline (a double exponential) and to fit the initial stage of the exotherm (an asymmetric double sigmoidal). At all temperatures $R^2 > 0.99$. The difference between the sample trace and the calculated baseline was measured. Since DSC and T-jump data reflect the rate of heat release directly, the deflection from the baseline, b, is directly proportional to the rate of reaction, $d\alpha/dt$, where α is the degree of conversion. Thus,

$$\beta b = d\alpha/dt = k(1-\alpha) \qquad (1)$$

where β is a proportionality constant and k is the rate constant. The relationships in equation (1) are valid for small values of α. Hence, $\ln b = \ln k/\beta + \ln (1-\alpha)$. For a first order reaction $\ln (1-\alpha) = -kt + c$, where c is a constant. By substituting and combining constants, $\ln b = C - kt$ is obtained, and rate constants for a first order process can be obtained directly from a plot of ln b vs t. Figure 3 shows the rate data and Table 1 contains the Arrhenius constants. A similar procedure was attempted for the initial exotherm in the DSC thermogram of Figure 2, but was inconclusive because of large uncertainty in the integration of this small exotherm.

Finally, zeroth-order induction time kinetics based on the Semenov model [4, 5] of the time-to-exotherm (TTX) [22] was explored. Here the time-to-exotherm as a function of temperature was obtained from the data in Figure 1. Equation (2) relates E_a and $\ln A$ to these data, where B is the intercept and C_p is the specific heat.

$$\ln \mathrm{TTX} = \frac{E_a}{RT} + \frac{C_p R T^2}{\Delta H_d B E_a} \qquad (2)$$

A plot of $\ln(1/\mathrm{TTX}, s^{-1})$ vs $1/T$ and equation (2) yields the apparent Arrhenius data in Table 1.

Thermochemistry

The integrated area of the control voltage trace should be directly proportional to the heat generated by PSP provided that the heat transfer coefficient between the filament and film of PSP is very large and little heat is transferred to any part of the system (e.g. the surrounding atmosphere) other than the filament. Of course, neither of the presumptions is strictly true, making the amount of heat sensed by the filament always less than the absolute amount produced by the sample. The fall-back position is to take the amount of heat generated from the decomposition of PSP (ΔH_d) which was determined above by DSC, and to correlate this value with a specific area defined by the control voltage deflection from the baseline. Figure 4 shows that the area from the average of five runs with a series of masses of PSP is approximately linearly related to the area of the control voltage trace, ΔV, but that the range of uncertainty is large. Equation (3) on Figure 4 gives the mass-area relationship. If equation (3) is used for calibration purposes, then equation (4) relates the heat generated by a compound x, ΔH_d (x), to the area ΔV, for a specific mass of x. For 200 μg of PSP, γ = 13.1 cal/volt-sec.

$$\Delta H_d(x) = \frac{\Delta H_d(PSP) \bullet \Delta V(x)}{\Delta V(PSP)} = \Delta V(x) \bullet \gamma \qquad (4)$$

DISCUSSION

The Arrhenius constants (Table 1) that are obtained for PSP from the deviation of the voltage trace from the baseline trace by T-jump/FTIR spectroscopy reflect the initial reaction stage before the process becomes strongly autothermal. The resultant activation energy of E_a = 39 kcal/mol lies in the range of values for thermal homolysis of dialkyl peroxides of 30-39 kcal/mol [23]. However, ln (A, s^{-1}) = 45.9 from the T-jump/FTIR data on solid PSP is larger than the highest value reported [23] for dialkyl peroxides in the gas phase [ln(A, s^{-1} = 16.5)]. The meaning of ln A for solid phase decomposition processes is much less certain than that for the gas phase. The larger A factor for the solid phase process could mean that the heat released during decomposition accelerates the rate to some extent compared to the reaction of more isolated molecules in the gas phase. The value of E_a = 39 kcal/mol resembles the O-O single bond strength of 38 kcal/mol for a dialkyl peroxide [24]. These facts suggest that the control voltage trace during flash thermolysis of PSP is capturing the homolysis rate of the O-O bond of PSP, although probably with an extraneous contribution from the autothermal nature of the process.

The value of E_a obtained in this work by DSC is lower than the value reported by Kishore [8], which was based on three data points in the 405-415 K range. No A factor was reported. Since ln A was determined from the DSC data in Figure 2, a comparison of rates by DSC, T-jump/FTIR spectroscopy and TTX can be made in Figure 5. Despite the apparent differences in E_a in Table 1, the compensation effect between E_a and A produces approximately the same rate of the overall process in the 400±20 K range. This suggests that all of the measurements are sensing essentially the same process, namely O-O homolysis. Extrapolation of the rate measured by any of these techniques into another temperature range yields a rather different prediction.

Unlike the kinetic analysis by T-jump/FTIR spectroscopy, the determination of ΔH_d for a bulk material at high temperature is subject to a rather large uncertainty. However the uncertainty appears to be least when approximately 200 μg sample are used. An uncertainty in ΔH_d of ±20% would be likely.

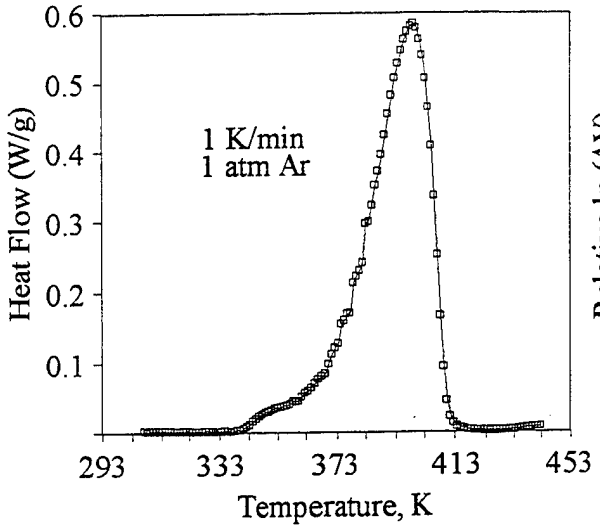

Figure 2. DSC thermogram for PSP.

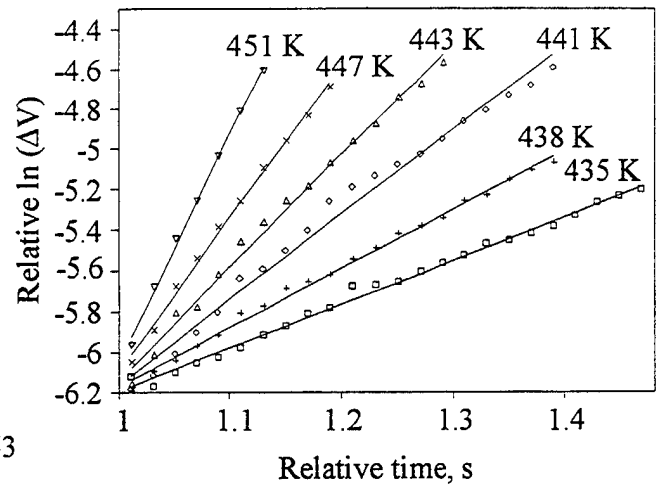

Figure 3. Rate data for PSP from T-jump data in Figure 1.

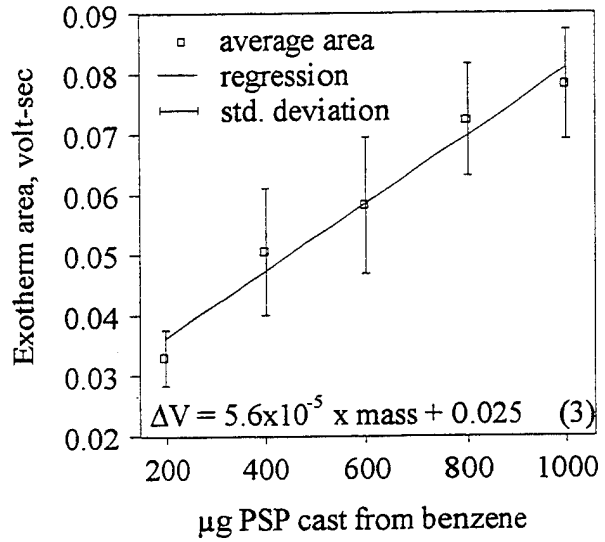

Figure 4. Relationship between the area of the thermal trace in Figure 1 and the sample mass.

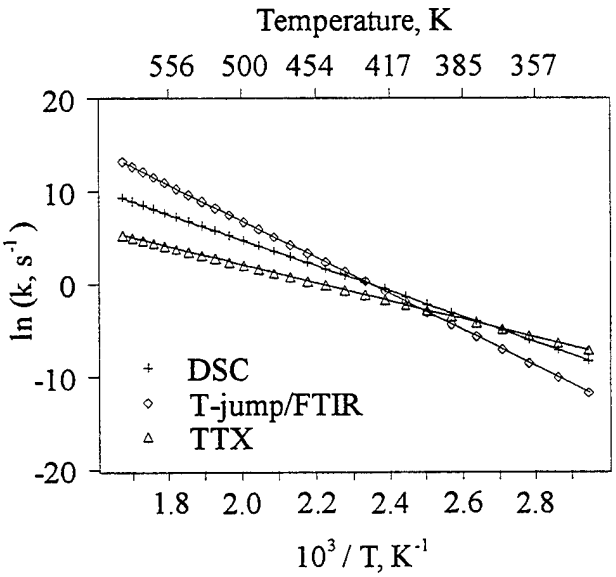

Figure 5. Comparison of the Arrhenius plots from data in Table 1.

CONCLUSIONS

In principle, the rates of decomposition and the heat released from energetic materials heated at high rates to high temperatures can be obtained by T-jump/FTIR spectroscopy. The degree of success on the kinetics of PSP is good, but the thermochemistry is only marginally acceptable. From experience with the thermal traces of other energetic materials, we know that the successful analysis of the kinetics for PSP is partly attributable to the gradual slope of the exotherm before the violent release of heat occurs. Other energetic materials with this behavior can, therefore, be analyzed. On the other hand, the kinetics of decomposition of compounds which release a great deal of heat very early in the decomposition scheme (e.g. azide-containing polymers [25]) probably could not be characterized in this manner.

ACKNOWLEDGMENT

We are grateful to the Air Force Office of Scientific Research (NA) for support on F49620-94-1-0053.

REFERENCES

1. T. B. Brill, H. Arisawa, P. J. Brush, P. E. Gongwer and G. K. Williams, J. Phys. Chem. **99**, p. 1384 (1995).
2. T. B. Brill, J. Propul. Power **11**, p. 740 (1995).
3. J. Wenograd, Trans. Farad. Soc. **57**, p. 1612 (1961).
4. A. G. Merzhanov, Combust. Flame **11**, p. 201 (1967).
5. N. N. Semenov, Z. Phys. **48**, p. 571 (1928).
6. T. B. Brill, P. J. Brush, K. J. James, J. E. Shepherd and K. J. Pfeiffer, Appl. Spectrosc. **46**, p. 900 (1992).
7. R. P. Rastogi, K. Kishore and B. K. Chaturvedi, AIAA Journal **12**, p. 1187 (1974).
8. K. Kishore, J. Therm. Anal. **21**, p. 15 (1981).
9. K. Kishore and K. Ravindran, Macromolecules **15**, p.1638 (1982).
10. K. Kishore, V. Gayathri and K. Ravindran, J. Macromol. Sci. Chem. **A19**, p. 943 (1983).
11. K. Kishore and T. Mukundan, Nature **324**, p. 130 (1986).
12. R. E. Cais and F. A. Bovey, Macromolecules **10**, p. 169 (1977).
13. K. Kishore, J. Chem. Eng. Data **25**, p. 92 (1980).
14. K. Kishore and K. Ravindran, J. Anal. Appl. Pyrolysis **5**, p. 363 (1983).
15. R. T. C. Brownlee, D. G. Cameron, R. D. Topsom, A. R. Katritzky and A. J. Sparrow, J. Mol. Struct. **16**, p. 365 (1973).
16. T. Nakanaga, S. Kondo and S. Saëki, J. Chem. Phys. **76**, p. 3860 (1982).
17. A. W. Coates and J. P. Redfern, Nature **201**, p. 68 (1964).
18. K. E. J. Barrett, J. Appl. Polym. Sci. **11**, p. 1617 (1967).
19. J. E. Shepherd and T. B. Brill, 10th International Detonation Symposium, Office of Naval Research, Arlington, VA 1993, pp. 849-855.
20. S. T. Thynell, P. E. Gongwer and T. B. Brill, J. Propul. Power, submitted.
21. R. N. Rogers, Anal. Chem. **44**, p. 1336 (1972).
22. G. K. Williams and T. B. Brill, Combust. Flame **102**, p. 481 (1995).
23. R. Hiatt in Organic Peroxides, Vol. III, D. Swern, Ed. (John Wiley & Sons, Inc., New York, 1972), pp. 1-66.
24. S. W. Benson and R. Shaw in Organic Peroxides, Vol I, D. Swern, Ed. (John Wiley & Sons, Inc., New York, 1970), pp. 106-140.
25. T. B. Brill, P. J. Brush, D. G. Patil and J. K. Chen, 24th Symposium (International) on Combustion, The Combustion Institute, Pittsburgh, PA 1992, pp. 1907-1914.